A COMPARATIVE STUDY OF VPO CATALYSTS IN THE OXIDATION OF BUTANE TO MALEIC ANHYDRIDE

by

NISHLAN GOVENDER
B.Sc (Hons)

School of Pure and Applied Chemistry
University of Natal
Durban
4041

Submitted in fulfillment of the academic
requirements for the degree of
Master of Science in the
School of Pure and Applied Chemistry,
University of Natal
Durban

March 2002

DECLARATION

I hereby declare that the work presented in this thesis is my own work and has never before been submitted for any degree at this or any other university.

_____

N. GOVENDER

_____ day of _____ 2002

ABSTRACT

Co promoted and unpromoted vanadium-phosphorous-oxide (VPO) catalysts were synthesized via an organic route. The catalyst precursor was calcined and then conditioned in a reactor, forming the active vanadyl pyrophosphate, $(VO)_2P_2O_7$, phase. Different promoter loaded catalysts were synthesized and their effect on the yield of maleic anhydride (MA) from *n*-butane oxidation was examined at different temperatures and gas hourly space velocities (GHSV). The catalysts were tested as a powder. The catalysts were examined in the oxidation of *n*-butane gas, over air as an oxidant, in a specially designed and constructed continuous flow, fixed-bed catalytic micro-reactor equipped with an on-line gas chromatography (GC) monitoring system. A thermal conductivity detector (TCD) was employed for carbon oxide monitoring and a flame ionization detector (FID) for all other products.

The catalysts were characterised by X-ray diffraction (XRD) to determine the phases present in the precursor, calcined and used catalysts. The Brunauer-Emmet-Teller (BET) surface area was calculated for the different promoter loaded catalysts. Fourier transform infrared (FT-IR) spectra, via the KBr pellet method, and attenuated total reflectance (ATR) spectra were recorded to determine the anions present in the bulk and surface of the catalyst respectively. Energy dispersive X-ray (EDX) and inductively couple plasma-atomic emission spectroscopic (ICP-AES) techniques were employed to determine the elemental composition on the surface and in the bulk of the catalyst respectively. Scanning electron microscopic (SEM) images of the catalysts during different stages of their investigation were recorded. The average vanadium oxidation state (AV) in the bulk of the catalyst was determined via a titrimetric method. The catalysts were optimized to a high yield and selectivity of MA. The operating temperature, GHSV and promoter loading on the catalyst were the parameters that were changed during the testing of the catalyst. Different stages of the catalyst's life were characterised via the techniques mentioned above. The catalysts were monitored over a 200-hour period on average, usually taking approximately 24 hours to equilibrate. One such Co promoted catalyst yielded 45 % MA at 275°C and GHSV of 2878 hr^{-1} on equilibration, with an *n*-butane conversion of 73 %, whilst all previously reported VPO catalysts produce far lower MA yields at this temperature.

ACKNOWLEDGEMENTS

I would, at the outset, like to thank my sponsoring company SASOL for the financial support throughout this project, without whom this project would not have taken off the ground. From an academic perspective, thank you to my supervisor, Dr Holger Friedrich, for imparting his knowledge to me as well as for his encouragement and kindness to me through the duration of this project. A special thank you to my mentor Dr Sadesh Sookraj (SASOL R&D) for the academic support and encouragement. Thank you to Dr Thys Botha (SASOL R&D), Dr Matthys Janse van Vuuren (SASOL R & D), Miss Louisa Griesel (SASOL R&D), Dr Klaus Möller (UCT) and Prof. Neil Coville (WITS) for academic and technical advice. Thank you to Prof. B.S. Martincigh and Dr A. Kindness. From a technical perspective I would like to extend a heartfelt thanks to Mr John Swinley (Scientific Group) for information with regard to the on-line GC monitoring system design and Mr Basil Chassoulas (WITS) for technical assistance. My gratitude extends to Prof. A. Spark for sharing his expertise with regard to GC modifications. Thank you to the workshop technician at the University of Natal, Durban, Mr Jodie Couling, for assistance in setting up the reactor, Sastech R&D for performing the XRD and BET analyses and Dr Fiona Graham of the electron microscope unit at the University of Natal for performing the EDX and SEM analyses. The Technical staff at the University of Natal, Durban was invaluable in their support, assistance and efficiency. The efficient staff includes Mrs J. Govender, Mr G. Moodley, Mrs T. Naidoo, Mr R. Suchipersad, Mr S. Peterson, Mrs Z. Sayed-Ally, Mr K. Singh and Mr B. Parel. Thank you to my friends Rivash, Jonathan, Sam, Manuja, Nirad, Vikash and Martin for their support.

The project was very intensive with regard to setting up and networking with the right people. It was hard work at times, yet exciting. I want to thank my spiritual guide for giving me the strength and capability to see the project through. The research and academic skills I have acquired in this project are invaluable.

Thank you to my parents, Bala and Rumba and sister, Preesha, for their love and support throughout this project, which spurred me on through the rough times. Thank you to my aunts, uncles and grandmother for the encouragement. To my grandfather, who is no longer here, whose spirit has been my guiding light.

PUBLICATIONS

The following work from this dissertation has already been presented.

Conference contributions:

1. 'A VPO catalyst for the oxidation of *n*-butane', N. Govender and H.B. Friedrich, *Sasol Technology Symposium*, Rand Afrikaans University, South Africa, 2000.

2. 'A comparative study of VPO catalysts and promoters in the oxidation of *n*-butane', N. Govender and H.B. Friedrich, *35th Convention of the South African Chemical Institute,* Potchefstroom, South Africa, 2000.

3. 'A comparative study of VPO catalysts and promoters in the oxidation of *n*-butane', N. Govender and H.B. Friedrich, *Fifteenth Indian National Symposium on Catalysis and Second Conference of the Indo-Pacific Catalysis Association*, (CATSYMP-15 & IPCAT-2), Pune, India, 2001.

4. 'Oxidation of *n*-butane on a cobalt-promoted vanadyl pyrophosphate catalyst', N. Govender and H.B. Friedrich, *SACI Young Chemists Colloquium*, University of Natal, Pietermaritzburg, 2001.

5. 'Cobalt promoted VPO catalysts in the selective oxidation of *n*-butane to maleic anhydride', N. Govender and H.B. Friedrich, *CATSA/SACI Conference on Catalysis and Inorganic Chemistry*, Pilanesburg, South Africa, 2001.

6. 'Cobalt promoted VPO catalysts in the selective oxidation of *n*-butane', H.B. Friedrich and N. Govender, *4th World congress on oxidation catalysis*, Potsdam, Berlin, Germany, 2001.

DEDICATION

This thesis is dedicated to my loving parents Bala and Rumba and my darling sister Preesha for their undying support. They have been my pillar of strength.

The Three P's of Success: Passion, Persistence and Patience.
-Unknown-

Success is knowing what you're doing, loving what you're doing, and believing what you're doing.
-Napoleon Hill-

ABBREVIATIONS

acac	=	acetylacetonate
ATR	=	attenuated total reflectance
AV	=	average oxidation state of vanadium
BET	=	Brenauer-Emmet-Teller (surface area characterization technique)
EDX	=	electron dispersive X-ray spectroscopy
FID	=	flame ionization detector
FT-IR	=	fourier transform-infrared
GC	=	gas chromatograph
GC-MS	=	gas chromatography-mass spectrometry
GHSV	=	gas hourly space velocity
ICP-AES	=	inductively coupled plasma-atomic emission spectroscopy
lel	=	lower explosive limit
MA	=	maleic anhydride
m.p	=	melting point
NH_3-TPD	=	ammonia-thermoprogrammed desorption
PA	=	phthalic anhydride
PE GC	=	Perkin Elmer GC
ppm	=	parts per million
PRV	=	pressure release valve
TCD	=	thermal conductivity detector
TPR	=	temperature programmed reduction
uel	=	upper explosive limit
VPO	=	vanadium-phosphorous-oxide
XPS	=	X-ray photoelectron spectroscopy
XRD	=	X-ray diffraction

DEFINITIONS AND CALCULATIONS

1. Gas hourly space velocity (GHSV) = $\frac{\text{flowrate (ml.hr}^{-1})}{\text{volume of catalyst bed/ml}}$

2. Specific yield = $\frac{\text{molar yield of species}}{\text{total surface area of catalyst}}$

3. Specific rate = $\frac{\text{rate of reaction}}{\text{total surface area of catalyst}}$

4. Average vanadium oxidation state (AV) = $5 - \frac{\text{(volume } KMnO_4 \text{ solution)}}{\text{(volume } Fe(NH_4)_2(SO_4)_2 \text{ solution)}}$

   This is a titrimetric method employed that is explained in Section 3.5.3.7.

5. Carbon mass balance calculation

   $$n\text{-Butane feed} + O_2 \rightarrow \text{MA} + CO + CO_2 + \text{unreacted } n\text{-butane}$$

   i.e. 4 carbons + 0 carbons → 4 carbons + 1 carbon + 1 carbon + 4 carbons

   carbon mass balance = $\frac{\text{n(products) X 100}}{\text{n(feed)}}$ (n = number of moles)

   $= \frac{[4 \text{ X nMA} + 1 \text{ X nCO} + 1 \text{ X nCO2} + 4 \text{ X n(unreacted } n\text{-butane)}] \text{ X 100}}{4 \text{ X n(}n\text{-butane feed)}}$

6. Percentage conversion of n-butane = $\frac{\text{n(}n\text{-butane reacted) X 100}}{\text{n(}n\text{-butane feed)}}$

7. Percentage selectivity MA = $\frac{4 \text{ X nMA X 100}}{1 \text{ X nCO} + 1 \text{ X n}CO_2 + 4 \text{ X nMA}}$

   The percent selectivity towards CO and CO_2 were calculated in the similar way, with either CO or CO_2 replacing MA in the numerator.

8. Percentage yield MA = $\frac{\text{percentage selectivity MA X percentage conversion of } n\text{-butane}}{100}$

9. Catalyst effectiveness = $\frac{\text{diffusion path of reactant molecule/nm}}{\text{catalyst particle dimension/nm}}$

10. Upper explosive limit (uel): ratio below which gaseous mixture will explode on ignition.

11. Lower explosive limit (lel): ratio above which gaseous mixture will explode on ignition.

CONTENTS

Page No(s).

Page No(s).

Page No(s).

LIST OF FIGURES

Page No(s).

Page No(s).

Page No(s).

LIST OF TABLES

CHAPTER 1

INTRODUCTION

1.1. General: historical background

Maleic anhydride (MA), $C_4H_2O_3$, has the IUPAC name 2,5-furandione. It crystallizes as orthorhombic crystalline needles and is available from producers either as molten liquid or as briquettes. The m.p of MA is 53°C. MA is a strong eye irritant and can cause conjunctivitis and temporary double vision. A material safety data sheet for MA is included in Appendix 1.

MA is important in a large number of chemical processes; unsaturated polyester resins being a major use amongst others such as lube additives, paper reinforcement, agriculture and specialty chemicals (Hodnett, B.K.; (1985)). The polyester resin is formed from the reaction between MA, ethylene glycol and a vinyl monomer. Polyester resins are in turn used in the production of fibreglass composites for boats, cars and other consumable products. Polyester resins are also involved in the construction and electrical industries. MA and maleic acid find use in fragrances. Smaller amounts of MA are used in pesticides and growth inhibitors.

Specialty chemical products from MA include 1,4 butanediol, γ-butyrolactone, tetrahydrofuran, polybutyleneterethalates (PBT), polyurethanes, copolyester elastomers (COPE), pyrrolidones, polytetramethylene ether glycol (PTMEG) and tetrahydrothiophene. These products are used in various engineering plastics, automotive products, solvents for the manufacture of pharmaceuticals, videotapes and specialty fibers. Within Dupont, the principal end use of MA is in the production of PTMEG for which tetrahydrofuran (THF) is a precursor. The main outlet for PTMEG is in the manufacture of Spandex fibres and COPE for products such as Lycra®, Hytrel® and other consumable products (Stadig, W.E. (1992)). The worldwide demand for MA has escalated through the years. An estimated 171 000 tons of MA were produced in 1978. In 1995, the global production of MA had grown to an estimated 900 000 tons, with a value of $700 million. Over the last few years, consumption throughout the world

has increased at an average annual rate of 5.8 %. The forecast has the consumption of MA rising at an annual rate of 3 % in the U.S. and 7-8 % in Asia (Centi, G. *et al.* (2001)). The fastest growth is occurring in Asia, where MA is used as an intermediate for production of 1,4-butanediol. MA derivatives of growing importance are those obtained by hydrogenation such as butanediol and γ-butyrolactone. The main end uses of MA are highlighted in Table 1.1. The percentage indicates what proportion of the MA produced in the region is used in the respective end products.

End uses	Europe, %	North America, %	Japan, %
Unsaturated polyester resins (UPR)	55	51	38
Fumaric and maleic acids	6	7	11
Agricultural chemicals	6	6	-
Additives for oils	5	12	3
Alkydic resins	6	-	-
γ-Butyrolactone	-	-	4
Detergents	6	-	-
Copolymers	-	8	7
Others	16	16	37

Table 1.1. End uses of MA (Centi, G. et al. (2001))

Since 1933, production of MA has been mostly via the selective oxidation of benzene over V_2O_5-MoO_3 catalysts (Fig. 1.1) (Malow, M; (1980)).

As early as 1962 a plant was constructed in the United States for the conversion of *n*-butenes to MA. At that time, however, the process was found not to be economically viable by comparison with the contemporary benzene oxidation process (Malow, M.; (1980)).

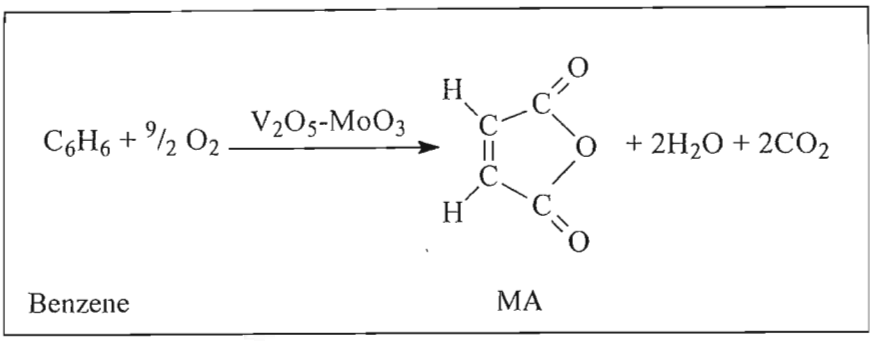

Fig. 1.1. Oxidation of benzene to MA (Hodnett, B.K. (1985))

In the 1970s two developments occurred which tilted the balance of economic advantage in favour of the C_4 process: (i) A substantial price differential developed between benzene and C_4 feedstocks. The differential continued to grow due to scarcity of benzene, caused by its increasing use in unleaded automobile fuels, coupled with generally increasing oil prices. (ii) The introduction of strict controls, particularly in the United States, on benzene emission from MA plants; for new plants these prohibit any detectable benzene emission (De Maio, D.A; (1980)). Benzene has the ability to cause leukemia, a fatal cancer of the white cell producing tissue (Centi, G. *et al.* (2001)). It was as a direct result of these factors that interest intensified in the C_4 partial oxidation route during the 1970s. Vanadium-phosphorous-oxide catalysts (VPO) were found to be best suited for the task, and interest was successively focussed on butadiene, *n*-butenes, and *n*-butane as feedstocks. It was initially generally thought that oxidation of alkane hydrocarbons was difficult, however, now *n*-butane seems to be the most favoured feedstock (Fig. 1.2) (Malow, M.; (1980)). *n*-Butene oxidation produces undesirable by-products including organic salts, which can cause corrosion and problems in separation. *n*-Butane is a more attractive feed than benzene because there is theoretically no carbon loss during its oxidation. In terms of product quality, *n*-butane oxidation is a very clean reaction with minimal formation of by-products (apart from the carbon oxides, only minimal amounts of acetic acid are produced) (Sookraj, S.H. *et al.* (1999)). The catalysts involved in the *n*-butane route were also found to have a longer lifespan than catalysts used in the production of MA using butene. Butene reactivity is higher and there are fewer reaction steps involved in the process, yet, the increased

selectivity and cleaner reaction lead commercial producers to choose *n*-butane as the preferred feed. The flammability limit for *n*-butane is lower than that for benzene, resulting in safer operating conditions.

n-Butane selective oxidation on the VPO catalyst is a much studied reaction in heterogenous catalysis. Monsanto operated the first commercial process starting with *n*-butane in 1974 and

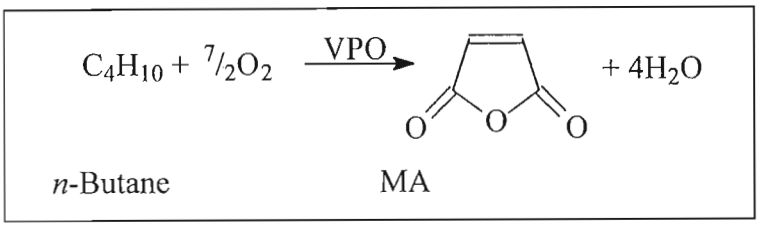

Fig. 1.2. Oxidation of n-butane to MA

the use of *n*-butane in MA synthesis remains the only large-scale commercial partial oxidation process that uses an inexpensive alkane as a direct feedstock (Ebner, J.R. *et al.* (1988)). The reactor technology that has been developed thus far shall be discussed in detail in Chapter 2.

1.2. Background into reaction chemistry

Most of the MA produced worldwide is now obtained by direct catalytic oxidation of *n*-butane on the VPO catalyst surface. The VPO system is highly selective and active and therefore the most effective catalyst. The required catalyst structure for the use of *n*-butane is considerably more complex than the catalyst involved in the benzene process. There are two main synthetic routes for VPO catalysts: the aqueous and the organic route. The catalysts are generally prepared by mixing the vanadium pentoxide with a nearly anhydrous phosphoric acid and an organic solvent for an organic preparation. Concentrated hydrochloric acid and water are used in the aqueous preparation. HCl accomplishes reduction of the V^{5+} starting compound, for aqueous preparation and isobutyl, benzyl, and allyl alcohols for the organic preparations (Busca,

G. *et al.* (1986a)). In both preparations, almost pure vanadyl hydrogen phosphate is obtained, but with different microstructures (Busca, G. *et al.* (1986b)). The vanadyl hydrogen phosphate product is dried and calcined. Once the calcined product is loaded into the reactor, it is conditioned to form the active catalyst by heat treatment over an *n*-butane feed stream. The temperature used in the conditioning varies in different publications and patents. The study of this system has been the subject of extended research, for industrial reasons, due to the economic importance of MA as a chemical intermediate, and for fundamental reasons, as this reaction is very complex, involving a 14 electron oxidation, with 8 H-abstractions, three O-insertions, and subsequent electron transfers (Fig. 1.2). There are numerous publications on the physicochemical aspects of the VPO system (Centi, G *et al.* (2001)), however, few studies have been devoted to kinetics and the mechanism of this reaction. Centi *et al.* (1984) and Pepera *et al.* (1985) have published data on the kinetics and mechanism of this reaction in separate papers. The main reason for little focus being placed on the kinetic and mechanistic aspects of this reaction is that there are many possible reaction pathways and the absence of well-identified intermediates in steady state conditions. It has been suggested that the oxidation of *n*-butane may proceed without intermediate desorption from the active site (Aguero, A. *et al.* (1988)), but through a preliminary dehydrogenation step to butene and subsequent oxidation to MA (Centi, G. *et al.* (1988)). The density of oxidising sites has been considered as a tool for modifying the selectivity in reactions of mild oxidation (McKay, J.; URL; (1999)) and this can be controlled by the catalytic conditions such as *n*-butane/air ratio, temperature of reaction and contact time. There are many discrepancies in the open literature concerning the nature of the active phase. Most of the kinetic studies have been drawn toward the vanadyl pyrophosphate phase, $(VO)_2P_2O_7$, which is considered to be the active phase for *n*-butane to MA oxidation (Centi, G. *et al.* (1984a), Pepera, M.A. *et al.* (1985)). In the former study (Centi, G. *et al.* (1984a)), it was concluded that $(VO)_2P_2O_7$ catalyses the oxidation of *n*-butane to MA via redox reaction of its surface layer according to a Mars and van Krevelen mechanism as illustrated in Fig. 1.3.

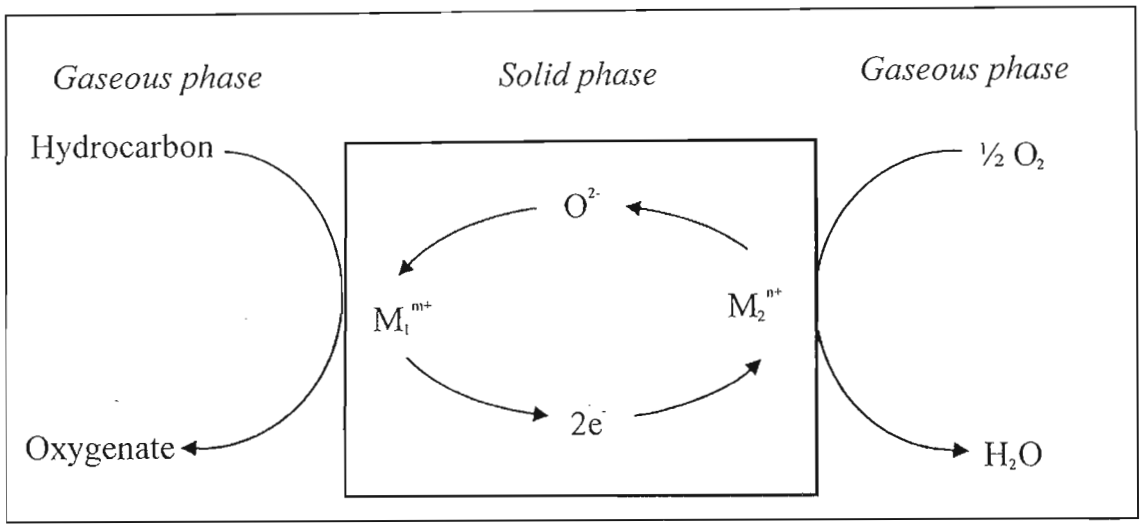

Fig. 1.3. Mars and van Krevelen mechanism (adapted from Mars, P. et al. (1954))

There are three essential properties the catalyst should possess in order to obey a Mars and van Krevelen mechanism: (i) the catalyst should contain a feasible redox couple at the operating temperature, which is possible with transition metal ions; (ii) it should exhibit high electrical conductivity to favour electron transfer and (iii) it should have a high lattice oxygen anion mobility within the material to ensure the reoxidation of the reduced catalyst.

According to this mechanism, the substrate is oxidized by the solid and not directly by molecular oxygen of the gaseous phase. The role of dioxygen is to regenerate or maintain the oxidized state of the catalyst. The oxygen species introduced in the substrate stems from the lattice and is at an oxidation state of –2. The mechanism involves the presence of two distinctive active sites: an active cationic site that oxidizes the substrate and another active site for dioxygen reduction.

V^{4+} at the surface of pyrophosphate is proposed to activate molecular oxygen, while the surface layer can be oxidised to a certain extent to V^{5+}, which provides the capacity to oxidise adsorbed hydrocarbons.

In a former study (Pepera, M.A. *et al.* (1985)), the reactivity of the various oxygen species was examined by thermogravimetric techniques and transient reaction studies. It was shown that intermediates such as butene, butadiene and furan desorb when the $(VO)_2P_2O_7$

catalyst works in more reducing conditions with high hydrocarbon/air ratios, i.e. above the upper explosive limit of 8.5 % (Appendix 1). Furan is readily converted to MA on a partially oxidised surface. These results suggest that there are several active oxygen species involved: activated oxygen, which was suggested to be formed by the irreversible dissociative chemisorption of dioxygen via oxidation of V^{4+} to surface V^{5+}, was considered to be responsible for the oxidation of the C-H bonds of *n*-butane and furan, while a surface lattice oxygen anion should be responsible for allyl oxidation and ring insertion (Pepera, M.A. *et al.* (1985)).

Although, in all industrial processes, a vanadyl pyrophosphate-base catalyst is used in the conversion of *n*-butane to MA, its specific characteristics in terms of nature and quantity of the promoters, method of preparation and textural/mechanical properties, shape and characteristics of the pellets (and additives to obtain the required properties) and procedures of catalyst activation and regeneration are different for the various processes. As a consequence of all these variables, the various processes perform quite differently in terms of selectivity and productivity, even though all of them use the same type of catalytic active phase.

Compared to other industrially practiced hydrocarbon selective oxidation reactions, MA production is the most complex (Centi, G. *et al.* (1984b)). It is the only example of an industrially practiced selective oxidation reaction involving alkane activation (Birkeland, K.E. *et al.* (1997)).

Dehydrogenation reactions are reversible due to the hydrogen evolved, and the alkane conversion is limited by thermodynamic equilibrium. In order to shift it towards the formation of dehydrogenation products, the reactions are carried out at relatively high temperatures (400-500°C). At these temperatures, however, cracking of hydrocarbons to coke occur, reducing the selectivity of the reaction. The coke deposition causes a decrease in catalyst activity and the need for frequent regeneration. One of the more difficult technological problems to be solved is the necessity to provide high temperatures, which usually makes the process energy and capital intensive. Many of the obstacles can be overcome by providing the heat necessary for the reaction via *in situ* oxidation of hydrogen evolved as a product of pure dehydrogenation. The

reaction, therefore, becomes exothermic and able to proceed at much lower temperatures, at which formation of carbon and cracking products is insignificant (Mamedov, E.A. *et al.* (1995)). A further advantage is that the conversion is no longer limited by thermodynamic factors. Molecular oxygen is the most attractive reactant for industrial purposes because of its low cost and less severe environmental impacts. Dioxygen can react directly with the hydrocarbon molecule on the catalyst surface yielding the products of oxidative dehydrogenation. The aim is to develop a catalyst capable of activating only the C-H bonds of the alkane molecule in a flow of oxygen. This problem becomes one of global importance in the light of expectation that the petrochemical industry will in the future be based on the direct use of alkanes as raw materials instead of alkenes (Sookraj, S.H., Engelbrecht, D.; (1999)). A number of investigations relating catalyst structure to catalytic activity and selectivity, and comparing one system with another, have appeared in the literature. The literature also shows the catalyst phase composition or/and structure being controlled, to a large degree, by the preparation method. For supported catalysts, the nature of the support becomes one more variable in determining the final catalytic properties.

1.3. Catalyst models

Heterogeneous catalysis is a science at the interface of different areas of chemistry and engineering. Each new development stems from applications of concepts from these different areas. A heterogeneous catalytic system should be, in fact, correctly regarded as a three phase system: a gas phase, a solid phase and a two-dimensional surface region at the gas-solid interface composed of the surface solid phases and interacting adsorbed molecules (Centi, G. *et al.* (1985)). The structure and properties of this surface region may be modified either by changing the composition of the gas phase or by altering the properties of the solid catalyst.

The VPO system is characterised by the facile formation of a number of crystalline phases, in the V^{4+} and V^{5+} oxidation states. In hydrated $VOPO_4$, the layer lattice is built up of neutral $VOPO_4$ layers and interlayer water molecules. The V atom lies on a fourfold axis and is

surrounded by six oxygen atoms to give a distorted octahedron. The four equitorial oxygens are provided by four different phosphate tetrahedra. One of the axial vanadium-oxygen bond distances is very short, corresponding to a vanadium-oxygen double bond (V=O). The structure of α-$VOPO_4$ is composed of chains of highly distorted VO_6 octahedra sharing four oxygen atoms with four different PO_4 groups (Centi, G. *et al.* (1988)). These groups are arranged to form layers. This is discussed further in the next section. A description of the catalyst phases present in the VPO catalyst appear in Appendix 1.

The two main effects observed in the preparation of the $VOHPO_4 \cdot {}^1/_2H_2O$ catalyst precursor may be, in fact, strictly connected to intercalation properties. Firstly, non-stoichiometry is easily accommodated as evidenced by the preparation of compounds with 0.9-1.2 P:V atomic ratios without any apparent modification of structural and morphological properties (Centi, G. *et al.* (1985)). Secondly, the preparation conditions have a pronounced effect on the microstructure (Centi, G. *et al.* (1985), Cavani, F. *et al.* (1985a)), i.e. on the morphology, solid-state reactivity, and the presence of disorder in the stacking fold of crystalline planes of its layered structure. The layers of vanadyl hydrogen phosphate ((010) planes) are interconnected in a three dimensional structure by weak H bonding of phosphates and water molecules. The organic alcohol, which was added as a solvent and reducing agent only in the organic synthetic route, competes with this effect, reducing the bonding between the planes and allowing the formation of crystals in which these (010) planes are predominantly exposed, revealing a platelike morphology (Wenig, R.W. *et al.* (1986), Johnson, J.W. *et al.* (1984)). This effect, in addition to the increase in surface area (Cavani, F. *et al.* (1984)), modifies the surface properties due to a change in the relative ratio of crystalline planes at the surface. The alcohol can also remain intercalated between layers (Busca, G. *et al.* (1986a)). This effect induces some local modification of the vanadyl hydrogen phosphate structure, which can strongly modify its solid-state reactivity (Busca, G. *et al.* (1986a)).

Because the VPO system is characterised by the facile formation of a number of crystalline phases, the structure of the active phase must be discussed in terms of factors such as

the method of preparation of the precursor (type of reagents, reducing agents and aliphatic or aromatic solvents (Horowitz, H.S. *et al.* (1988), Cornaglia, L. *et al.* (1993)), temperature, use of dry or wet milling), oxidation state, P:V ratio (Horowitz, H.S. *et al.* (1988)), the use of additives, removal of excess P by washing, activation and conditioning procedure for the precursor at high temperature and crystal phase transformations under reactant atmosphere such as reduction time, temperature and amount of water. The various crystal phases can interconvert as a function of the reducing or oxidising properties of the reactants, the time on stream and the reaction temperature (Bordes, E. *et al.* (1985), Bordes, E. *et al.* (1979)). Fig. 1.4 indicates the structural changes and interconversion of VPO phases during the activation of $(VO)HPO_4 \cdot 1/_2H_2O$ (Cavani, F. *et al.* (1996)).

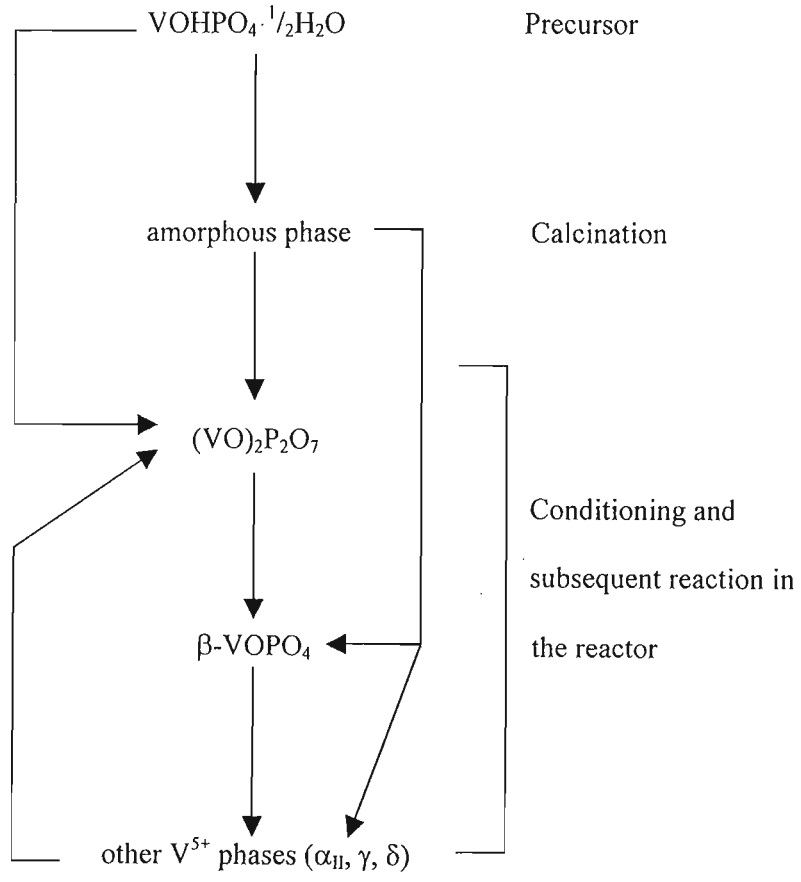

Fig. 1.4. Interconversion of the VPO phases from precursor stage through to activated stage in the reactor

The orthophosphate ($VOPO_4$) phases are transformed to $(VO)_2P_2O_7$ by reaction with the hydrocarbon mixture. This transformation involves two water-loss steps, the first associated with water of crystallization and the second with the transformation of hydrogen phosphate to pyrophosphate. The two transformations can occur simultaneously or consecutively, depending on the nature of the precursor phase and the heat treatment (Cavani, F. *et al.* (1985b)). When oxygen is present in the atmosphere, there is also oxidation, leading to various possible V^{5+} phases (α_I, α_{II}, β, γ, δ), again depending on both the nature of the precursor phase and the conditions of the heat treatment. Thus there is a broad range of possibilities in terms of catalyst composition after the heat treatment or the calcination step, with identification of some of the phases, being amorphous or well dispersed on the vanadyl pyrophosphate phase, being difficult. Many of the studies on the structure-activity and selectivity relationships on VPO catalysts have focused on identification of the different phases present in the catalyst after this heat treatment, with the aim of correlating the types and amounts of phases present to the catalytic behaviour and thus identifying the active phase/s. There are different VPO phases, with V in the +5, +4 and +3 oxidation state for which structures have been resolved (Bordes, E.; (1987)). The V^{5+} phases are hydrated {$VOPO_4 \cdot {}^1/_2H_2O$, $VOPO_4 \cdot 2H_2O$} or dehydrated phosphates {α_I-, α_{II}-, β-, γ-, δ-$VOPO_4$} (Bordes, E.; (1987)). The V^{4+} phases are hydrogen phosphates {$VOHPO_4 \cdot {}^1/_2H_2O$ (Torardi, C.C. *et al.* (1984)), $VOHPO_4 \cdot 4H_2O$ (Johnson, J.W. *et al.* (1984)) and $VO(H_2PO_4)_2$ (Bordes, E.; (1987))}, pyrophosphate {$(VO)_2P_2O_7$} and metaphosphate {$VO(PO_3)_2$} (Bordes, E.; (1987)). The V^{3+} phases are VPO_4 (Bordes, E.; (1987)) and $V(PO_3)_3$ (Tofield, B.C. *et al.* (1975)). A description of the phases appears in Appendix 1.

The transformation of V^{4+} and V^{5+} phases into vanadyl pyrophosphate is an important step in forming active catalysts. By thermal treatment at ca. 400°C, the $VOHPO_4 \cdot {}^1/_2H_2O$ dehydrates to $(VO)_2P_2O_7$.

Wenig and Schrader (Wenig, R.W. *et al.* (1986)) claim that only $(VO)_2P_2O_7$ is the active and selective phase in *n*-butane oxidation to MA. VPO catalysts are composed of binary oxides.

When P is present in excess of the stoichiometric ratio, the catalysts become resistant to oxidation (Hodnett, B.K. (1985)). They can operate during catalytic work with most of the V in the +4 oxidation state, even in oxygen rich feeds.

1.4. An idealized model for the orthorhombic structure of vanadyl pyrophosphate

VPO systems have a complex, yet fascinating structural chemistry. $(VO)_2P_2O_7$ exhibits exceptional selectivity in the 14-electron oxidation of *n*-butane to maleic anhydride (Centi, G. *et al.* (1988)). The catalytic performance of this phase was shown to be correlated with crystal morphology and size, and is strongly influenced by the presence of non-stoichiometric P and variations in the bulk oxidation state of V (Cornaglia, L.M. *et al.* (1991)). In order to fully understand the structure/performance dependance of this system and the mechanistics of site isolation at the active/selective surfaces parallel to the basal (100) plane (Fig. 1.5), a thorough investigation of the crystallography and variation in the structure of vanadyl pyrophosphate has been necessary.

A molecular description of the surface structure and surface chemistry of vanadyl pyrophosphate requires an acceptable crystallographic model of the bulk. Unfortunately, a great deal of confusion has surrounded attempts to determine the structure of this material. For example, crystals and crystallites of vanadyl pyrophosphate have been observed to have defects. The nature of these defects can cause severe problems with the refinement of the crystallographic models in single crystal X-ray diffraction studies and this has resulted in lack of confidence in previous structural assignments. Other points of confusion revolve around the fact that vanadyl pyrophosphate catalysts are known to exhibit a structure sensitivity related to the method of preparation (Cavani, F. *et al.* (1985a)) and that differences in catalytic performance are likely due both to the modification of crystal morphology as well as structure.

The solid-state dehydration reaction, which transforms the vanadyl hydrogen phosphate hemisolvate precursor into the vanadyl pyrophosphate product, has been reported to be topotactic (Bordes, E. *et al.* (1979)), with an amorphous intermediate phase required to

complete the transformation. Based on symmetry arguments alone, it is clear that this reaction cannot proceed as simple topotaxy of the published crystal structures of $VOHPO_4 \cdot {}^1/_2H_2O$ and $(VO)_2P_2O_7$. $VOHPO_4 \cdot {}^1/_2H_2O$ and $(VO)_2P_2O_7$ are representative of the precursor and product, respectively. The point group symmetry around the face-shared vanadyl dimeric unit in the precursor is C_{2V}, while that of the edge-shared dimer in the vanadyl pyrophosphate product is C_1. It is apparent that there is a considerable reorganization of structure as the catalyst precursors pass through an amorphous intermediate phase during calcination and, after conditioning in the presence of the feedstream in the reactor, yield the catalytically active $(VO)_2P_2O_7$ phase (Thompson, M.R. *et al.*(1994)).

Large single crystals of vanadyl pyrophosphate vary in colour (either emerald-green or red-brown) and possess subtle structural differences due to variation in the symmetry of the V atom sites within the asymmetric unit (Thompson, M.R. *et al.* (1994)). No variation in P atom positions are indicated in the single crystals, however, there is evidence of P disorder in catalyst powders.

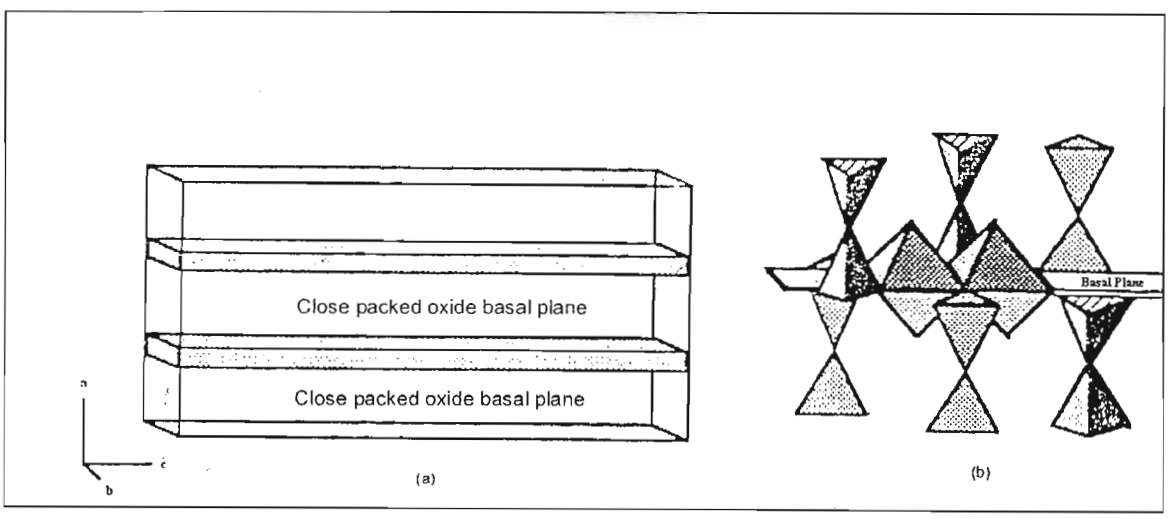

Fig. 1.5. (a) The close-packed oxygen basal planes for the unit cell of vanadyl pyrophosphate. (b) The relationship between the coordination spheres of vanadium (octahedra) and phosphorous (tetrahedra)

The crystal structure of vanadyl pyrophosphate contains two close-packed layers of oxygen atoms that lie parallel to the bc plane at approximately ¼ and ¾ along the a-axis as illustrated in Fig. 1.5.

These layering planes are made up entirely of the basal oxygens of V octahedra and pyrophosphate tetrahedra (Fig.1.5. (b)). The close-packed pattern for the basal-plane and the relative positions of the V and P sites in the octahedral and tetrahedral interstices are illustrated in Fig. 1.6. The refinement of the crystallographic model indicates a degree of non-planarity and distortion of the oxygen basal plane. These distortions are minor.

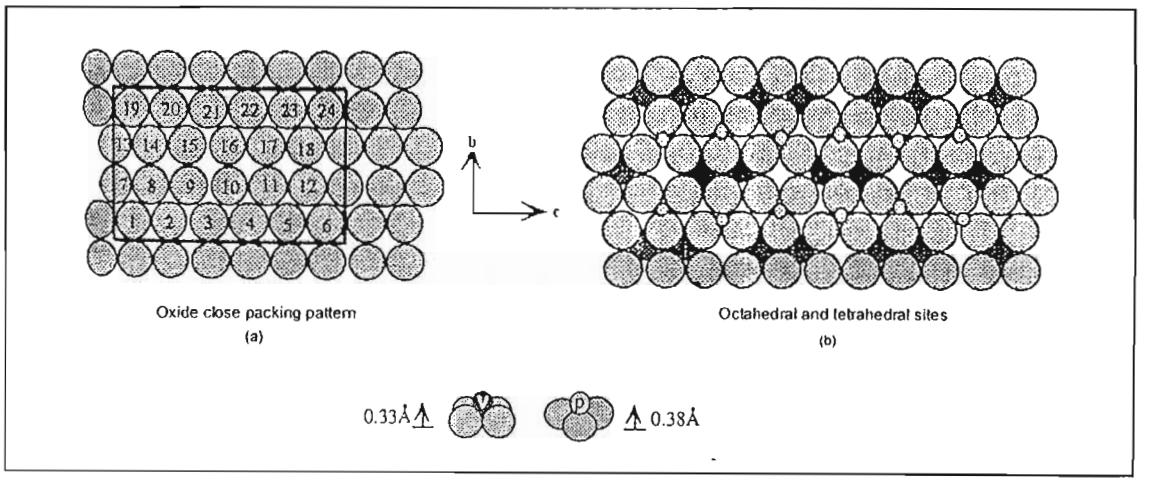

Fig. 1.6. (a) Basal oxygen close-packing pattern. (b) Location of the octahedral and tetrahedral interstices (Thompson, M.R. et al. (1994))

The V octahedra are square-pyramidally distorted. The V atoms lie approximately 0.33 Å out of the basal plane oriented toward the vanadyl oxygen, i.e. V=O. The P atoms lie approximately 0.38 Å out of the basal plane. Fig. 1.7 (a) illustrates the coordination geometry about the V atoms, and Fig. 1.7 (b) the geometry for the P atoms, each idealized from experimental models.

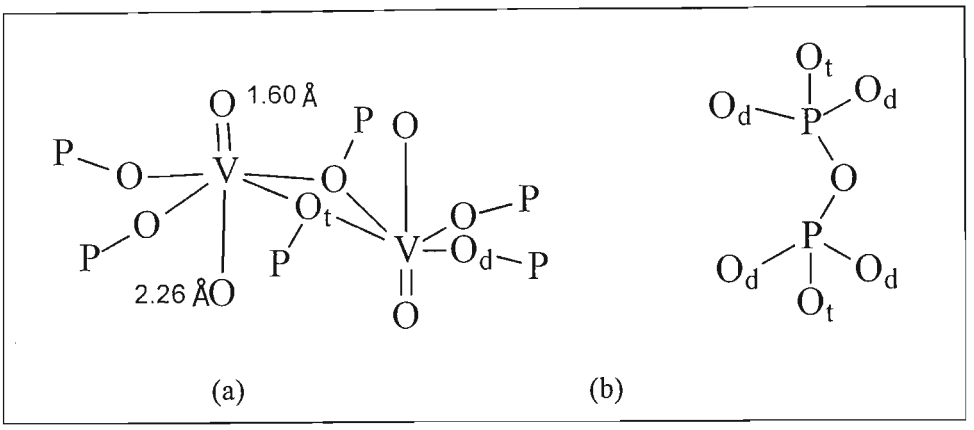

Fig. 1.7. (a) The vanadium coordination sphere and (b) the phosphorous atoms in the idealized model of vanadyl pyrophosphate. Subscripted oxygen atoms represent double-bridged positions (O_d) and triple-bridged positions (O_t)

Four classes of oxygen atoms exist within the structure: double bridging oxygen, triple bridging oxygen, vanadyl oxygen (V=O) and pyrophosphate oxygen (P-O-P). The double- and triple-bridging oxygens lie in the basal plane. The other vanadyl oxygens lie within the unit cell. It is important to note that the positions of the vanadyl oxygens are invariant to the direction of the vanadyl bond. The directional sense of the vanadyl column relative to the a-axis is determined by the position of the V ions in that column (Fig. 1.5 (b)). Two positions are possible for each V atom: above or below the basal plane. If the V atoms lie above the basal planes at ¼, the direction of the vanadyl column will be aligned with the direction of the a-axis, and if they lie below these planes at ¾, then the direction of the column will be anti-parallel to a. Within every vanadyl column, one V atom will be positioned between any two basal planes of the structure. Similar to the situation for the V atoms, the P atoms can lie above or below the planes at ¼ and ¾ on the a-axis. However, both P atoms of an individual pyrophosphate group must lie between two adjacent basal layers. Therefore a column vacancy will occur in every other layer. There are eight pyrophosphate columns within the unit cell, each of which possess two possible orientations. In summary there are 104 atoms contained within the unit cell of

vanadyl pyrophosphate: 48 basal oxygen atoms, 16 vanadyl oxygen atoms, 16 V atoms (8 pairs) and 8 pyrophosphates (24 atoms).

The XRD patterns of vanadyl pyrophosphate catalysts exhibit significant differences when compared with the diffracted intensities from the single crystals. The most probable explanation is that there is a significant amount of variation in the structure of the vanadyl pyrophosphate in the microcrystalline catalysts (Thompson, M.R. *et al.* (1994)). The structures of the single crystals are only two of a great number of possible polytypes for vanadyl pyrophosphate. For the observed cell volume, there are 8 columns of vanadyl groups each possessing two possible orientations and 8 columns of pyrophosphates each with two possible orientations, yielding 2^{16} (65 536) variations.

The idealized model of vanadyl pyrophosphate has been presented here primarily to illustrate the point that there are many conceivable variations in the structure of this material. There does not seem to be a simple symmetry preserving mechanistic path between vanadyl hydrogen phosphate and the structures of the emerald-green and red-brown crystal, and therefore, we should not be surprised that an amorphous intermediate phase results during the preparation of the catalyst. Theoretical results point to the fact that the experimental structures may be representative of the most thermodynamically favorable structures for this material (i.e. lowest crystal energy). There is a common misconception that the bulk structure of the vanadyl pyrophosphate is characterized as a compact solid oxide. Consideration of the symmetry of the vanadyl and pyrophosphate building blocks more appropriately leads to a description of the bulk as a material with a series of interlayer vacancies or pores. One hypothesis is that the surface topology parallel to the (100) plane in vanadyl pyrophosphate must possess three-dimensional character (Centi, G., Trifirò, F.; (1988)). This stems from the fact that these surfaces cut across bulk vacancies. If vanadyl pyrophosphate can exhibit variations in its bulk structure, then the sizes and the symmetries of these vacancies at the surface termination would likewise be expected to be variable.

1.5. Influence of reducing agent and solvent

Hydrochloric acid and water are the two most widely used reducing agents and solvents for preparations of VPO catalysts via the aqueous method. Alcohol solvents such as ethanol, benzyl alcohol, *iso*-butanol and allyl alcohol are used as reducing agents and solvents for the organic preparations of the catalyst. Conversion, yield or selectivity, always expressed in molar terms, observed at a given temperature or at the temperature required to obtain a given conversion are the parameters usually compared between catalysts. An important characteristic of VPO is the oxidation state of the V ions. Usually a mixture of +5, +4 and +3 oxidation states is present. Values for the average V oxidation state (AV) between +4 and +5 are common. The redox level of these catalysts is conveniently expressed in terms of the AV, which is usually slightly greater than +4.

A study revealed that catalysts prepared using HCl as a reducing agent are typically activated in air at 100°C higher than catalysts where *iso*-butanol or allyl alcohol acted as a combined solvent and reducing agent (U.S. Patent (1982), U.S. Patent (1981)). Since most VPO in this particular study operated at similar AV values, this finding implies that the former catalysts were more highly reduced before activation. The strength of the reducing agent determines the initial AV of the precursor and plays a role in determining the temperature at which the catalyst must be activated. The use of organic solvents can lead to increased surface areas but improved catalytic performance does not always follow. The nature of the solvent and the temperature at which the precursor is isolated by filtration can influence the final phase composition of the catalyst. The preparation chemistry of this phase is thus very complex. Indeed, with *iso*-butanol, non-agglomerated platelets (rosette morphology) form with preferential exposure of the basal (001) plane (Horowitz, H.S. *et al.* (1988)), whereas using secondary or tertiary butyl alcohol, well-formed non-agglomerated platelets form. With benzyl alcohol, platelets with stacking faults form with the alcohol trapped between the layers (Cavani, F. *et al.* (1985a)). Miyake and Doi (Miyake, T. *et al.* (1997)) showed that the morphology of the catalyst precursor changes with the use of different alcohols in a comparative study. They also

showed that selective synthesis of MA is related to exposed face of the catalyst and that catalyst activity is related to surface area.

1.6. Influence of P:V ratio

The P:V ratio is a crucial factor in determining the final characteristics of VPO catalysts. Influences of this can be conveniently classified as follows:

1. Influence on redox properties, i.e. the reducibility of the catalyst by hydrogen or hydrocarbons and oxidizability by oxygen.
2. Influence on the phase composition of crystalline catalysts.
3. Influence on the distribution of V oxidation states in amorphous or poorly crystalline catalysts.

Each of these classifications is considered below.

Determination of the P:V ratio must be taken into consideration, whether the precursor is isolated by evaporation of the solvent or the precursor is precipitated.

A slight excess of P in the catalyst, i.e. a molar P:V ratio greater than 1 is necessary to stabilise the active phase. It is generally accepted that P above the stoichiometric amount stabilises the V^{4+} valence state and limits its oxidation (Hodnett, B.K.; (1985), Haber, J.; (1984)). The P:V ratio is a key parameter in determining catalysts selectivity and activity according to Wenig *et al.* (1986). Selectivity towards MA increases with catalyst P loading, whereas specific activity of both selective and non-selective oxidation decreases on increase of P content in the 0.9 – 1.2 P:V range. Buchanan and Sunderasen (Buchanan, J.S. *et al.* (1986)), in an extensive kinetics study, found that a catalyst with a P:V ratio of 1.0 was approximately twice as active as a catalyst with a P:V ratio of 1.1, while selectivities to MA were similar. It can thus generally be stated that a good VPO catalyst has a P:V ratio of about 1 (Trifirò, F.; (1993)). Bither (1984) showed that the MA decomposition rate increases at P:V ratios less than 1, which results in reduced selectivity. Bither (1984) also showed that a slight excess of P (P:V ratio = 1 to 1.2) with one or some of promoters such as In, U, Zn, Sb, Ta and Si, etc. is advantageous. Despite

the extensive use of promoters in patent literature, fundamental studies on the effect of promoters have been very limited.

Ai (1970) showed from earlier work in this field that adding P to vanadium-oxide catalysts lowers the overall activity but increases the selectivity towards MA formation from C4 feedstocks. Study of this effect indicated that when P was present at a P:V ratio close to or in excess of unity, the +4 oxidation state of V was stabilised even during high temperature calcination in air, i.e. temperatures exceeding 400°C (Nakamura, K. *et al.* (1974), Poli, G. *et al.* (1981)). It was also reported that when calcination is carried out below 380°C, excess P remains on the surface as PO_4^{3-}; above this temperature P enters the solid to stabilise the +4 oxidation state by solid-state reaction (Poli, G. *et al.* (1981)). Centi *et al.* (1988) showed that this high P:V ratio hinders the oxidation of V^{4+} in vanadyl pyrophosphate. The reactivity of near surface regions to reduction by hydrogen or re-oxidation by oxygen of catalysts calcined at 500°C was essentially independent of the P:V ratio but depended strongly upon the surface area. However, the reactivity of the bulk of these catalysts was found to be strongly dependent on the P:V ratio, and a slight excess of P strongly inhibited the mobility of lattice oxygen through the bulk. The fact that oxidation can proceed rapidly in near surface regions may result in an uneven distribution of oxidation states between the surface and the bulk.

Reducibility of V^{5+} to V^{4+} (or the inverse reaction) is not the only important parameter of catalyst behaviour; the V^{4+} to V^{3+} reducibility is significant as well, although this aspect has often not been properly considered. The formation of V^{3+} was observed during the catalytic reaction and the amount of V^{3+} depended on the feed composition and thus changed along the axial direction of the fixed-bed reactor (Centi, G. *et al.* (1988)). A change in redox properties not only changes the surface structure and P:V surface ratio, but also the intrinsic nature of the catalyst surface during the catalytic reaction as well as the possibilities of its dynamic *in operandi* restructuring.

Several studies have shown that the P:V parameter can have an overriding influence on the AV, hence on the phase composition of VPO catalysts. In general, well-crystallised

materials can be obtained from this system after thermal treatment at or above 450°C in simple oxidising or inert atmospheres. Some phases which have been detected for VPO catalysts are α-$VOPO_4$, β-$VOPO_4$, $(VO)_2P_2O_7$, $VPO_5 \cdot 2H_2O$, $VO(PO_3)_2$ and $VO(H_2PO_4)_2$. Amorphous precursors were obtained for P:V ratios between 0.95-1.07:1 and employing an organic synthetic route, whilst crystalline precursors were obtained for HCl reduction, via an aqueous method of catalyst synthesis (Hodnett, B.K.; (1985)).

When calcination of the organic prepared catalysts were carried out at 500°C, crystalline β-$VOPO_4$ developed very quickly for P:V ratios of less than unity. When the molar P:V ratio was greater than unity, a V^{4+}-containing phase labelled β* developed initially and then transformed slowly into β-$VOPO_4$. As the molar P:V ratio was increased from 1.03:1 to 1.10:1, the β*-phase became more stable against oxidation to β-$VOPO_4$ (Hodnett, B.K. (1985)). A description of the phases appears in Appendix 1.

A suitable choice of molar P:V ratio can play a pivotal role in the final redox state attained by VPO catalysts during steady-state working conditions. P in excess of the P:V = 1.1 ratio reduces the reactivity of the bulk of the materials. This ratio is primordial in determining the phase composition of relatively well-crystallised catalysts. However, for poorly crystalline or amorphous catalysts activated or calcined at low temperatures, viz. below 400°C, the P:V ratio, in combination with the reducing agent used, determines the distribution of V and P ions within the bulk of these catalysts.

1.7. Activation of the VPO catalyst

As outlined earlier (Section 1.5.), the reducing agent plays an important role in establishing the initial AV of the VPO catalyst at the stage of isolation of the solid precursor. Suitable choice of P:V ratio can stabilize this parameter during thermal treatments. However, the efficacy of this stabilization depends upon the conditions, notably the temperature and atmosphere during activation or catalytic testing. The activation procedure leads to a decrease in

the rate of *n*-butane over-oxidation and a significant increase in selectivity. Deactivation of the catalyst, on the other hand, results in over-oxidation products, viz. CO and CO_2.

Low temperature activation procedures result in poorly crystalline or amorphous VPO catalysts. The catalyst is usually calcined in an oxygen-free atmosphere at temperatures higher than 400°C, followed by introduction of the *n*-butane in air reactant mixture. In this procedure, pure crystalline vanadyl pyrophosphate is formed after the calcination step, and then, after addition of the reaction mixture, partial oxidation may occur (Horowitz, H.S. *et al.* (1988)).

1.7.1. Activation in air

Catalysts prepared by HCl reduction with a P:V ratio close to unity and calcined by slowly heating in air to 380°C consisted of an amorphous pyrophosphate and a V^{5+}-containing phosphate, which was described as a form of α-$VOPO_4$ modified by the presence of V^{4+} ions between its layer structure; subsequent calcination at 500°C led to the formation of β-$VOPO_4$.

For catalysts with P:V > 1.1 and calcined slowly, the precursor, hydrated pyrophosphate $\{(VO)_2P_2O_7 \cdot 2H_2O\}$, decomposed below 380°C to form an amorphous pyrophosphate; at 380°C a mixture of non-crystalline α-$VOPO_4$ and β-$VOPO_4$ formed, and these two constituents were again observed after further calcination to 500°C. By contrast, rapid approach to a calcination temperature of 500°C produced β-$VOPO_4$ and a crystalline V^{4+} phosphate. It was reported that rapid approach to the final calcination temperature prevented a reaction between amorphous pyrophosphate and excess P (to form the β-phase), but favoured the formation of the new V^{4+} phosphate (Poli, G. *et al.* (1981)). On calcination, the surface area of the calcined catalyst is greater than that of the precursor.

1.7.2. Activation in hydrocarbon-air mixtures

During testing of catalysts in *n*-butane-air flow at 500°C, the pre-reduced catalysts attained steady state activities much faster and these were also more active and selective. It was

established that the pre-reduced catalysts oxidised considerably under the test conditions, whereas the calcined analogs were found to become slightly reduced (Hodnett, B.K. (1985)).

It is clear from this that VPO catalysts, even with excess P, can respond to some extent to the redox potential of their environment. However, in the normal operating temperature range of these catalysts (350-450°C), AV values always stabilise in the range +4 to +4.5 for *n*-butane/air mixtures below the explosive limit. It is also clear that the slow approach to the ultimate temperature at which calcination in air or activation in hydrocarbon-air mixtures is carried out can lead to catalysts with different phase compositions compared to catalysts calcined with a rapid approach to the ultimate temperature. The AV values obtained by pre-reducing the catalyst precursor in a hydrocarbon/air mixture are similar to those obtained by catalysts calcined with a rapid approach to the ultimate temperature. Non-equilibrated solids cannot be used to interpret the behaviour of equilibrated catalysts as temperature and time on stream play a vital role in the activation and subsequent selectivity as well as yields (Cornaglia, L.M. *et al.* (1999)).

1.8. Promoted vanadium-phosphorous-oxide catalysts

According to Hutchings (1991), dopants for VPO catalysts can be classified into two main groups:

(i) those that promote the formation of the required VPO phase or avoid the formation of spurious phases.

(ii) those that form solid solutions with the active phase and regulate the catalytic activity.

Addition of these ions can interact with free phosphoric acid as a means of fine-tuning the optimum surface P:V ratio and acidity. Examples are basic ions such as Zn^{2+} that also act to prevent the migration and loss of P. Certain ions can substitute for P in the precursor, such as Si^{4+} and S^{6+}. The partial or total elimination of these ions by calcination from the vanadyl pyrophosphate structure influences the morphology and leads to defects in the $(VO)_2P_2O_7$

structure. Addition of elements that substitute for V can act as modifiers of the reactivity, forming stable solid solutions. Ti, Zr, Ce and Mo fall into this last category.

Numerous attempts have been made to synthesise improved VPO catalysts by adding various amounts of other metallic elements. Although reports of some of these attempts have appeared in the open literature, the vast majorities are found in the form of patents (Hodnett, B.K.; (1985)).

Promoters are introduced by one of the following three methods: by (i) dissolution with the V component before or during reduction or co-precipitation with the final catalyst; (ii) mixing into a solution containing both the V and P components and co-precipitation to form the final catalyst and (iii) impregnation into the solid precursor before calcination and subsequent activation (Hodnett, B.K.; (1985)).

An interesting development relates to MoO_3 promoted catalysts with *n*-butane/oxygen feed gases featuring hydrocarbon compositions above the explosive limit (Higgins, R. *et al.* (1982). In this case MoO_3 was added as a promoter. Higher selectivities resulted as compared to the unpromoted catalyst. The feed gas composition influenced the promoter effect. The promoter shifts the hydrocarbon/air composition from which optimal AV values result. The AV value governs the MA selectivity as discussed in Section 1.2. The P:V ratio is another factor that can be expected to have similar effects as the MoO_3 promoter, with P acting as a promoter. However, it is not fully understood how promotional effects influence or are influenced by the P:V ratio. The question remains open as to whether promoters are effective in catalysts that comprise largely V^{4+} or whether promotional effects would also be observed for VPO catalysts with V in its +5 oxidation state.

Promotional effects in VPO catalysts are many and varied but little understood. In a general way they may be classified into two groups: (i) where the promoter is added to the bulk of the catalyst and (ii) cases where the promoter is added in such a way as to favour its location at the surface. Several studies have concluded that the way in which the promoters are added is of crucial importance. It appears that an optimal promoter:V ratio can be identified for several

series of catalysts; this ratio in turn seems to depend upon the P:V ratio of the catalysts. Little is known about the solubility of promoters in VPO catalysts, but it has been hypothesised that optimum promoter:V ratios represent compositions beyond which further addition would lead to surface segregation of some promoters, which in their oxidised forms, are highly active in total oxidation. By contrast, certain promoters such as Mn, Co, Sn, Fe, Cu, Li, Zn, Ce and Ni seem to act exclusively upon the surface properties of these catalysts (Hodnett, B.K.; (1985)).

1.8.1. Cobalt as a promoter for *n*-butane oxidation over a VPO catalyst

Metal dopants can greatly affect the performance of a catalyst. The addition of promoters can readily induce both structural as well as electronic changes to the bulk of the catalysts. Catalysts with modifying elements whose ions possess an incomplete outer electron shell exhibit higher selectivity and yields of MA than those in which the introduced ions possess a complete outer electron shell (Brutovsky, M. et al. (1982)). Co contains an incomplete outer electron shell. Even authors who used the same method of catalyst preparation, expressed conflicting views on the influence of the same dopant element in *n*-butane oxidation, e.g. different results were published as to the role of Co: it worsens the properties of the basic composition (Young, L.B. Fr. Patent (1974)), exerts a positive influence (Katsumoto, K. *et al.* (1980)), or does not affect properties of the VPO catalyst (McDermott, J. GB Patent (1979)).

The form in which the dopant is present in the VPO catalyst, determines its influence on catalytic properties. Metal additions can be present in the VPO catalyst in four types of phases: (i) metallic, (ii) metal oxide, (iii) metal phosphate and (iv) bi-metal phosphate. It is well known, in the case of alkaline-earth metal additions, that there is bi-metal phosphate formation. Transition metal addition, such as Co, may form bi-metal phosphates as well, such as $CoVOP_2O_7$ and $CoVOPO_4$ (Lozano-Calero, D. (1993)). Several studies have concluded that the way in which promoters are added is of crucial importance. It must be noted that the "pure" VPO system is already promoted since the P:V ratio employed in all industrial catalysts exceeds unity and cannot be claimed to be a simple single-phase system. According to these data, metal

ions are distributed in empty channels of pyrophosphate or orthophosphate networks. The binding energy of Co $2p_{3/2}$ electrons is 2-3 eV higher than expected for Co in oxide systems (Wagner, C.D. *et al.* (1979)). Such a large shift can be related to a state of high dispersion and/or to strong interactions between Co and other atoms in the VPO matrix. The low concentration and high dispersion of these bi-metal phosphate units in the basic framework of the $(VO)_2P_2O_7$ does not allow detection by X-ray phase analysis (Zazhigalov, V.A. *et al.* (1996)). A temperature programmed reduction (TPR) experiment can be done to determine the types of Co interactions and/or phases in the catalyst. Characteristic peaks of Co oxides are exhibited with the Co doped catalyst. The TPR profile of the equilibrated catalysts is different from non-equilibrated catalysts in that there are peaks at much higher temperatures in the equilibrated catalysts (ca. 1000 K), symptomatic of the presence of less reducible Co-containing species. The non-equilibrated catalyst refers to the catalyst precursor that has been calcined and the equilibrated catalyst refers to the calcined catalyst that has been conditioned in the reactor.

There is higher scattering of Co in the bulk of the equilibrated catalyst as compared with the non-equilibrated catalyst. Co addition leads to P enrichment on the surface of the catalyst precursor, which is less significant in the equilibrated and non-equilibrated catalyst (Cornaglia, L.M. *et al.* (1999)). The catalyst tested above was prepared via a benzyl alcohol and *iso*-butanol mixture reduction of V_2O_5. The molar surface P:V ratios of these catalyst precursors were in the region of 3.

VPO catalysts usually contain a slight excess of P with respect to the stoichiometric amount as a means of fine tuning the optimal surface P:V ratio and acidity. The basic ions such as Co that are added can act in preventing the migration and loss of P. 20 mol % Co:V introduced into the VPO catalyst, increased the surface P:V ratio and favoured the stabilisation of the catalyst's properties compared with the unpromoted catalyst. Comparison of catalysts with the same % Co:V shows that when the P:V ratio is decreased, the promotional effect of Co decreases. The optimum Co:V ratio is thus P:V ratio dependant. A % Co:V ratio in excess of 20 causes segregation of Co on the surface and gives rise to lower selectivities by catalysing total

oxidation reactions. Below a value of 2 mol % Co:V, Co enters into solid solution, reduces the surface area and diminishes the reactivity of VPO with hydrogen (Zazhigalov, V.A. *et al.* (1993)).

A high BET surface area of the VPO catalyst is generally associated with a high development of the basal (100) $(VO)_2P_2O_7$ face. A Co doped catalyst shows that the addition of the metal leads to a slight variation in the ratio of the relative intensities of the (001) and (220) reflections, from 3.4 to 2.7. This alludes to the fact that the addition of dopants leads to slightly different morphologies for the $VOHPO_4 \cdot {}^1/_2H_2O$ precursor, in agreement with different surface areas. The catalyst precursor is always composed of $VOHPO_4 \cdot {}^1/_2H_2O$, irrespective of the method of preparation and of Co content, as discovered by phase analysis. It is also noteworthy that the promoted catalysts do not require the detailed heat pretreatment required for the unpromoted catalysts (Lemal, R.; U.S. Patent. (1976)). XRD spectra showed the presence of $(VO)_2P_2O_7$ and three diffraction lines (d = 7.12, 3.55 and 3.04 Å) for both doped and undoped catalysts that have been attributed to a hydrated phase possessing an AV close to +5, with stoichiometry $VOH_{0.16}PO_4 \cdot 1.9H_2O$ (Albonetti (1996)). The reflection at the highest d value could also possibly be attributed to the $VOPO_4 \cdot 2H_2O$ phase.

At these concentrations, it is proposed that Co serves to stabilize the loss of oxygen anions during reduction, hence rendering the catalyst less active but more selective (Hodnett, B.K. (1985)). A study of a Co promotion of β-$VOPO_4$ showed that addition of Co stabilized the oxygen anions present in the structure. The incorporation of elements, which can easily donate electrons to the structure of vanadyl phosphate, leads to an increase in effective negative charge on the oxygen atom as compared to the unpromoted catalyst. This electron donation is confirmed by X-ray photoelectron spectroscopy (XPS). An increase of negative charge on oxygen should cause an increase of its basic properties. This increase in basicity is also shown by the increased adsorption of CO_2 on the surface of the catalyst (Zazhigalov, V.A. (1996)).

The cations present in the solid solution can therefore (i) stabilize the AV that would enable improved initial dehydrogenation of *n*-butane and (ii) control the oxygen diffusion and

adsorption thereby minimizing the non-selective oxidation route. Evidence to confirm that promoters aid the control of the optimum oxidation state is found in studies made above the upper explosion limit of 7.1 % on *n*-butane/air mixtures (Higgins, R. *et al.* (1982)) (Refer to p vii). It is proposed that the formula for the solid solution is $((VO)_{1-x}M_x)_2P_2O_7$, where M = promoter element. Co hardly changes the structure of the catalyst precursor, $VOHPO_4 \cdot {}^1/_2H_2O$. Co does, however, promote the *n*-butane oxidation reaction by the formation of defect sites because of the inclusion of the cation into the $(VO)_2P_2O_7$ lattice (Brutovsky, M. *et al.* (1982)). FT-IR shows that there is a shift in the absorption bands in the 900 – 1300 cm^{-1} wavenumber region for the catalysts containing promoters. This suggests that the promoter ion is located in the crystal lattice of $(VO)_2P_2O_7$ (Takita, Y. et al. (1993)). According to the literature, impregnation of the final catalyst with Co also gives enhanced activity with a significant loss in selectivity and, additionally, the rate of MA oxidation is increased. This optimum promoter loading depends on the method of preparation of catalyst. Hence, Co must be added at the precursor stage for the promotional effect to be observed and this indicates that this plays a role in the formation of the final active surface (Hutchings, G.J. *et al.* (1996)).

The optimum promoter loading, i.e the loading that gives the greatest yield of MA, is correlated to a maximum surface area of the catalyst (Sajip, S. *et al.* (2001)). Addition of dopant beyond this optimum loading results in a decrease in surface area of the catalyst.

There was a decrease in selectivity towards MA after operating the catalyst for 2000 hrs. The above increase in activity and subsequent decrease in selectivity holds true in the 0.20 to 0.50 mol ratio Co:V promoter loading region. This decrease in selectivity was attributed to the loss of P from the surface zone of the catalyst. Introduction of alkali and alkali-earth metals to the VPO catalyst causes an increase of surface P:V ratio. This rise of P concentration on the surface is accompanied by simultaneous enrichment of the surface in oxygen and increase of oxygen basicity. These changes lead to changes in acidic properties of the catalyst (Zazhigalov, V.A. *et al.* (1996)). At low acidity of the surface, desorption of adsorbed acid-like products of the reaction is hindered and further oxidation occurs with CO_x formation. On the other hand,

high acidity of the surface does not favour the adsorption of intermediates with acidic properties. Promoter ions may also substitute for phosphorus in the precursor. This causes defects in the structure of the catalyst, which aids in selectivity (Cavani, F. *et al* (1997)). Benzyl alcohol has the same effect in that it remains trapped inside the structure of the catalyst precursor during the preparation in an alcoholic medium. Addition of transition elements can possibly substitute for V and act as modifiers of the reactivity by forming a stable solid solution. Zazhigalov *et al.* (1993) have shown the formation of $Co_2P_2O_7$ when Co was co-precipitated with V and P. This Co phosphate formation prevents the formation of inactive or deleterious VPO compounds, e.g. $VO(H_2PO_4)_2$. It can be expected that the highly dispersed $Co_2P_2O_7$ phase, which is uniformly distributed in the bulk of the catalyst, may fill the voids and macrodefects in the structure, hindering the P transport from the bulk towards the surface. The presence of Co, in effect, reduces the losses of P and thus prolongs the catalyst lifetime. Increasing amounts of Co beyond the optimum promoter loading, which depends on method of preparation, leads to a decrease in the catalytic activity, with a corresponding increase in the selectivity towards MA. This was attributed to an increase in surface acidity. The ideal Co:V molar ratio is between an unpromoted catalyst and 0.20 % loading. Acidity of a catalyst is measured via NH_3-TPD (ammonia-thermoprogrammed desorption) (Zazhigalov, V.A. *et al.* (1987)). It was experimentally shown in this study that adsorption of ammonia increases with increasing Co content, within the above-mentioned promoter loading range, which indicates increased acidity. Introduction of small amounts of Co into the VPO catalyst mainly causes the appearance of weak acid sites, whereas the number of strong acid sites rises to a lesser extent (Zazhigalov, V.A. *et al.* (1993)). There are different acid sites on the surface of the catalyst.

Patents claim that a Co dopant increases both activity and selectivity (Zemal, R.Z. *et al.* (1977), Hutchings, G.J. *et al.*(1981)). This discrepancy in activity to the above studies is due mainly to preparation conditions, Co loading and reagents. It is generally considered that the Co dopant is capable of increased selectivity towards MA. Ben Abdelouahab *et al.* (1995) have

found that Co remarkably improved the selectivity to MA. The observed effects were attributed to a different dispersion of $VOPO_4$ phases on the $(VO)_2P_2O_7$ matrix.

A Co promoted catalyst prepared by the reduction of $VOPO_4 \cdot 2H_2O$ by *iso*-butanol is known to give a particular morphology of $VOHPO_4 \cdot {}^1/_2H_2O$ by developing crystallites in the [110] direction as revealed by XRD studies (Sananes-Schulz, M.T. *et al.* (1996)). From a physical perspective, a platelike morphology was revealed by scanning electron microscopy (SEM) images of the catalyst surface. The Co doped catalyst, however, showed larger plate-like crystals as compared to the undoped one. For the Co-doped VPO precursor (Co:V = 5 mol %), α_I- and α_{II}-$VOPO_4$ first appear, and then $(VO)_2P_2O_7$ on conditioning the catalyst. It has been shown that the $VOPO_4/(VO)_2P_2O_7$ dispersion can be modified by using dopants (Ben Abdelouahab, F. *et al.* (1995)). V switches between V^{5+} ($VOPO_4$) and V^{4+} ($(VO)_2P_2O_7$) during the oxidation of *n*-butane to MA.

The temperature at which MA is first detected is 234°C and detection is noted up to 430°C, when the Co doped catalyst is prepared by adding Co acetylacetonate salt to the *iso*-butanol solvent and V_2O_5, and refluxed. The presence of α_{II}-$VOPO_4$ is shown by Raman spectroscopy. This phase plays a role in the formation of a disorganized VPO matrix (Sananes-Schulz, M.T. *et al.* (1996)). XRD spectra of both undoped and Co doped catalysts show the presence of $(VO)_2P_2O_7$ and α_I-$VOPO_4$ phases. Both α_I- and α_{II}-$VOPO_4$ have the same properties in the lattice of the catalyst. XRD spectra of these two catalysts are similar. Discrepancy with XRD patterns can be explained by taking into account that all anhydrous oxidized $VOPO_4$ phases (with the exception of β-$VOPO_4$) are in a hydration/dehydration equilibrium with $VOPO_4 \cdot 2H_2O$ (Ben Abdelouahab, F. *et al.*(1994)). The relative intensities of the $(VO)_2P_2O_7$ reflections are the same for unpromoted and promoted catalysts and show that the corresponding crystallites present the same morphology after doping with Co. The slight difference in XRD patterns is only seen above a 15 mol % Co:V promoter loading. There are few extra lines present for the Co doped catalyst (Zazhigalov, V.A. *et al.* (1993)) and the peak

intensity of the modified catalyst is lower than the unmodified catalyst. The lowered reflection intensities indicate that the dimension of particles and degree of arrangement of the catalyst structure are lowered. This is characteristic of solid solutions, where the presence of additional or substituent atoms or holes in the solvent lattice of $(VO)_2P_2O_7$ results in changed intensity of reflections. There is a decrease in lattice energy related to the substitution of low valent cations into the crystal lattice. Modified VPO catalysts have Fourier-transform-infrared spectra (FT-IR) that are less complex than unmodified catalysts. The former lack the individual intensive maxima and breaks of the basic bands, which is characteristic of unmodified catalysts. This can be explained by the decreased degree of structural order. Individual bands in spectra of modified catalysts are shifted by 5-20 cm^{-1}, which can be explained by the change in dimension of particles and effect of admixtures on bond relations. The intensities of bands in the region 1 300 - 900 cm^{-1} reveal an increase in absorption in the spectra of most modified catalysts as compared with the unmodified ones. The observed changes can be explained by a change of dipole moment of P-O bonds in the modified catalysts. The incorporation of the dopant and distribution of electron density in the anions causes polarity changes in the corresponding bonds, which results in intensity changes of absorption and in the observed shift of maxima of the individual bands (Brutovsky, M. *et al.* (1982)).

Co doped catalysts appear to be more crystalline compared to the undoped VPO catalyst. This is consistent with ^{31}P NMR spectra by spin echo mapping which show an increase of the contribution of the signal at 2400 ppm attributed to crystalline $(VO)_2P_2O_7$ (Sananes-Schulz, M.T. *et al.* (1997)).

Doping with Co results in a decrease of the V^{5+} contribution (from 47 to 37 %) (Sananes-Schulz, M.T. *et al.* (1996)). The redox ability of the Co-dopants have a favourable effect on the $VOPO_4$ (V^{5+}) and $(VO)_2P_2O_7$ (V^{4+}) couple. MA formation is directly correlated to the surface V^{4+}/ V^{5+} ratio. The V^{4+}/V^{5+} ratio in used catalysts is generally higher than in freshly calcined catalysts. It can be thus confirmed that during conditioning, the reaction environment reduces the V^{5+}. Characterisations of used catalysts indicate V^{5+} phases, besides the crystalline

$(VO)_2P_2O_7$. The effect of doping depends not only on the nature of the dopant, but also the morphology of the precursor. Doping permits the control of $VOPO_4/(VO)_2P_2O_7$ dispersion during the activation process and this factor is important for industrial catalysts and should be monitored for "equilibrated catalysts" after long time-on-stream (Sananes-Schulz, M.T. *et al.* (1996)). The relative amounts of the phases present, as well as the nature of the oxidized $VOPO_4$ phases are affected by the presence of the dopant (Cavani, F. *et al.* (1997)).

Co generates a significantly crystalline $(VO)_2P_2O_7$ together with poorly crystalline $(VO)_2P_2O_7$ structures, a combination that gives enhanced catalytic performance. This structure can be correlated with the presence of V^{4+} cations and V^{4+}-V^{5+} dimers (Sananes-Schulz, M.T. *et al.* (1997)).

XPS measurements show that binding energies of O 1s, V 2p and P 2p photoelectrons remain unchanged in the precursors and in the catalysts after use. This concludes that the valence states of Co and V do not change in the course of the transformation of the precursors into VPO catalysts (Zazhigalov, V.A. *et al.* (1993)).

1.8.2. Case studies

The method of preparation of the promoted catalysts leads to the formation of a higher surface area catalyst and thus an enhanced catalyst activity (Hutchings, G.J. (1993)). A Co doped catalyst showed a promotional effect by increasing the yield per unit surface area (Cornaglia, L.M. *et al.* (1999)). A precursor catalyst prepared via the organic route utilizing only *iso*-butanol as solvent showed a decrease in surface area with the doped catalyst compared to the undoped catalyst (Cavani, F. *et al.* (1997)). In contrast there was a 20 % increase in surface area of the equilibrated Co doped catalyst, with a 20 molar % Co:V loading, compared to the undoped catalyst (Hutchings, G.J. *et al.* (1996)). This catalyst had a 17 m^2/g surface area and was synthesized using an HCl/*iso*-butanol reduction mixture. There is thus some

discrepancy with regard to surface area and Co doping, however, the results are dependant on the method of preparation.

In another study, it was experimentally found that a Co doped VPO catalyst gave higher specificity to the formation for phthalic anhydride from *n*-pentane oxidation, which occured at the expense of MA (Cavani, F. *et al.* (1997)).

An optimum selectivity of 76 % was obtained for a 0.25 mol ratio Co:V loaded catalyst prepared via the organic route. The catalyst was prepared with *iso*-butanol as solvent. The salt utilized in the synthesis was $CoCl_2 \cdot 6H_2O$. There was an optimum P:V ratio linked to this optimum selectivity which was around a molar P:V ratio of 1.7 (Zazhigalov, V.A. *et al.* (1993)). Above this P:V ratio it is thought that some other factors begin to dominate, whilst the concentration of strong acid sites remain constant, to cause the decrease in selectivity. This molar P:V ratio is higher than most published P:V ratios which lie between 1.0 and 1.2.

A patent claims a 95 % conversion of *n*-butane with a 60 % yield of MA (U.S Patent (1980)). HCl was used in the reduction stage of the synthesis. $CoCl_2$ was used as the promoter and the impregnation method of addition was utilised. The promoter loading was 6.5 mol % Co:V. 1.5 % *n*-butane in air was fed into the reactor and the testing was carried out at 420°C.

The Union Carbide (UCB) system utilized a catalyst capable of a 55 % yield of MA. The catalyst has a molar P:V ratio of 1.14:1 and a Co:V ratio of 0.19:1. The feedgas is 1.5 % *n*-butane in air. The operating temperature is 450°C, with a GHSV of 1893 hr^{-1}. The aqueous HCl method is used in this synthesis (Lemal, R.; US Patent (1976)). The non-aqueous catalyst synthesis method, utilizing *iso*-butanol as solvent produced a MA yield of 59 %. This catalyst operated at 380°C.

Chevron produced an unpromoted catalyst capable of a 57 % yield of MA. The catalyst was synthesized using *iso*-butanol solvent. The feed gas consisted of 1.5 % *n*-butane in air. The operating temperature was 380°C. The conversion of *n*-butane was 90 mol % and the selectivity towards MA was 69 mol % (Schneider, R.A.; U.S. Patent. (1977).

1.8.3. Conclusion

The essential role of promoters in VPO catalysts for *n*-butane to MA oxidation is to modify the structural nature of the catalyst. The promoter is incorporated into a solid solution. An optimum promoter loading into these solid solutions is obtained. This optimum promoter loading correlates with the largest catalyst surface area. The promoter controls the catalyst oxidation state and surface segregation of phases. Promotion effects have been mainly examined on the $(VO)_2P_2O_7$ phase. The combination of the promoters and excess P results in a VPO catalyst with appropriate oxidizability and morphology to give high yields of MA, i.e. greater than 50 %. The addition of additives can increase the rate of *n*-butane oxidation to maleic anhydride.

1.9. Surface acidity of the VPO catalyst

Catalysts prepared by both the organic and aqueous route show the presence of strong Brϕnsted acid sites, attributed to surface P-OH groups, and medium strong Lewis sites, attributed to V^{4+} coordinatively unsaturated ions exposed on the surface (Busca, G. *et al.* (1986c)). The presence of these centers is related to the $(VO)_2P_2O_7$ structure itself and is fairly independent of the $(VO)_2P_2O_7$ preparation method. $(VO)_2P_2O_7$ prepared in an organic medium and to a lesser extent in the $(VO)_2P_2O_7$ prepared in an aqueous medium show very strong Lewis sites. The enhancement of the rate of *n*-butane activation in the $(VO)_2P_2O_7$ prepared in an organic medium is attributed to the presence of these sites.

It was found in a previous study (Centi, G. *et al.* (1984c)), that the rate-limiting step of the reaction,

$$n\text{-butane} \longrightarrow \text{maleic anhydride}$$

over a VPO catalyst, is the activation of the hydrocarbon to form an intermediate, which can desorb as butenes in conditions avoiding their successive oxidation.

The adsorption of ammonia, pyridine and acetonitrile indicates that strong Brϕnsted sites as well as medium strong Lewis sites are present on the vanadyl pyrophosphate surface. The Brϕnsted acidity is attributed to the presence of surface P-OH groups, whose $\delta_{in\text{-}plane}$ deformation is perturbed by the adsorption of ammonia and water (Busca, G. *et al.* (1986c)). The medium strong Lewis acidity is attributed to coordinatively unsaturated V^{4+} ions exposed on the surface in V=O double bonds.

Adsorption of acetonitrile, which is a weak base, indicates the presence of medium strong Lewis sites in greater quantities in the $(VO)_2P_2O_7$ prepared in an organic medium as compared with that prepared in an aqueous medium. The medium strong Lewis acidity is due to an inductive effect considering the higher electronegativity of P in the V-(O-P) bond. Less CO and CO_2 adsorption agrees with this interpretation (Busca, G. *et al.* (1986c)). Since the specific rate of *n*-butane activation on $(VO)_2P_2O_7$ prepared in an organic medium is higher, the enhancement of catalytic properties in *n*-butane oxidation by the vanadyl pyrophosphate prepared in an organic medium is attributed to the presence of the very strong Lewis sites bonded to the V=O moiety. These are the active sites for *n*-butane selective oxidation. The specific rate is the rate of reaction per unit surface area.

The formation of the very strong Lewis sites can be attributed to the topotactic mechanism of formation of vanadyl pyrophosphate from $VOHPO_4 \cdot {}^1/_2H_2O$. In the organic preparation of $VOHPO_4 \cdot {}^1/_2H_2O$, the organic alcohol utilized as a reducing agent remains trapped between the layers of the $VOHPO_4 \cdot {}^1/_2H_2O$ structure during the transformation to $(VO)_2P_2O_7$ and induces deformations in the vanadyl pyrophosphate structure creating a partial lack of coordination sites on the V^{4+} ions and enhances the Lewis acid strength (Busca, G. *et al.* (1986c)).

1.10. Relationship between catalyst preparation, phase composition and selectivity

Improved understanding of the factors that determine the structure of VPO catalysts has made renewed attempts at elucidating the detailed mechanism of C_4 transformation to MA possible.

Several reports have appeared which link catalytic activity and selectivity of VPO catalysts with an optimal AV value. It was reported that with catalysts operating below 400°C in 1 % *n*-butane in air feed, deactivation only occurred after 200-300 hours on stream and was attributed to the loss of P by sublimation. Organic P compounds may be added (continuously or during batch regeneration) to maintain catalyst performances.

It is important to maintain an optimal oxidation state for the catalyst to maintain a certain selectivity of MA production. For the supported catalysts prepared by Nakamura (Nakamura, K. *et al.* (1974)), the optimum AV value for all catalysts was close to +4. When this parameter fell below +4, selectivity diminished dramatically. This indicated that the presence of some V^{5+} ions was necessary for MA formation and that a redox cycle between V^{4+} and V^{5+} was involved. It was remarked that only catalysts with metal-oxygen double bonds were active in MA formation and V=O bonds were postulated as active sites. It was concluded that facile movement of electrons through the aggregated reduced structures facilitated dissociation of $O_{2(g)}$ and formation of the necessary surface V=O active sites with V in the +5 oxidation state.

It is postulated that the β- and α-$VOPO_4$ phases are in dynamic equilibrium with the position shifting depending upon the composition of the gas phase (more oxidising favouring α-$VOPO_4$) and the reaction temperature. β-$VOPO_4$ tended to form when catalysts were calcined at 500°C in air. It was reported that this phase was somewhat more difficult to reduce than α-$VOPO_4$, so that dynamic equilibrium between it and the β-phase could not occur as readily.

Few detailed studies of the relationship between the phase composition of VPO catalysts and their catalytic activities for *n*-butane selective oxidation have been carried out. Catalysts were generally tested at a reaction temperature of 400°C for *n*-butane oxidation where changes

in bulk composition of catalysts were minimal (Hodnett, B.K. *et al.* (1984)). Greater activities were observed after pre-reduction in hydrogen; this treatment also increased the selectivity of catalysts with low P:V ratios, i.e. P:V ratios below 1, but no changes in selectivity were observed after reduction of catalysts with high ratios. This effectively meant that higher yields were observed as a result of the higher conversions.

Extremely high initial selectivities in MA, of the order of 80 %, were observed when *n*-butane was contacted with the calcined catalyst in the absence of gas-phase oxygen (Hodnett, B.K. *et al.* (1984)). However, for all P:V ratios studied, selectivity and yield decreased as *n*-butane reacted with the catalysts under these conditions and fell to zero for decrease in AV of approximately 1. These results suggested that catalysts with maximum activity and high selectivity are constituted of oxidised surface layers built upon a reduced core. The reduced core could be produced either by pretreatment in hydrogen or through structural stabilisation of the V^{4+} ions by excess P (Hodnett, B.K. *et al.* (1984)). The non-reactive core is postulated as a means whereby the availability of surface oxygen was controlled. Oxygen incorporated into the MA product is envisaged as originating from near surface layers (Hodnett, B.K. *et al.* (1985)). This model is similar to that proposed by Centi, G. *et al.* (1984c), who found that selectivity in MA is increased when the *n*-butane concentration was increased. However, conversion is lower under these circumstances and very little V^{5+} remains in the catalyst. Centi, G. *et al.* (1984c) and Ziolkowski, J. (1983) concluded in separate studies, that selectivity in MA was determined by the amount of surface oxygen available in the vicinity of the adsorption site.

1.11. Proposed mechanism for *n*-butane oxidation to MA over a VPO catalyst

The rate-determining step of this reaction is the activation of *n*-butane through abstraction of a proton (Zazhigalov, V.A. *et al.* (1993)). This step is accelerated via the increased basicity of the surface oxygen atoms. This has been found experimentally by the linear dependance of the rate of *n*-butane oxidation on the binding energy of O 1s-electrons (Zazhigalov, V.A. *et al.* (1996)).

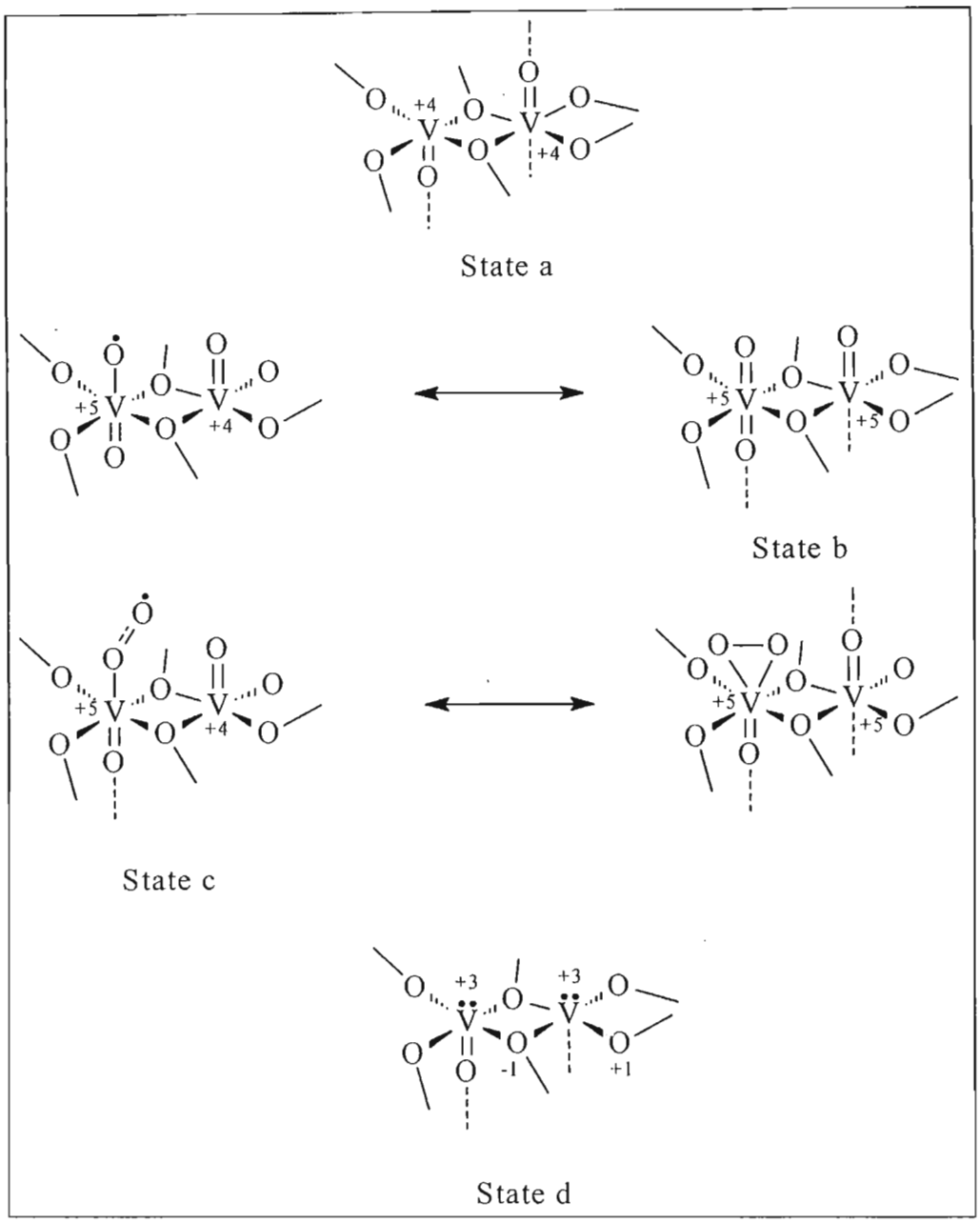

Fig. 1.8. Possible states of the active sites (Agaskar, P.A. et al. (1994))

The proposed mechanism for the selective oxidative transformation of *n*-butane to maleic anhydride on the (100) face of the $(VO)_2P_2O_7$ crystallites, suggests that each of the four dimeric active catalytic groups per geometrically isolated surface cluster (as illustrated in Section 1.4) can assume the four distinct states a, b, c and d as illustrated in Fig. 1.8.

- State a: "ground" state of the active site, it has only one oxygen associated with it.
- State c: molecule of dioxygen is adsorbed on the Lewis acid site of state a, this chemisorbed dioxygen could either be a superoxo or peroxo species.
- State b and d: two additional possible states that the active sites can assume.

The first step of the mechanism involves the initial activation of *n*-butane. This is accomplished by the abstraction of a methylene hydrogen by a superoxo species to give a surface bound hydroperoxy group, and simultaneously the capture of the alkyl radical by the adjacent vanadyl group to give a surface bound alkoxy group as illustrated in Fig. 1.9. The hydroperoxy group can then rapidly abstract another hydrogen, from either the same methylene group or from one of the adjacent -CH_x groups, to generate a molecule of water and a metal bound ketaloxy or glycoloxy group respectively. The surface species formed as a result of this step can also be considered to be 2-butanone and 1- or 2-butene, strongly adsorbed on the active site in state a or b respectively (Agaskar, P.A. *et al.* (1994)).

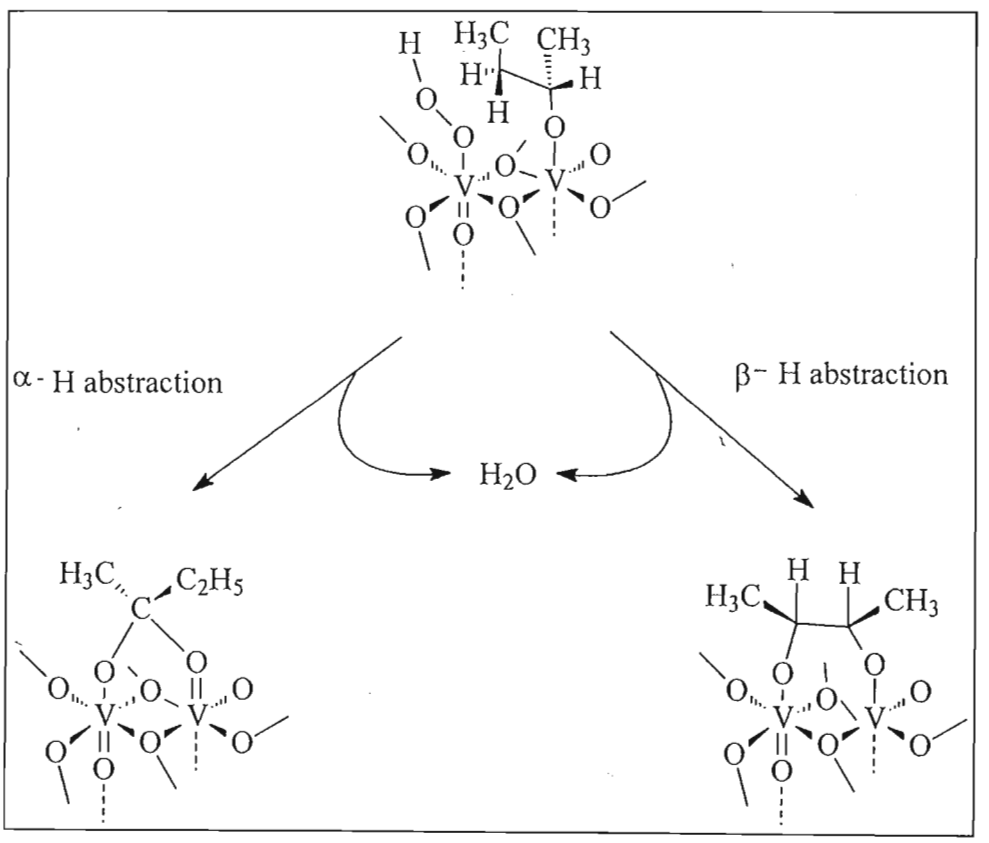

Fig. 1.9. n-Butane activation

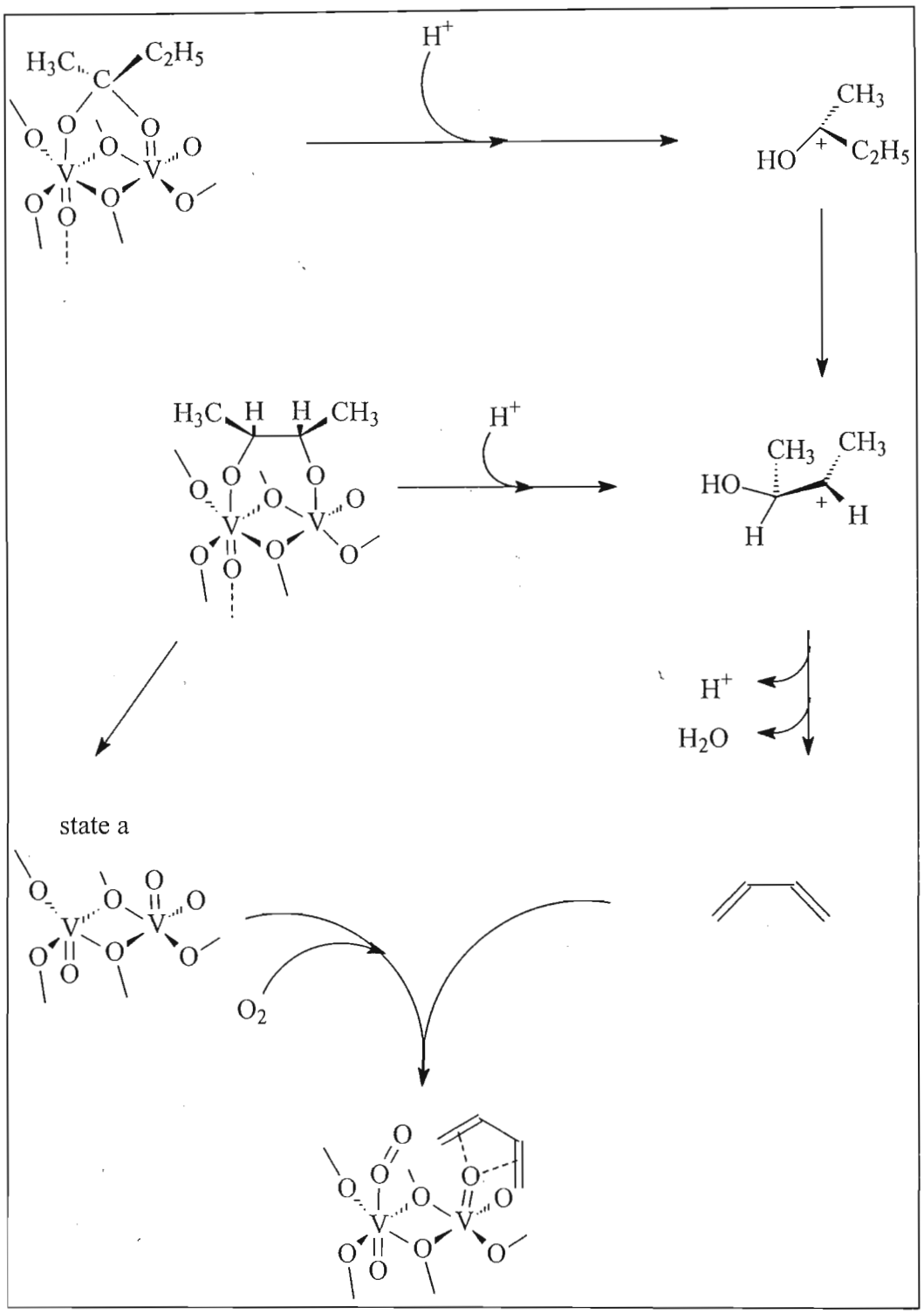

Fig. 1.10. Butadiene formation on the surface of the catalyst

The next step in the mechanism involves the acid catalysed conversion of partially bound surface intermediates to 1,3-butadiene. The active site is first converted to state a which is capable of adsorbing a molecule of dioxygen and is therefore converted to state c as illustrated in Fig. 1.10.

The vanadyl oxygen is used in reaction with 1,3 butadiene producing 2,5-dihydrofuran (Fig. 1.10).

An interaction between one of the oxygens in the adsorbed molecular oxygen species and the C-H bond in the 2-position of the 2,5-dihydrofuran becomes possible; the interaction thus leads to a transfer of a hydrogen atom from 2,5-dihydrofuran to the peroxo species giving a surface bound hydroperoxide group (Fig. 1.11). With this orientation of the two adsorbed species a considerable C-O interaction (bond length = 1.60 Å) is present. The OH group can therefore transfer to the neighbouring 2,5-dihydrofuran derivative giving the corresponding 2-hydroxy derivative (Fig. 1.11).

The asymmetric lactone can be obtained by first transferring a hydrogen atom from the 2-lactone hydroxy derivative giving a surface hydroxy group. The second hydrogen atom can be transferred to give the desired asymmetric lactone and one molecule of water (Fig. 1.11) (Wenig, R.W. *et al.* (1987). This process can repeat itself until maleic anhydride is formed (Agaskar, P.A. *et al.* (1994)).

The transformation of *n*-butane to maleic anhydride is a multi-step polyfunctional reaction mechanism occurring entirely on the surface and is the only industrially practiced selective oxidation involving an alkane. Knowledge gained through study and understanding of this system may contribute to advances in alkane oxyfunctionalisation in general.

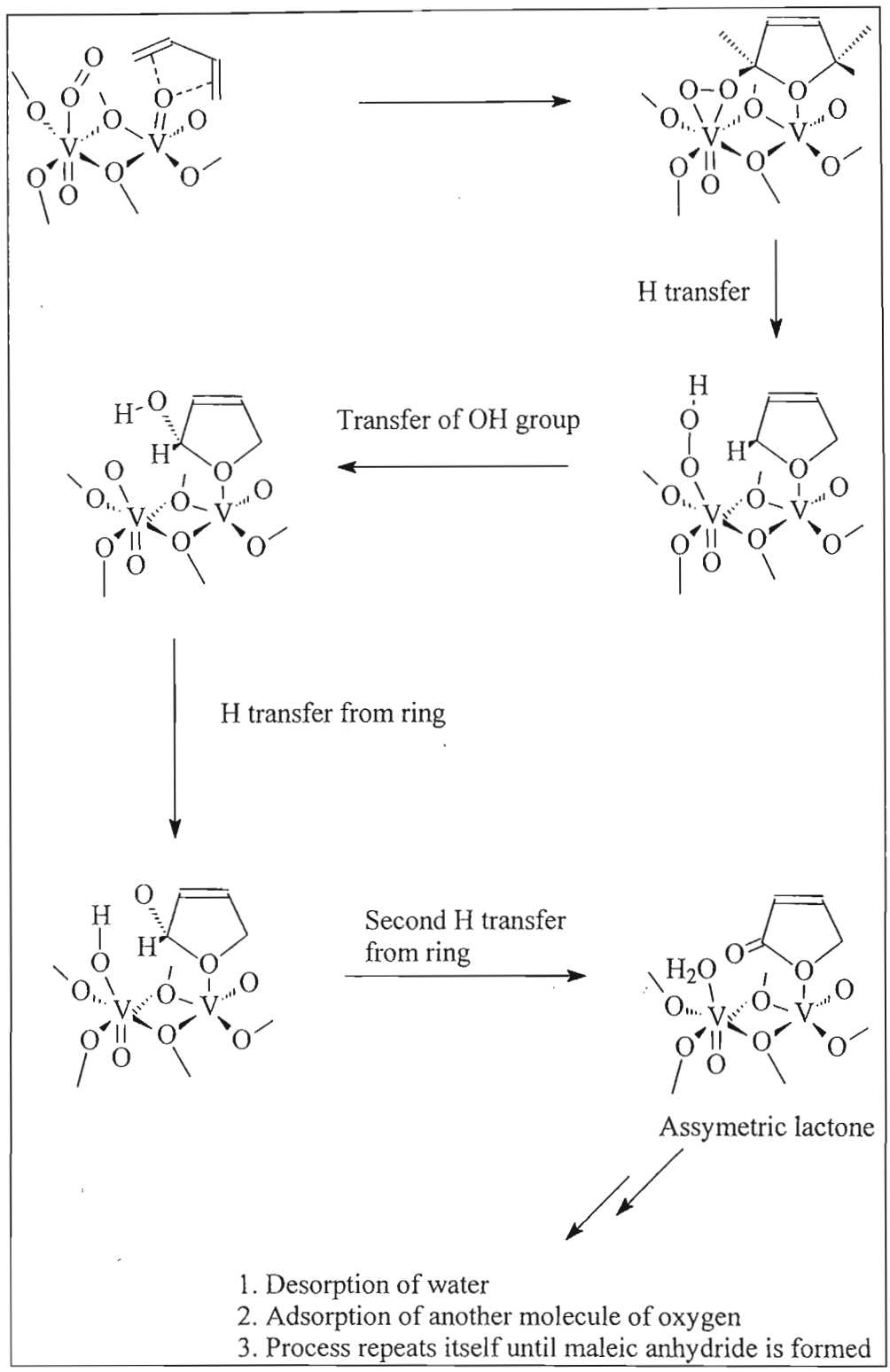

Fig. 1.11. 2,5-Dihydrofuran and consequent lactone formation (Sookraj, S.H. et al. (1997))

1.12. Directions for future research

Understanding this catalyst system is restricted to model systems in the laboratory which often possess well-defined crystal structures, have been activated under fairly severe conditions, and give much lower yields and selectivities of MA than their industrial analogues. These two streams must be united if better catalysts are to be developed.

Two approaches from which advances can be expected are:

1. Developments in the engineering of a given process, such as the use of fluidised-bed reactors, or, for fixed-bed reactors, working with *n*-butane in air mixtures above the explosive limit.
2. By a more systematic and detailed study of all the factors which influence the preparation of the industrial VPO catalysts.

For the latter a great deal of fundamental work is required for catalysts that are capable of yields and selectivities of the order of 50 % at close to 100 % conversion. The systematic approach, which must be adopted, is similar to that required for all bulk oxide catalysts. The first step would involve monitoring the solution chemistry and fully characterising the precursor which is obtained vis-à-vis it's AV value, P:V ratio, distribution of this ratio within the catalyst, and the phases which form. XPS (see Appendix 3) is of considerable help in that it could indicate the P:V ratio at the surface for various locations in the bed. These factors also need to be investigated for used catalysts, but an additional factor needs to be investigated here, viz. the manner in which lattice oxygen is involved in the reaction. Studies have shown that the availability of lattice oxygen at the catalyst surface determines it's final selectivity (Centi, G. *et al.* (1984c)). The prerequisite for this type of study is the determination of the catalyst structure followed by an investigation of the mechanism of mobility of lattice oxygen within the bulk of the catalysts. The final challenge will be the identification, on the molecular scale, of the nature of the surface sites responsible for the individual steps of the transformation.

Examining a catalyst as it functions *in situ* means evaluating or characterising it at elevated temperatures and pressures and as the reactant gases flow over it, ideally under the

temperature and flow conditions that would be typical of industrial applications. Researchers at Dupont's Ames laboratory observed that cycling the catalyst between reducing and oxidizing environments improved activity, selectivity and yield. But this new operation also brought with it new questions that only could be answered through fundamental research. If conditions fluctuated completely, new characterisation techniques had to be developed. The fundamental questions for this system are "Why does it operate better? Is it changing its structure or oxidation state? Are the rates for partial oxidation higher? Is the mechanism different? Finding the answers has opened up a whole new area in catalysis research involving forced oscillation kinetics, or unsteady states" (Schrader, G.; URL; (1996)).

1.13. References

Agaskar, P.A.; DeCaul, L.; Graselli, R.K.; *Catal. Lett.*; **23** 339 (1994)

Aguero, A.; Sneddon, R.P.A.; Volta, J.C.; *Heterogenous Catalysis and Fine Chemicals - Studies in Surface Science and Catalysis*, Elsevier, Amsterdam; **41** p 353, (1988)

Ai, M.; *Bull. Chem. Soc., Jpn.*; **43** 3490 (1970)

Albonetti, S.; Cavani, F.; Trifirò, F.; Venturoli, P.; Calestani, G.; Lopez Granados, M.; Fierro, J.L.G.; *J. Catal.*; **160** 52 (1996)

Ben Abdelouahab, F.; Olier, R.; Ziyad, M.; Volta, J.C.; *J. Catal.*; **157** 687 (1995)

Ben Abdelouahab, F.; Volta, J.C.; Olier, R.; *J. Catal.*; **148** 334 (1994)

Birkeland, K.E.; Babitz, S.M.; Bethke, G.K.; Kung, H.H.; *J. Phys. Chem. B*; **101** 6895 (1997)

Bither, T.A.; U.S Patent 4,442,226 (1984)

Bordes, E.; *Catal. Today*; **1** 499 (1987)

Bordes, E.; Courtine, P. J.; *J. Catal.*; **57** 236 (1979)

Bordes, E., Courtine, P. J.; *Chem. Soc., Chem Commun.*; 294 (1985)

Brutovsky, M.; Gerej, S.; *Czechslovak Chem. Commun.*; **47** 403 (1982)

Buchanan, J. S.; Sunderasen, S.; *Appl. Catal.*; **26** 211 (1986)

Busca, G.; Cavani, F.; Centi, G; Trifirò, F.; *J. Catal.*; **99** 400 (1986a)

Busca, G.; Centi, G.; Trifirò, F.; *Appl. Catal.*; **25** 265 (1986b)

Busca, G.; Gabriele, C.; Ferruccio, T.; Lorenzelli, V.; *J. Phys. Chem.*; **90** 1337-1344 (1986c)

Cavani, F.; Centi, G.; Trifirò, F.; *Appl. Catal.*; **9** 191 (1984)

Cavani, F.; Centi, G.; Trifirò, F.; J. *Chem. Soc., Chem Commun.*; 492 (1985a)

Cavani, F.; Centi, G.; Trifirò, F.; Poli, G.; *J. Thermal Anal.*; **30** 1241 (1985b)

Cavani, F.; Colombo, A.; Giuntoli, F.; Trifirò, F.; Vazquez, P.; Venturoli, P.; *Advanced Catalysis and Nanostructured Materials*, Academic Press: New York; Chapter 3 p 43 (1996)

Cavani, F.; Colombo, A.; Trifirò, F.; Sananes-Schulz, M.T.; Volta, J.C.; Hutchings, G.J.; *Catalysis Letters*; **43** 241-247 (1997)

Centi, G.; Cavani, F.; Trifirò, F.; *Selective Oxidation by Heterogenous Catalysis*; Kluwer academic/Plenum publishers; p 144 (2001)

Centi, G.; Fornasari, G.; Trifirò, F.; *J. Catal.*; **89** 44 (1984a)

Centi, G.; Manenti, I.; Riva, A.; Trifirò, F.; *Appl. Catal.*; **9** 177 (1984b)

Centi, G.; Trifirò, F.; *Appl. Catal.*; **12** 1 (1984c)

Centi, G.; Trifirò, F.; *Chem. Rev.*; **88** 56 (1988)

Centi, G.; Trifirò, F.; Poli, G.; *Appl. Catal.*; **19** 225 (1985)

Cornaglia, L.M.; Carrara, C.R.; Petunchi, J.O.; Lombardo, E.A.; *Appl. Catal. A: General*; **183** 177-187 (1999)

Cornaglia, L.M.; Caspani, C.; Lombardo, E.; *Appl. Catal.*; **74** 15 (1991)

Cornaglia, L.; Sanchez, C.A.; Lombardo, E.A.; *Appl. Catal. A: General.*; **95** 117 (1993)

De Maio, D.A.; *Chem. Eng.*; 104 (1980)

Ebner, J.R.; Gleaves, J.T.; *Oxygen Complexes and Oxygen Activation by Transition Metals*, Plenum, New York; p 273 (1988)

Haber, J.; *In Proceedings, 8th International Congress on Catalysis*, Dechema: Frankfurt am Main, **1** 85 (1984)

Higgins, R.; Hutchings, G.J.; U.S. Patent 4 317 777 (1982), assigned to Imperial Chemical Industries

Hodnett, B.K.; *Catal. Rev-Sci. Eng.*; **27(3)** 373-424 (1985)

Hodnett, B.K.; Delmon, B.; *Appl. Catal.*; **15** 141 (1985)

Hodnett, B.K.; Delmon, B.; *Ind. Eng. Chem. Fundam.*; **23** 465 (1984)

Horowitz, H.S.; Blackstone, C.M.; Sleight, A.W.; *Appl. Catal.*; **38** 193 (1988)

Hutchings, G.J.; *Appl. Catal.*; **72** 1 (1991)

Hutchings, G.J.; *Catal. Today*; **16** 139 (1993)

Hutchings, G.J.; Higgins, R.; GB Patent 1 601 121 (1981)

Hutchings, G.J.; Higgins, R.; *J. Catal.*; **162** 153-168 (1996)

Johnson, J. W.; Johnson, D.C.; Jacobson, A.J.; Brody, J.F.; *J Am. Chem. Soc.*; **106** 8123 (1984)

Katsumoto, K., Marqius, D.M.; US Patent 4 187 235 (1980)

Lemal, R.; Vekemans, J.; US Patent 3 987 063 (1976), assigned to UCB

Lozana-Calero, D.; Bruque, S.; Aranda, M.A.G.; Martinez-Lara, M.; Moreno, L.; J. *Solid State Chem.*; **103** 481 (1993)

Malow, M.; *Hydrocarbon Process*; p 149 (1980)

Mamedov, E.A.; Corberan, V.C.; *Appl. Catal. A: General*; **127** 1-40 (1995)

Mars, P.; van Krevelen, D.W.; *Chem. Eng. Sci. Special Suppl.*; **3** 41 (1954)

McDermott, J.; GB Patent 2 001 861 (1979)

McKay, J. http://www/che.lsu.edu/COURSES/4205/1999/mckay/paper.html, *"The Production of Maleic Anhydride"*

Miyake, T.; Doi, T.; *3rd World Congress on Oxidation Catalysis; Studies in Surface Science and Catalysis*, Elsevier Science: Amsterdam; **110** 835 (1997)

Nakamura, K.; Kawai, K.; Fujiwara, Y.; *J.Catal.*; **34** 345 (1974)

Pepera, M. A.; Callahan, J. L.; Desmond, M.J.; Millberger, E. C.; Blum, P. R.; Bremer, N. J.; *J. Amer. Chem. Soc.*; **107** 4883 (1985)

Poli, G.; Resta, I.; Ruggeri, O.; Trifirò, F.; *Appl. Catal.*; **1** 395 (1981)

Sajip, S.; Bartley, J.K.; Burrows, A.; Rhodes, C.; Volta, J.C.; Kiely, C.J.; Hutchings, G.J; *Phys. Chem. Chem. Phys.*; **3** 2143-2147 (2001)

Sananes-Schulz, M.T.; Ben Abdelouahab, F.; Hutchings, G.J.; Volta, J.C.; *J. Catal.*; **163** 346 (1996)

Sananes-Schulz, M.T.; Tuel, A.; Hutchings, G.J.; Volta, J.C.; *J. Catal.*; **166** 388-392 (1997)

Schneider, R.A.; U.S. Patent 4 043 943 (1977), assigned to Chevron Research Co.

Schrader, G.; http://www.external.ameslab.gov/News/Inquiry/spring96/circle.html; (1996)

Sookraj, S.H.; Engelbrecht, D.; *Catal. Today*; **49** 161 (1999)

Sookraj, S.H.; Engelbrecht, D.; *Confidential Report Number 290/97; Sastech R&D Applied Catalysis Research*; p 24 (1997)

Stadig, W.E.; *Chem. Proc.*; p 27 (1992)

Takita, Y.; Tanaka, K.; Ichimaru, S.; Mizihara, Y.; Abe, Y.; Ishihara, Y.; *Appl. Catal. A: General*; **103** 281 (1993)

Thompson, M.R.; Hess, A.C.; Nicholas, J.B.; White, J.C.; Anchell, J.; Ebner, J.R.; *New Developments in Selective Oxidation II*; p 167 (1994)

Tofield, B.C.; Crane, G.R.; Aspeur, G.A.; Sherwood, R.C.J.; *J. Chem. Soc. Dalton Trans.*; 1806 (1975)

Torardi, C.C.; Calabrese, J.C.; *Inorg. Chem.*; **23** 1308 (1984)

Trifirò, F.; *Catal. Today*; **16** 91 (1993)

U.S. Patent 4,209,423 (1980)

U.S. Patent 4,244,879 (1981)

U.S. Patent 4,317,778 (1982)

Wagner, C.D.; Riggs, W.M.; Davis, L.E.; Moulder, J.F.; Mullenberg, G.E.; *Handbook of X-Ray Photoelectron Spectroscopy*, Perkin-Elmer, Physical Electronics Division, Eden Prairie, MN.; (1979)

Wenig, R. W.; Schrader, G. L.; *J. Phys. Chem.*; **90** 6480 (1986)

Wenig, R.W.; Schrader, G.L.; *J. Phys. Chem.*; **91** 5674-5680 (1987)

Young, L.B.; Weinstein, B.; Jurewicz, A.T.; Fr. Patent 2 187 752 (1974)

Zazhigalov, V.A.; Haber, J.; Stoch, J.; Bacherikova, I.V.; Komashko, G.A.; Pyatnitskaya, A.I.; *Appl. Catal. A: General*; **134** 225-237 (1996)

Zazhigalov, V.A.; Haber, J.; Stoch, J.; Pyatnitzkaya, A.I.; Komashko, G.A.; Belousov, V.M.; *Appl. Catal. A: General*; **96** 135 (1993)

Zazhigalov, V.A.; Konovalova, N.D.; Zaytzev, Yu. P.; Belousov, V.M.; Stoch, J.; Krupa, R.; Haber, J.; *Ukr. Khim. Zhurn.*; **53** 1145 (1987)

Zemal, R.Z.; Vekemans, J.A.; GB Patent 1 475 309 (1977)

Ziolkowski, J.; *J.Catal.*; **84** 317 (1983)

CHAPTER 2

INDUSTRIAL AND LABORATORY PROCESSES

2.1. Introduction

This chapter focuses on heterogeneous gas-phase oxidation processes from a reactor technology viewpoint. Existing and emerging catalytic reactors are described and both advantages and disadvantages are discussed. The theory behind the testing of catalysts shall be briefly explored, focusing on factors that affect the catalyst and product analysis.

Because oxidation reactions often involve breaking of saturated or unsaturated carbon-carbon or carbon-hydrogen bonds, the reactions are highly exothermic. The degree of exothermicity can be quite significant when non-selective combustion reactions occur in series or parallel with the selective reactions. This is the primary reason why reactor selection and design are of critical importance for industrial oxidation processes. The reactor system must be capable of controlling the temperature within certain safety-designed limits by proper management of the high heat load. This places some specific requirements on their design (Pratt, K.C.; (1987)).

Depending on the composition of the hydrocarbon/air feed to the reactor, the mixture can spontaneously ignite; therefore safe operation of oxidation reactors requires avoiding the flammability region. Newer emerging processes based upon re-circulating solids reactors are operated with hydrocarbon-rich feed gas whose composition is above the upper limit of the flammability region so that safe operation is ensured (Emig, G. *et al.* (1994)).

The smallest possible size for a micro-reactor is advisable for plug flow conditions. A preheater is necessary to maintain isothermal conditions in the catalyst bed. It is easier to achieve isothermal or near isothermal conditions with a small catalyst charge than a large one. The smallest possible particle size is also recommended, at most 40 or 60 mesh.

2.2. Fixed-bed micro-reactors

Fig. 2.1 lists some of the key issues that must be considered when modeling fixed-bed reactors for vapour phase catalytic systems (Froment, G.F. *et al.* (1990)). A wide range of length scales must be traversed in a realistic model of the fixed-bed reactor. The individual catalyst sites represent the micro-scale where the catalyst reactions occur. Reaction kinetic measurements using state-of-the-art laboratory reactors and information derived from catalyst characterization instrumentation provide the basis for development of kinetic models and identification of kinetic parameters based upon a sequence of elementary steps.

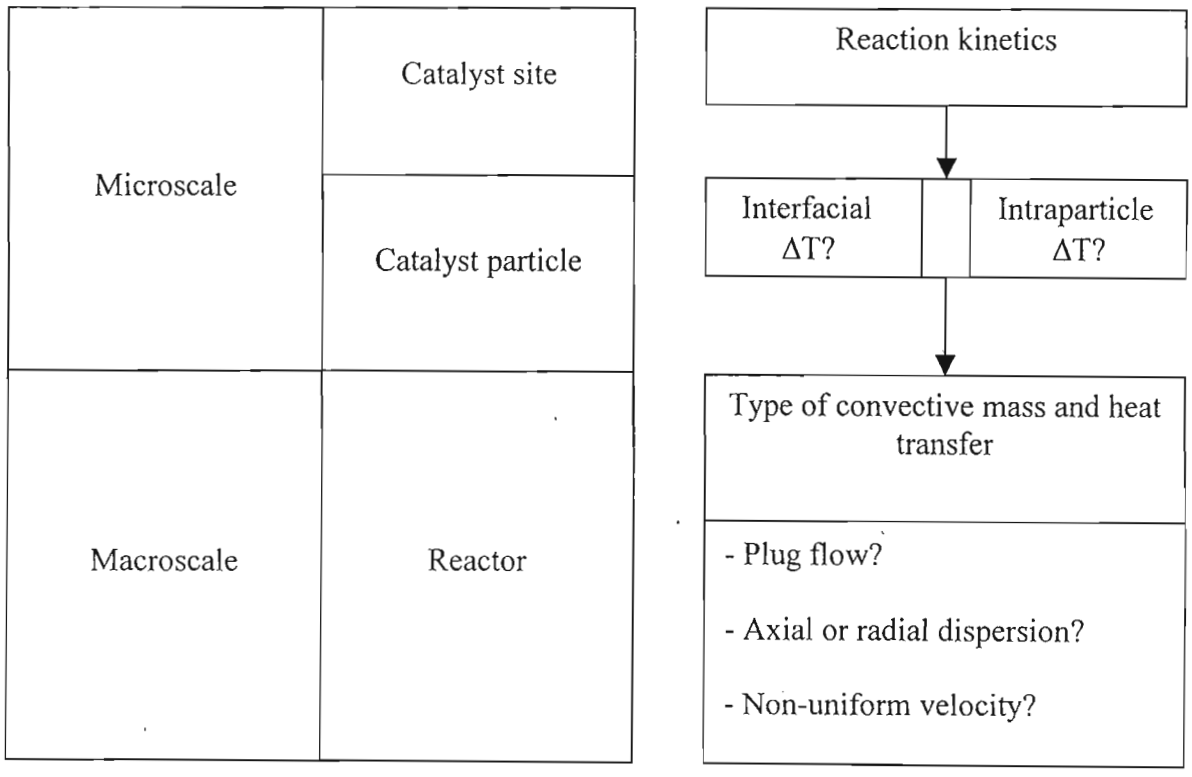

Fig. 2.1. Parameters to consider when designing a fixed-bed reactor (Froment, G.F. (1990))

The bed of catalyst particles corresponds to the macro-scale level. Here, transport processes that occur on characteristic dimensions of the reactor, such as the reactor diameter and overall length of the fixed-bed are the focus. This includes a description of deviations of the gas

flow pattern from ideal plug-flow and deviations of the temperature within the catalyst particles and in the gas bulk from an ideal isothermal condition.

Fixed bed reactors are among the most widely used reactors in the hydrocarbon processing and petrochemical industry. An analysis is made up of factors that pose a limit to representative downscaling of catalyst testing in a continuous fixed-bed operated with either gas or gas-liquid flow. By taking advantage of radial diffusion to cancel the effect of uneven velocity distributions and by resorting to catalyst bed dilution with fine inert particles, representative experiments are possible on a very small scale, with amounts of catalyst down to a few grams or even less. Results obtained on such a small scale are in good agreement with those obtained in industrial reactors under comparable conditions. A need, however, remains for laboratory catalytic tests which simulate the commercial operations close enough to give results on catalytic process performance that are directly meaningful for industrial practice, preferably without requiring translations of which the validity is uncertain (Sie, T.; (1996)).

Reducing the scale of experiments in the laboratory has a number of important advantages, such as (i) lower cost of construction and installation of equipment; (ii) less consumption of materials and less waste products to be disposed of; (iii) reduced demands on laboratory infrastructure because of lower space requirements, less facilities for storage and transport of feeds and products; (iv) increased intrinsic safety: reduced hazards of fire, explosions and emission of toxic materials and (v) generally reduced manpower needs.

In principle, the safest way to represent an industrial reactor on a laboratory scale is to reduce the diameter while keeping the bed length the same. In a well-designed industrial fixed-bed reactor, where proper care is taken to ensure uniform distribution of feed over the cross section of the bed, there are theoretically no cross sectional differences. Hence, a more slender but equally tall test reactor would be a good representation of the commercial reactor, provided that the diameter of the test reactor is not so small that wall effects, such as axial dispersion, become appreciable (Zimmerman, S.P. *et al.* (1986)).

Axial dispersion in the reactor is caused by the more or less random variations of fluid velocity at the scale of the particle diameter and is an intrinsic property of a random packing of particles. Aside from these microscopic fluctuations of velocity, there can be more systematic differences of fluid velocities in the bed. A transverse velocity profile extending from wall to wall may be present as a consequence of uneven packing, i.e. unequal compaction of the packing in different parts of the bed or, in the case of a catalyst having a size distribution, unequal average particle size caused by segregation during filling of the reactor. Whereas such non-conformity in the packing need not exist if the reactor is filled with sufficient care, the perturbation of the random packing by the reactor wall is a cause of velocity differences, which cannot be avoided (Zimmerman, S.P. *et al.* (1986)).

Fixed bed reactors are generally chosen for processes with relatively low intrinsic reaction rates. Riser reactor technology becomes preferable for very fast reactions. Here, the catalyst is regenerated with air in a separate reactor. Therefore, most fixed bed processes operate under conditions where, within the above window, the catalyst effectiveness (defined in the list of definitions on p. (vii)) is 1 or not very much below 1, implying that the diffusion paths of reactant molecules inside the catalyst particles are not much shorter than the particle dimensions. Transformations of reactant to product in most practical fixed-bed processes are mainly governed by chemical reaction rates and intra-particle diffusion. A well-designed fixed-bed micro-reactor is a close approximation of an ideal integral reactor that fulfills the following criteria: (i) all volume elements of the feed contribute to the overall conversion, which implies that they have to spend the same time in the reactor. This criterion applies to conversions with a reaction order greater than zero, i.e. conversions for which the fixed-bed reactor is an appropriate choice and (ii) all parts of the catalyst bed must contribute maximally to the overall conversion, which means that all catalyst particles must be adequately contacted by the reactant. Aside from the requirement of a sharp residence time distribution, the ideal fixed-bed reactor should also allow all parts of the catalyst bed to fully participate in the overall conversion. With a single fluid phase, this condition is generally met when the plug flow criterion is obeyed, since

in this case there is uniform flow through the bed. However, in two phase flow, such as co-current trickle flow, the ratio of the liquid to gas flow may be different in different parts of the bed: a situation may prevail where liquid flows preferentially through a certain part of the bed, while gas flows predominantly through the other parts. This mal-distribution is commonly referred to as incomplete wetting of the catalyst. Therefore the requirement for an ideal reactor is better stated as "even irrigation" of all parts of the catalyst bed (Sie, T. (1996)).

Molecular diffusion can be an important cause of a spread in residence time, particularly at low velocities (low space velocities and short bed lengths), therefore it is important in micro-reactors with gas flow. Axial molecular diffusion is not a function of particle size or velocity of fluid but rather based on molecular diffusion.

2.2.1. Catalyst bed packing and dilution with fine particles

In testing catalysts, only relatively small particles can be used in a bench-scale or micro-flow reactor to comply with the criteria for axial convective dispersion in the packing, the wall effect, and even irrigation. Particles of such small size (diameter below 0.5 mm) give rise to unacceptably high pressure drops in industrial fixed-bed reactors and practical catalysts for these reactors generally have particle diameters in the range of 1 to 3 mm. When the effectiveness factor of such practical catalysts is 1, i.e. there is no intra-particle diffusion limitation at all; crushing or grinding the catalyst to obtain smaller particles can be a way to assess catalyst performance in small-scale laboratory reactors. However, even if the main reaction is not limited by diffusion, other reactions (side reactions or consecutive reactions involving larger molecular species) can still be diffusion limited. In this case, testing of catalysts in crushed form may give misleading results on selectivity or stability of the catalyst even when activity data are correct. In many processes of interest to the hydrocarbon processing industry, the size and shape of the catalyst has been chosen as a compromise between catalyst effectiveness and pressure drop. Hence, with effectiveness factors for the main reaction somewhat below 1, intra-particle diffusion is generally a factor to be reckoned with. Its effect is

not easily quantified since the processing of a practical feedstock involves the conversion of a large variety of molecules with widely different reaction rates and therefore the translation of catalyst performance data obtained with crushed particles to that of the actual catalyst may be difficult and of questionable validity. A way out of the dilemma is to use a bed of small particles in small laboratory reactors and yet determine the performance of a practical catalyst of much larger particle size by embedding the latter particles in much finer inert particles. Thus, by diluting the catalyst bed with 1-3 times its volume of fine inert material, the hydrodynamics will largely be dictated by the packing of the fine inert particles, whereas the performance measured is that of the catalyst in the actual form. It can be seen that bed dilution with fine inert particles results in a considerable improvement in the plug-flow character of the reactor, which supports the idea that the dispersion is largely determined by the packing of fine particles (Carruthers, J.D. *et al.* (1988)).

Fixed-bed reactors can in principle be operated in two different ways, viz.

- isothermally, i.e. the temperature is the same in every part of the bed, or
- adiabatically, i.e. the reaction heat is taken up or supplied by the reactant stream without heat being released or supplied to the environment.

Small laboratory reactors are most easily operated as isothermal reactors.

2.2.2. Isothermally operated reactors

In an isothermal reactor, the temperature of the reactant stream is constant in the axial direction. Hence, this stream does not take up reaction heat (in the case of an exothermic reaction) and all heat generated within the bed must be transported radially to the reactor wall. If the bed radius is too large and the effective heat conductivity of the bed too low, a radial temperature profile will develop with appreciable differences between the centre of the bed and near the wall. The temperature profile will be more pronounced as the radial distances are longer and as fluid velocities are lower, hence, wide and short reactors are likely to suffer from radial temperature inhomogeneity.

An effective way to improve the isothermicity of reactors is to dilute the catalyst with inert particles, preferably of a material with high heat conductivity, such as silicon carbide which has a heat conductivity in the solid state about 40 times that of porous alumina. In the diluted bed, the heat generated per unit volume of bed will be lowered, and together with increased effective heat conductivity this will result in a more even radial temperature distribution.

2.2.3. Adiabatically operated reactors

In a true adiabatic reactor there is no flow of reaction heat to or from the surroundings, and the reaction heat (in the case of an exothermic reaction) heats up the reactant stream so that the temperature difference between the outlet and inlet stream is equal to the theoretical adiabatic temperature rise, ΔT_{ad}. In a laboratory, one attempts to obtain this situation by surrounding the reactor with heating zones to compensate for natural heat losses. However, even when the heating power is adjusted in such a way that the net heat loss from the reactor is zero and consequently the temperature difference between the outgoing and incoming stream equals the theoretical adiabatic temperature rise, the temperature distribution in the bed may still deviate from that in a true adiabatic reactor when the number of heating zones is limited and their temperature setting is non-optimal (Satlerfield, C.)

Temperature deviations of the fluid and reactor wall from a true adiabatic profile for a specific case are quite appreciable, notwithstanding the fact that the reactor system is "adiabatic" in the sense that the temperature difference between the outgoing and incoming stream equals the adiabatic temperature rise and the net overall heat loss is zero. The deviations are caused by significant axial heat conduction through the metal wall of the reactor, which tends to flatten the temperature profile, and by radial conduction of heat from the interior of the bed to the wall. Furthermore, end effects play a role as well, and the actual temperature of the fluid when it enters the reaction zone does not necessarily have to be equal to the temperature of

the reactor wall or the fluid temperature in the reactor. It is clear that deviations from true adiabaticity may seriously affect the results of catalyst testing, particularly with regard to selectivity and deactivation behavior (Anderson, D.H. *et al.* (1989)).

For improperly designed laboratory reactors the axial and radial heat flows can be quite appreciable even when the net heat loss is zero. It thus follows that the radial heat flow is reduced as the bed diameter is increased, whereas the axial heat flow diminishes as the reactor length is increased. Hence, long pilot plant reactors of wide diameter will perform best as adiabatic reactors even with sub-optimal design of compensation heaters. To prevent heat losses at the reactor ends, the catalyst containing adiabatic part of the reactor is preceded and followed by an isothermal part filled with inert material (Anderson, D.H. *et al.* (1989)).

2.2.4. Fixed-bed reactors in relation to fluidized-bed and transport-bed reactors

Process, licensor	Type of reactor	Product recovery
ALMA (Lonzagroup,Lummus)	Fluidised bed	Anhydrous
Lonzagroup	Fixed bed	Anhydrous or aqueous
BP (Sohio)-UCB	Fluidised bed	Aqueous
Denka Scientific Design	Fixed bed	Aqueous
DuPont	Transport bed	Aqueous
Mitsubishi Kasei	Fluidised bed	Aqueous
Monsanto	Fixed bed	Anhydrous

Table 2.1 Industrial technologies for MA synthesis (Mills, P.L.)

The main features of the industrial technologies currently used for MA production are summarized in the Table 2.1 below. The various processes differ in terms of: (i) type of reactor (fixed-bed, fluidized-bed or transport-bed reactors); (ii) composition of feed (i.e. usually referring to the concentration of *n*-butane in air); (iii) product recovery (referring to the method

of recovery of MA where an aqueous or organic solvent may be used and the product is purified via distillation). Some well-established industrial processes shall be briefly discussed. Table 2.1 highlights some of the industrial technologies employed in MA synthesis.

The Mitsubishi Process: The hydrocarbon source in the Mitsubishi plant is the crude C_4 fraction from naphtha crackers, so it represents a departure from the older benzene-based processes and a move towards more recent processes based upon *n*-butane. The crude C_4 fraction and air are fed into the reactor where the hydrocarbon concentration is high enough that it exists in the explosive range (i.e. between 1.8 and 1.9 mol %). Because of the rapid gas-solids mixing and associated hydrodynamics, an ignition cannot occur, so that safe operation is possible. The hot reactor off-gas, which contains the crude MA, is quenched in a spray tower so that an aqueous solution of crude maleic acid is produced. Dehydration and purification of the crude maleic acid stream obtained from the quenched tower bottoms is performed by evaporation and distillation. The purified MA vapours are taken overhead and condensed for subsequent pelletisation and packaging (Contractor, R.M.; (1987)).

The Alusuisse/Alma process: Unlike the Mitsubishi Chemicals process, *n*-butane is used as the hydrocarbon source. The *n*-butane and air are fed separately to maintain a certain mol % of hydrocarbon in the mixed stream. A distinguishing feature of this process is that it uses a proprietary anhydrous MA recovery system with an organic solvent where the boiling point of the latter exceeds that of MA (ca. 202°C at 1atm). This is claimed to minimize the formation of unwanted by-products that are otherwise formed in aqueous recovery processes involving the evaporation of aqueous maleic acid (Contractor, R.M.; (1987)).

The Dupont process: Dupont's Ames laboratory developed a system of cycling the catalyst between a reducing and oxidizing environment, thereby improving activity, selectivity and yield. Normally these processes are steady-state processes; the catalyst is brought up to a certain temperature and pressure, and the reactant gases continually flow over it (Schrader, G.; URL; (1996)).

The choice of reactor determines the conversion-yield relationship, the control of the heat of reaction (and thus the feed composition), and the feasibility of catalyst regeneration. Fluidised-bed reactors have a number of advantages over fixed-bed reactors including: (i) excellent heat transfer and no hot spots; (ii) high tolerance for feed impurities; (iii) safe operation with inlet gas compositions within the flammability limits; (iv) higher productivity; (v) improved turndown, turnoff, and flexibility; (vi) reduced limitations for heat and mass intragranular transfer; (vii) shorter downtime for catalyst replacement; (viii) constant catalyst performance (continuous catalyst makeup is possible); (ix) production of higher value steam; (x) single train operation up to 50,000 tons/year (about twice that for fixed-bed) and (xi) investment cost advantage for production of higher than about 10,000 tons/year. On the other hand, fluidized-bed reactors suffer from: (i) lower selectivity because of back-mixing; (ii) the necessity of making hard catalyst particles (must be mechanically resistant to high attrition conditions) using additives that often lower catalyst performance and (iii) problems in scale-up. Transport-bed reactors, e.g. continuous flow fluidized bed reactors (CFIBRS), operate in the hydrodynamic regime of transport of the catalyst with the feed (*n*-butane virtually without oxygen, although a small quantity of oxygen is added to improve productivity) in the riser reactor with regeneration of the catalyst (with air) in a separate reactor (usually a fluidized-bed reactor) (Centi, G. (2001)).

The advantages of CFIBR technology using a dense-bed transport reactor with respect to fluidized-bed and fixed-bed reactors are: (i) higher throughput, because of the higher gas velocity and the ability to independently optimize the kinetic conditions for the two stages of the redox mechanism as reduction and re-oxidation occur in physically separated reactors; (ii) higher selectivity; (iii) excellent intragrain and interphase heat and mass transfer; (iv) high turndown (solid and gas retention times can be adjusted independently); (v) higher product concentration (improved recovery) and (vi) greater intrinsic safety. However, there are disadvantages: (i) the need for a catalyst with an exceptionally high attrition resistance; (ii) significant uncertainty in scale-up; (iii) the need for temperature control in the riser; (iv) the

very high energy costs associated with catalyst re-circulation; (v) high catalyst makeup; (vi) possible side reactions, which include condensation and polymerization, that occur in the absence of oxygen; (vii) low productivity per mass of circulating solid and (viii) production of significant quantities of carbon oxides in the regeneration unit (Centi, G. (2001)).

2.3. Catalyst testing

Coke is sometimes the final product of a series of consecutive reaction steps. Coke can block active catalytic sites on the catalyst surface and thus lead to deactivation of the catalyst. The feed conversion drops as a result of a smaller active catalytic surface area. Deactivation rates, therefore, might also depend on the conversion level (Csicsery, S.M. (1992)). The catalyst is only tested after reaching an equilibrium state, referred to as conditioning a catalyst, i.e. when the percent conversion of feed and selectivity towards the required product stabilizes under set reactor conditions.

2.3.1. The feed delivery system

The feed system should deliver a homogenous feed at an even flowrate at the required temperature and pressure to the reactor. It is difficult to determine whether or not mixing has been complete. One possible method to check is to connect the bypass line to the TCD of the GC, whilst maintaining the same pressure as that through the catalyst bed. A straight horizontal line obtained from the integrator shows complete mixing. A wavy line shows poor mixing (Csicsery, S.M. (1992)).

Significant space velocity fluctuations could occur unless the pump and most of the feed delivery system are kept at constant temperature. It is, however, difficult to keep a constant temperature as gauges, valves and joints have large dead volumes. Opening windows or doors can change ambient temperature of the feed delivery system that can affect actual flowrates. Laboratory reactors need not be miniature copies of commercial reactors as the purpose of the reactor is to generate information and not to manufacture and sell a product.

Glass wool should be packed after the catalyst bed to ensure that fines do not get into the sampling or control valves.

2.3.2. Mass transport phenomena in a catalyst

Catalytic reactions proceed through several distinct steps. There are gas diffusions of the reactants, adsorption, surface reaction/s, desorption, and gas diffusions of the products. Surface diffusion may also take place. Any one of these steps could be rate limiting. Fig. 2.2 shows some of the mass transport steps during the oxidation of *n*-butane to MA. Mass transport becomes rate limiting when the surface reaction is faster than the supply of reactants and/or the removal of the products by any of several diffusion steps. Most catalyst screening studies rank catalysts in order of intrinsic catalytic activities. Therefore, it is imperative to test catalysts under conditions where mass transfer is not rate limiting.

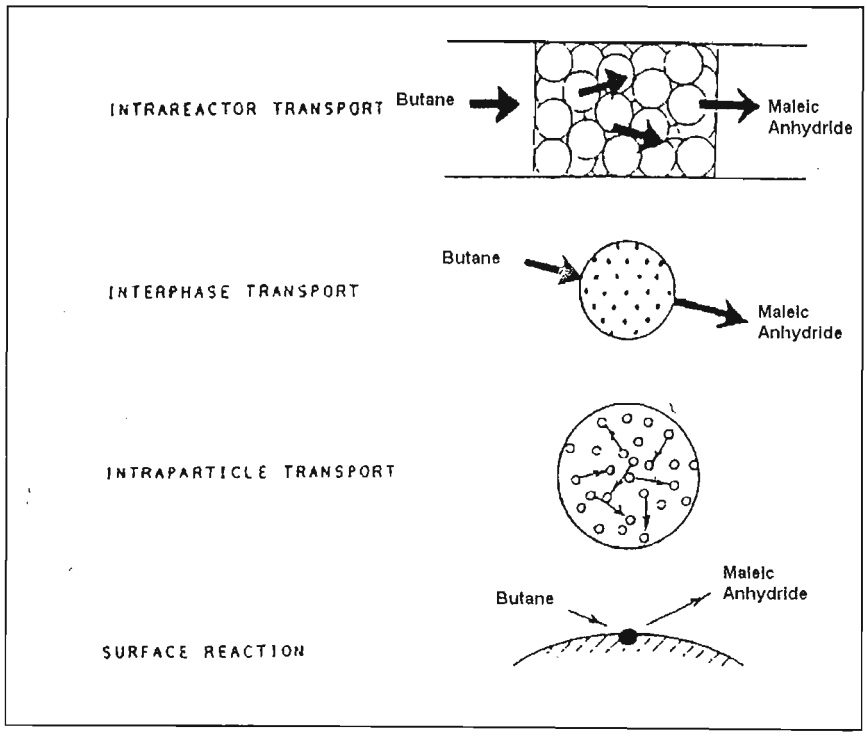

Fig. 2.2. Mass transport phenomena in a reactor (Csicsery, S.M. (1992))

2.3.3. Product analysis

Greaseless, no-dead volume sampling valve systems are essential in the analysis of products in a micro-reactor. The no-grease feature is particularly important here because greases could selectively absorb some components from the product. This, of course, would change sample compositions before analysis. Gas chromatographs are the most important analytical instruments used in catalytic reaction studies. The analytical and sampling instruments should be kept in top shape for best results. Recalibration of the gas chromatograph retention times and response factors at regular intervals, preferably daily, are necessary. Heated transfer lines between the sampling valve and the gas chromatograph prevent condensation of the products from the reactor. Recording and comparing total GC areas of the on-line sample analyses is one of the most powerful and simplest methods to detect errors. As long as the total GC areas are within 5 % of each other, probably everything is working as it should. The following can affect the total GC area: (i) improper feed rates; (ii) leaks in the joints connecting the reactor; (iii) leaks in the sampling, sample transfer, and GC carrier gas lines; (iv) splitter problems and (v) faulty detectors and improper GC carrier gas rates. Results that show GC areas more than 5-10 % higher or lower than their proper value should be ignored and the experiment repeated.

2.3.4. Catalyst life cycle

The life of most heterogeneous catalysts may be divided into three periods as illustrated in Fig. 2.3. The first period is called "line-up" or "activation" or "induction". Some catalysts rapidly deactivate in this time period and others become more active. This period can be anything from a few seconds to several days or even weeks. "Line-up" is usually followed by a long "steady state" period. Deactivation is usually slow and steady during this stage. In the "end of run" period the catalyst deactivates rapidly. The catalyst activities, selectivities and other kinetic parameters are determined during the steady state period.

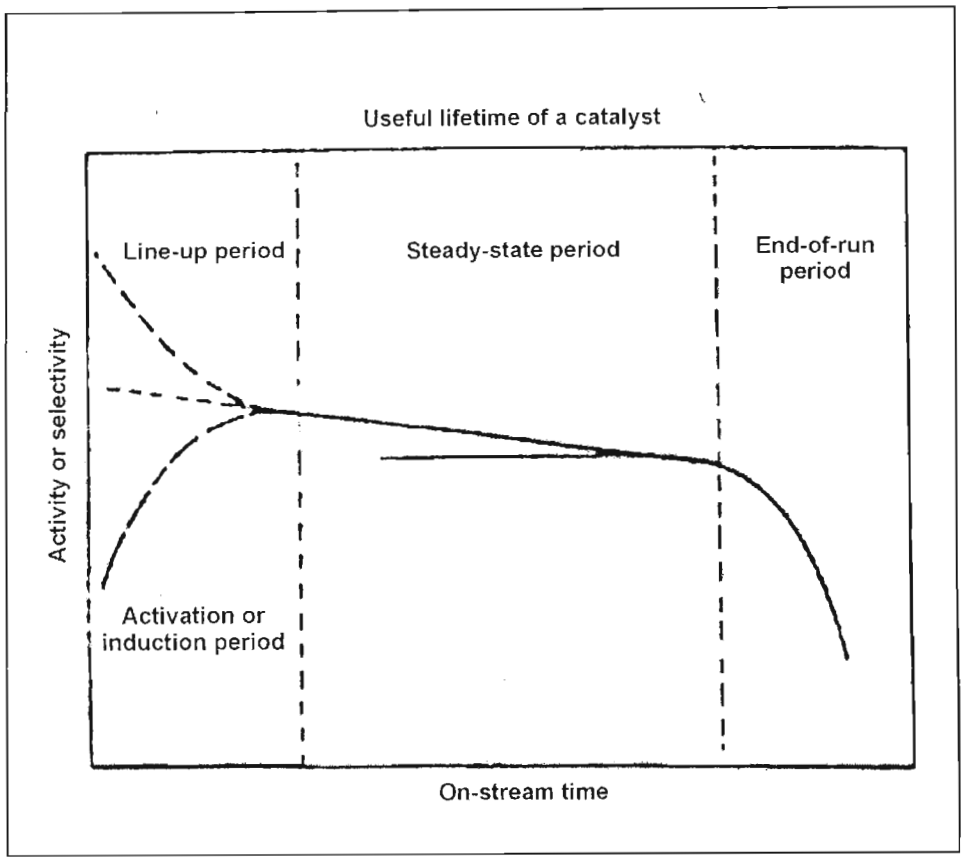

Fig. 2.3. Life cycle of a catalyst (Csicsery, S.M. (1992))

Activity may be expressed as conversions reached at constant pressure, temperature, and space velocity.

Selectivities may depend on temperature, pressure, space velocity, diffusion, catalyst particle size and shape, reactor geometry and other factors. Selectivities should always be compared at constant temperature, pressure and conversion.

2.3.5. Heat transfer effects

High axial and/or radial temperature gradients are the most frequent sources of incorrect data in continuous tubular flow reactors. The problem increases with increasing reactor diameter and increasing catalyst bed volume. Temperatures between the hottest and coldest points could differ more than 30-40°C even in small (10 mL) catalyst beds and even with moderately exothermic or endothermic reactions. However, even larger temperature differences might remain undetected because few micro-reactors provide enough space for more than two

thermocouples. It is thus recommended to determine the axial temperature profile of the catalyst bed. The temperature should be within 2°C. The temperature gradient increases with increasing conversion. Ways of minimizing the temperature gradient would be: (i) to dilute the catalyst with inert material; (ii) using the smallest possible diameter reactor and the highest practical linear flow rate and (iii) encouraging turbulent flow rate by using small particles. The particle diameter should be less than one tenth of the reactor diameter and about one-hundredth the length of the catalyst bed. The catalysts should be tested at low conversions. Most of these measures will increase the pressure drop along the catalyst bed, however, pressure changes usually affect reaction rates much less than temperature changes.

2.4. Conclusion

As can be inferred from Table 2.1, it is not possible to indicate a clear reactor-type preference for the synthesis of MA from *n*-butane, but different options may exist depending on factors such as the up- and downstream integration of the process and the cost of *n*-butane. It may be noted, however, that the choice of reactor determines reaction conditions, which in turn affect the characteristics of the "optimal" catalyst, and thus catalyst optimization is not an independent variable with respect to the choice of the final process reactor technology.

Oxidation processes that are economically viable require the development of catalyst and reactor technology where the yield of the desired product is maximized. Optimal yields of the desired product can only be obtained if the product does not undergo thermal decomposition in the given reaction environment and in any downstream unit operations associated with product recovery.

Compared to other types of vapour-phase catalytic reactors, fixed-bed reactors have received the most attention from the perspective of application and reaction engineering analysis. For this reason, the level of understanding for this configuration is perhaps the greatest when compared to other reactor types.

Due to the beneficial effect of radial diffusion in gas-phase processes in counteracting transverse velocity profiles caused, for instance, by the perturbation of packing homogeneity near the reactor wall, and by taking advantage of the improvements in axial dispersion and catalyst irrigation resulting from dilution of the catalyst bed with fine inert material, it is possible to obtain reproducible and meaningful results from tests in micro-reactors.

From the analysis of limiting factors as discussed thus far, it follows that even smaller reactors than micro-reactors may be used, since the bed diameter of the latter can be further reduced without adverse consequences, as long as the reactor tube can still accommodate the catalyst particles. Thus, catalyst testing may be done in reactors having diameters in the millimeter range containing less than one gram of catalyst.

Due to the exothermic nature of the reaction it is important to ensure that the reactor is isothermal. If the temperature in the catalyst bed is not properly controlled the reaction could easily become unstable and temperature runaway would occur in both an industrial and laboratory reactor setup.

2.5. References

Anderson, D.H.; Sapre, A.V.; *Chem. Eng. Progress*; **85(7)** 54 (1989)

Bither, T.A.; U.S Patent 4,442,226 (1984)

Carruthers, J.D.; Dicamillo. D.J.; *Appl. Catal.* **43** 253 (1988)

Centi, G.; Cavani, F.; Trifirò, F.; *Selective Oxidation by Heterogenous Catalysis*; Kluwer Academic/Plenum Publishers; p 146 (2001)

Contractor, R.M.; *Catalysis Today*; **1** 587 (1987)

Csicsery, S.M.; *Catalyst Testing: How and How Not To Test Catalysts*; Catalysts Consultants Publishing Company. A Member of The Catalyst Group; pp 1-21 (1992)

Emig, G.; Uihlein, K.; Hacker, C. J.; *New Developments in Selective Oxidation II*; p 243 (1994)

Froment, G.F.; Bischoff, K.B.; *Chemical Reactor Analysis and Design*; 2nd Edition, Wiley, New York; pp 475-515 (1990)

Mills, P.L.; Harold, M.P.; Lerou, J.J.; *Industrial Hetergenous Gas-Phase Oxidation Processes*; p 331 Chapter 4

Pratt, K.C.; *Catalysis: Science and Technology*; Springer-Verlag: New York; **8** Chapter 4 (1987)

Schrader, G.; http://www.external.ameslab.gov/News/Inquiry/spring96/circle.html; (1996)

Satlerfield, C.; *Heterogenous Catalysis for Industrial Practice*; p 473 Chapter 11

Sie, T.; *Small Scale Testing of Catalysts for Fixed Bed Processes*; p 7 Chapter 2 (1996)

Zimmerman, S.P.; Ng, K.M.; *Chem. Eng. Sci.*; **34** 1350 (1979)

CHAPTER 3

EXPERIMENTAL

3.1. Reactor setup

A fixed-bed continuous flow micro-reactor and on-line gas chromatograph (GC) monitoring system was designed and constructed for the purpose of this project. The fixed-bed reactor was chosen for its low cost of construction and installation of equipment as opposed to the other types of reactors mentioned in Chapter 2. The *n*-butane to MA reaction has a low intrinsic reaction rate, thus the fixed-bed reactor was appropriate. High intrinsic reaction rates require the use of fluidized-bed technology. The fixed-bed reactor occupies less lab space compared to other types of reactors and a small amount of catalyst is used in a catalytic run.

An overall picture of the reactor and analytical system is illustrated in Appendix 1 (Fig. 1). A 1 % *n*-butane in air premix was fed into the reactor. The reason for using a 1 % *n*-butane in air premix, as opposed to any other amount, was due to a supplier restriction. The feed lines to the reactor were $^1/_8{}^{th}$ inch copper tubing. The lines from the reactor outlet to the gas-sampling box were $^1/_8{}^{th}$ inch stainless steel tubing. The lines from the gas-sampling valve to the GC were $^1/_{16}{}^{th}$ inch stainless steel tubing. The *n*-butane feed was monitored and controlled by a pressure gauge, needle valve (NV1) and rotameter (R1) that were mounted on a control panel. The arrangement of valves and guages are shown in Fig. 3.1. The supply pressure was kept at 100 kPa, as this was the supply pressure under which the rotameters had been calibrated. The needle valve served to stop the flow of feed gas from the supply cylinder. Calibration gas was fed via a separate line. The calibration gas cylinders contained premixes of CO, CO_2, *n*-butane and the balance being air. The calibration gas was monitored and controlled by a pressure gauge, needle valve (NV2) and rotameter (R2). An on/off valve (NV3) was employed at the T-junction where the feed gas met the calibration gas to avoid a bleed of calibration gas during catalytic runs. Mixing coils served to mix the *n*-butane in air before entering the reactor. A pressure gauge before the reactor served to monitor the supply pressure to the reactor. After the pressure gauge, the supply gas met a three-way valve that either diverted the gas to a bypass line or to the

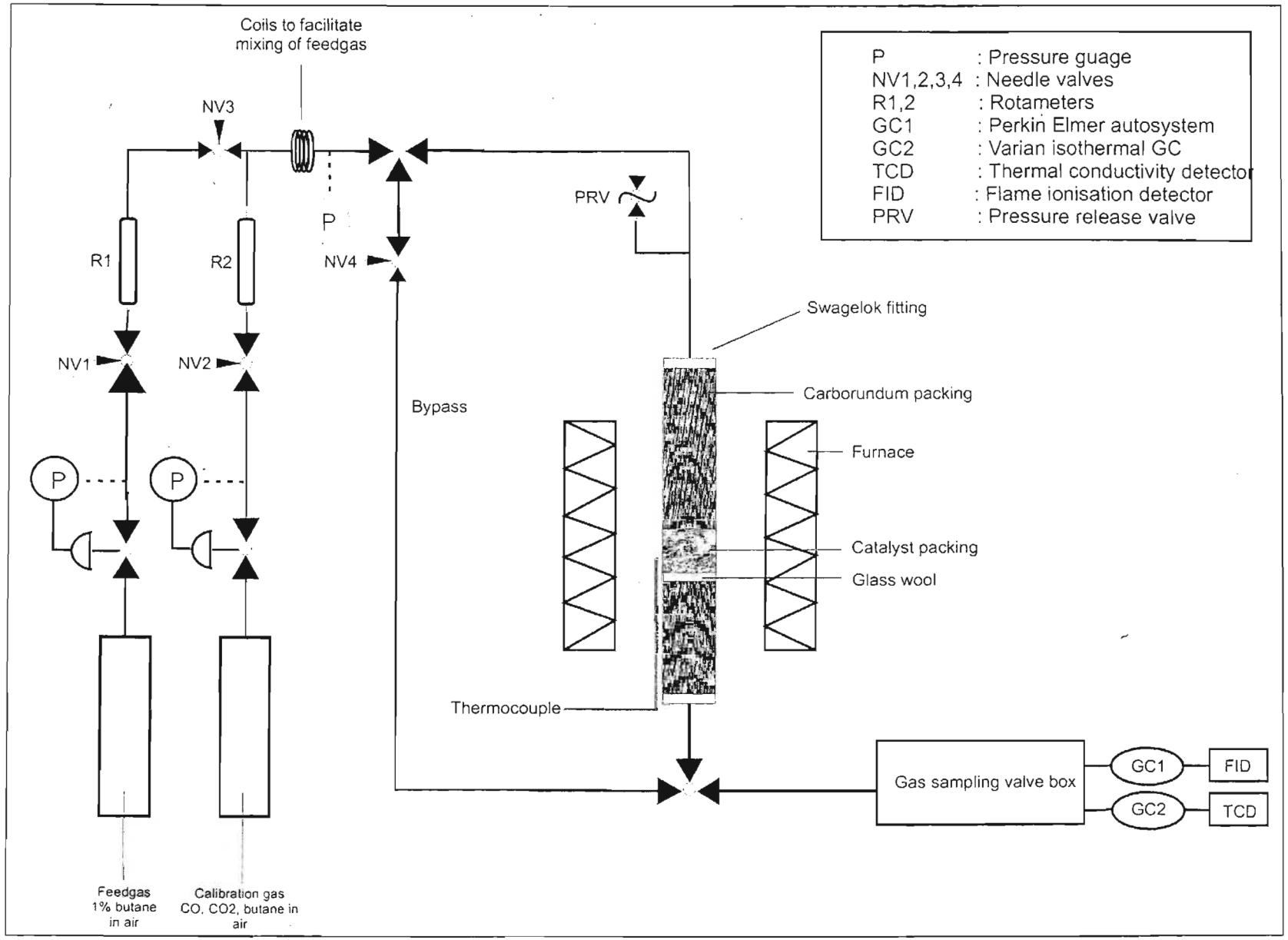

Fig. 3.1. Reactor setup

reactor. The bypass line was used for calibration purposes and checking the mass balance. The line was fitted with an on/off valve (NV4) to prevent bleed of gas when not in use. A pressure release valve (PRV) ensured a safe operating pressure for the reactor tube, which was quartz. The PRV was set at 120 kPa. The supply line to the reactor was fitted with a rubber o-ring connector to connect the copper tube to the 10 mm outer diameter and 7 mm inner diameter quartz reactor tube.

A rubber o-ring sealed the connection at both the inlet and outlet points of the reactor (Fig. 2, Appendix 1). A 300 mm long split block furnace was employed to supply heat for the reaction of *n*-butane with air under catalytic conditions. The products from the reactor were corrosive at high temperature and thus stainless steel tubing was employed after the reactor. 1 g neat catalyst was packed towards the middle of the 500 mm quartz reactor tube as illustrated in Appendix 1. The reactor tube had a 7 mm inner diameter and a 10 mm outer diameter. Carborundum was packed on either side of the catalyst. The carborundum packing before the catalyst further mixed the feed stream gases. It was also necessary to preheat the gases before they reached the catalyst bed to ensure a constant temperature in the catalytic zone. The carborundum packing served this purpose as well. Glass wool was packed at the ends of the reactor tube. The carborundum and glass wool after the catalyst bed served to prevent any particulate matter from entering the product stream and entering the valves downstream from the reactor. A thermocouple was placed on the outside wall of the reactor tube to monitor the temperature of the catalyst. The thermocouple was connected to a temperature controller that was mounted on a control panel. The stainless steel product stream line leaving the reactor was heated to 160°C to prevent condensation of any solid product in the lines. A three-way valve after the reactor controlled flow from either the bypass or the reactor to the gas sampling box which was the initial step in the analytical process.

3.2.The analytical system

3.2.1 The gas sampling box

Two GCs were employed in the analysis of the products from the reactor. An isothermal Varian 3700 GC separated and monitored air, CO and CO_2. A Perkin Elmer XL autosystem GC separated and monitored all other products, which included unreacted *n*-butane, MA and acetic acid. The gas-sampling box contained two Valco rotary valves connected to electronic switches that controlled them (Fig. 3, Appendix 1). The lines entering the gas-sampling box were the reactor product stream line and the return line from the pre-column of the Varian 3700 GC. The lines exiting the gas-sampling box were the sample feed to the pre-column of the Varian 3700 GC, feed line to analytical column of the Varian 3700 GC and the feed line to the Perkin Elmer GC. There was a 10 port rotary valve as well as a 6 port rotary valve in the gas sampling box. Both valves contained a 500 μL sampling loop. These rotary valves were attached to a heater plate that kept them at a temperature of 160°C to prevent condensation of the products from the reactor in the valves. The 10 port rotary valve sampled to the Varian 3700 GC, whilst the 6 port rotary valve sampled to the Perkin Elmer GC. The Varian 3700 GC was equipped with a pre-column that trapped components that are solid at room temperature and only allowed the gases, i.e. air, CO and CO_2 to go through to the analytical column and be detected by the thermal conductivity detector (TCD). The pre-column in the Varian GC was maintained at room temperature, thus making it possible to trap all products except gaseous products at room temperature. This column was flushed after every week of operation by increasing the temperature of the column to 180°C and applying a flow of helium gas through the column and out to waste.

3.2.2. Operation of the sampling valves

The operation of the 10 port valco rotary valve is illustrated in Fig. 3.2. The valves were electronically controlled by the Perkin Elmer GC. Pressurised air was used to turn the valves. The pressure was built and released automatically in the control of the valves. Helium gas,

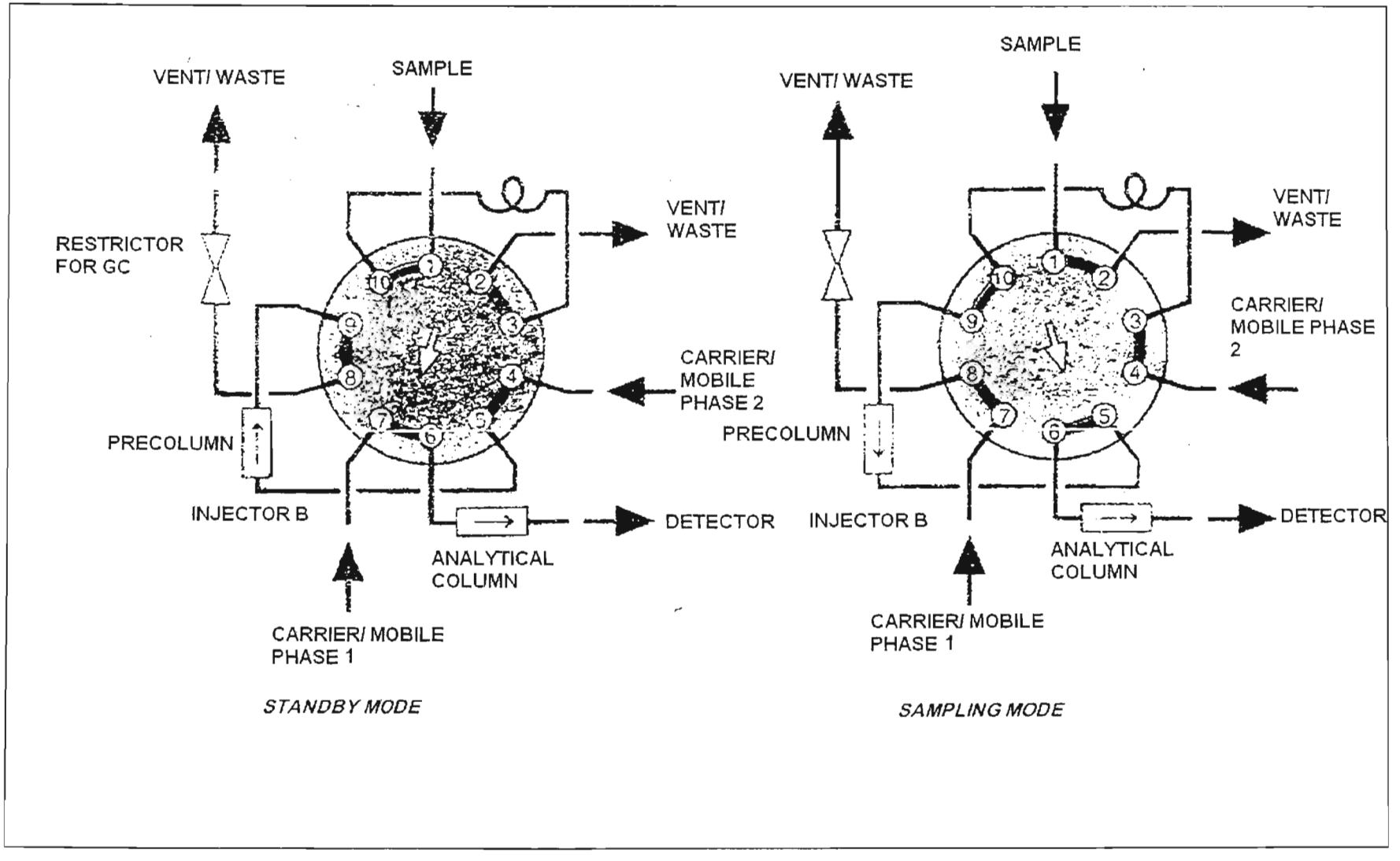

Fig. 3.2. 10 port Valco rotary valve that samples to the isothermal Varian 3700 GC

which was the carrier gas, flowed into port 7 and out through port 6 and then through the analytical column and the detector in the standby position of the valve. The mobile phase flowed in through port 4 and then out port 5, through the injector and through the pre-column, into port 9 and out through port 8, through a restrictor and then vented. Sample from the reactor flowed in through port 1, through the sample loop and then vented. The restrictor regulated the pressure in the system. In the sampling mode, that was when the valve was automatically turned clockwise, carrier gas flowed through port 7 and out through 8 to waste.

Carrier gas also flowed into port 4 through the sample loop, containing sample from the reactor and then followed a sequence through the pre-column, the analytical column and the detector. When the valve turned back to the standby mode, flow through the pre-column was in the opposite direction towards the waste line, which prevented any solid material traveling in the direction of the TCD. The pre-column thus enabled only the carbon oxides and air to pass through to the analytical column and subsequently to the TCD because when the valve turned, the sample containing essentially carbon oxides entered the analytical column in the Varian 3700 GC whilst the other products in the sample were flushed out.

The 6 port rotary valve that sampled to the Perkin Elmer GC, operated in the same manner. There was no pre-column attached to the 6 port valve. When the 6 port valve turned from standby to sampling mode, the sample in the sample loop was flushed directly into the analytical column in the Perkin Elmer GC. The only difference between the 6 port and 10 port valve setup was the inclusion of a pre-column with the 10 port valve.

3.3. Materials

The CO, CO_2 and *n*-butane standards for GC calibration were taken from a premix gas cylinder containing these components in a balance of air.

Material	Usage	Molar-mass /g.mol^{-1}	Supplier	% Purity
n-butane in air	Feedgas	58.12	Fedgas	1 % *n*-butane, balance air special mixture
Phthalic anhydride (PA)	Calibration	148.12	Saarchem	99 %
MA	Calibration	98.06	Saarchem	99 %
CO, CO_2, *n*-butane in air	Calibration	CO : 28.01 CO_2: 44.01	Fedgas	1.0 % CO, 1.1 % CO_2, 1.0 % *n*-butane in air 0.58 % CO, 0.62 CO_2, 0.58 % *n*-butane in air 0.19 % CO, 0.18 % CO_2, 0.19 % *n*-butane in air
Acetic acid	Calibration	60.05	Acros	99.8 %
1-Butene	Calibration	56.11	SASOL	99 %

Table 3.1. Feed and product materials

3.4. Product analysis

A CP-Sil 24CB column, which was installed in the PE GC, was capable of separating unreacted *n*-butane, MA, acetic acid and phthalic anhydride. A typical gas chromatogram is included in Appendix 1. The retention times were as follows: unreacted *n*-butane (0.76 s), acetic acid (0.844), MA (2.85) and phthalic anhydride (11.29). The Carboxen™ 1000 column, which was installed in the Varian 3700 GC, was capable of separating CO and CO_2. The retention times were as follows: CO (5.54) and CO_2 (56.98) (Appendix 1). A chromosorb WHPSP pre-column was installed in the Varian 3700 GC and was used to separate gaseous products from other products at room temperature. The specifications of these columns appear in Appendix 1.

3.5. Catalyst

3.5.1. Catalyst preparation

Reagent	Molar-mass/ g.mol^{-1}	Supplier	% purity
V_2O_5	181.88	Aldrich	98+ %
ortho-H_3PO_4	98.00	Fluka	98+ %
Benzyl alcohol	104.14	Aldrich	99 %
Iso-butanol	74.12	Rochelle chemicals	98.5 %
$Co(acac)_3$	356.26	Acros	99 %

Table 3.2. Reagents for catalyst preparation

An organic synthetic route was followed in the synthesis of the VPO catalyst. V_2O_5 (10 g, 0.055 mol) was added to a 3:2 volumetric ratio of *iso*-butanol:benzyl alcohol solvent mixture (100 ml) which reduced the V_2O_5. Powdered $Co(acac)_3$ was added to the mixture before refluxing. The $Co(acac)_3$ amounts, added during the reduction stage of the synthesis, were varied for different promoter loaded catalysts: VPO-1 (0 g); VPO-2 (0.49 g, 0.0014 mol); VPO-3 (0.97 g 0.0027 mol) and VPO-4 (1.94 g, 0.0055 mol). The mixture was refluxed for seven hours. The reflux mixture was cooled overnight. *ortho*-H_3PO_4 (11 g, 0.11 mol) was added to the cooled mixture and refluxed for a further 3 hours. The mixture was cooled and filtered through hardened (541) ashless filter paper to yield a precipitate, which was the catalyst precursor. The precipitate was washed with 20 ml *iso*-butanol solvent. The precipitate was initially dried overnight in an oven set at 100°C under an air atmosphere and then calcined under a nitrogen atmosphere at 450°C for 5 hours to yield a black catalyst regarded as the calcined catalyst (Sookraj, S.H. *et al.* (1999). The unpromoted catalyst (VPO-1) was similarly synthesized with the exception of adding $Co(acac)_3$ during the reduction step.

3.5.2. Labeling the catalysts

The catalysts with different promoter loading and P:V ratios shall be labeled as indicated in Table 3.3. The BET surface areas of the calcined catalysts and the average V oxidation states (AV) of the precursor, calcined and used catalysts are presented as well.

		ICP-AES RESULTS		EDX RESULTS		AV	BET
Label	Catalyst	% Co:V(molar)	P:V(molar)	% Co:V(molar)	P:V(molar)		Area(m2/g)
VPO-1p	precursor	0.00 (±0.00)	1.09 (±0.02)	0.00 (±0.00)	0.80 (±0.04)	4.30 (±0.02)	
VPO-1c	calcined	0.00 (±0.00)	1.11 (±0.01)	0.00 (±0.00)	0.85 (±0.01)	3.98 (±0.05)	14.83
VPO-1u	used	0.00 (±0.00)	1.11 (±0.01)	0.00 (±0.00)	0.81 (±0.10)	4.39 (±0.02)	
VPO-2p	precursor	1.31 (±0.04)	1.04 (±0.02)	1.22 (±0.18)	0.73 (±0.04)	4.17 (±0.01)	
VPO-2c	calcined	1.24 (±0.04)	1.06 (±0.02)	1.18 (±0.06)	0.88 (±0.05)	4.21 (±0.02)	16.87
VPO-2u	used	1.23 (±0.03)	1.04 (±0.02)	1.06 (±0.02)	0.79 (±0.08)	4.32 (±0.03)	
VPO-3p	precursor	2.33 (±0.03)	1.06 (±0.03)	2.76 (±0.07)	0.74 (±0.06)	4.22 (±0.01)	
VPO-3c	calcined	2.27 (±0.04)	1.05 (±0.02)	2.44 (±0.04)	0.79 (±0.10)	4.14 (±0.02)	22.93
VPO-3u	used	2.24 (±0.01)	1.06 (±0.01)	2.41 (±0.06)	0.80 (±0.03)	4.36 (±0.02)	
VPO-4p	precursor	4.21 (±0.05)	1.04 (±0.03)	4.13 (±0.16)	0.75 (±0.03)	4.24 (±0.01)	
VPO-4c	calcined	4.32 (±0.02)	1.02 (±0.01)	4.19 (±0.26)	0.85 (±0.03)	4.24 (±0.01)	13.22
VPO-4u	used	4.07 (±0.02)	1.04 (±0.02)	4.12 (±0.11)	0.74 (±0.05)	4.33 (±0.01)	

Table 3.3. Catalysts labeled according to their molar P:V ratios and Co:V molar percentages

3.5.3. Catalyst characterization

The catalyst under study was a Co promoted VPO catalyst. Fourier transform-infrared (FT-IR), attenuated total reflectance (ATR), X-ray diffraction (XRD), Brunauer-Emmet-Teller (BET) surface area, Energy dispersive X-ray spectroscopy (EDX), Scanning electron microscopy (SEM), Inductively coupled plasma-atomic emission spectroscopy (ICP-AES) and average V oxidation state (AV) analyses were used to characterize the catalyst. The theoretical aspects of each of these techniques are discussed in more detail in Appendix 3.

3.5.3.1. X-ray diffraction measurements

The XRD spectra were recorded on a Philips PW1130 instrument. Details of the instrument appear in Appendix 2.

3.5.3.2. Scanning electron microscopy (SEM)/Energy dispersive X-ray (EDX) analyses

The catalyst samples were analysed and viewed on a Hitachi S520 scanning electron microscope fitted with a Link ISIS energy dispersive X-ray analytical system. A spatula tip of catalyst sample was used in the SEM and EDX analyses. The sample was stuck onto a disk that

had an adhesive face. The disk was placed on a stage in the instrument before examination and analysis. The catalyst was coated in Au to obtain a stable SEM image of the catalyst by preventing movement of the catalyst during examination under a 10 000 X magnification whilst being bombarded with X-rays.

3.5.3.3. Fourier-transform-infrared (FT-IR) spectroscopy measurements

Fourier transform-infrared (FT-IR) spectra were recorded on a Nicolet 400D infrared spectrometer. The IR spectra were recorded via the KBr pellet sample preparation technique. A spatula tip amount of catalyst sample was placed in a mortar with a spatula full amount of dried KBr powder. All the equipment that made contact with the sample in the preparation of the KBr pellet was ensured to be hot during preparation to prevent moisture being absorbed by the sample. The sample and KBr powder was intimately ground, mixed and eventually compressed into the pellet. The absorption background was the same, as was the concentration of the catalysts in the KBr discs and the procedure of their preparation for all catalysts under investigation. The background for analysis was obtained from the spectrum of a KBr pellet not containing sample.

3.5.3.4. Attenuated total reflectance (ATR)

A Spectra-tech zinc selenite crystal was used to record the IR spectra of the catalyst samples via the attenuated total reflectance technique. The crystal had a refractive index of 2.4. The neat powdered sample was placed on the zinc selenite crystal so as to completely cover the crystal. Pressure was applied to the powdered catalyst sample, by tightening a pressure plate that forms part of the ATR apparatus, to ensure intimate contact between the sample and the crystal. The crystal was placed in the ATR cell. The ATR cell was placed on the stage of the infrared instrument so as to allow the IR beam to pass through the prism of the cell. The IR beam entered the cell on one end, impinged off the interface between the zinc selenite crystal and sample, and

left on the other end. The exit beam met the detector of the instrument. The infrared spectrum was thus recorded.

3.5.3.5. Brunauer-Emmet-Teller (BET) surface area measurements

The catalyst sample was out-gassed at 200°C overnight under a nitrogen flow. The sample was placed into position in a Tristar where it was evacuated prior to being immersed in liquid nitrogen for the analysis. A measured portion of nitrogen was placed in the evacuated sample cell. The sample absorbed a certain amount related to its own intrinsic capacity. This measured volume of gas was then used in calculations to determine volume adsorbed at monolayer coverage for BET, i.e. in the range 0.05 to 0.3 P/P_o, which was the ratio of the pressure in the sample cell to the atmospheric pressure. The pressure in the sample cell was thus compared to atmospheric pressure. The BET total surface area was calculated via the standard calculation developed by Brunauer, Emmet and Teller. The analysis was performed at the Sastech Research and Development Laboratory in Sasolburg.

3.5.3.6. Inductively coupled plasma-atomic emission spectroscopy (ICP-AES) measurements

The P:V molar ratio and Co:V molar percentage was determined using inductively coupled plasma-atomic emission spectroscopy (ICP-AES). The instrument used was a Jobin-Yvon (JY 24). Multi-element standards were prepared containing P, V and Co over the concentration range illustrated in Table 3.2. Microwave digestion was employed to digest the catalysts for ICP-AES analysis. Approximately 0.1 g of catalyst sample was digested in aqua regia (3.5 ml HCl and 1.5 ml HNO_3), following the digestion temperature program set on the microwave. Details of the temperature program are included in Appendix 4. The precursor, calcined and used catalysts were analysed in the same manner. A residue was obtained from the digest of the calcined and spent catalysts. The residue was analysed via EDX to determine the presence of any undigested P, V or Co compounds. The supernatant was separated and made up in 100 ml volumetric flasks with deionised water. The sample solution was diluted 20 times to

yield a concentration within the calibration range. The sample solution was then analysed via ICP-AES. A blank consisting of aqua regia in the same concentration as in the sample solution was made up. A blank correction was employed by subtracting the signal obtained from the blank solution from the sample solution. Multi-element standard solutions consisting of P, V and Co were prepared. The concentrations of elements in the calibration standards appear in Table 3.4.

Element	Wavelength	Standard 1/ ppm	Standard 2/ ppm	Standard 3/ ppm	Standard 4/ ppm	Standard 5/ ppm
P	213.581	10	20	30	40	50
V	309.483	10	20	30	40	50
Co	236.536	2	4	6	8	10

Table 3.4. Selected wavelengths and concentration of calibration standards used for ICP-AES analyses

The procedure of analysis via ICP-AES follows: The extractor fans and gases to the ICP torch were turned on. The extractor fans extract the waste gases from the chamber containing the ICP torch. The ICP flame was ignited. The computer was turned on. A zero order search was performed, which is a method of obtaining a baseline for analysis every time the instrument is turned on. The nebuliser is turned on, ensuring the tube that feeds sample into the ICP flame is immersed in deionised water. The nebuliser controls the flow of sample into the ICP flame. The flame is allowed to stabilise for half an hour. In this time, the method for analysis on the instrument is set.

The wavelength used for analysis of each element, as indicated in Table 3.4, is determined by the detection limit required. These wavelengths are thus selected accordingly. The instrument is set to automatically search for the wavelength specific to the emitting element that is being pumped into the flame. Corrections are employed for any slight variation in

wavelength. The voltage for analysis is set while pumping the highest concentrated standard into the ICP flame.

Calibration graphs for all three elements in the five multi-element standards were obtained from the computer. The zero emission point on the calibration curve was set using water. The computer used the calibration graphs to give concentrations of elements in the samples in the ppm scale. The P:V molar ratios and Co:V molar percentages were calculated using these results.

3.5.3.7. Average vanadium oxidation state (AV)

The average V oxidation state (AV) was determined by a redox titration procedure, largely the same as that employed by Nakamura *et al.* (1974). About 0.1 g of catalyst was dissolved in 17 ml of 12 M *ortho*-H_3PO_4 (98+ %) and boiled till a clear solution was obtained. This solution was added to a mixture of 10 ml concentrated H_2SO_4 in 250 ml water. Graphite was removed by filtration. All V ions were oxidized to V^{5+} by titration with 0.05 N $KMnO_4$ solution. The pentavalent ions were reduced to V^{4+} using a 0.05 N $Fe(NH_4)_2(SO_4)_2$ solution, with 1 % diphenylamine in concentrated H_2SO_4 as an indicator. The average V oxidation state was calculated as:

$$AV = 5 - \frac{(volume\ KMnO_4\ solution)}{(volume\ Fe(NH_4)_2(SO_4)_2\ solution)}$$

3.5.3.8 Gas chromatography-mass spectrometry (GC-MS) analysis

The product from the reactor was bubbled into water. The product was dried on a hotplate and analysed via GC-MS. Cyclohexane solvent was used in the analysis. The mass spectrum indicated the presence of MA when compared to library data.

3.5.4. Experimental procedure for catalyst testing

1 g (approximately 2 cm^3) of neat calcined catalyst was packed tightly in the middle of the 7 mm inner diameter (10 mm outer diameter) quartz reactor tube. The catalyst packing length was approximately 50 mm, which varied according to the particle size of the catalyst. Carborundum, which is inert SiC, was packed on the feed stream end of the reactor tube. The carborundum served to preheat the feed gas before entering the catalyst bed. A plug of glass wool was placed immediately after the catalyst bed to prevent particulate matter from entering the on-line sampling valves and, subsequently, the gas chromatographs.

The gas hourly space velocities (GHSV) and temperatures were varied in the examination of the Co promoted catalyst's ability in selectively converting *n*-butane to MA. The optimum conditions were thus obtained. Optimum conditions were the parameters (temperature, GHSV, Co loading) that gave the highest yield of MA.

Each catalytic run was approximately 200 hrs. The catalyst was maintained at a constant temperature and GHSV for approximately 200 hrs. The first 24 hrs were allowed for conditioning the catalyst at the operating temperature. Conditioning of the catalysts yielded equilibrated catalysts, i.e. catalysts that gave stabilized yields of MA with time on stream.

3.5.5. Gas chromatography for product monitoring

The products were monitored via gas chromatography. A description of the columns employed in the analysis of products from the reactor is given in Appendix 1. The control parameters for both GC's are also provided. The sampling was done automatically via on-line sampling as described in Section 3.2.

3.6. References

Nakamura, K.; Kawai, K.; Fujiwara, Y.; *J.Catal.*; **34** 345 (1974)

Sookraj, S.H.; Engelbrecht, D.; *Cat. Today*; **49** 162 (1999)

CHAPTER 4

RESULTS AND DISCUSSION

4.1. Catalyst synthesis

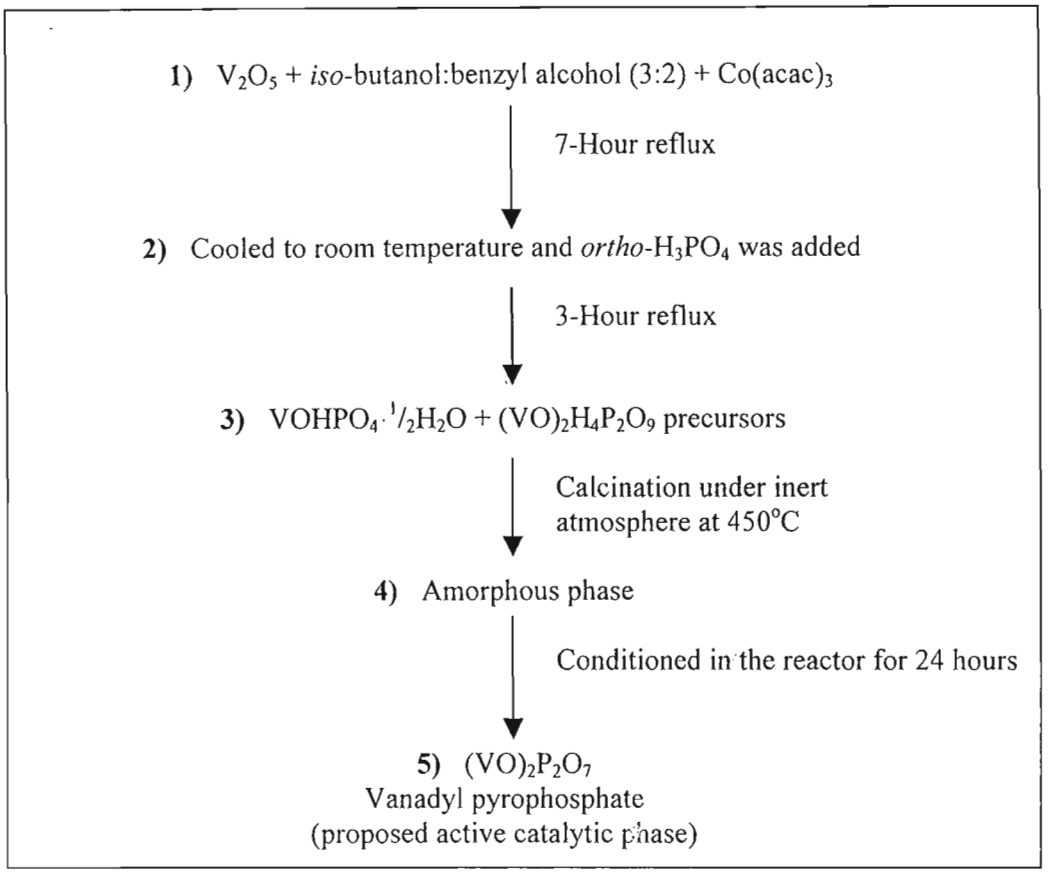

Fig. 4.1. Flow diagram of the synthetic route towards the active VPO catalyst

A flow diagram indicating the major steps towards the synthesis of the active VPO catalyst is presented as Fig. 4.1. Details of the synthesis appear in section 3.5.1. In step 1, shown in Fig. 4.1, the V_2O_5, an alcohol bi-mixture and the Co promoter in the form of a salt is mixed and refluxed for 7 hours.

Co was selected as a promoter in this study due to its known ability to stabilize the loss of oxygen anions during reduction, hence rendering the catalyst less active but more selective (Hodnett, B.K. (1985)). Co is also known to be a structural promoter by creating disorganization in the catalytically active $(VO)_2P_2O_7$ phase, which results in improved selectivity (Cornaglia,

L.M. *et al.* (1999). This disorder creates local modifications, inducing the formation of new active centers for the activation of *n*-butane (Busca, G. *et al.* (1986)). $Co(acac)_3$ was used as the source of the Co promoter as it was available and easily reduced. A 2.5 molar % Co:V promoted catalyst was initially tested. A % Co:V in excess of 20 causes segregation of Co on the surface and gives rise to lower selectivities by catalysing total oxidation reactions and below a value of 2 mol % Co:V, Co enters into solid solution, reduces the surface area and diminishes the reactivity of VPO with hydrogen (Zazhigalov, V.A. *et al.* (1993)), thus 2.5 % was selected. Values around this value was later chosen to determine the optimum promoter loading for the catalyst.

For the unpromoted catalyst, the Co salt addition is excluded in step 1. After a 7-hour reflux, the alcohol solvents are expected to have reduced the V in the mixture from V^{5+} to V^{4+}. Isobutanol solvent was selected as one of the solvents as it is known to reduce V_2O_5. Benzyl alcohol was the other alcohol used due to its ability to become trapped in the interstices of the catalyst and result in defects in the catalyst structure, which are known to improve selectivity towards MA. The Co phases were not seen in the XRD spectra (Appendix 2). This was probably due to the amorphous nature of the phases or their low concentrations in the catalyst. The reflux mixture from step 1 was cooled to room temperature before the addition of *ortho*-H_3PO_4. The addition of *ortho*-H_3PO_4 and further 3-hour reflux completed the reduction of any unreduced V^{5+} to V^{4+} from step 1. A cake was obtained on filtration of the reflux mixture through ashless filter paper. The cake was dried in an oven to give a powder. This powder was known as the catalyst precursor. The yield of the catalyst precursors could not be calculated due to the simultaneous production of two vanadium phases, $VOHPO_4 \cdot {}^1/_2H_2O$ and $(VO)_2H_4P_2O_9$, as revealed by X-ray diffraction (XRD) analysis (Appendix 2). The ratio of these two phases is unknown. The powders of the different promoter loaded catalysts had different colours: VPO-1p (light blue), VPO-2p (light green), VPO-3p (green) and VPO-4p (dark blue). The precursor catalysts were calcined under nitrogen at 450°C to yield an amorphous phase. All calcined catalysts were black in colour. The calcined catalyst was packed into the reactor and conditioned for 24 hours and

tested for approximately 200 hours at different operating temperatures. The catalyst removed from the reactor after testing was referred to as the used catalyst. XRD studies of this catalyst showed the presence of $(VO)_2P_2O_7$, which is the active catalytic phase for the oxidation of *n*-butane to maleic anhydride.

4.2. Catalyst characterization

4.2.1. X-ray diffraction (XRD)

The XRD spectra of the catalyst precursors (VPO-1p, VPO-2p, VPO-3p and VPO-4p) (Appendix 2) were recorded. The calcined catalyst was amorphous in nature and could not be recorded because the X-ray diffraction spectrum is obtained from diffraction of X-rays off the crystalline surface of the sample. The theoretical aspects of this analysis appear in Appendix 3. The XRD pattern of VPO-3u, which was the 2.3 % Co loaded used catalyst, was recorded. It was possible to record the XRD pattern of VPO-3u due to the crystalline nature of the catalyst after reaction on stream in the reactor. There was thus a transition of the catalyst from an amorphous state (calcined catalyst) to a crystalline state (used catalyst). The XRD spectrum of the used VPO catalyst indicated an orthorhombic structure of the catalyst, which was characteristic of the $(VO)_2P_2O_7$ phase (Appendix 2).

The XRD pattern of the precursor catalysts VPO-1p through to VPO-4p (Appendix 2) indicated the presence of two species, viz. $(VO)_2H_4P_2O_9$ and $VO(HPO_4)\cdot{}^1/_2H_2O$. $(VO)_2H_4P_2O_9$ and $VO(HPO_4)\cdot{}^1/_2H_2O$ also gave IR signals in the 900-1 300 cm^{-1} region of the IR spectra of VPO-1p through to VPO-4p (Appendix 5 (FT-IR results) and Appendix 6 (ATR results)). The $(VO)_2H_4P_2O_9$ phase decomposes above 375°C according to Horowitz, H.S. *et al.* (1988).

Only the $(VO)_2P_2O_7$ phase was present in the used catalyst of this study, as at this stage, the catalyst had been exposed to a temperature greater than 400°C during calcination and testing. Coulston, G.W. *et al.* (1997) state that the only detectable phase in aged industrial catalysts is vanadyl pyrophosphate, $(VO)_2P_2O_7$, which contains V^{4+} cations. Nevertheless, Hutchings, G.J. *et al.* (1994) state that $VOPO_4$ (V^{5+}) phases have been observed in working

catalysts through *in situ* laser Raman studies. The $VOPO_4$ phase is probably only seen *in situ*, during a catalytic run, but has not been seen in the XRD spectra of the *ex situ* catalysts (Appendix 2). This $VOPO_4$ phase may be elucidated via on-line XPS or Raman spectroscopic phase characterization techniques. The XRD pattern of the used catalyst in this study (VPO-3u) (Appendix 2) indicated the presence of $(VO)_2P_2O_7$, which is known to be the active catalyst for *n*-butane oxidation to maleic anhydride (Appendix 2). This indicates the presence of the +4 oxidation state of V. Hutchings *et al.* (1991) have shown that the catalyst is more selective towards MA production with most of the V in the +4 oxidation state as opposed to a +5 oxidation state. The average V oxidation (AV) for the used catalyst, however, is just above +4 (Table 4.5). This is indicative of V^{5+} phases also present in the used catalyst. These phases may be in the amorphous state and could not be detected via XRD spectroscopy. One such phase could be the $VOPO_4$ mentioned above. Horowitz (1988) describes the $(VO)_2P_2O_7$ phase as the active catalytic phase and Centi *et al.* (1990) describes the XRD pattern of the used catalyst as being pure $(VO)_2P_2O_7$. However, amorphous phases are not seen along with the crystalline $(VO)_2P_2O_7$ phase. The XRD pattern obtained for VPO-3u, which was the used catalyst, agreed with the literature (Centi, G. *et al.* (1990)).

It was evident from the XRD spectra of VPO-1p through to VPO-4p that the (200) plane reflection intensity decreased with increasing Co loading from VPO-1p through to VPO-4p (Appendix 2). A decrease in intensity was indicative of an amorphous character.

A high BET surface area is indicative of the development of the (100) basal plane of $(VO)_2P_2O_7$ (Sananes-Schulz, M.T. *et al.* (1997)). This plane could not be seen in the XRD spectra because it was not exposed. A picture of the basal plane, however, appears in Fig. 1.5. The catalyst with the highest BET surface area from all four catalysts tested was VPO-3c (Table 4.7). This was the most effective catalyst tested for oxidation of *n*-butane to maleic anhydride as shall be shown later.

The specific reaction rate is known to increase linearly with increasing exposure of the (020) reflection plane. The (020) plane of $(VO)_2P_2O_7$ is characterized by the presence of paired V pseudo-octahedra oriented *trans* to one another, and is claimed to be the catalytically

2θ obtained					Assignment
VPO-1p	VPO-2p	VPO-3p	VPO-3u	VPO-4p	
			14.450		(110)[1]
17.858	17.527	18.038		17.571	(020)[1]
21.412	21.433		21.456	21.542	(111)[1]
22.763	22.746	22.681		22.676	(200)[2]
			26.723		(121)[1]
28.150	28.113	28.119		28.093	(201)[1]
31.499	31.560	31.438		31.369	(031)[1]
33.325	33.365	33.424	33.138	33.132	(102)[1]
			34.167		(131)[1]
35.497	35.424	35.414	34.826	35.526	(112)[1]
37.354	37.224	37.271		37.164	(040)[1]
		39.923	39.316	39.935	(202)[1]
43.724	43.725	43.746	43.647	43.714	(400)[3]
		47.216		47.494	(241)[1]
			50.576		(113)[1]

Table 4.1. 2θ Values obtained from diffractograms (Appendix 2) and respective assignments

[1] Johnson, J.W.; Johnston, D.C.; Jacobson, A.J.; Brody, J.F.; *J. Am. Chem. Soc.*; **106** 8125 (1984)
[2] Sananes-Schulz, M.T.; Tuel, A.; Hutchings, G.J.; Volta, J.C.; *J. Catal.*; **166** 390 (1997)
[3] Brutovsky, M.; Gerej, S.; Vasilco, F.; Gerejova, J.; *Collection Czech. Chem. Commun.*; **47** 1294 (1982)

selective plane (Horowitz, H.S. *et al.* (1988)). The (020) plane reflection was present in all catalysts from VPO-1p through to VPO-4p. Promoters are said to induce the preferential exposure of the (020) plane leading to high activity and selectivity. The (020) plane reflection intensity appeared lower and the peaks broader for promoted catalysts (VPO-2p through to VPO-4p) compared to unpromoted catalyst (VPO-1p) (Appendix 2). Addition of the Co promoter had thus changed the morphology of the catalyst. A decrease in intensity of the (020) plane reflection is known to be attributed to disorder in the plane caused by *trans* to *cis* arrangement of the V=O units about the (020) plane of the idealized $(VO)_2P_2O_7$ structure (Busca, G. *et al.* (1986)). The idealized *trans* conformation of the $(VO)_2P_2O_7$ structure is illustrated in Fig. 4.1.

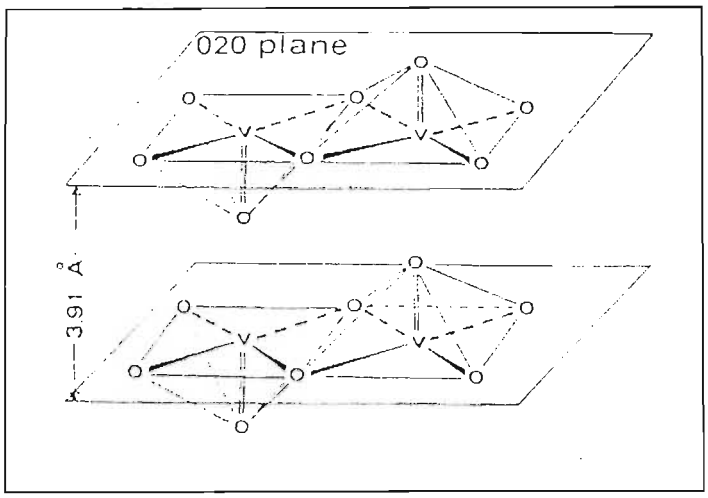

Fig. 4.2. The (020) plane on the surface of the VPO catalyst showing the trans conformation of the $(VO)_2P_2O_7$ structure (Busca, G. et al. (1986))

When transformed to the *cis* isomer, both oxygens on V=O lie above the plane. Busca, G. *et al.* (1986) said that this arrangement leads to the formation of a highly reactive pair of V ions, able to activate the paraffin with a coordinative attack. The (020) plane, which is responsible for enhanced selectivity towards MA, has been less exposed by the addition of the Co promoter, which was evident from the decreased peak intensities in the XRD spectra of the promoted catalysts compared to the unpromoted catalyst. The selectivity towards MA was greatest for catalyst VPO-3 compared to the other catalysts with respect to different conversions of *n*-butane as shown in Fig. 4.18. The addition of the Co promoter did not give spectra which entirely agree with the literature in that there was no increase in (020) plane exposure, however, there was an increase in selectivity towards MA at the optimum promoter loading, which is further discussed in section 4.3.3.

The XRD spectra, nonetheless, showed the presence of the (020) plane. The oxidation of *n*-butane to MA is a 14-electron oxidation involving the abstraction of eight hydrogen atoms and insertion of three oxygen atoms. The (020) plane has been shown to possess Brønsted acid sites and active lattice oxygen (V=O species), which are the two strong functions necessary for the selective oxidation of *n*-butane to MA (Busca, G. *et al.* (1986)). The (020) plane was not

seen in the used catalyst (VPO-3u). An amorphous state of this phase may have been responsible for this.

The intensity of reflections in the XRD spectrum of VPO-4p appeared to be lower than the other catalysts. Brutovsky, M. *et al.* (1982) showed that there is a trend towards modified catalysts generally having lower intensity reflections than the unmodified catalysts. This indicates that the dimension of particles and degree of arrangement of the catalyst structure are lowered with the addition of dopants. In this study there was a low concentration of dopants in the catalysts and there were few discernable changes in the XRD spectra going from VPO-1 (unpromoted catalyst) through to progressively increasing Co loaded catalysts. It was only with an addition of 4.3 molar % Co:V in VPO-4p that this decreased intensity of reflections became apparent (Appendix 2). Looking at the intensity of the (200) plane reflection, which corresponded to a small angle of reflection, it was seen that VPO-4p had the smallest intensity compared to the other catalysts. There was an increase in the line width of the (200) plane reflection in VPO-2p through to VPO-4p compared to unpromoted catalyst VPO-1p. This was indicative of the decreasing size of the crystallites (Guliants, V. *et al.* (1996)). The degree of disorder increased the line width.

VPO-4p appeared to be more amorphous in nature, which was indicated by the lowered reflection intensities in the XRD spectrum compared to the spectra of lower dopant loaded catalysts, viz. VPO-1p, VPO2p and VPO-3p.

4.2.2. Fourier transform-infrared spectroscopy (FT-IR)

FT-IR spectra of the catalyst precursors, calcined catalysts and used catalysts were recorded. A data sheet with assignment of peaks to vibrating species responsible appears in Table 4.2. The catalyst appeared largely amorphous after calcination as indicated by the distinct IR features in the FT-IR spectra shown by the catalyst precursors (VPO-1p through to VPO-4p) in the 900-1300 cm^{-1} region being replaced by a broad absorption band in the calcined catalysts (VPO-1u through to VPO-4u), alluding to a variety of degrees of phosphate condensation

(Appendix 3). The spectra of the calcined catalysts were somewhat simpler than the catalyst precursor spectra. The used catalyst showed distinctive IR features again. The catalyst thus reverted to fewer phosphate phases here, the essential phosphate phase being $(VO)_2P_2O_7$, which was the active catalyst phase (Zazhigalov, V.A *et al.* (1993)). The presence of this phase was confirmed by an XRD spectrum of VPO-3u (Appendix 2).

The FT-IR spectra of the used catalysts, VPO-1u and VPO-4u (Appendix 3), showed a lesser degree of crystallinity compared to VPO-2u and VPO-3u. This was noted by the less distinctive IR features in the spectra of VPO-1u and VPO-4u compared to VPO-2u and VPO-3u in the 900-1300 cm^{-1} region. The used unpromoted catalyst (VPO-1u) revealed a similar IR spectrum as the used 4.2 mol % loaded catalyst (VPO-4u). The optimally functioning used catalyst VPO-2u and VPO-3u, which had intermediate Co loadings, showed similar IR spectra. These catalysts indicated a more crystalline state. The peak intensities of the modified and unmodified catalysts appeared to be the same.

Spectra of the catalyst precursor showed the following adsorption bands in the region 1200-420 cm^{-1}: 1196, 1131, 1102, 1051, 975, 928, 685, 640, 547, 475, 422 cm^{-1} (Table 4.2). The bands with wavenumbers greater than 700 cm^{-1} were attributed to valence vibrations of P-O bonds in various anions of P with O, and the bands in the region below a wavenumber of 700 cm^{-1} were assigned to deformation vibrations of these groupings (Brutovsky, M. *et al.* (1982)). The intense absorption bands occurred in the wavenumber region of 970-1200 cm^{-1}, which are indicated by (s) for strong in the Table 4.2. Weak and medium intensities are indicated by (w) and (m) respectively in the table. The molecules and their respective anion responsible for the stretching frequencies are given in Table 4.2.

The FT-IR spectra of the unmodified catalysts have been studied (Bordes, E. *et al.* (1979); Nakamura, M. *et al.* (1974)) and the results published agreed with those obtained in this study.

VPO-1p	Signal Strength	VPO-1c	Signal Strength	VPO-1u	Signal Strength	VPO-2p	Signal Strength	VPO-2c	Signal Strength	VPO-2u	Signal Strength	Vibration	Anion
422	m											Deformation Vibrations	
										435	m		
475	m					482	w						
547	m	580	m	558	m	533	w			512	w		
								589	w	559	s		
640	s			631	m	639	m			632	s		
685	m					697	w					ν_sPOP	Cycl. $P_4O_{12}^{4-}$
735	w			743	m	731	w			743	w	ν_sPOP	Cycl. $P_4O_{12}^{4-}$ $P_2O_7^{4-}$
785	w					787	w			798	w	ν_sPOP	Cycl. $P_4O_{12}^{4-}$
928	m			937	s	926	m	937	s	947	s	ν_{as}POP	$P_2O_7^{4-}$
975	s					974	s	988	s	1013	m	ν_{as}POP	$P_2O_7^{4-}$
1051	m			1061	s	1049	m			1061	s	$\nu_s PO_3$	$P_2O_7^{4}$
1102	s	1108	s			1102	s	1105	s	1128	m	ν_sO-PO$^-$	Cycl. $P_4O_{12}^{4-}$
1131	m			1125	s	1129	m			1154	s	ν_sO-PO$^-$	Cycl. $P_4O_{12}^{4-}$
1196	s			1157	s	1198	s			1248	s	ν_{as}O-PO$^-$	Cycl. $P_4O_{12}^{4-}$
1361	w											ν_{as}O-PO$^-$	PO_3^-
1381	w					1382	w					ν_{as}O-PO$^-$	PO_3^-
1453	w					1454	m						
1495	w					1501	w	1634	m	1636	w		
1642	w	1619	w	1631	m	1638	m						
						1713	w						
2341	m	2341	w	2331	w	2334	w	2322	m			CO	
2359	m	2359	w	2357	w	2365	w	2364	m			CO	
2852	w					2846	w						
2919	w					2929	w						
						3032	w						
						3068	w						
3360	s	3345	w	3426	s	3388	s	3345	m	3431	m		
3668	w												

Table 4.2. FT-IR spectroscopy data from bulk analysis of catalyst sample

VPO-3p	Signal Strength	VPO-3c	Signal Strength	VPO-3u	Signal Strength	VPO-4p	Signal Strength	VPO-4c	Signal Strength	VPO-4u	Signal Strength	Vibration	Anion
411	s							412	w			Deformation Vibrations	
								440	w				
479	m					486	w	465	w				
528	m	527	w			520	w	519	w	512	w		
		568	w	585	m	552	w			559	m		
640	s	639	w	640	m	641	m	646	w	634	m		
		665	w			668	m	665	w				
684	m					696	m					ν_sPOP	Cycl. $P_4O_{12}^{4-}$
				749	w	746	w			742	w	ν_sPOP	Cycl. $P_4O_{12}^{4-}$ $P_2O_7^{4-}$
781	w					808	w			792	w	ν_sPOP	Cycl. $P_4O_{12}^{4-}$
920	m					924	m	931	s	938	s	ν_{as}POP	$P_2O_7^{4-}$
973	s	970	s	968	s	975	s	978	s			ν_{as}POP	$P_2O_7^{4-}$
1049	m			1090	m	1047	m	1104	s	1063	s	$\nu_s PO_3^-$	$P_2O_7^{4}$
1102	s	1108	s			1103	s			1132	s	ν_sO-PO$^-$	Cycl. $P_4O_{12}^{4-}$
1139	m			1147	m					1153	s	ν_sO-PO$^-$	Cycl. $P_4O_{12}^{4-}$
1200	s			1250	m	1202	s	1195	s	1216	s	ν_{as}O-PO$^-$	Cycl. $P_4O_{12}^{4-}$
						1328	w					ν_{as}O-PO$^-$	PO_3^-
						1404	w					ν_{as}O-PO$^-$	PO_3^-
1459	w					1450	w						
1646	m	1625	w	1642	w	1639	w	1632	w	1631	w		
		1730	w										
1980	w												
2236	w												
2335	m	2327	w	2333	w	2342	s	2336	m	2340	w	CO	
2361	m	2360	w	2367	w	2359	s	2361	m	2357	w	CO	
		2851	w	2855	w			2847	w	2844	w		
		2920	w	2925	w			2924	w	2913	w		
3323	s	3356	m	3439	m			3341	m	3440	m		
3613	w					3589	w						

Table 4.2. (continued) FT-IR spectroscopy data from bulk analysis of catalyst sample

Bordes, E. *et al.* (1979) considered the bands in the region 1050-1200 cm^{-1} (Table 4.2) to belong to the corresponding vibrations of ortho-, pyro-, tri- and higher linear phosphate ions. This region produced the strong stretching frequencies. The used catalyst, which XRD studies indicated as $(VO)_2P_2O_7$ (Appendix 2), showed stretching frequencies in the FT-IR spectra of VPO-1p through to VPO-4p at wavenumbers: 743, 937 and 1061, which were assigned to vibrations ν_s(POP), ν_{as}(POP) and $\nu_s(PO_3)$ respectively. Bordes, E. *et al.* (1979) assigned the wavenumbers of the anions ν_s(O-PO^-) and ν_{as}(O-PO^-). These peaks are often very close and therefore it was difficult to assign the observed bands unambiguously. These assignments appear in Fig. 4.3. It is also noteworthy that Bordes, E. *et al.* (1979) are of the opinion that an absorption at about 1000 cm^{-1} is due to the valence vibration of the V=O bond in the catalysts. Nakamura, M. *et al.* (1974) has shown that in the spectra of Co doped catalysts, the absorption band of the V=O bond is shifted towards lower wavenumbers and is overlapped by the more intensive band ν_{as}(POP) at about 980 cm^{-1}.

The Co doped catalyst precursors exhibited an absorption band in the region of 680 cm^{-1}. This was assigned to the $P_4O_{12}^{4-}$ ion with C_{2h} symmetry (chair conformation). The intensity of this band was lower for the optimally performing VPO-3p catalyst compared to the other catalysts.

The intense bands present around wavenumbers 970, 1100 and 1200 cm^{-1}, which were assigned to ν_{as}(POP) [$P_2O_7^{4-}$ anion], ν_s(O-PO^-) [cyclic $P_4O_{12}^{4-}$ anion] and ν_{as}(O-PO^-) [cyclic $P_4O_{12}^{4-}$ anion] respectively, appeared in the doped and undoped precursor and used catalysts.

The fact that the XRD spectra of the modified catalysts contained practically only the reflections due to $(VO)_2P_2O_7$, whereas the FT-IR spectra exhibited bands that could be assigned to vibrations of two anions ($P_2O_7^{4-}$ and cyclic $P_4O_{12}^{4-}$), can be explained by these latter anions being present in the X-ray amorphous state. The band at around 3400 cm^{-1}, which appeared in spectra of the precursor, calcined and used catalysts, did not match a standard water peak when compared. It was most likely due to the alcohol mixture (benzyl alcohol and *iso*-butanol) used in the synthesis of these catalysts, which became trapped in the lattice of the catalyst.

4.2.3. Attenuated total reflectance (ATR)

The zinc selenite crystal had a transmission range from 20 000 cm^{-1} to 650 cm^{-1}; thus deformation vibrations could not be seen in the attenuated total reflectance (ATR) spectra.

The peak around 3400 cm^{-1}, which appeared in the precursor, calcined and used catalysts FT-IR spectra (Appendix 5), did not appear in the calcined and used catalyst ATR spectra (Appendix 6). This peak was attributed to the presence of the alcohol mixture (benzyl alcohol and *iso*-butanol) used in the synthesis. ATR was a surface study of the catalyst. This indicated that the alcohol was absent on the surface of the calcined catalyst but rather trapped in the lattice (Appendix 5). Thus the alcohol from the surface of the catalyst appeared to have evaporated during calcination of the catalyst precursor, as would be expected.

Comparison of the peak assignments in Table 4.3 with Table 4.2 showed that the same types of bands were present in both the FT-IR and ATR spectra. This showed that the anions present on the surface of the catalysts, revealed by the ATR study results (Table 4.3), were also present in the bulk of the catalyst shown by the FT-IR study results (Table 4.2). The used catalysts showed a single strong sharp band in the region of 940 cm^{-1} in the ATR spectra compared to the broad band seen in FT-IR spectra of these used catalysts. The surface of the catalyst contained the crystalline $(VO)_2P_2O_7$ phase as revealed by the XRD spectrum of the used catalyst VPO-3u (Appendix 2). This presence of a single distinct crystalline phase is thus believed to be responsible for this sharp band in the ATR study.

VPO-1p	Signal Strength	VPO-1c	Signal Strength	VPO-1u	Signal Strength	VPO-2p	Signal Strength	VPO-2c	Signal Strength	VPO-2u	Signal Strength	Vibration	Anion
								678	w			ν_sPOP	Cycl. $P_4O_{12}^{4-}$
695	m					701	m					ν_sPOP	Cycl. $P_4O_{12}^{4-}$
733	w	743	w			750	m	752	w	750	w	ν_sPOP	Cycl. $P_4O_{12}^{4-}$ $P_2O_7^{4-}$
868	w					835	w					ν_sPOP	Cycl. $P_4O_{12}^{4-}$
927	m	937	s	941	s	927	m	932	s	947	s	ν_{as}POP	$P_2O_7^{4-}$
972	s					974	s	982	s			ν_{as}POP	$P_2O_7^{4-}$
1048	m			1070	w	1053	m			1071	m	$\nu_s PO_3^-$	$P_2O_7^{4-}$
1099	s	1083	s			1103	s	1103	s			ν_sO-PO$^-$	Cycl. $P_4O_{12}^{4-}$
1126	w					1135	w	1136	s	1128	w	ν_sO-PO$^-$	Cycl. $P_4O_{12}^{4-}$
1189	s			1256	w	1191	s			1258	w	ν_{as}O-PO$^-$	Cycl. $P_4O_{12}^{4-}$
						1309	w					ν_{as}O-PO$^-$	PO_3^-
1446	w					1456	w						
						1494	w	1539	w				
						1594	w						
1638	w	1604	w										
						1700	m						
		2332	m	2341	m	2336	m	2325	w				
		2359	m	2356	m	2364	m	2359	w				
						2878	m						
3350	w					3348	m						

Table 4.3. ATR spectroscopy data from the surface analysis of the catalyst sample

VPO-3p	Signal Strength	VPO-3c	Signal Strength	VPO-3u	Signal Strength	VPO-4p	Signal Strength	VPO-4c	Signal Strength	VPO-4u	Signal Strength	Vibration	Anion
		681	w									ν_sPOP	Cycl. $P_4O_{12}^{4-}$
		716	w			703	m					ν_sPOP	Cycl. $P_4O_{12}^{4-}$
		763	w	737	w	750	m			742	w	ν_sPOP	Cycl. $P_4O_{12}^{4-}$ $P_2O_7^{4-}$
834	w									792	w	ν_sPOP	Cycl. $P_4O_{12}^{4-}$
934	m	929	s			926	m	932	s	922	s	ν_{as}POP	$P_2O_7^{4-}$
981	s	976	s	965	s	973	s	979	s			ν_{as}POP	$P_2O_7^{4-}$
1056	m	1098	s			1055	m	1050	s	1058	w	$\nu_s PO_3^-$	$P_2O_7^{4-}$
1106	s					1101	s	1098	s	1126	w	ν_sO-PO$^-$	Cycl. $P_4O_{12}^{4-}$
1140	m	1132	s	1140	m	1137	m	1190	s			ν_sO-PO$^-$	Cycl. $P_4O_{12}^{4-}$
1198	s	1235	w	1234	m	1207	s			1267	w	ν_{as}O-PO$^-$	Cycl. $P_4O_{12}^{4-}$
		1358	w									ν_{as}C-PO$^-$	PO_3^-
		1439	w			1447	w						
		1479	w										
		1513	w										
		1571	w			1541	w						
1639	w	1634	w			1646	w	1610	w				
1706	w					1699	w						
2331	m	2335	s	2330	w	2325	w	2333	w				
2358	m	2361	s	2356	w	2354	w	2356	w				
3355	w					3373	m						

Table 4.3. (continued) ATR spectroscopy data from surface analysis of catalyst sample

4.2.4. Scanning electron microscopy (SEM)

SEM images of the catalyst precursors, calcined catalysts and used catalysts were recorded. The SEM images of the catalyst precursors and calcined catalysts revealed a plate-like morphology (Appendix 8). There was deviation from the ideal rosette shape platelets of typical VPO catalysts. VPO-3p showed a more agglomerated platelet arrangement compared to VPO-1p. The Co doped catalyst (VPO-3p) thus underwent a change in morphology compared to the undoped catalyst (VPO-1p). The platelets on the surface of VPO-1p are larger than those on VPO-3p. An increase in P:V ratio is known to increase the platelet size (Cheng, W.; (1996)). The P:V ratio of VPO-1p was slightly greater than the other catalysts as seen from ICP-AES results (Table 4.4). Larger platelets formed as a result of calcining VPO-3p to yield VPO-3c. The used catalysts show signs of disintegration on the surface as can be seen from the SEM images of VPO-1u through to VPO-4u. The SEM images of VPO-1u through to VPO-3u were similar, however, the SEM image of VPO-4u was different in that pitting occurred on a smoother surface. The platelike morphology on the surface of all used catalysts was lost.

4.2.5. Inductively coupled plasma-atomic emission spectroscopy (ICP-AES)

		Theoretical		Experimental	
Label	Catalyst	%Co/V(molar)	P:V(molar)	%Co/V(molar)	P:V(molar)
VPO-1p	precursor	0.00	1.00	0.00 (±0.00)	1.09 (±0.02)
VPO-1c	calcined			0.00 (±0.00)	1.11 (±0.01)
VPO-1u	used			0.00 (±0.00)	1.11 (±0.01)
VPO-2p	precursor	1.26	1.00	1.31 (±0.04)	1.04 (±0.02)
VPO-2c	calcined			1.24 (±0.04)	1.06 (±0.02)
VPO-2u	used			1.23 (±0.03)	1.04 (±0.02)
VPO-3p	precursor	2.48	1.00	2.33 (±0.03)	1.06 (±0.03)
VPO-3c	calcined			2.27 (±0.04)	1.05 (±0.02)
VPO-3u	used			2.24 (±0.01)	1.06 (±0.01)
VPO-4p	precursor	4.95	1.00	4.21 (±0.05)	1.04 (±0.03)
VPO-4c	calcined			4.32 (±0.02)	1.02 (±0.01)
VPO-4u	used			4.07 (±0.02)	1.04 (±0.02)

Table 4.4. Co:V molar percentages and P:V molar ratios determined by the ICP-AES technique

ICP-AES was a technique used for the analysis of the P:V molar ratio and Co:V molar % in the bulk of the catalyst as opposed to the energy dispersive X-ray (EDX) spectroscopic technique, which was a surface study (Table 4.4).

The samples were prepared for ICP-AES via microwave digestion. The catalyst sample was digested in aqua regia. The digestion temperature program and reagents used are included in Appendix 4. A brittle, orange residue was obtained on completion of the digestion of the calcined and used catalysts. Analysis of the residue via EDX indicated the absence of P, Co or V (Appendix 4). The digested samples separated from the residue were thus representative of the catalyst in terms of P, V and Co content. The EDX study did, however, show the presence of C, O and Cl (Appendix 4). The Cl and O were from the aqua regia, whilst the C was from the alcohol solvents used in the synthesis of the catalyst. An SEM image of the residue indicated the presence of bubbles on the surface (Appendix 4). The FT-IR spectra of the digestion residues of both promoted and unpromoted calcined and used catalysts lacked the presence of the typical phosphate condensation stretches in the region 900-1300 cm^{-1} (Appendix 4). The FT-IR spectra of both promoted and unpromoted calcined catalyst residues appeared similar. This residue formed only in the digests of calcined and used catalysts and not in the digest of precursor catalysts. The residue precursor is thus believed to have formed at the high temperatures (~450°C) to which the catalysts were subjected during calcination.

From Table 4.4 it can be seen that the largest deviation from the theoretical value for the P:V molar ratio was 9 % for VPO-1p. The other catalysts were within 6 % deviation from the theoretical molar P:V ratio. This was probably due to Co fitting into the catalyst lattice more readily than P, therefore reducing the P:V molar ratio. The unpromoted catalyst, VPO-1, thus had a higher P:V ratio. The P:V ratios obtained experimentally were generally higher than the theoretical values. Catalysts VPO-2p through to VPO-4p showed experimental P:V molar ratios within experimental error of each other. The Co:V molar % obtained experimentally deviated by +4 % for VPO-2p, -6 % for VPO-3p and -18 % for VPO-4p from the theoretical values. As can be seen the molar % Co:V values obtained via ICP-AES were generally lower than the

theoretical values (Table 4.4). This indicated that there was less Co incorporated into the lattice of the VPO catalyst with increasing the Co dopant added during synthesis. The excess Co appeared to have been eliminated after synthesis via washing.

4.2.6. Average vanadium oxidation state (AV)

Label	Catalyst	
VPO-1p	precursor	4.30 (±0.02)
VPO-1c	calcined	3.98 (±0.05)
VPO-1u	used	4.39 (±0.02)
VPO-2p	precursor	4.17 (±0.01)
VPO-2c	calcined	4.21 (±0.02)
VPO-2u	used	4.32 (±0.03)
VPO-3p	precursor	4.22 (±0.01)
VPO-3c	calcined	4.14 (±0.02)
VPO-3u	used	4.36 (±0.02)
VPO-4p	precursor	4.24 (±0.01)
VPO-4c	calcined	4.24 (±0.01)
VPO-4u	used	4.33 (±0.01)

Table 4.5. Average vanadium oxidation states with respective standard deviations

Brutovsky, M. *et al.* (1982) found that the optimum AV for a VPO catalyst is just above 4 for oxidation of *n*-butane to maleic anhydride. The AV obtained for all catalysts in this study were between 4 and 4.4 (Table 4.5). The used catalysts had a stabilized AV of between 4.3 and 4.4. The AV of the precursor and calcined catalysts were lower than the used catalysts.

Considering that V switches between oxidation states +4 and +5 during the oxidation of *n*-butane to MA (Section 1.2), it was expected that the catalyst maintained an AV between +4 and +5. Excess P is known to stabilize the +4 oxidation state (Section 1.6) and therefore the stabilized AV was closer to +4 than to +5. V^{5+} is known to activate molecular oxygen (Section 1.2). V^{4+} is known to oxidize *n*-butane. By maintaining most of the V in the +4 oxidation state, the chances of over-oxidation products forming are lower.

4.2.7. Energy dispersive X-ray (EDX) study

		Bulk theoretical values		Experimental	
Label	Catalyst	%Co/V(molar)	P:V(molar)	%Co/V(molar)	P:V(molar)
VPO-1p	precursor	0.00	1.00	0.00 (±0.00)	0.80 (±0.04)
VPO-1c	calcined			0.00 (±0.00)	0.85 (±0.01)
VPO-1u	used			0.00 (±0.00)	0.81 (±0.10)
VPO-2p	precursor	1.26	1.00	1.22 (±0.18)	0.73 (±0.04)
VPO-2c	calcined			1.18 (±0.06)	0.88 (±0.05)
VPO-2u	used			1.06 (±0.02)	0.77 (±0.00)
VPO-3p	precursor	2.48	1.00	2.76 (±0.07)	0.74 (±0.06)
VPO-3c	calcined			2.44 (±0.04)	0.79 (±0.10)
VPO-3u	used			2.41 (±0.06)	0.80 (±0.03)
VPO-4p	precursor	4.95	1.00	4.13 (±0.16)	0.75 (±0.03)
VPO-4c	calcined			4.19 (±0.26)	0.85 (±0.03)
VPO-4u	used			4.12 (±0.11)	0.74 (±0.05)

Table 4.6. P:V molar ratios and Co:V molar percentages determined by the EDX technique

Energy dispersive X-ray (EDX) spectrometry was a non-destructive surface study of the catalyst and is a technique that analyses a specific area on the catalyst surface. A distribution map of the elements on the surface of the catalyst is shown in Appendix 8. The first frame (top left) shows an SEM image of the catalyst surface for VPO-1p (Appendix 8). Going in a clockwise direction from the first frame shows O distribution and then V and P distribution. Likewise, the first frame for catalyst VPO-3p shows the SEM image of the catalyst surface and going in a clockwise direction, O, P, Co and V. The elements occupied the catalyst surface evenly, as shown by EDX spectroscopy measurements. The promoted catalysts were tested in the same manner, indicating an even distribution of Co on the surface. Typical output data from the EDX instrument for sample composition is included in Appendix 3, for an unpromoted (VPO-1) and promoted catalyst (VPO-3).

The molar % Co:V, obtained from the EDX study (Table 4.6), on the surface of VPO-2p compared well within experimental error with the experimental molar % of Co:V in the bulk, obtained from the ICP-AES study (Table 4.4).

The Co:V molar % on the surface of the VPO-3 catalyst was greater than the value obtained for the bulk, when comparing the results obtained from ICP-AES (Table 4.4.) and

EDX (Table 4.6) analyses. For the other catalysts investigated, the bulk values were higher than the surface values. Co is known to stabilize the AV (discussed in Section 1.8.1) so as to improve initial dehydrogenation of *n*-butane and controls the oxygen diffusion and adsorption, thereby minimizing the non-selective oxidation route. This greater Co:V molar % on the surface could thus have improved the activity and selectivity of VPO-3. This was the optimally performing catalyst that shall be discussed later.

The molar P:V ratio on the surface of the catalyst was lower than that in the bulk. The molar P:V ratio on the surface was 0.80 on average for all catalysts. The experimental values obtained via ICP-AES (Table 4.4) for the bulk were around 1.00 for all catalysts. There thus appears to be a greater amount of P below the surface (molar P:V ratio of greater than 1.00) of the catalyst. It must be noted that this is an *ex-situ* study of the catalyst.

4.2.8. Brunauer-Emmet-Teller (BET) surface area measurements

Catalyst	Surface Area (m^2/g)	Bulk Molar % Co:V
VPO-1c	14.83	0.00 (± 0.00)
VPO-2c	16.87	1.18 (± 0.06)
VPO-3c	22.93	2.44 (± 0.04)
VPO-4c	13.22	4.19 (± 0.26)

Table 4.7. Surface area measurements

The surface areas of the calcined catalysts were determined. There was an increase in surface area with increasing promoter loading as indicated by the surface area values from VPO-1c through to VPO-3c as shown in Table 4.7. VPO-4c, however, showed a drop in surface area, yielding a value lower than the unpromoted catalyst, VPO-1c. This suggested that there was an optimum Co:V molar % loading of around 2.3 for VPO-3c for a maximum catalyst surface area. Hodnett (1985) and Sartoni *et al.* (2001) discovered that optimum promoter:V ratios exist for a maximum catalyst surface area, beyond which further addition leads to surface

segregation. This, in turn, leads to a decrease in surface area of the catalyst. The catalysts under study agreed with the literature.

4.2.9. Reactor Variables

4.2.9.1. Residence times

Catalyst	Reaction conditions		Residence Time/s
	Temp/°C	Flowrate/ml.min^{-1}	
VPO-1	Varying	120	1.00
VPO-2	Varying	120	1.31
VPO-3	Varying	120	1.21
VPO-3	400	80	2.16
	400	60	2.69
	400	40	3.75
	300	80	2.16
	300	60	2.69
	300	40	3.75
VPO-4	Varying	120	0.97

Table 4.8. Residence times of n-butane feedgas over different catalysts

The residence time was calculated as the time the feed-gas spent in the catalyst bed and was calculated as follows:

$$\textit{Residence time} = \frac{\textit{volume of catalyst bed/(ml)}}{\textit{volumetric flowrate/ml.s}^{-1}}$$

All catalysts (1 g) were packed tightly into the reactor. There was a difference in the residence time for VPO-1 through to VPO-4 although a constant flowrate was employed through the catalyst bed. The reason was due to a difference in the volume of the catalyst bed. The different catalysts had different surface areas and thus different particle sizes (Table 4.7). For VPO-1c and VPO-4c, the catalyst particles with smaller surface areas, occupied a smaller volume in the reactor by packing more tightly together. VPO-1c and VPO-4c thus yielded shorter residence times compared to VPO-2c and VPO-3c, which had higher surface areas.

The VPO-3 catalyst tested under varying flowrates of feedgas, as anticipated, had varying residence times in the reactor. Larger feedgas flowrates resulted in lower residence times (Table 4.8).

4.2.9.2. Gas hourly space velocity (GHSV)

Catalyst	Reaction conditions		GHSV/hr^{-1}
	Temp/°C	Flowrate/$ml.min^{-1}$	
VPO-1	Varying	120	3598
VPO-2	Varying	120	2751
VPO-3	Varying	120	2878
VPO-3	400	80	1663
	400	60	1336
	400	40	959
	300	80	1663
	300	60	1336
	300	40	959
VPO-4	Varying	120	3981

Table 4.9. GHSV calculated values

The gas hourly space velocity is the ratio of feedgas flowrate over the volume of the catalyst bed in the reactor:

$$GHSV = \frac{flowrate\ (ml.hr^{-1})}{volume\ of\ catalyst\ bed/ml}$$

Catalysts VPO-1 through to VPO-4 were tested at a constant flowrate of 120 $ml.min^{-1}$, however the GHSV values differed. The reason was the same as that for the varying residence times (Table 4.8). Those catalysts that occupied smaller volumes in the reactor had larger GHSV values. The catalyst loading in the reactor was kept constant at 1 g for all catalytic runs.

4.3. Catalyst testing

4.3.1. Setting constant parameters from preliminary results

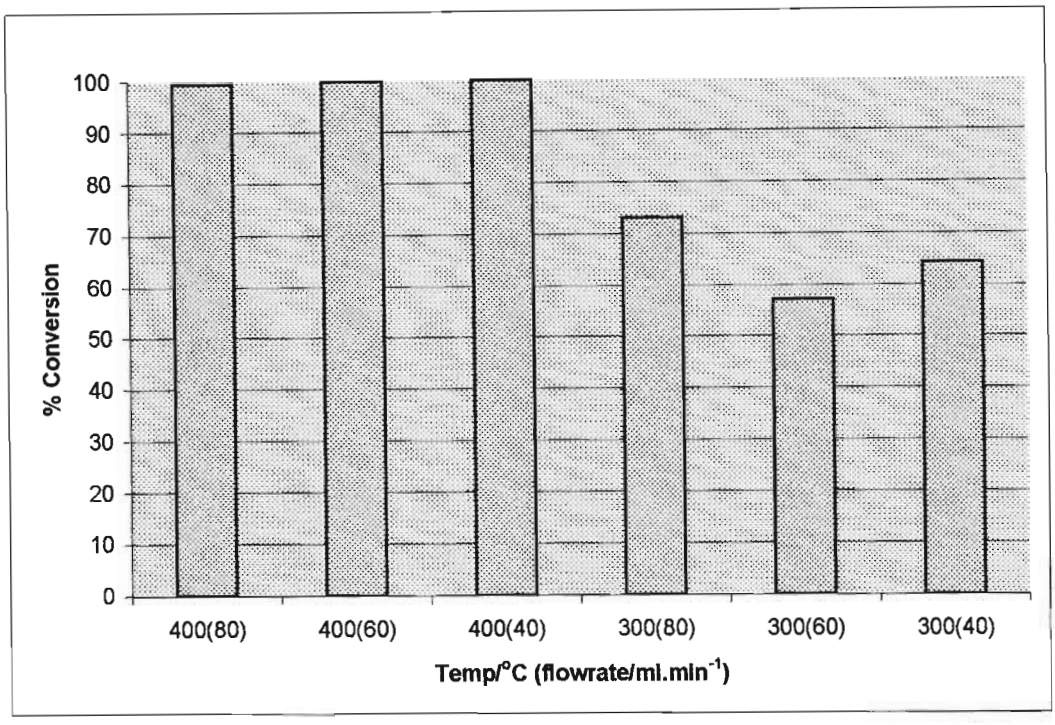

Fig. 4.3. % Conversion of n-butane over VPO-3 with varying temperature and flowrate

Error bars are included on all graphical data. All catalytic runs lasted approximately 200 hours at a constant temperature and GHSV.

The 2.3 % Co promoted catalyst (VPO-3) was initially tested at different temperatures and feed-gas flowrates as shown in Fig. 4.3. The molar carbon mass balance was between 95 and 105 % for all catalytic runs on this catalyst. The P:V molar ratio was 1.06 and the Co:V molar % was 2.33, which were both determined by ICP-AES (Table 4.4). The BET surface area of the catalyst was 22.9 m^2/g (Table 4.7). Conversions of 100 % occurred at a temperature of 400°C. The same high conversions were evident at different flowrates, viz. 80, 60 and 40 $ml.min^{-1}$. The corresponding GHSV values were 1663, 1336 and 959 hr^{-1}. The same flowrates and GHSV values were employed at a lower temperature of 300°C. The % conversion of *n*-butane increased with increasing the GHSV from 959 hr^{-1} to 1663 hr^{-1}, whilst maintaining a

constant temperature of 300°C. Although the % conversion *n*-butane is high at higher temperatures, the yields and selectivities towards MA are low as seen in Figs. 4.4 and 4.5.

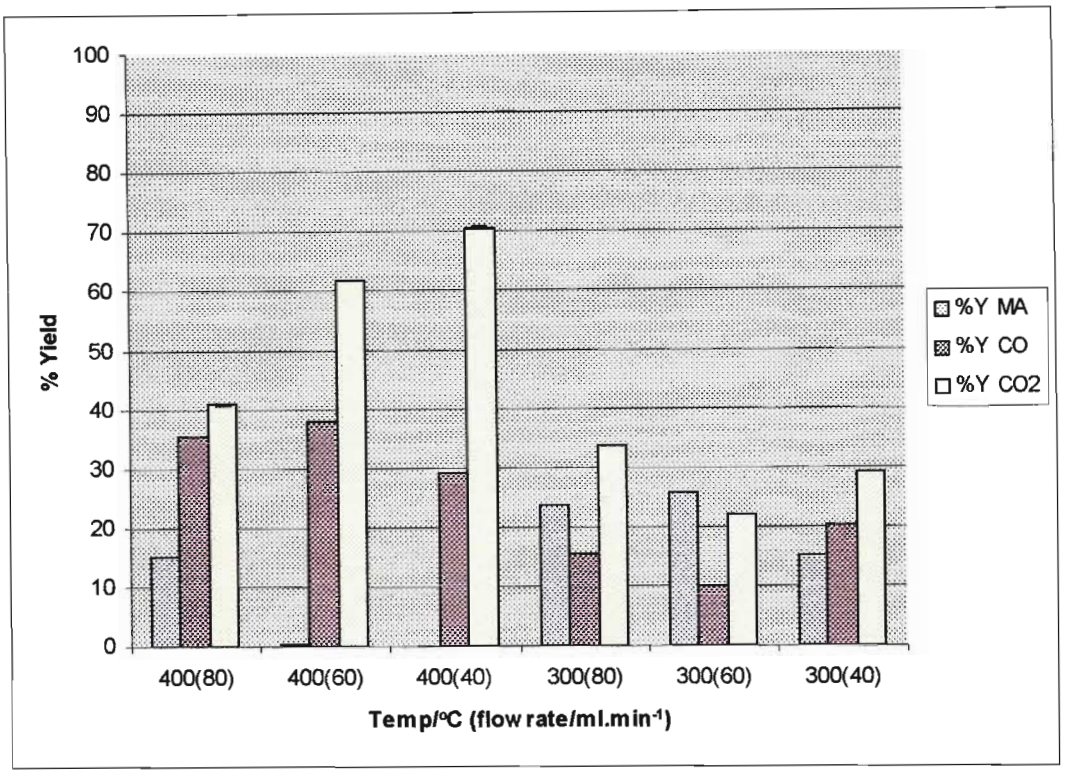

Fig. 4.4. % Yield (%Y) products over VPO-3 with varying temperature and flowrate

Since a Co promoter gives increased selectivity compared to undoped catalysts, a Co promoter was selected and used in this study. A discussion on the motivation for the use of Co as a promoter is given in Section 1.8.1. There appeared to be a greater % yield of MA at 300°C compared to 400°C (Fig. 4.4). The yield of carbon oxides at 400°C dropped significantly with a change in GHSV from 959 hr^{-1} (40 $ml.min^{-1}$) to 1663 hr^{-1} (80 $ml.min^{-1}$) (Fig. 4.4). Higher flowrates at high temperatures appeared to be favourable for MA production. This was seen from the improved yield (Fig. 4.4) and selectivity (Fig. 4.5) towards MA. The low flowrates meant a higher residence time for feed in the catalyst bed. This led to over-oxidation of the MA product and thus higher carbon oxide production at a temperature of 400°C (Fig. 4.4). Over-oxidation occurred readily at higher temperatures, viz. 400°C, hence this trend of lower carbon oxide production at higher GHSV values was not observed at a lower temperature of 300°C. The

optimum flowrate for MA production at 300°C was 60 ml.min^{-1} (GHSV=1336 hr^{-1}). This was marked by the highest yield of MA (Fig. 4.4) and selectivity towards MA (Fig. 4.5). Higher selectivities towards MA were obtained at lower temperatures (Fig. 4.5), however, it must be noted that the % conversions of *n*-butane were 30 % lower at an operating temperature of 300°C compared to 400°C for a 80 ml.min^{-1} flowrate (Fig. 4.6). A higher conversion of *n*-butane was obtained at a flowrate of 120 ml.min^{-1} (Fig. 4.12).

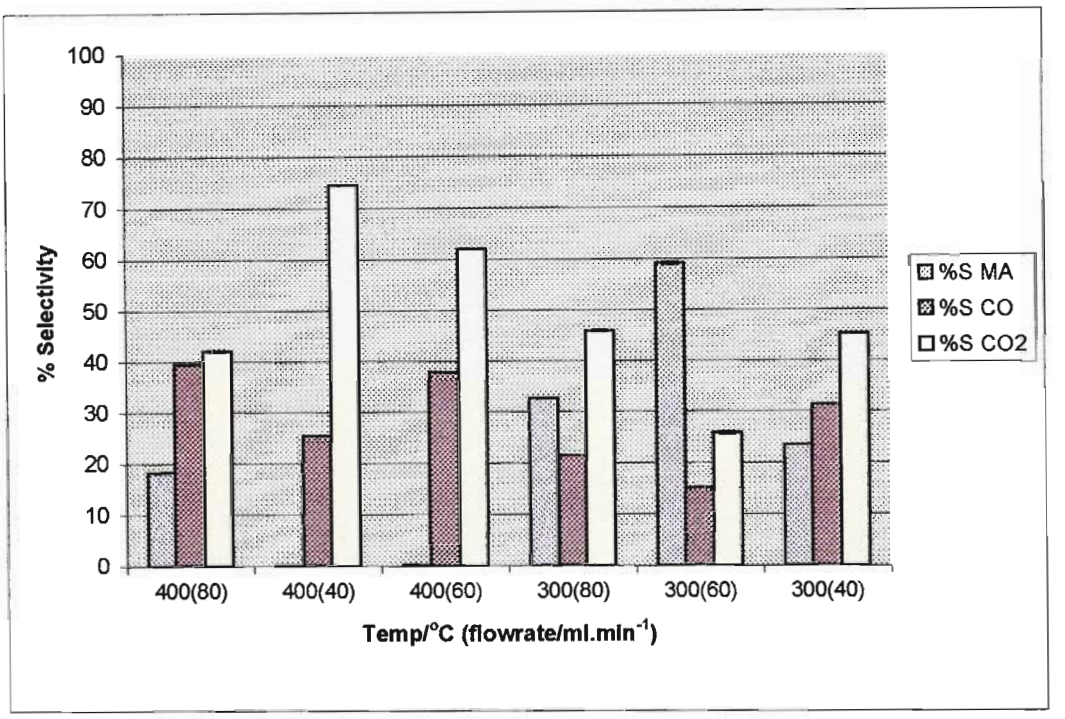

Fig. 4.5. % Selectivity (%S) products over VPO-3 with varying temperature and flowrate

The aim was to develop a catalyst that gave high conversion of *n*-butane whilst maintaining a high selectivity towards MA at a low operating temperature, i.e. below 400°C, which is generally employed by industry. Higher conversions resulted at higher temperatures (400°C), however, there was the problem of over-oxidation products. Reducing the residence time of the feed by increasing the flowrate of the feed-gas resulted in less carbon oxide production relative to MA as shown in Fig. 4.5.

A constant flowrate of 120 ml.min^{-1} was maintained for all successive studies on this catalyst and the other modified catalysts whilst varying the temperature. This flowrate was selected because it gave the highest conversion of *n*-butane at a temperature of 300°C (Fig. 4.12). This was also the highest obtainable flowrate in the reactor. The plug of powdered catalyst in the reactor prevented any higher flowrate through. Modified catalysts referred to the varying concentrations of Co dopant in the catalysts. Each catalyst shall be discussed separately.

4.3.2. Systematic testing of catalysts

4.3.2.1. VPO-1

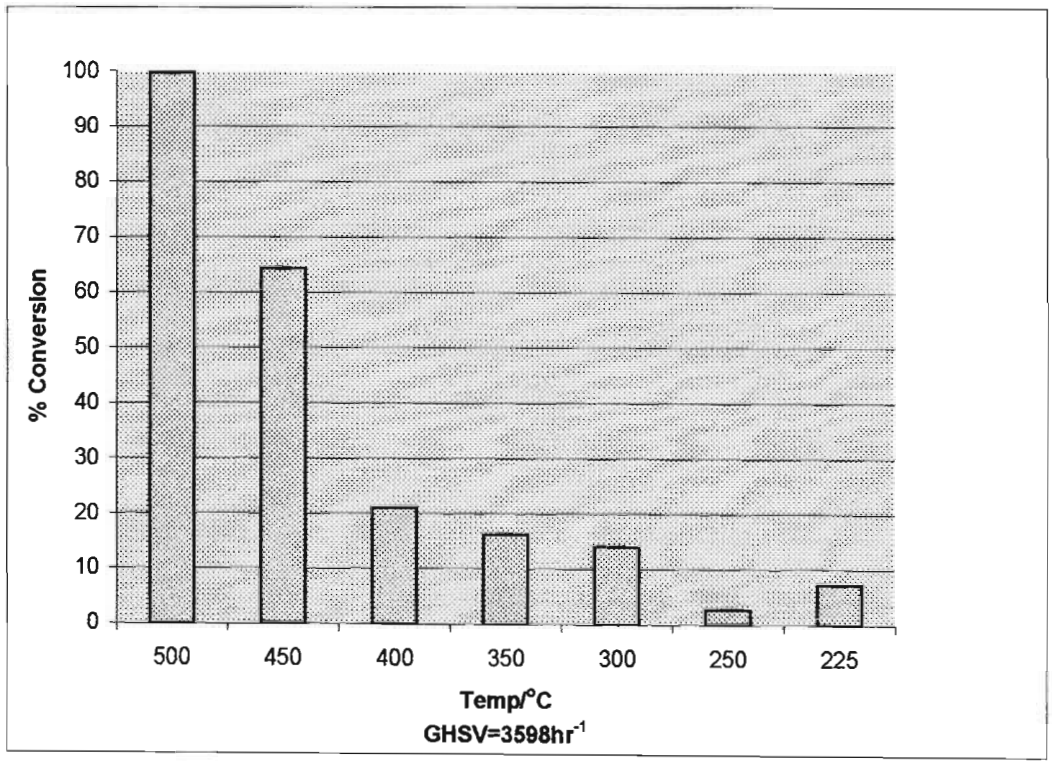

Fig. 4.6. % Conversion of n-butane for VPO-1 at a constant GHSV of 3598 hr^{-1}

This catalyst precursor had a molar P:V ratio of 1.09 (Table 4.4) and was unpromoted. The surface area was 14.8 m^2/g (Table 4.7). The molar carbon mass balance was between 95 and 105 % for all tests carried out on this catalyst. A GHSV of 3598 hr^{-1} was calculated.

A 100 % conversion of *n*-butane was obtained for the 500°C run and this significantly decreased with decreasing temperature (Fig. 4.6). The conversion of *n*-butane at 500°C was mainly due to carbon oxides and only negligible amounts of MA were obtained.

The highest molar % selectivity of 87 % MA was obtained at a temperature of 225°C with a low % conversion of *n*-butane of 7 %. The catalyst had low activity at low temperatures, and therefore the conversion was low at these temperatures. The yield of over-oxidation products at low conversions of *n*-butane dropped to below 2 % (Fig. 4.8).

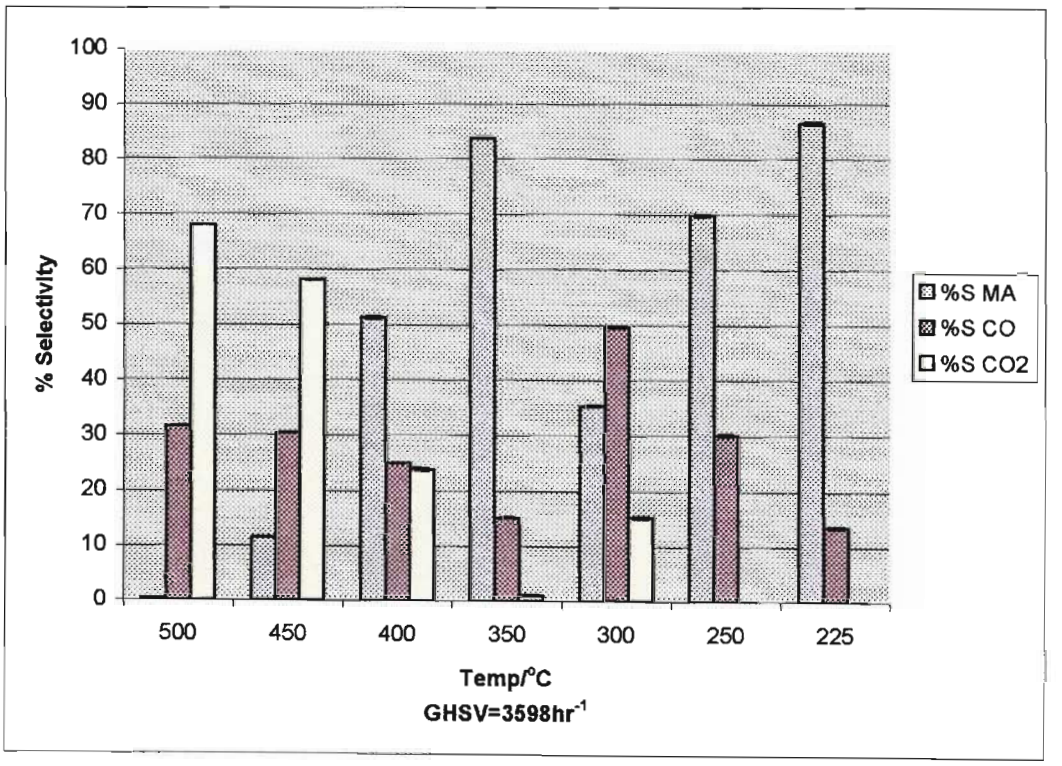

Fig. 4.7. % Selectivity (%S) products for VPO-1 at a constant GHSV of 3598 hr^{-1}

There was a resulting increase in selectivity towards MA, which reached 87 % at a temperature of 225°C, at these low conversions (Fig. 4.7). The selectivity may have been good, however, these were not ideal conditions, considering that the feedgas needs to be recycled due to the low conversion. A more favourable result would have both high % conversion of *n*-butane

and % selectivity towards MA. The optimum parameters for catalyst testing were thus assessed by the highest yield obtained.

$$\textit{\% Yield} = \textit{\% conversion X \% selectivity / 100}$$

A maximum molar yield of 14 % MA was obtained at a temperature of 350°C (Fig. 4.8). The % selectivity towards MA at this temperature was 84 %. A low yield of 3 % CO was obtained with negligible amounts of CO_2 (Fig. 4.8). The conversion of *n*-butane at this temperature was only 18 % (Fig. 4.6).

There was an increase of selectivity towards MA from 300°C down to 225°C (Fig. 4.7). The yields of MA, however, were very low in this range (Fig. 4.8).

In summary, VPO-1 proved to be less active at temperatures below 500°C as seen from the % conversion of *n*-butane shown in Fig. 4.6.

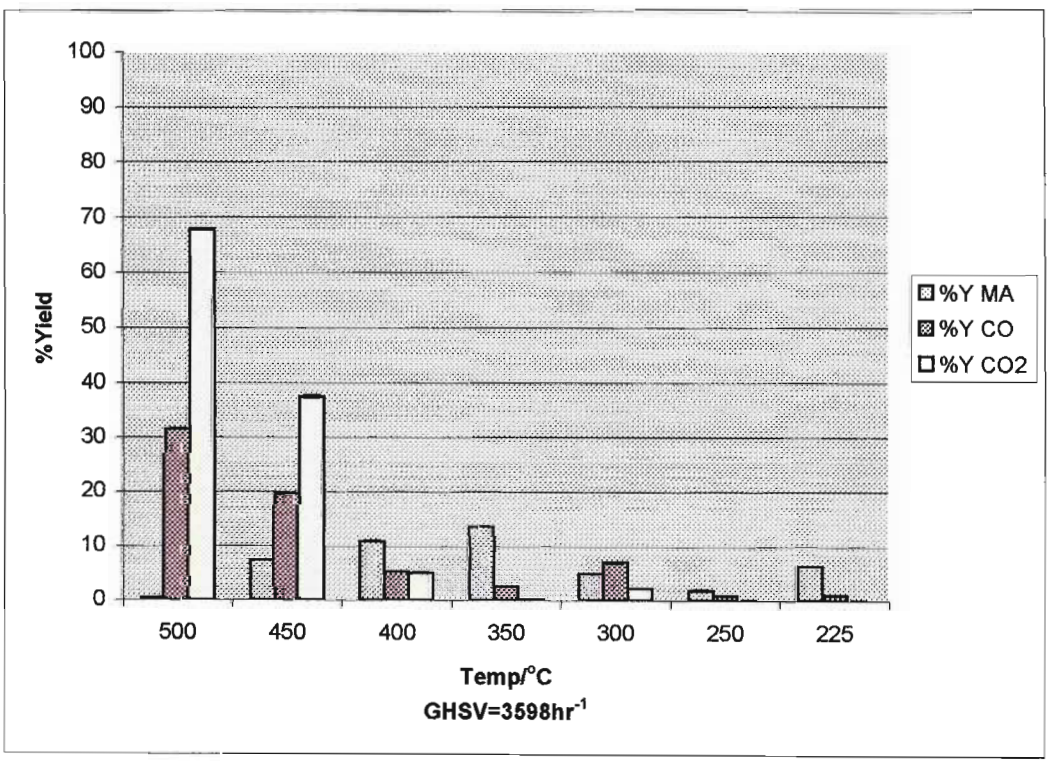

Fig. 4.8. % Yield (%Y) products for VPO-1 at a constant GHSV of 3598 hr^{-1}

4.3.2.2. VPO-2

This catalyst precursor had a P:V molar ratio of 1.04 and Co:V molar % of 1.31 as shown by ICP-AES results (Table 4.4). The surface area of the catalyst was 16.9 m^2/g (Table 4.7).

The molar carbon mass balance was between 95 and 105 % for all tests carried out on this catalyst. A 90 % conversion of *n*-butane was obtained at a temperature of 425°C and this decreased with a decrease in temperature (Fig. 4.9). From 350°C and lower temperatures, the % conversion of *n*-butane was below 10 %.

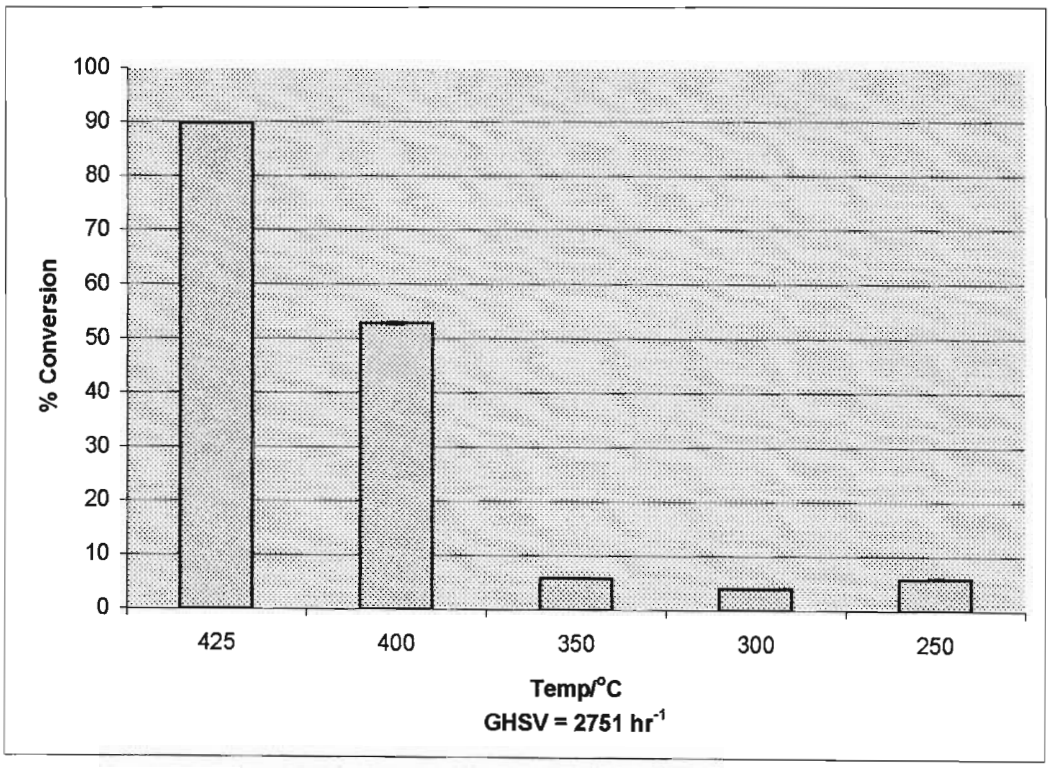

Fig. 4.9. % Conversion of n-butane over VPO-2 with a constant GHSV of 2751 hr^{-1}

Above an operating temperature of 350°C, VPO-2 had greater activity compared to VPO-1. This was seen by from the increase in *n*-butane conversion. The Co dopant appeared to be playing a positive role in increasing the conversion of *n*-butane.

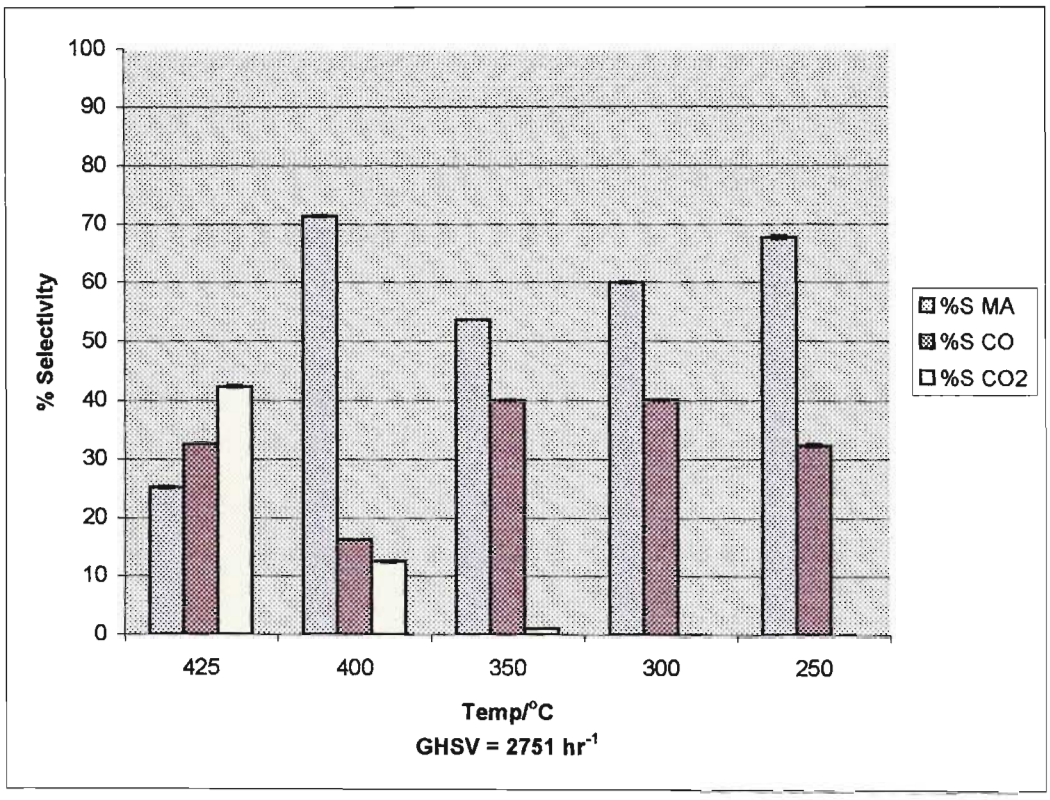

Fig. 4.10. % Selectivity (%S) products over VPO-2 with a constant GHSV of 2751 hr^{-1}

An optimum selectivity of 72 % MA was obtained at 400°C (Fig. 4.10) with a 52 % conversion of *n*-butane (Fig. 4.9). A yield of 38 % MA was obtained at this temperature (Fig. 4.11) and the carbon oxide yields at this temperature were below 10 %. There was a trend of increasing % selectivity towards MA with decreasing temperature in the temperature range 350°C to 250°C, as seen for VPO-1. The % conversion of *n*-butane in this range was below 10 %.

Negligible amounts of MA formed at a temperature of 225°C. Further analysis below 225°C was thus not carried out.

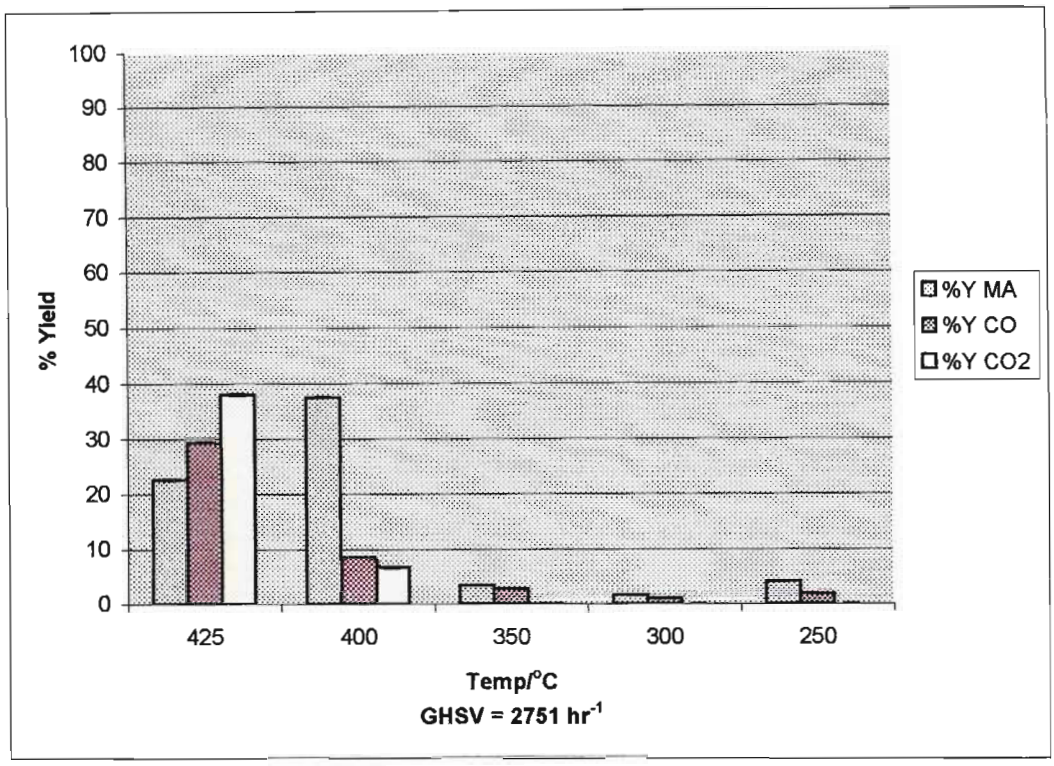

Fig. 4.11. % Yield (%Y) products over VPO-2 with a constant GHSV of 2751 hr^{-1}

4.3.2.3. VPO-3

This catalyst precursor had a molar P:V ratio of 1.06 and Co:V molar % of 2.33 (Table 4.4). The surface area was 22.9 m^2/g (Table 4.7). The catalyst was operated at a GHSV of 2878 hr^{-1}.

The carbon mass balance was between 95 and 105 % for all tests carried out on this catalyst. A trend of decreasing conversion of *n*-butane with decreasing temperatures was observed. A 100 % conversion of *n*-butane was obtained at an operating temperature of 325°C and a GHSV of 2878 hr^{-1} (Fig. 4.12) whilst a conversion of *n*-butane around 61 % was obtained for VPO-3 at an operating temperature of 275°C.

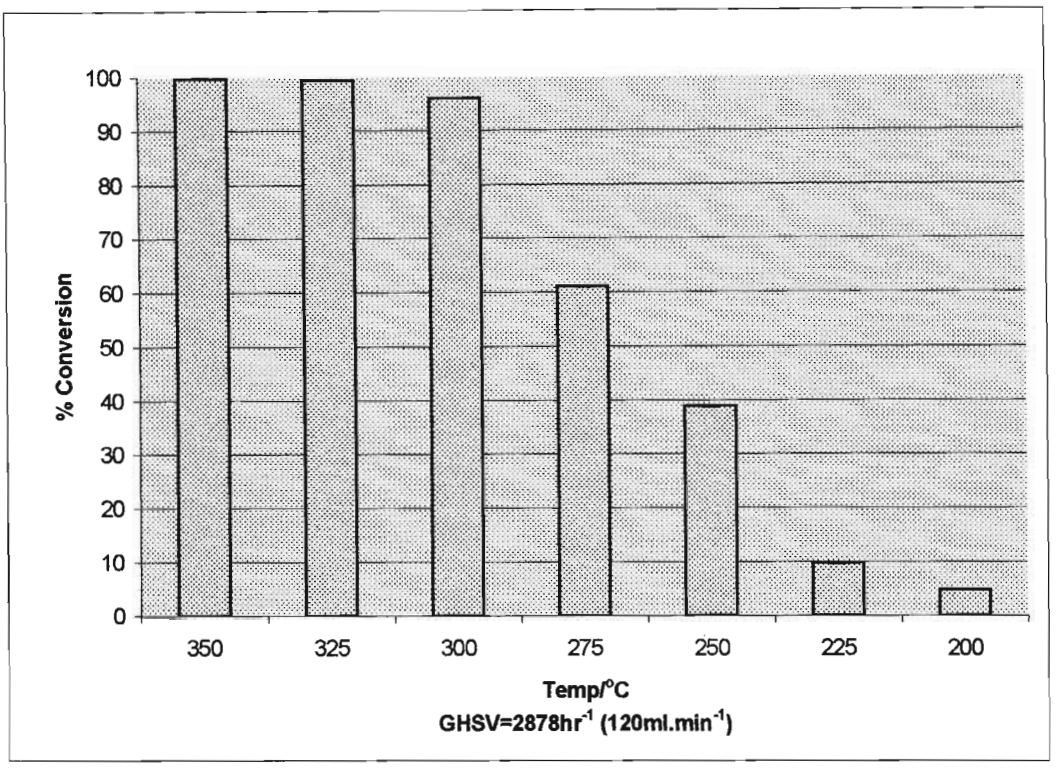

Fig. 4.12. % Conversion of n-butane over VPO-3 for a constant GHSV of 2878 hr^{-1}

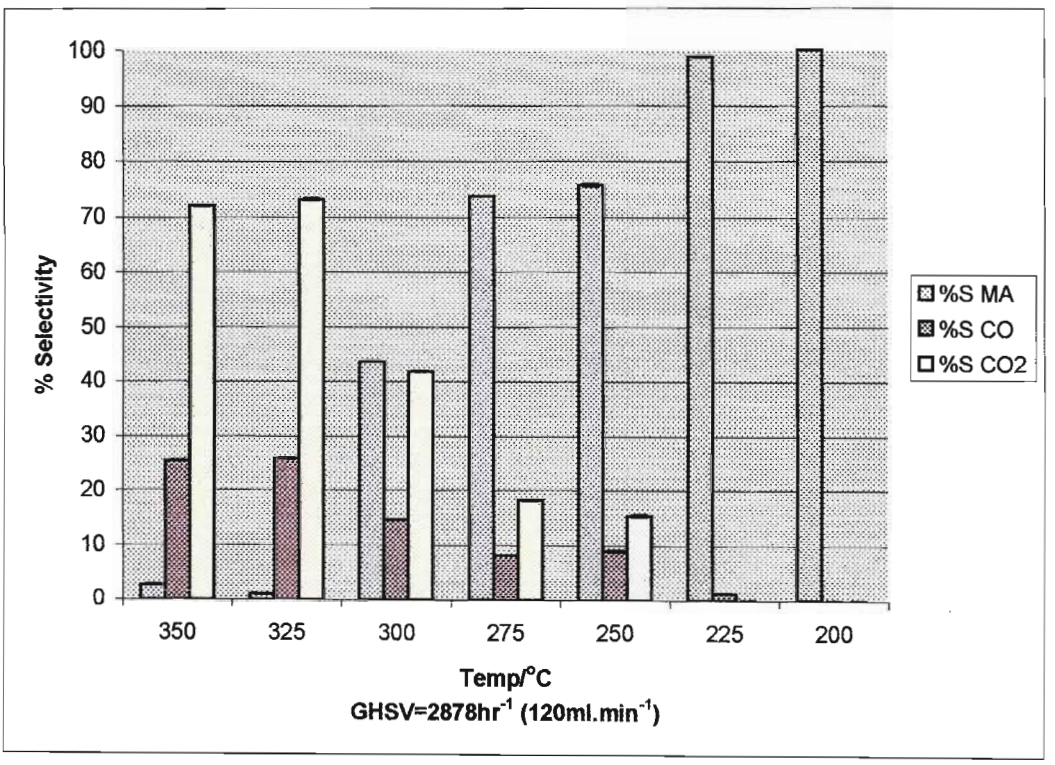

Fig. 4.13. % Selectivity (%S) products over VPO-3 at a constant GHSV of 2878 hr^{-1}

A maximum yield of 45 % MA was obtained at this temperature (Fig. 4.14) and at this temperature the selectivity towards MA was 74 % (Fig. 4.13).

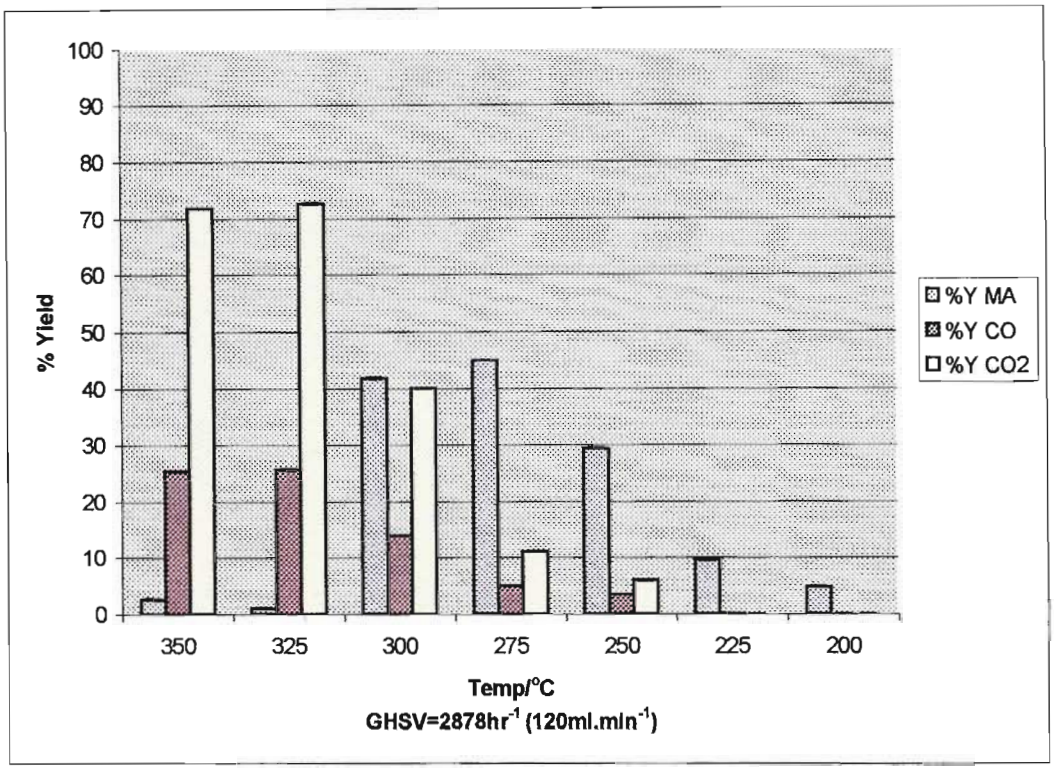

Fig. 4.14. % Yield (%Y) products over VPO-3 at a constant GHSV of 2878 hr^{-1}

4.3.2.4. VPO-4

This catalyst precursor had a P:V molar ratio of 1.04 and a molar % Co:V loading of 4.2 % (Table 4.4). The molar carbon mass balance was between 95 and 105 % for all tests carried out on this catalyst. The BET surface area was 13.2 m^2/g (Table 4.7). An *n*-butane conversion of 42 % was obtained at 450°C and this decreased with decreasing temperature (Fig. 4.15).

A maximum yield of 21 % MA was obtained at 400°C (Fig. 4.17). The % selectivity towards MA at this temperature was 84 % (Fig. 4.16) with a conversion of *n*-butane of 25% (Fig. 4.15).

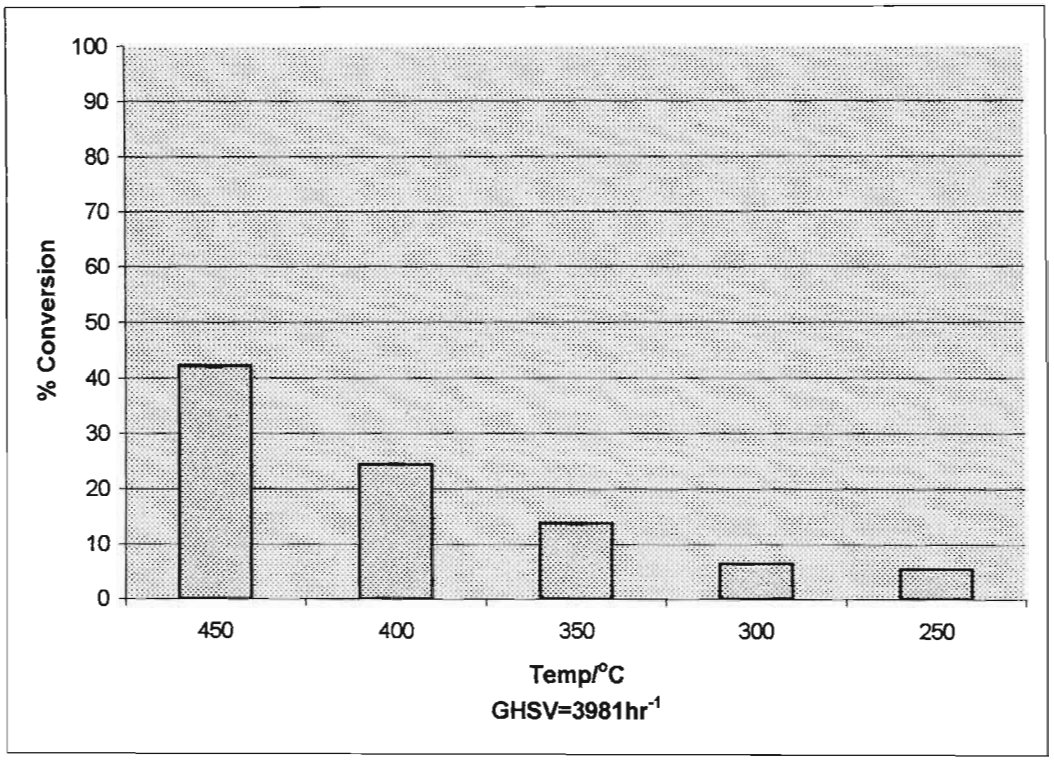

Fig. 4.15. % Conversion of n-butane over VPO-4 for constant GHSV of 3981 hr^{-1}

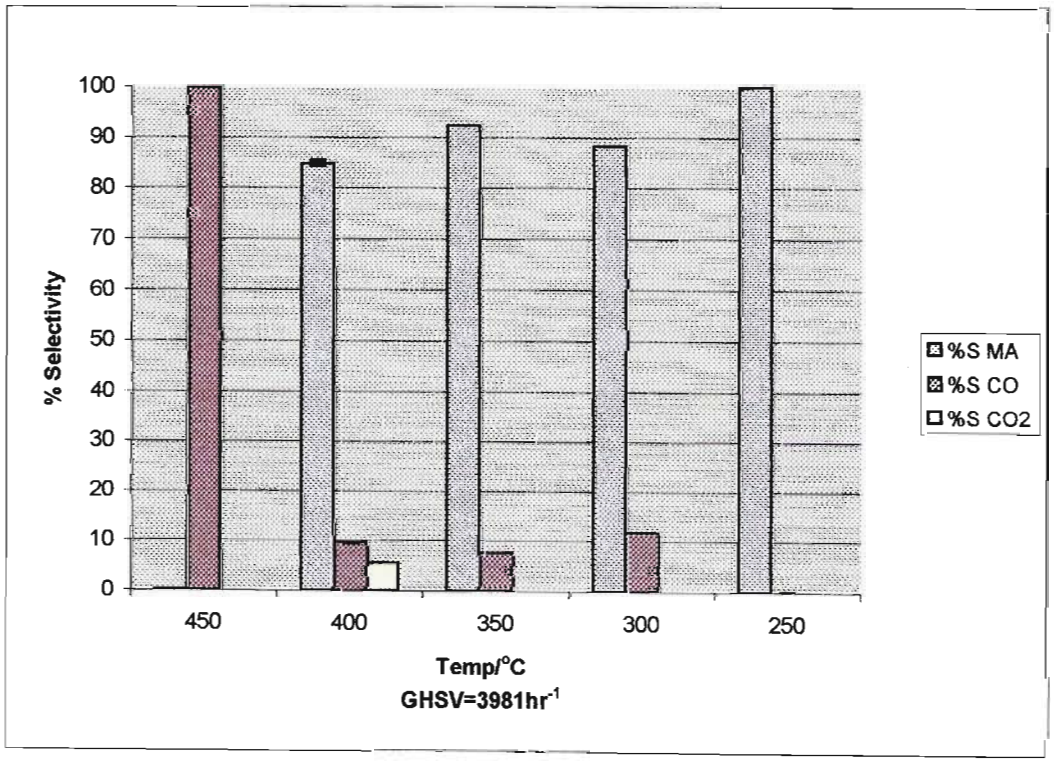

Fig. 4.16. % Selectivity (%S) products over VPO-4 with a constant GHSV of 3981 hr^{-1}

This catalyst had the lowest activity from all the catalysts examined as seen from the lowest % conversions obtained over the temperature range investigated.

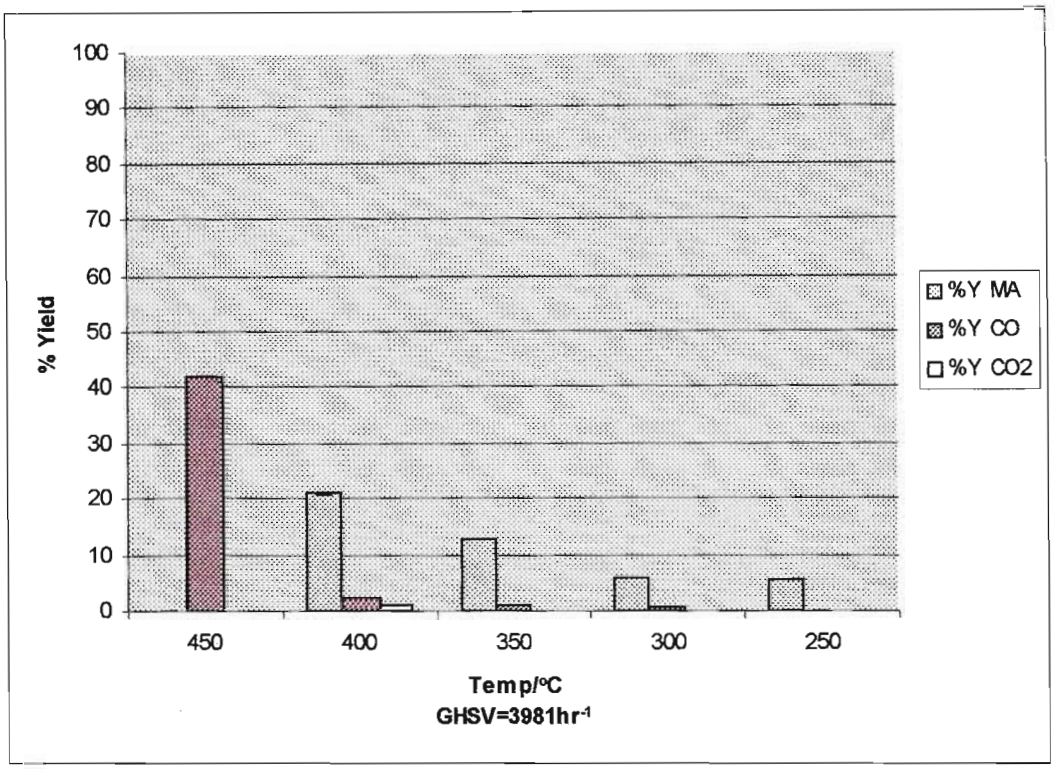

Fig. 4.17. % Yield (%Y) products over VPO-4 with a constant GHSV of 3981 hr^{-1}

4.3.3. % Selectivity towards MA and its relationship to % conversion of *n*-butane

Different promoter loaded catalysts gave different conversions of *n*-butane and selectivities towards MA when compared at the same operating temperature. The relationship between conversion of *n*-butane and selectivity towards MA for all catalysts tested is examined in this section. A graph of % selectivity towards MA vs % conversion of *n*-butane for the four different promoter loaded catalysts generally showed a trend of increasing % selectivity towards MA with a decreasing conversion of *n*-butane (Fig. 4.18). The operating temperature decreases on moving from left to right on the y-axis of the graph in Fig. 4.18. The operating temperature range was between 200°C and 450°C. VPO-3 showed a gradual decrease in % selectivity towards MA with an increase in % *n*-butane conversion. It was only on approaching 100 % conversion of *n*-butane that the selectivity plummeted. VPO-2 followed a similar trend to VPO-

3, however the % selectivities towards MA were lower. VPO-4 showed a steep drop in selectivity towards MA between a conversion of *n*-butane of 30 and 40 %. The 2.3 % Co loaded catalyst (VPO-3) maintained a high selectivity throughout the *n*-butane conversion range, which only dropped rapidly at *n*-butane conversion greater than 95 %.

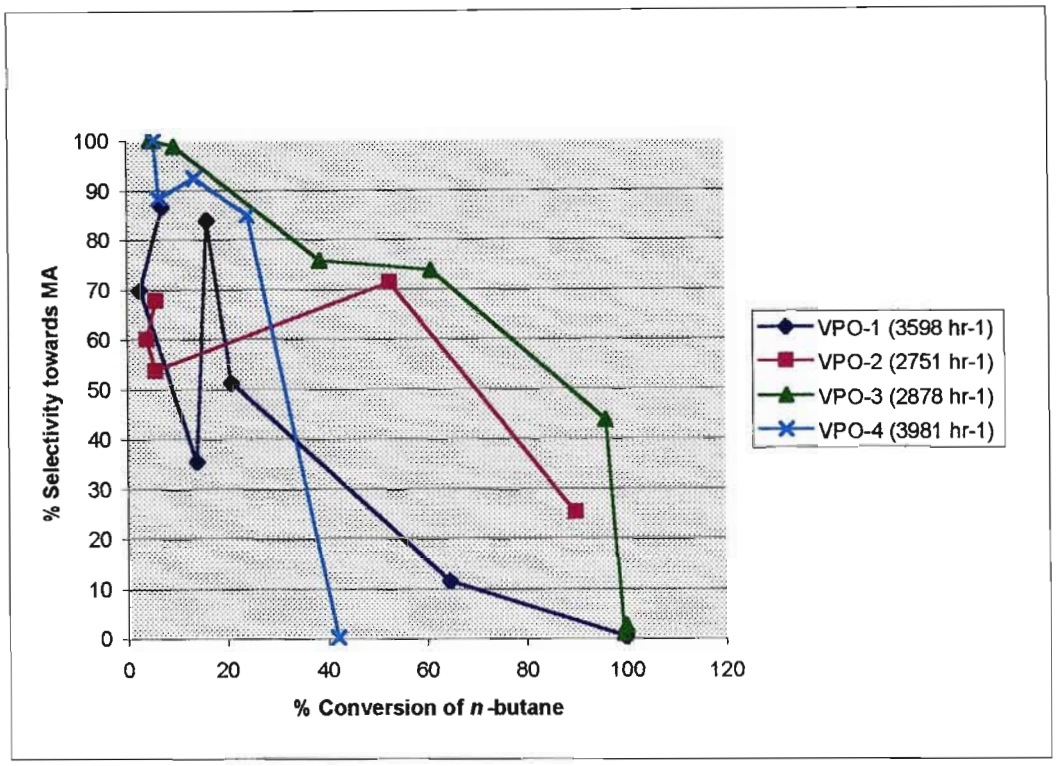

Fig. 4.18. % Selectivity towards MA vs % conversion of n-butane for four different promoted catalysts, VPO-1 through to VPO-4

Examining the relationship between the selectivity towards MA and temperature for all four catalysts tested, viz. VPO-1 (Fig. 4.7), VPO-2 (Fig. 4.10), VPO-3 (Fig. 4.13) and VPO-4 (Fig. 4.16), it could be seen that the selectivities towards MA peaked for VPO-1 (Fig. 4.7) and VPO-2 (Fig. 4.10) at 350°C and 400°C respectively, which corresponded to the maximum yields of MA obtained for these catalysts. After peaking, the selectivities decreased and then progressively increased again with decreasing operating temperature. VPO-3 (Fig. 4.13) gave progressively increasing selectivities towards MA without peaking with decreasing operating temperature. VPO-4 (Fig. 4.16) showed no distinct peaking. The selectivity towards MA is

defined as the ratio of yield of MA to the conversion of *n*-butane. The conversion of *n*-butane decreased with decreasing operating temperature.

The relationship between yield and conversion is shown in Fig. 4.19. The MA yields peak at different conversions of *n*-butane for the different catalysts. Catalyst VPO-3 had the highest yield of 45 % at the highest conversion of 61 % of all the catalysts tested.

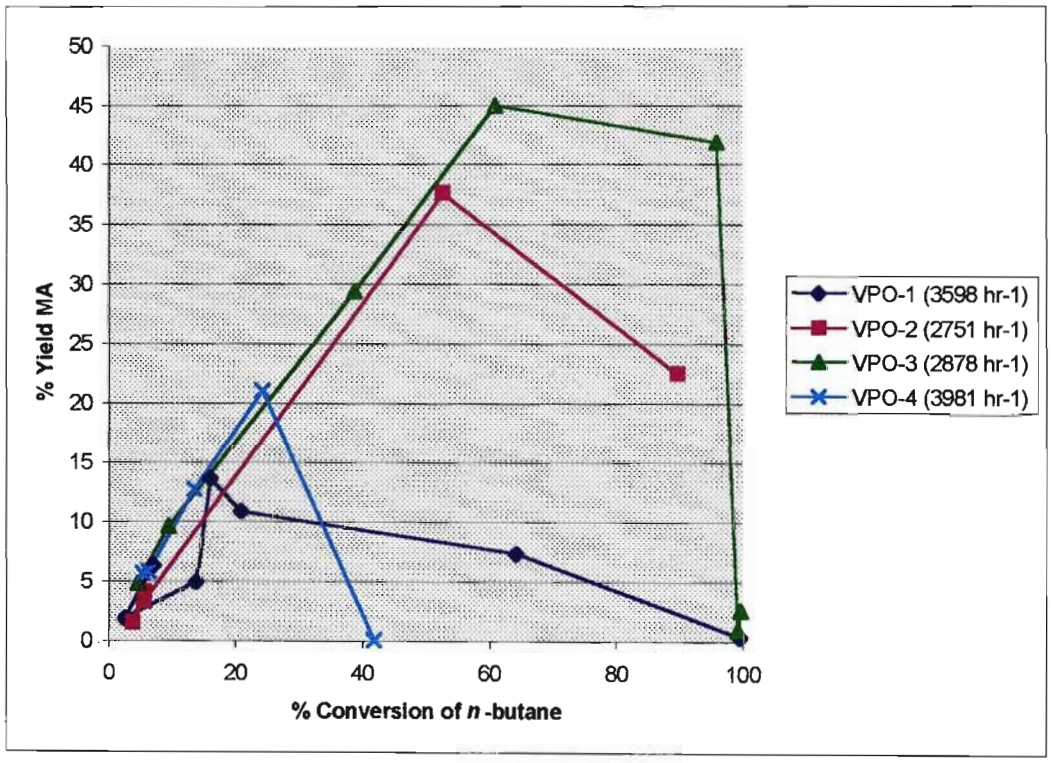

Fig. 4.19. % Yield MA vs % conversion of n-butane for four different promoted catalysts, VPO-1 through to VPO-4

Fig. 4.20 is a graphical representation of all the optimally performing catalysts. Each calcined catalyst was tested for approximately 200 hrs at each operating temperature over a constant feedgas flowrate of 120 ml.min^{-1}. Four catalysts with different Co promoter loadings were tested in this fashion. Optimally performing catalysts were identified as those catalysts that gave the highest yield MA at a particular temperature and GHSV.

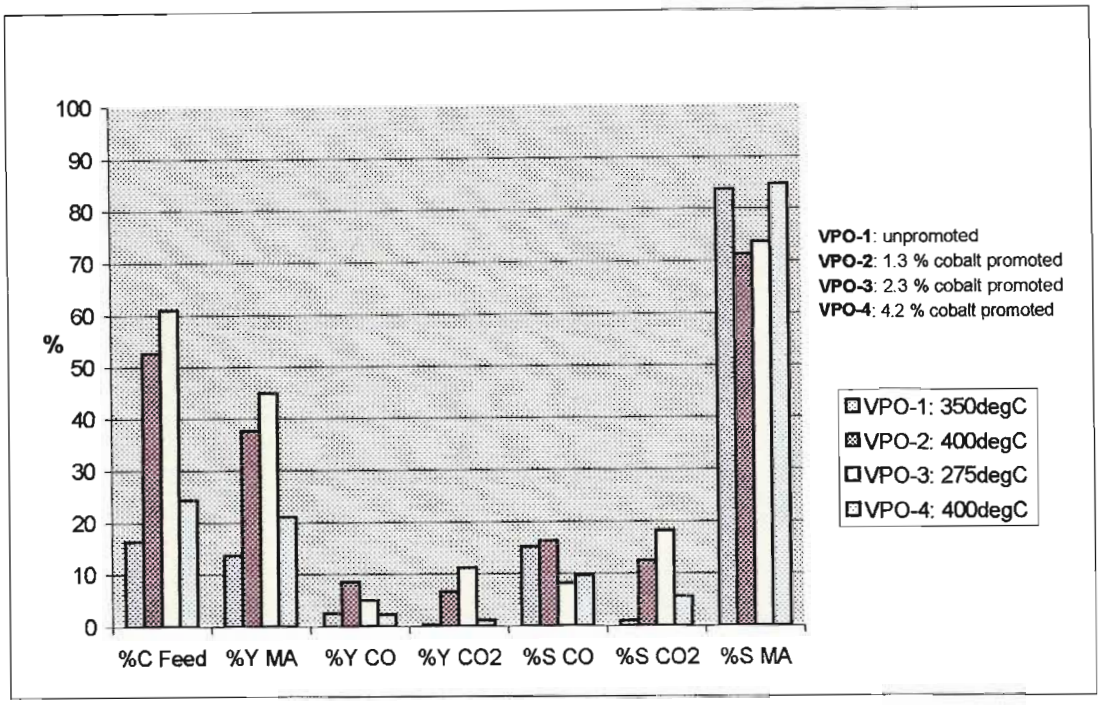

Fig. 4.20. Composite graph of yield (Y) and selectivity (S) of products and conversion (C) of n-butane feedgas, indicating operating temperatures for optimum yields of MA obtained from the four catalysts tested. GHSV = 3598 hr^{-1} (VPO-1), 2751 hr^{-1} (VPO-2), 2878 hr^{-1} (VPO-3) and 3981 hr^{-1} (VPO-4)

It is usual for % conversion of *n*-butane to increase with increasing temperature. Catalyst VPO-1 performed optimally at 350°C to yield 14 % MA with a 17 % conversion of *n*-butane. Catalyst VPO-2 performed optimally at 400°C to yield 37 % MA with a 53 % conversion of *n*-butane. A low conversion of *n*-butane was expected at a low temperature, however, VPO-3 revealed a MA yield of 45 % with a 61 % conversion of *n*-butane at 275°C. Catalyst VPO-4 gave a MA yield of 21 % with a 24 % conversion of *n*-butane at 400°C. There appeared to be an optimum Co promoter loading, which was a Co:V molar % of 2.3. CO yields were below 10 % for all optimally performing catalysts and the CO_2 yields were below 11 %. Higher selectivities than 73 % were obtained, under different conditions; however, these selectivities were obtained for lower conversions of *n*-butane.

4.3.4. Effect of surface area on % yield maleic anhydride

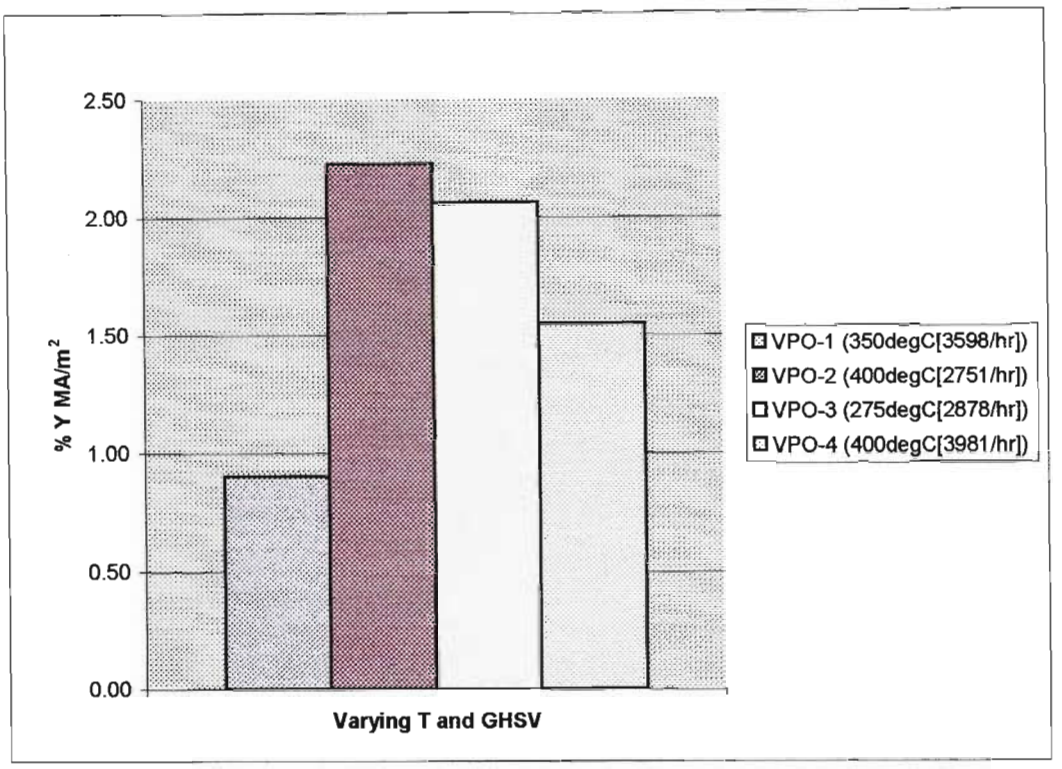

Fig. 4.21. Graph of specific % yield MA for optimum catalytic conditions for catalysts VPO-1 through to VPO-4 at respective temperatures and gas hourly space velocities

The effect of surface area was examined under the optimum operating conditions shown in Fig. 4.20 for each catalyst. Fig. 4.21 indicates that the specific yield of MA (i.e. the yield MA/total surface area of catalyst in the reactor) was different for the different catalysts at varying optimum operating temperatures. It was thus concluded that the varying surface areas of the catalyst could not exclusively explain the differences in yield under optimum conditions.

4.4. References

Bordes, E.; Courtine, P.; *J.Catal.*; **57** 236 (1979)

Brutovsky, M.; Gerej, S.; Vasilco, F.; Gerejova, J.; *Collection Czechoslovak Chem. Commun.*; **47** 1290-1300 (1982)

Busca, G.; Cavani, F.; Centi, G.; Trifirò, F.; *J. Catal.*; **99** 400-414 (1986)

Busca, G.; Centi, G.; Trifirò, F.; Lorenzelli, V.; *J. Phys. Chem.*; **90** 1337 (1986)

Centi, G.; Golinelli, G.; Busca, G.; *J. Phys. Chem.*; **94** 6814 (1990)

Cheng, W.; *Appl. Catal. A: General*; **147** 55-67 (1996)

Cornaglia, L.M.; Carrara, C.R.; Petunchi, J.O.; Lombardo, E.A.; *Appl. Catal. A: General*; **183** 177-187 (1999)

Coulston, G.W.; Simon, R.B.; Kung, H.; Birkeland, K.; Bethke, G.K.; Harlow, R.; Herron, N.; Lee, P.L.; *Science*; **275** 191 (1997)

Guliants, V.; Benziger, J.; Sundaresan, S.; Wachs, Y.; Jehng Roberts, J.U.; *Catal. Today*; **28** 275 (1996)

Hodnett, B.K.; *Catal. Rev. Sci. Eng.*; **27(3)** 412 (1985)

Horowitz, H.S.; Blackstone, C.M; Sleight, A.W.; Teufer, G.; *Appl. Catal.*; **38** 193 (1988)

Hutchings, G.J.; *Appl. Catal.*; **72** 1-32 (1991)

Hutchings, G.J.; Desmartin-Chomel, A.; Olier, R.; Volta, J.C.; *Nature*; **368** 41 (1994)

Lemal, R.; Vekemans, J.; U.S. Patent 3 987 063 (1976), assigned to U.C.B.

Nakamura, M.; Kawai, K.; Fujiwara, Y.; *J. Catal.*; **34** 345 (1974)

Sananes-Schulz, M.T.; Tuel, A.; Hutchings, G.J.; Volta, J.C.; *J. Catal.*; **166** 388-392 (1997)

Sartoni, L.; Wells, R.; Delmitis, A.; Burrows, A.; Kiely, C.; Herrman, J.; Roussel, H.; Volta, J.C.; 4th World Conference on Oxidation Catalysis; http://www.dechema.de/f-forschung-e.htm.; 'Synergistic effect of Ga on vanadium-phosphorous-oxide catalysts for *n*-butane oxidation to maleic anhydride'; (2001)

Zazhigalov, V.A.; Haber, J.; Stoch, J.; Pyatnitzkaya, A.I..; Komashko, G.A.; Belousov, V.M.; *Appl. Catal. A: General*; **96** 135 (1993)

CHAPTER 5

CONCLUSION

Co is known to stabilize P in the lattice of the catalyst and reduce or prevent the sublimation of P under the high operating temperatures around 400°C. The excess P above the stoichiometric value in the catalyst is required for the selective oxidation of *n*-butane. A discussion of this appears in Section 1.6. This was evident from the data obtained in this study. The molar P:V ratios of the catalysts from the precursor, through to the calcined and used catalysts, remained constant at around 1.1 in the bulk of the catalyst (Table 4.4) and 0.80 on the surface of the catalyst (Table 4.6).

Co stabilized the P:V molar ratio in this study. A discussion of this appears in Section 1.8. XRD spectra indicated the presence of the active catalytic phase, $(VO)_2P_2O_7$, in the used catalyst which was formed from the $VOHPO_4 \cdot {}^1/_2H_2O$ precursor. XRD spectra also showed the modification of the catalyst structure with the addition of dopants.

The composition of the surface and bulk of the catalyst appeared similar as indicated by the stretching bands in the IR spectra. It must be noted that these are *ex-situ* observations. The phases present in the active online catalyst may differ.

SEM images indicated the presence of larger platelet sizes with a slight increase in P:V molar ratio. The platelet size also increased for the Co promoted catalyst on calcination.

Alcohol solvent was trapped in the lattice of the catalyst. Microwave digestion of the calcined catalyst sample in aqua regia and subsequent EDX analysis revealed the presence of carbon. The only source of carbon was the alcohol solvent used in the synthesis of the catalyst. ATR analysis of the catalyst surface showed the absence of the alcohol on calcination of the catalyst precursor, however, the FTIR spectrum of the calcined and used catalysts, using the KBr pellet method of analysis, which was a bulk catalyst study, still showed the presence of the alcohol. This indicated that the alcohol was trapped in the lattice of the catalyst.

The AV was around 4.3 on average for all catalysts after conditioning and testing the catalysts in the reactor. This indicated an oxidation state switched between +4 and +5 in the oxidation of *n*-butane to MA.

The surface areas of the catalysts did not exclusively play a role in the performance of the catalyst at optimum operating conditions.

The Co promoter appeared to increase the surface area of the catalyst, up to an optimum value, and then excess Co caused a decrease in surface area.

There was a general increase in % selectivity towards MA with a decrease in % conversion of *n*-butane. The selectivity towards MA showed a peak for VPO-1 (Fig. 4.7) and VPO-2 (Fig. 4.10) over the different operating temperatures, however, no peak was evident for VPO-3 (Fig. 4.13) and VPO-4 (Fig. 4.16).

The maximum yields of MA obtained over the temperature range tested, viz. 250°C to 400°C, for the different promoter loaded catalysts were different at different conversions of *n*-butane.

Most industrial catalysts are capable of a conversion of *n*-butane in the region of 70-90 mol %. Their yields of MA are in the region of 55-65 mol %. Selectivities approach 90 mol % with lower conversions than those mentioned above. The selectivities are, however, generally around 60-70 mol % on average. A Co promoted catalyst was capable of a 59 mol % yield as shown industrially by Union Carbide. The selectivity towards MA obtained for this catalyst was 66 mol % and conversion of *n*-butane was 90 mol %. The operating temperature was 387°C and the GHSV was 1028 hr^{-1}. *Iso*-butanol solvent was used in the synthesis of the catalyst with a P:V ratio of 1.2 and molar Co:V ratio of 0.19 (Lemal, R. *et al.* U.S. Patent (1976)). The feedgas concentration was 1.5 % *n*-butane in air. The surface area of the catalyst was 20 m^2/g.

Table 5.1 highlights the different Co promoted catalysts developed by different institutions and their operating conditions and test results compared to the optimally performing catalyst in this study.

Company	Reducing Solvent/s	Synthetic route	*n*-Butane feedgas compositio	Operating Temp./ °C	Gas hourly space velocity/ hr^{-1}	Molar surface P:V ratio	BET surface area (m^2/g)	Bulk Cobalt concentrati on Co:V	Co salt and introduction	% Conversion	% Yield	% Selectivity	Reference
Academic	Isobutanol/ benzyl alcohol	Organic	1.00 % in air	275	2878	1.1	23	2.3	$Co(acac)_3$/ co-precipitation	61	45	73	Masters thesis, N. Govender, A Comparative Study of VPO Catalysts in the Oxidation of Butane to Maleic Anhydride
Chevron	Isobutanol	Organic	1.50 % in air	380	-	-	-	-	-	-	57	-	Schneider, R.A.; *U.S. Patent 4 043 943* (1977), assigned to Chevron Research Co.
US Patent	Aqueous HCl	Aqueous	1.50 % in air	420	6480	-	-	6.5	$CoCl_2$/ impregnation	95	59	62	*US Patent 4,209,423*; (1980)
Instituto de Investigaciones en Catalisis	Isobutanol/ benzyl alcohol	Organic	1.50 % in air	392	2500	2.6	-	7	Co acetate/ co-precipitation	74	29	39	Cornaglia, L.M.; Carrar, C.R.; Petunchi, J.O.; Lombardo, E.A.; *Appl. Catal. A: General*; **183** 177-187 (1999)
Instituto de Investigaciones en Catalisis	Isobutanol/ benzyl alcohol	Organic	1.50 % in air	392	2500	3.6	-	13	Co acetate/ co-precipitation	50	28	56	Cornaglia, L.M.; Carrar, C.R.; Petunchi, J.O.; Lombardo, E.A.; *Appl. Catal. A: General*; **183** 177-187 (1999)
Instituto de Investigaciones en Catalisis	Isobutanol/ benzyl alcohol	Organic	1.50 % in air	392	2500	3.7	42	13	Co acetate/ impregnation	85	30	35	Cornaglia, L.M.; Carrar, C.R.; Petunchi, J.O.; Lombardo, E.A.; *Appl. Catal. A: General*; **183** 177-187 (1999)
Instituto de Investigaciones en Catalisis	Isobutanol/ benzyl alcohol	Organic	1.50 % in air	392	2500	3.8	42	19	Co acetate/ impregnation	80	30	37	Cornaglia, L.M.; Carrar, C.R.; Petunchi, J.O.; Lombardo, E.A.; *Appl. Catal. A: General*; **183** 177-187 (1999)
Safarik University, Kosice	Aqueous HCl	Aqueous	1.00 % in air	407	2520	1.2	-	20	-	32	16	50	Brutovsky, M.; Gerej, S.; *Collection Czechoslovak Chem. Commun.*; **47** 406 (1983)
Union Carbide (UCB)	Aqueous HCl	Aqueous	1.5 % in air	450	1893	1.14	-	19	-	-	55	-	Lemal, R.; Vekemans, J.; *US Patent 3 987 063* (1976), assigned to UCB
Union Carbide (UCB)	Aqueous HCl	Aqueous	1.5 % in air	480	1893	1.14	-	10	-	-	45	-	Lemal, R.; Vekemans, J.; *US Patent 3 987 063* (1976), assigned to UCB
Union Carbide (UCB)	Aqueous HCl	Aqueous	1.5 % in air	453	1893	1.1	-	25	-	-	43	-	Lemal, R.; Vekemans, J.; *US Patent 3 987 063* (1976), assigned to UCB
Union Carbide (UCB)	Aqueous HCl	Aqueous	1.5 % in air	431	1439	1.14	-	19	-	-	46	-	Lemal, R.; Vekemans, J.; *US Patent 3 987 063* (1976), assigned to UCB
Union Carbide (UCB)	Isobutanol	Organic	1.5 % in air	387	1028	1.14	20	20	-	90	59	66	Lemal, R.; Vekemans, J.; *US Patent 3 987 063* (1976), assigned to UCB
Union Carbide (UCB)	Methanol	Organic	1.5 % in air	405	1028	1.14	-	20	-	-	60	-	Lemal, R.; Vekemans, J.; *US Patent 3 987 063* (1976), assigned to UCB
Standard Oil Co., Ohio	Hexachloro-butadiene	Organic	1.10 % in air	437	1890	1.2	-	20	-	89	50	56	Lemanski, M.F.; Bremer, N.J.; Milberger, E.C.; US Patent 4,293,498 (1981); assigned to Standard Oil Co., Ohio
Institut de Recherched sur la Catalyse	Isobutanol	Organic	$C_4H_{10}/O_2/He$ = 1.5/18.5/80	430	1000	-	9.1	1	$Co(acac)_3$/ co-precipitation	60	48	80	Sananes-Schulz, M.T.; Tuel, A.; Hutchings, G.J.; Volta, J.C.; *J. Catal.*; **166** 388-392 (1997)
Institut de Recherched sur la Catalyse	Isobutanol	Organic	1.5 % in air	430	2000	2.1	-	12.6	$Co(acac)_3$/ co-precipitation	51	12	23	Ben Abdelouahab, F.; Olier, R.; Ziyad, M.; Volta, J.C.; *J. Catal.*; **157** 687-697 (1995)
Academic	Isobutanol	Organic	$C_4H_{10}/O_2/He$ = 1.6/18/80 4	400	1000	1.1	16	1	$Co(acac)_3$/ co-precipitation	25	18	71	Sajip, S.; Bartley, J.K.; Burrows, A.; Sananes-Shulz, M.T.; Tuel, A.; Volta, J.C.; Kiely, C.J.; Hutchings, G.J.; *New J. Catal.*; **25** 125-130 (2001)
Academic	Isobutanol	Organic	$C_4H_{10}/O_2/He$ = 1.6/18/80 5	400	1000	1.1	10	5	$Co(acac)_3$/ co-precipitation	25	16	62	Sajip, S.; Bartley, J.K.; Burrows, A.; Sananes-Shulz, M.T.; Tuel, A.; Volta, J.C.; Kiely, C.J.; Hutchings, G.J.; *New J. Catal.*; **25** 125-130 (2001)

Table 5.1. Description of cobalt promoted catalysts from the literature

The optimum catalyst obtained in this study gave a yield of 45 mol %. The conversion of *n*-butane was 62 % with a corresponding % selectivity towards MA of 73 %. The optimally promoter loaded catalyst, VPO-3, gave the highest yield MA at the highest conversion of *n*-butane from all the catalysts tested in this study. The surface area of the catalyst was 23 m^2/g. The % yield MA was lower than that obtained from the UCB process, however, the operating temperature for the catalyst here was 275°C, more than a 100°C cooler than the UCB process.

In conclusion therefore, a catalyst was synthesized with a significantly lower Co loading compared to the UCB catalyst. This catalyst was tested under similar conditions to the industrial conditions mentioned above and operated at a significantly lower temperature.

5.1. Recommendations

Future recommendations for this research could include:

The use of a recycle loop for the optimum catalyst VPO-3 extending from the product stream and meeting the feed line to the reactor. The % selectivity was high, thus by-products entering the recycle line would be low. The by-products could be trapped before unreacted *n*-butane enters the feed stream of the reactor. The trap could be a water bubbler maintained at room temperature, where MA would condense and form maleic acid. The by-products, viz. carbon monoxide and carbon dioxide are soluble in water; however, *n*-butane is not and would exit the bubbler and meet the feed stream into the reactor. The maleic acid can be later purified via distillation and dehydrated to form pure MA. The composite feed to the reactor would be diluted with the excess air entering the feedstream from the by-pass line. Enriching the feedstream with *n*-butane will compensate for this.

The use of a diluent, such as silica, to reduce the chances of hot spots developing in the reactor, which could decrease the amounts of over-oxidation products at operating temperatures around 400°C. This would further increase selectivity towards MA at elevated temperatures.

X-ray photoelectron spectrometry (XPS) and Raman spectroscopy would be invaluable instrumental techniques to determine the Co and V oxidation states, and hence the possible

phases present with these oxidation states. On-line characterization of the catalyst via XPS would elucidate the phases present during oxidation of *n*-butane to MA.

APPENDIX 1

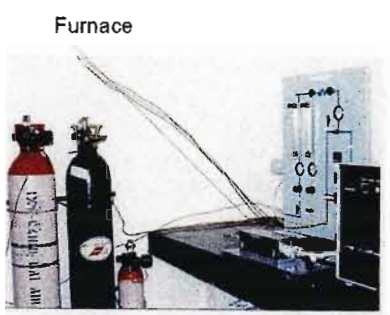

Fig. a

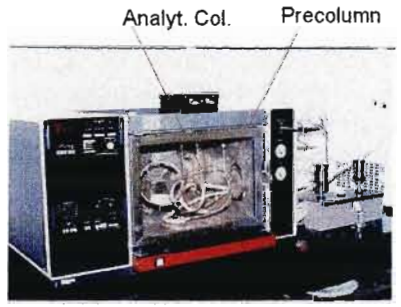

Fig. c

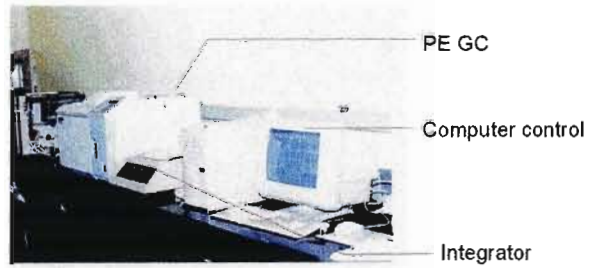

Fig. e

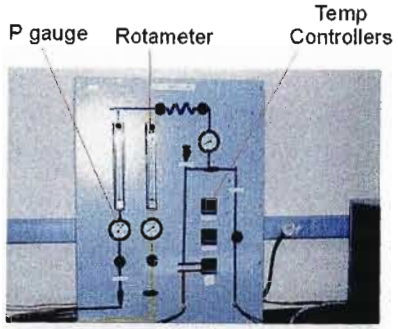

Fig. b

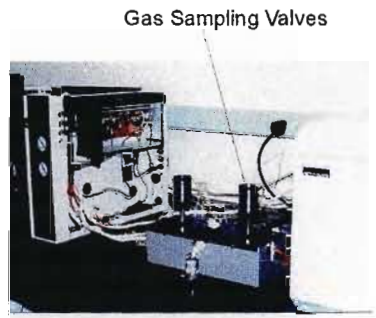

Fig. d

Fig. a Shows the feed gas cylinder, split block furnace and reactor control panel.

Fig. b A photo of the reactor control panel, showing the pressure gauges, rotameters, control valves and temperature controllers. Feed gas enters on the left hand side.

Fig. c Varian 3700 isothermal GC equipped with a thermal conductivity detector (TCD) for CO and CO_2 and air analyses. A pre-column in this gas chromatograph (GC) traps the products that condense at room temperature and allows the gaseous products to pass through to the TCD.

Fig. d Shows the gas sampling valve box in between the two gas chromatographs that samples to both gas chromatographs.

Fig. e Shows the Perkin Elmer XL autosystem GC on the left, followed by an integrator which is linked to the Varian 3700 GC, and a computer to analyse data from th e Perkin Elmer XL autosystem GC. The Perkin Elmer GC is equipped with a flame ionization detector (FID) for *n*-butane and MA amongst other analyses.

Fig. 1. Laboratory setup of reactor, control panel, GCs and automatic sampling system

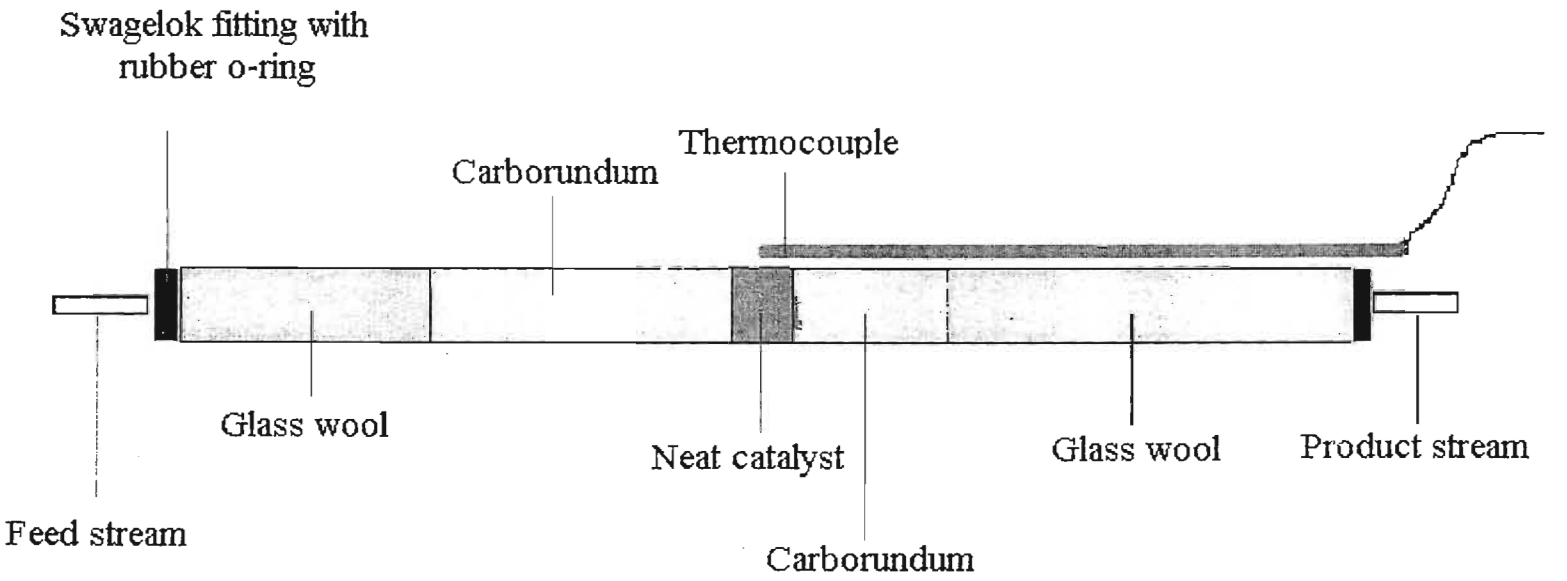

Fig. 2. Quartz reactor tube with catalyst packing

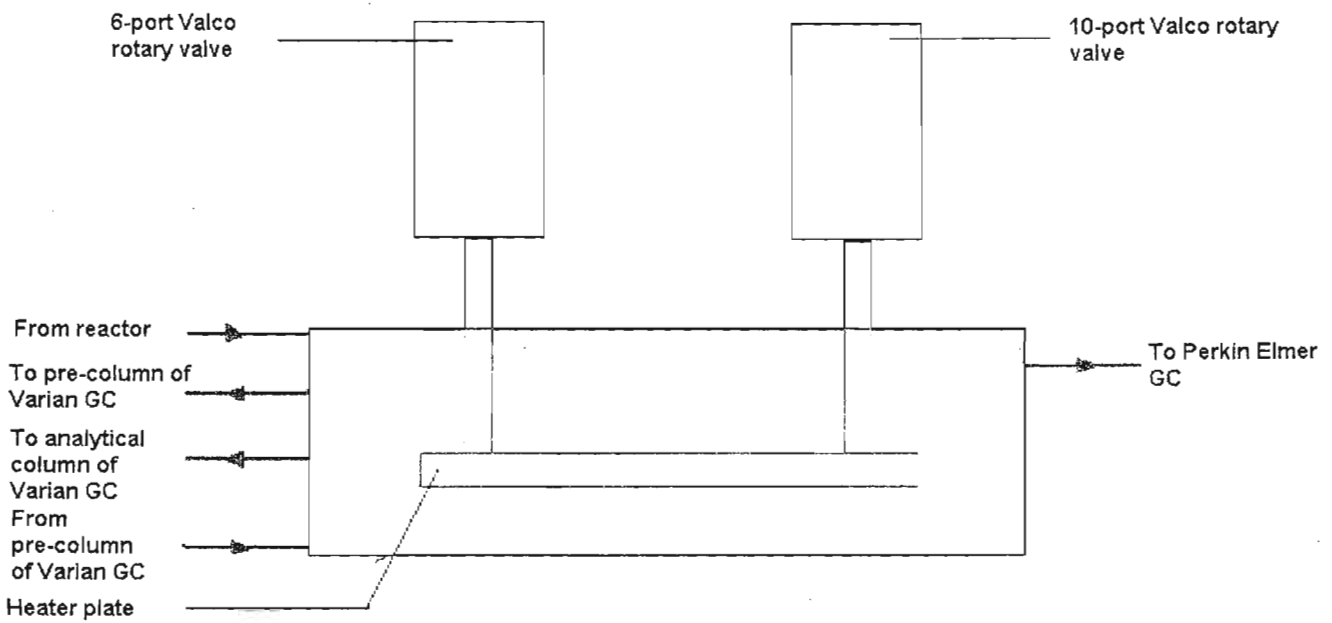

Fig. 3. Gas sampling valve box

COLUMNS USED IN VARIAN 3700 ISOTHERMAL GC

Precolumn

Stainless steel

Support.....Chromosorb WHPSP

Dimensions.....Length : 1m

OD : 1/8"

ID : 2.2mm

Mesh range.....80/100

Liquid phases.....OV-225 weight % 10

Temperature range.....20-275°C

Analytical Column

Stainless steel

Support.....Carboxen™ 1000

Dimensions.....Length : 2.5m

OD : 1/8"

ID : 2.2mm

Mesh range.....60/80

Maximum temperature.....225°C

COLUMNS USED IN PERKIN ELMER XL AUTOSYSTEM

Chrompak capillary column

Coating.....CP-Sil 24CB

Dimensions.....Length : 30m

ID : 0.32mm

OD : 0.45mm

Maximum allowable Temperature.....225°C

GC PARAMETERS SET FOR CATALYST TESTING

GC 1: Isothermal Varian 3700

Detector temperature.....130°C

Column temperature.....22°C

Injector temperature.....150°C

TCD filament temperature.....150°C

Output.....Negative

Range.....0.5mV

Carrier gas: He (instrument grade), Supplier: Afrox

GC 2: Perkin Elmer XL Autosystem

Detector temperature.....130°C

Injector A.....220°C

Carrier A.....9.0 psig

Split flow 50.2

Column temperature program for Perkin Elmer XL Autosystem

Initial.....70°C Held : 1 minute

Setpoint .....200°C Held : 2 minutes

Rate.....7°C/minute

Carrier gas: Nitrogen (instrument grade), supplier: Afrox

Flame gases for FID: Hydrogen and air (instrument grade), supplier: Afrox

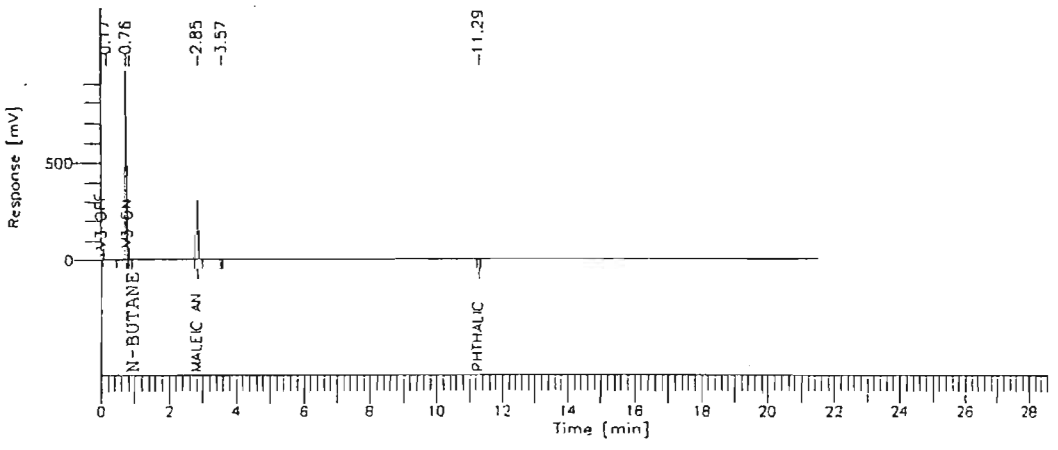

Report

Peak #	Time [min]	Component Name	Area [µV·s]	Area [%]	BL	Area/Height [s]	Amount of NBA ng\L
1	0.172		6260.92	0.30	BB	16.32	0.0063
2	0.755	n-Butane	961244.27	46.51	BB	0.93	0.9612
3	0.844	Acetic acid	30019.77	1.45	BB	0.95	0.0300
4	2.852	Maleic anhydride	1066140.68	51.58	BB	3.01	0.0001
5	3.570		1792.64	0.09	BB	2.50	0.0018
6	11.288	Phthalic anhydride	1337.20	0.06	BB	3.05	0.0001
			2066795.49	100.00			

Fig. 4. Typical gas chromatogram from Perkin Elmer XL Autosystem GC affixed with an FID

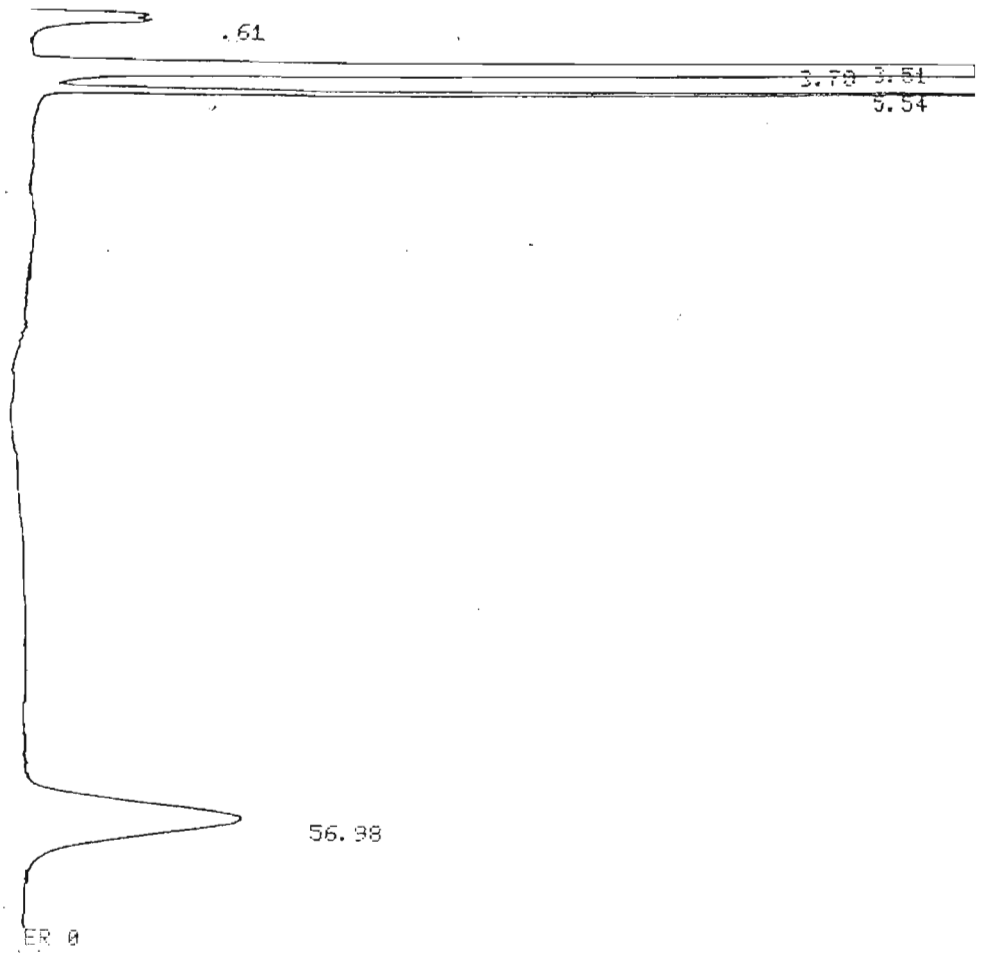

FILE 1. METHOD 0. RUN 7 INDEX 7

PEAK#	AREA%	RT	AREA	BC	
1	0.009	0.61	224	01	
2	14.74	3.51	378856	02	NITROGEN
3	81.706	3.7	2100064	03	OXYGEN
4	1.352	5.54	34748	01	CARBON MONOXIDE
5	2.193	56.98	56368	01	CARBON DIOXIDE
TOTAL	100.		2570260		

Fig. 5. Typical gas chromatogram from Varian 3700 GC affixed with a TCD

MALEIC ANHYDRIDE MATERIAL SAFETY DATA SHEET[1,2]

1. Product identification

Synonyms: cis-Butenedioic anhydride; 2,5-furandione; toxilic anhydride

Molecular weight: 98.06 $g.mol^{-1}$

Chemical formula: $C_4H_2O_3$

2. Hazards identification

Emergency overview

Corrosive substance. Causes burns to skin and eyes. May cause irritation and/or allergic reaction in the respiratory tract. Melted material causes thermal burns. May be harmful if swallowed.

Potential health effects

Inhalation:

Inhalation of the dust or vapor may cause irritation of the nose and throat. Coughing, sneezing and burning of the throat may be experienced. Can cause allergic respiratory reactions.

Ingestion:

Corrosive. Toxic. Swallowing can cause sore throat, abdominal pain and vomiting. May cause burns to the digestive tract.

Skin contact:

Corrosive. May not cause immediate burning of the skin, but prolonged contact with moist skin cause reddening and blistering or burns.

Eye contact:

Corrosive. Dust or vapor cause burns or irritation of the eyes with swelling. Sensitivity to light and double vision may occur.

Chronic exposure:

Repeated inhalation may cause chronic bronchitis of the asthmatic type. Repeated skin contact may lead to dermatitis or sensitization.

3. First aid measures

Inhalation:

Remove to fresh air. If not breathing, give artificial respiration. If breathing is difficult, give oxygen. Call a physician.

Ingestion:

Induce vomiting immediately as directed by medical personnel. Never give anything by mouth to an unconscious person.

Skin contact:

In case of contact, immediately flush skin with plenty of soap and water for at least 15 minutes while removing contaminated clothing and shoes. Wash clothing before reuse. Call a physician immediately.

Eye contact:

Immediately flush eyes with plenty of water for at least 15 minutes, lifting lower and upper eyelids occasionally. Get medical attention immediately.

4. Fire fighting measures

Fire:

Flash point: 102°C

Auto-ignition temperature: 477°C

Flammable limits in air % by volume: lower explosive limit = 1.4; upper explosive limit = 7.1

Explosion:

Above flash point, vapor mixtures are explosive within flammable limits noted above.

Fire extinguishing media:

Alcohol foam or carbon dioxide may be used to extinguish fires. DO NOT USE dry chemical, multipurpose dry chemical or loaded stream media because of explosion potential due to reactivity of basic compounds in these extinguishing media.

5. Physical and chemical properties

Appearance: White crystals

Odour: Sharp irritating acrid odour.

Solubility: 16.3 g/100ml water @ 25°C; slowly hydrolyses.

Specific gravity: 1.48

Boiling point: 202°C

Melting point: 53°C

Vapor density (Air=1): 3.38

Vapour pressure (mmHg): 0.16 @ 20°C

[1]Chemdat[R], The Merck Chemical Database, 2000
[2]http://www.jtbaker.com/msds/m0364.htm

Description of vanadium-phosphorous-oxide catalyst phases

Phase	*Structural characteristics*
β-$VOPO_4$	Isostructural with β-$VOSO_4$; V in the +5 oxidation state. Features corner sharing distorted VO_6 octahedra.[3]
α_I-$VOPO_4$	Isostructural with α-$VOSO_4$; V in +5 oxidation state. Features corner sharing distorted VO_6 octahedra.[3]
α_{II}-$VOPO_4$	Similar structure to α-$VOPO_4$ with elongation along the a-axis due to trapped water.[3]
$(VO)_2P_2O_7$	V in the +4 oxidation state. Features edge-sharing VO_6 octahedra.[3]
β*-phase	Features V in the +4 oxidation state. Transforms into B' phase at ~450°C and into β-$VOPO_4$ at 500°C and above.[3]
B'-phase	Reported to be oxidized equivalent to the β-phase. Also postulated to feature V in the +4 oxidation state.[3]
γ-$VOPO_4$, δ-$VOPO_4$	Polymorphic. Pairs of edge sharing octahedral with trans vanadyl oxygens are alternatively unshared or shared with phosphate tetrahedra.[4]

Table 1. Structural characteristics of phases present in the vanadium-phosphorous oxide catalyst

[3] Hodnett, B.K.; *Catal. Rev. Sci. Eng.*; **27(3)** 390 (1985)
[4] Centi, G.; Trifiró, F.; *Chem. Rev.*; **88** 57 (1988)

APPENDIX 2

XRD DATA FROM CHARACTERISATION OF CATALYSTS

Instrument: Philips PW1130

Experimental conditions

X-Ray source	:	Cobalt
Voltage	:	40 kV
Amperage	:	25 mA
Divergence slit	:	1 °
Receiver slit	:	0.15 °
Scan from	:	5 °2θ
Scan to	:	100 or 105 °2θ
Step size	:	0.05 °2θ
Count between steps	:	2 seconds

Peak positions

VPO-1p 2θ	**VPO-2p** 2θ	**VPO-3p** 2θ	**VPO-3u** 2θ	**VPO-4p** 2θ
17.858	17.526	18.038	14.450	12.598
21.412	21.433	22.681	16.358	17.571
22.763	22.746	28.119	21.456	21.542
28.150	28.113	31.438	26.723	22.676
31.499	31.560	33.424	33.138	28.093
33.325	33.365	35.414	34.167	31.369
35.497	35.424	37.271	34.826	33.132
37.354	37.224	39.923	39.316	35.526
43.724	43.725	43.746	43.647	37.164
56.112	56.063	47.216	50.576	39.935
57.619	57.587	51.726	55.134	43.714
75.010	74.918	54.378	58.172	47.494
		55.970	69.010	51.651
		57.694		54.294
		60.744		56.312
		66.050		57.572
		71.089		66.264
		72.283		74.957
		75.068		
		77.986		
		83.159		
		86.209		

Fig. 1. XRD experimental conditions and 2θ values obtained

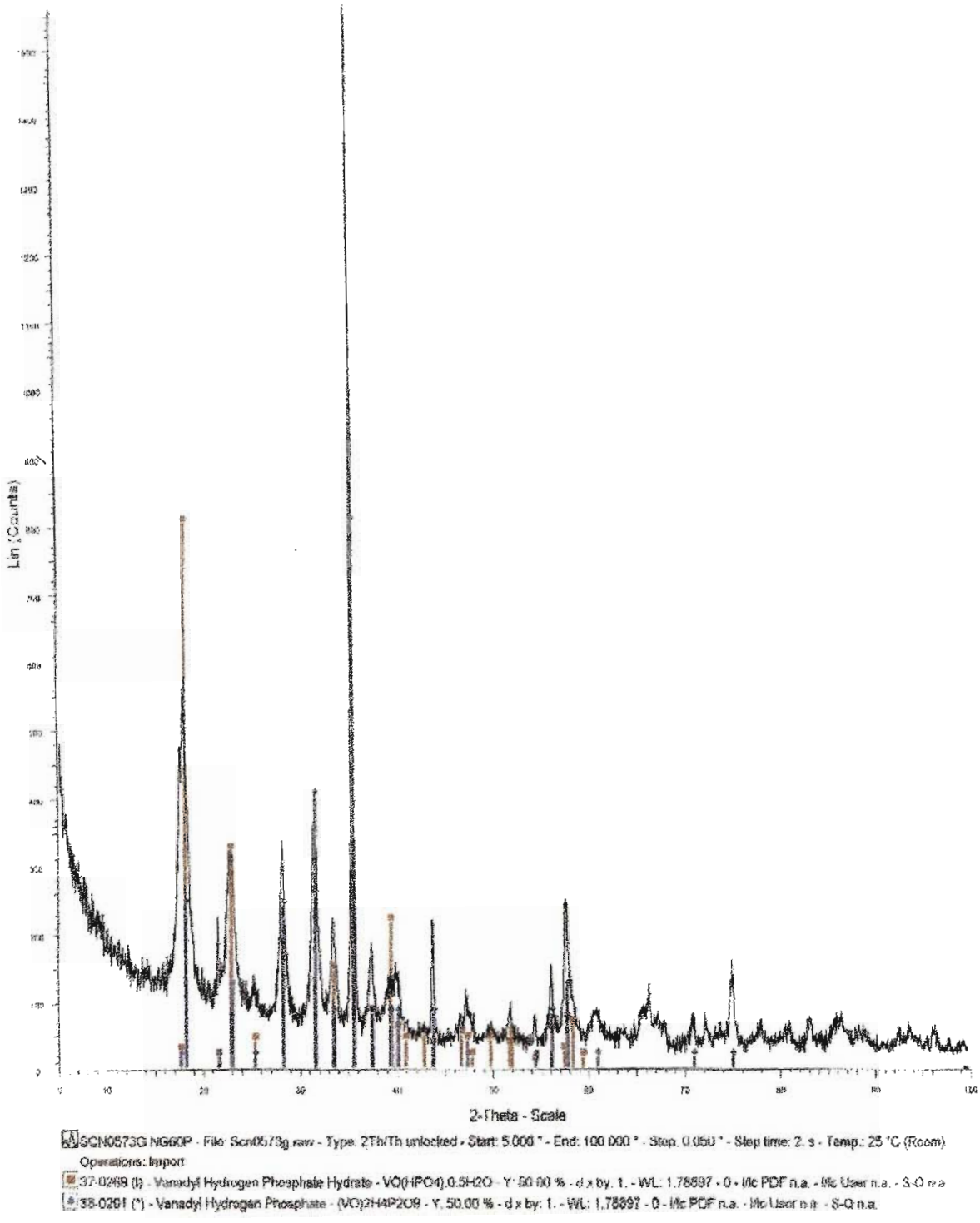

Fig. 2. X-ray diffraction spectrum of VPO-1p

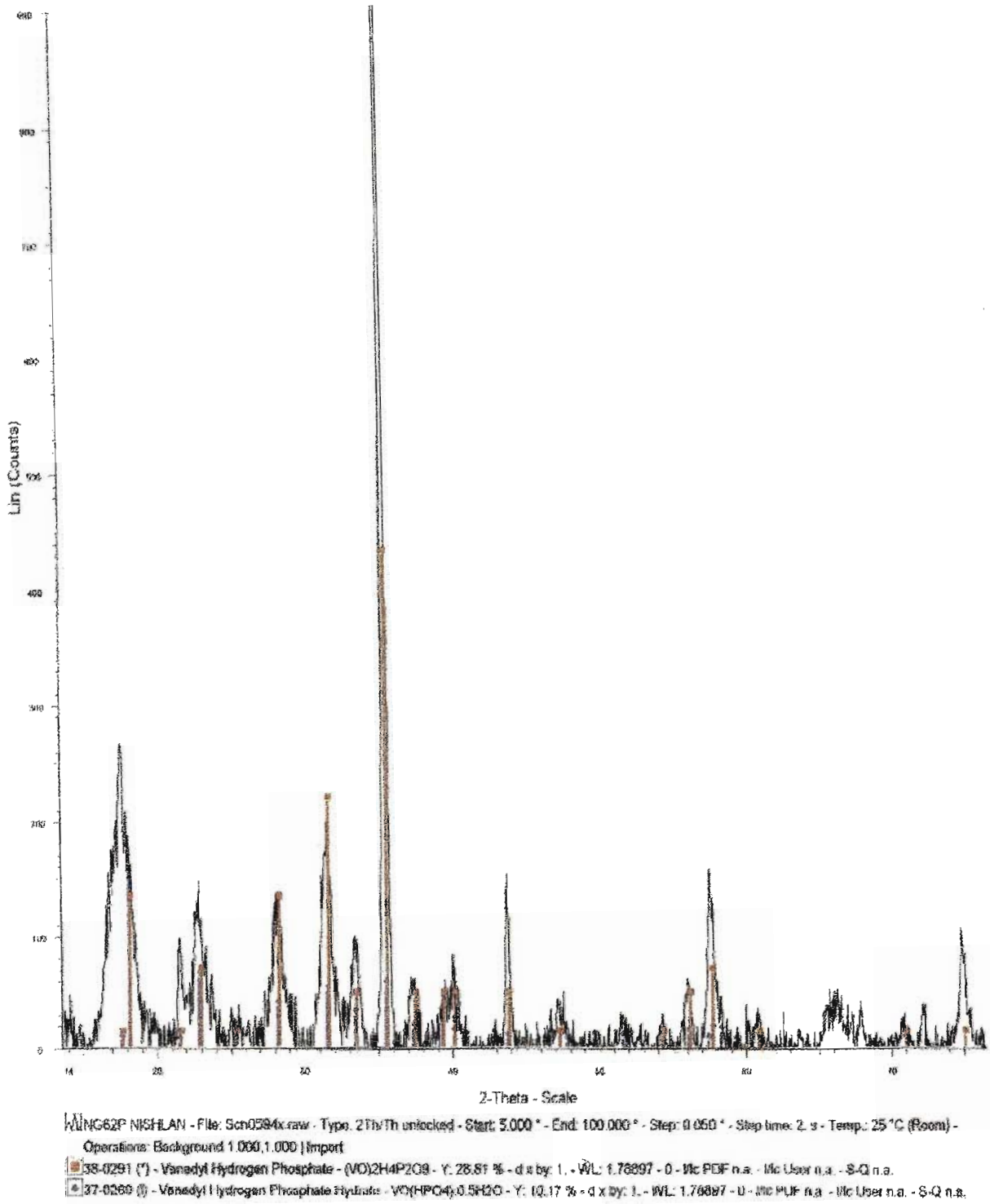

Fig. 3. X-ray diffraction spectrum of VPO-2p

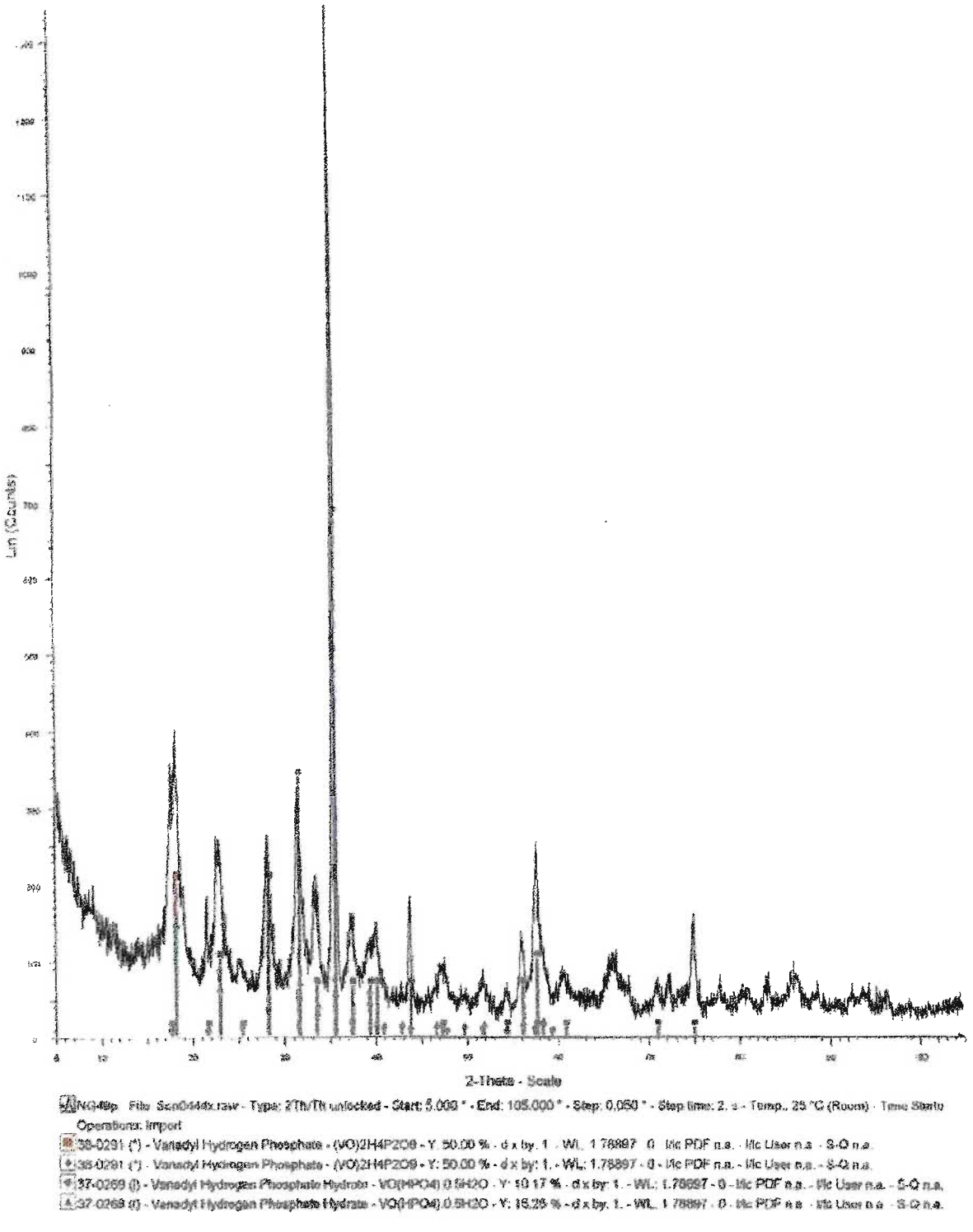

Fig. 4. X-ray diffraction spectrum of VPO-3p

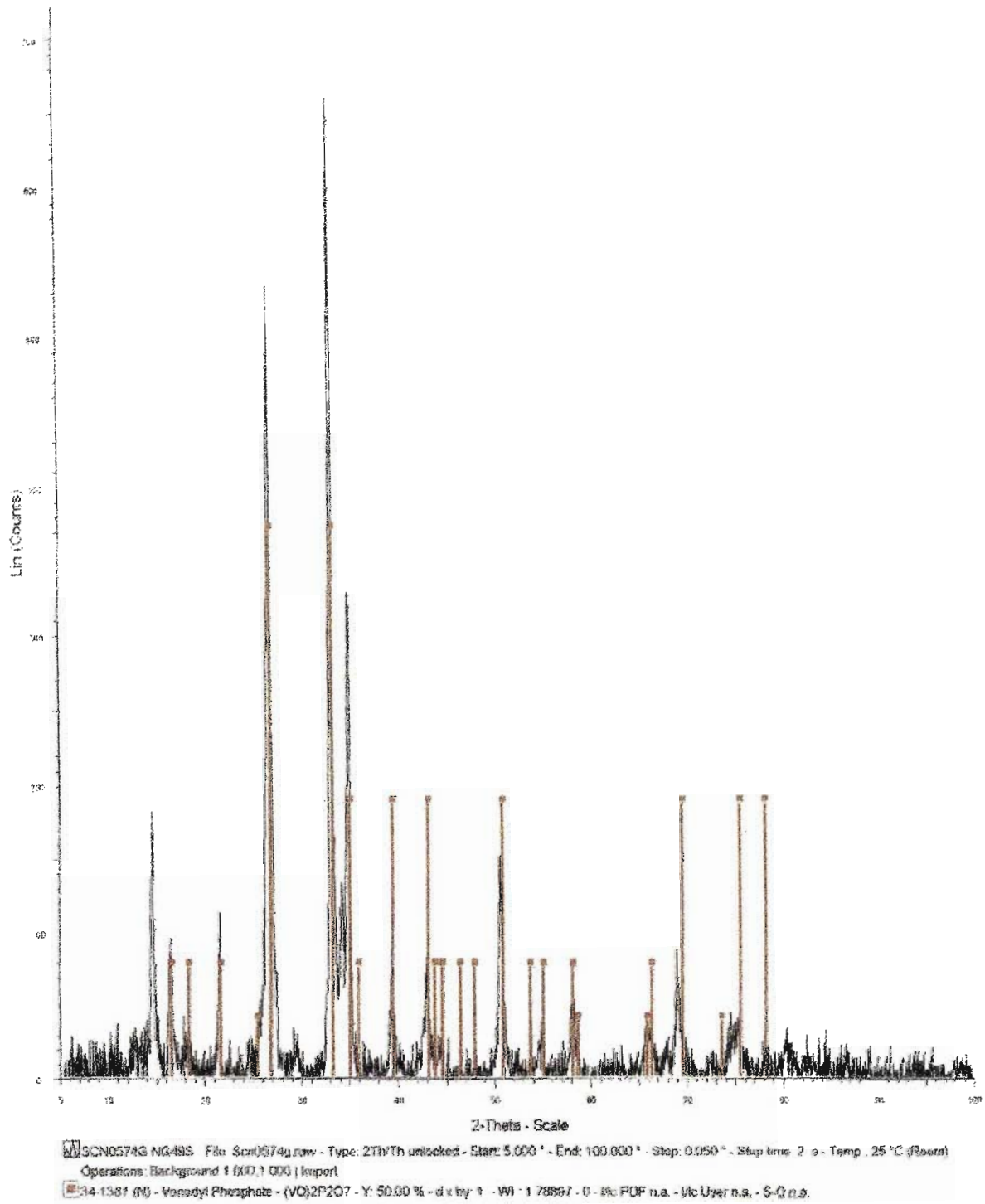

Fig. 5. X-ray diffraction spectrum of VPO-3u

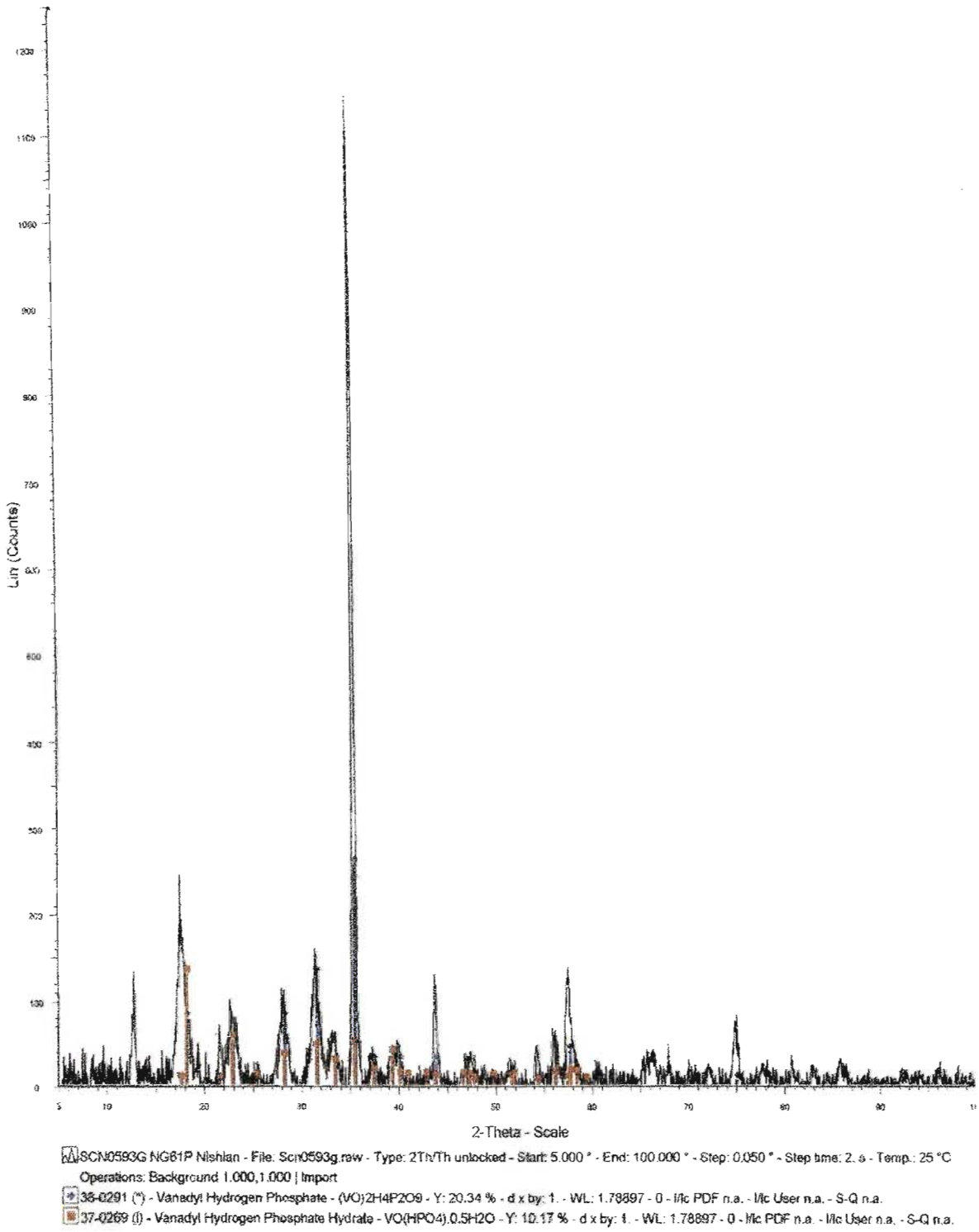

Fig. 6. X-ray diffraction spectrum of VPO-4p

APPENDIX 3

INSTRUMENTATION

1. Inductively coupled plasma – atomic emission spectroscopy (ICP-AES)[1]

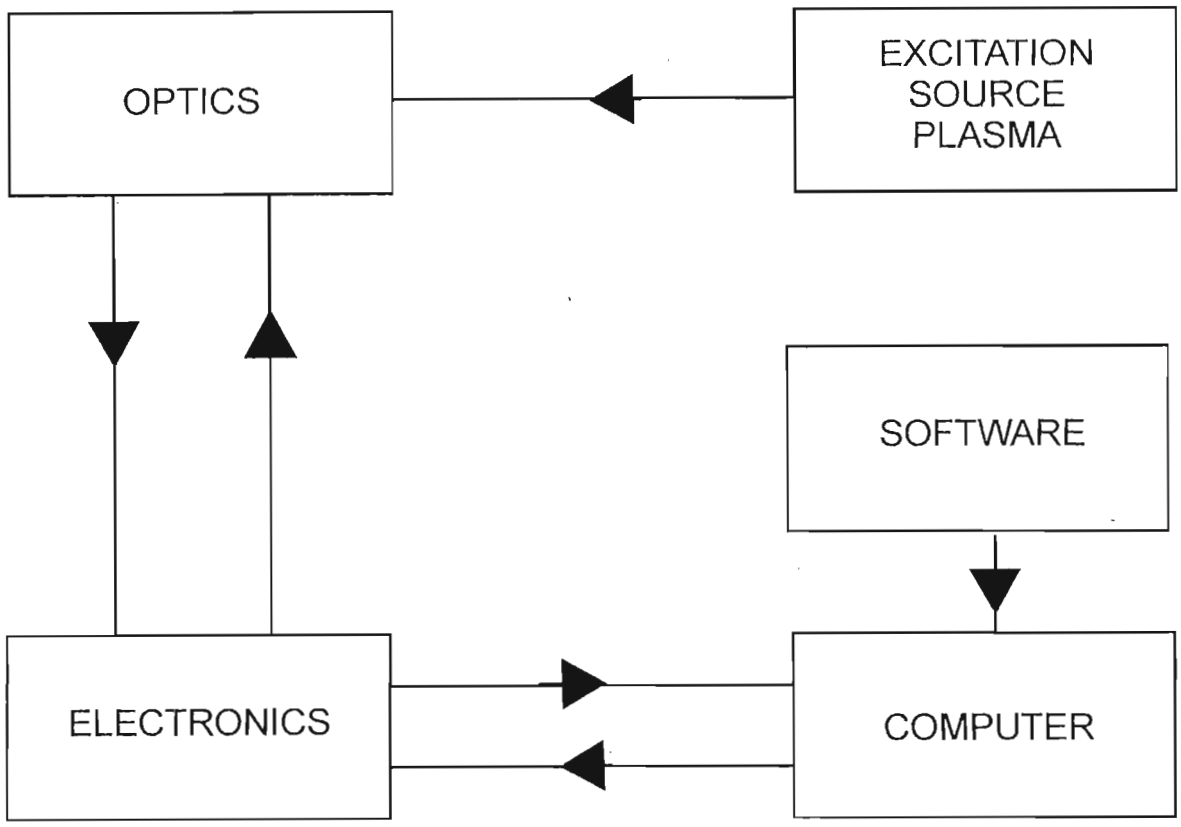

Fig. 1. Flow diagram of the standard configuration of an ICP-AES instrument

The inductively coupled plasma-atomic emission (ICP-AES) spectroscopic method of analysis is an essential tool in the assaying of elements as traces and in very high concentrations. ICP-AES analysis involves introducing the elements to be analysed into argon plasma induced by a high radio frequency (indicated by the "excitation source plasma" box in Fig. 1), where the temperature is in the order of 8000 K. The sample, in the form of an aerosol, is introduced into the plasma via a "torch", where it is excited. Each excited element produces a characteristic spectrum whose light intensity is directly proportional to the quantity of that element present in the sample.

When the atoms of an element are excited, their electrons change orbitals by absorbing energy and emit light with a wavelength characteristic of each element when they return to their initial orbital. Each element can thus be characterized by its emission wavelength.

A plasma generator supplies the energy required to make the electrons change their atomic orbital. High frequency radiation is used to heat a stream of argon and to form plasma via an induction coil. The temperature varies between 5000 K and 10000 K (depending on the zone of the plasma). The sample added to the plasma is reduced to the state of the individual atoms. When the plasma excites these atoms, they re-emit the energy acquired in the form of electromagnetic radiation (light). This energy is composed of wavelengths characteristic of the elements present. The discrimination of these wavelengths is performed by an optical system called a monochromator represented by the optics box in Fig. 1. The beam of light is focused by a convergent lens onto the primary slit of the monochromator and then reaches a holographic diffraction grating. The grating separates the beam into the component lines of its different wavelengths corresponding to the elements in the analysed sample. In this system, the only moving component is the grating. Rotation about its axis sends all the wavelengths present onto the plane of the exit slit. A photomultiplier behind the exit slit receives this radiation and transforms it into electrical signals that are captured by the data processing system. Each angular position of the grating corresponds to a well-defined wavelength. Thus, each beam of light passing through the exit slit of the monochromator is characteristic of the element analysed.

The intensity of the light beam captured by the photomultiplier, represented by the electronics box in Fig. 1, is measured. It is proportional to the concentration of each element analysed. A calibration curve for each element is entered in the data processing system represented by the computer and software boxes in Fig. 1. For a specific intensity, the computer system gives the concentration of the element analysed: this is the basis of quantitative analysis.

The torch and ICP plasma generator

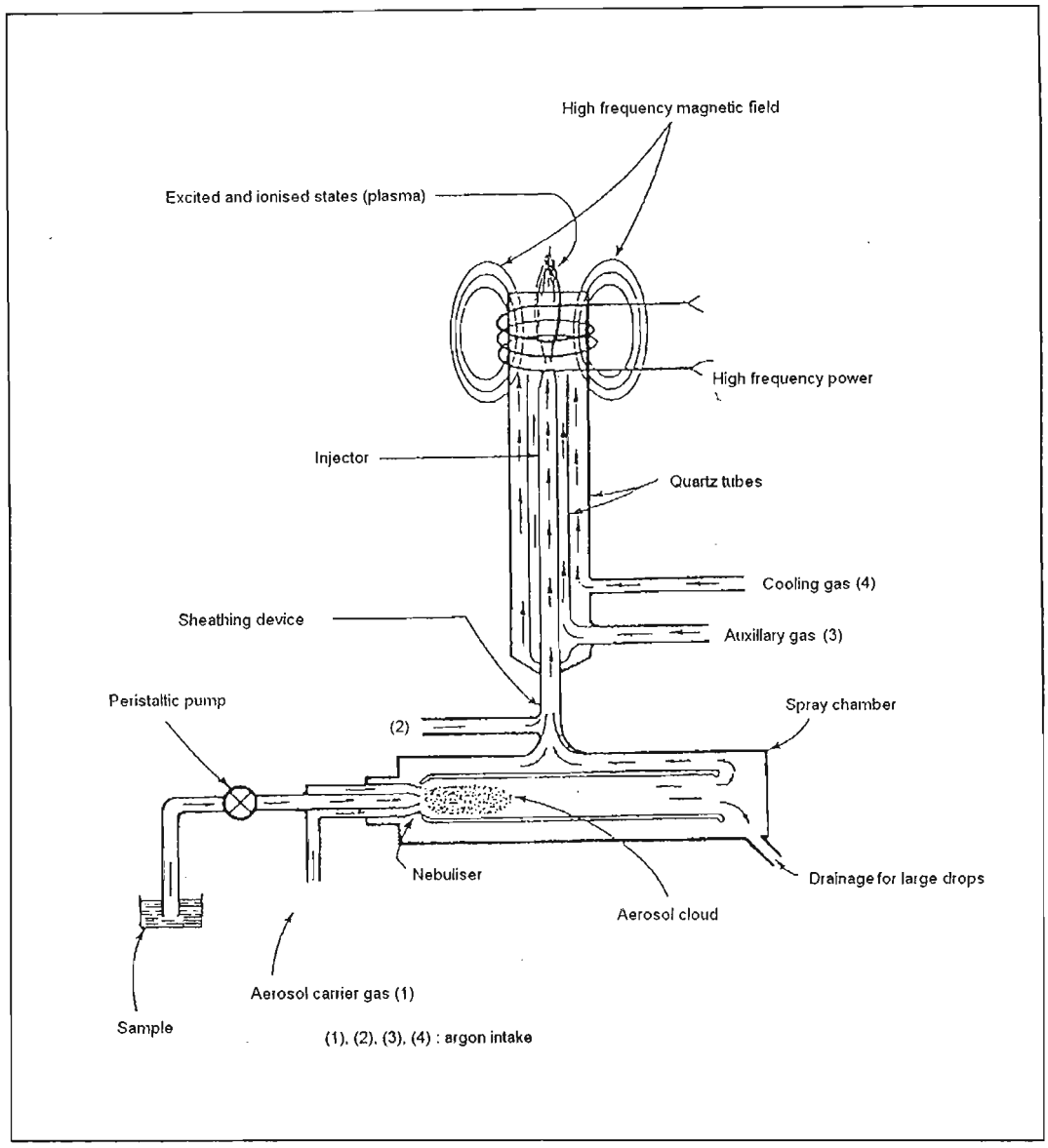

Fig. 2. Schematic view of the ICP source

An automatic water-cooling circuit built into the spectrometer regulates the temperature released by the plasma in the induction coil. The sample is drawn into a capillary tube with a peristaltic pump as shown in Fig. 2 and is sent to the nebuliser, where a fog of fine droplets is formed. The fog is carried to the spray chamber before being transferred to the torch, where it is ionized. The demountable ICP torch is formed from three concentric tubes, connected to the argon source of which two surrounds the central injector connected to the nebuliser via a

sheathing system. There are two argon inlets to the torch itself: one (4) for both cooling and supplying the plasma, the other (3) for the auxillary gas in the case of organic samples. The other inlets (1) nebuliser and (2) coating gas are used for the formation, transport and injection of the aerosol into the plasma core, at the same time contributing to plasma generation.

[1]Skoog, D.A; West, D.M.; Holler, F.J.; *Fundamentals of Analytical Chemistry*; 7th edition; Saunders College Publishing; p 632 Chapter 26 (1996)

2. Gas chromatography[2]

The word "chromatography," formed from the Greek word "chroma" meaning "color," and "graphein" meaning "to write," was coined by Tswett around 1900 to describe his process of separating mixtures of plant pigments. He washed the pigments down a column of adsorbent powder. Such a separation of the components of a mixture for qualitative or quantitative analysis, or for isolation and recovery of the components is the desired end of any type of chromatography.

A gas chromatograph consists of a flowing mobile phase or carrier gas, an injection port, a separation column containing the stationary phase and a detector as indicated in Fig. 3. The organic compounds are separated due to differences in their partitioning behaviour between the mobile phase and the stationary phase in the column. In gas chromatography, the mixture or solute to be separated is vaporized and swept over a relatively large absorbent or adsorbent surface inside a long narrow tube or column. A steady stream of inert carrier gas moves the solute vapours along the column. The different components are moved along the column at different rates and, under proper circumstances, become separated.

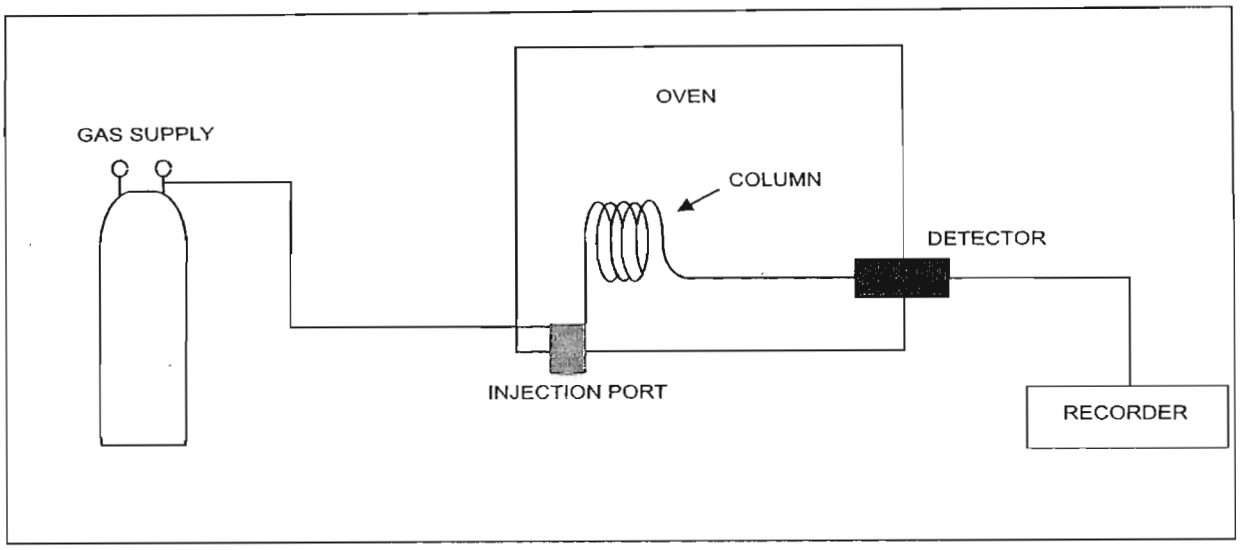

Fig. 3. Gas chromatograph

The gas chromatograph usually consists of a regulated supply of carrier gas which serves as a means of sample introduction, an injecton port, a column for separating the components of the sample, a detector for detecting and signaling the components as they emerge in sequence from the column, and a recorder for measuring and recording the signal from the detector. The arrangement of these components is shown in Fig. 3. The injection port consists of a rubber septum through which a syringe is inserted to inject the sample. Sampling loops were directly connected to the injection ports of both gas chromatographs in the setup used in this project. The sample from these loops was automatically flushed into the GC. The injection port is maintained at a higher temperature than the boiling point of the least volatile component in the sample mixture. Since the partitioning behaviour is dependant on temperature, the separation column is usually contained in a thermostatically controlled oven. Starting at a low oven temperature and increasing the temperature over time to elute the high-boiling components accomplish separating components with a wide range of boiling points.

Each component has a characteristic retention time in the column for a given set of instrumental conditions. These retention times serve as a means of qualitative analysis. The sensitivity of detection for a given detector varies according to peak height.

There are two types of GC columns, viz. packed and capillary columns. Packed columns are typically a glass or stainless steel coil that is filled with the stationary phase. Capillary columns on the other hand, are thin fused silica (purified silicate glass) capillaries (typically 10-100 m in length and 250 μm inner diameter that have the stationary phase coated on the inner surface. Capillary columns provide much higher separation efficiency than packed columns but are more easily overloaded by too much sample. The stationary phase can be polar, intermediate or non-polar in nature. The ideal stationary phase is judged by the types of components to be separated.

[2]http://www.chem..vt.edu/chem.-ed/sep/gc/gc.html

3. Fourier transform infrared spectroscopy[3]

3.1 Introduction to FT- IR

The vibrational and rotational energies of molecules can be studied by infrared spectroscopy. A common application of FT-IR spectroscopy is for "group frequency" analyses. In molecules certain functional groups show certain vibrations in which only the atoms in the group move. Since the rest of the molecule is mechanically uninvolved in the vibration, a group vibration will have a characteristic frequency that remains constant no matter what molecule the group is in. This group frequency can be used to reveal the presence or absence of the group in the molecule and this is frequently of tremendous help in characterizing the molecular structure. In IR spectroscopy the micron ($\mu = 10^{-4}$ cm) is more often used as the dimension for wavelength. Using this unit, the visible region is about 0.4-0.7 μ, the near infrared is about 0.7-2.5 μ, the fundamental infrared region is about 2.5-50 μ and the far infrared is about 50 μ to a fraction of a mm. The reason for a division at about 2.5 μ is that absorption caused by fundamental vibrational transitions fall on the long wavelength side of 2.5 μ. The reason for a division at about 50 μ is largely instrumental.

The properties that electromagnetic radiation and molecules have in common are energy and frequency. However, the frequency, ν, in hertz (Hz) in this part of the spectrum is an inconveniently large number so a number that is proportional to frequency is commonly used.

This is called the wavenumber, ω (cm^{-1}), which denotes the number of waves in a 1-cm-long wave train. This unit is related to the other units by:

$$\omega = \nu/c = 1/\lambda_{cm} = 10^4/\lambda_{\mu}$$

where λ_{cm} and λ_{μ} are the wavelengths expressed in cm and μ respectively. Grating instruments deliver spectra where the horizontal coordinate is linear with wavenumber. Results are reported in wavenumbers since these are proportional to molecular properties, frequency and energy. The vertical coordinate in an IR spectrum is usually presented linearly with sample transmittance. Transmittance is defined as the radiant power of the radiation which is incident on the sample, divided into the radiant power transmitted by the sample.

In a typical infrared spectrometer, a source simultaneously emits all the infrared frequencies of interest. These radiation frequencies are about the same order of magnitude as the molecular vibrational frequencies. The molecule that matches the vibrational frequency of the molecule shall absorb some of the radiation. Most of the other frequencies are transmitted. The absorption of radiation has occurred because this particular molecule has increased its vibrational energy. This occurs at the expense of the energy of the IR radiation that has been absorbed.

In order for any infrared absorption to occur, the molecular vibration must cause a change in molecular dipole moment.

[3]http://www.uksaf.org/tech/list.html

3.2 Attenuated total reflection (ATR)[4]

The attenuated total reflection method is a true reflection spectrum from the interface of a high refractive index transmitting prism and the substance under investigation. It is observed that if certain conditions were met, infrared radiation entering a prism made of a high refractive index infrared transmitting material such as an ATR crystal would be totally internally reflected as shown in Fig. 4. This internal reflectance creates an evanescent wave that extends beyond the surface of the crystal. In regions of the infrared spectrum where the sample absorbs energy, the envanescent wave will be attenuated.

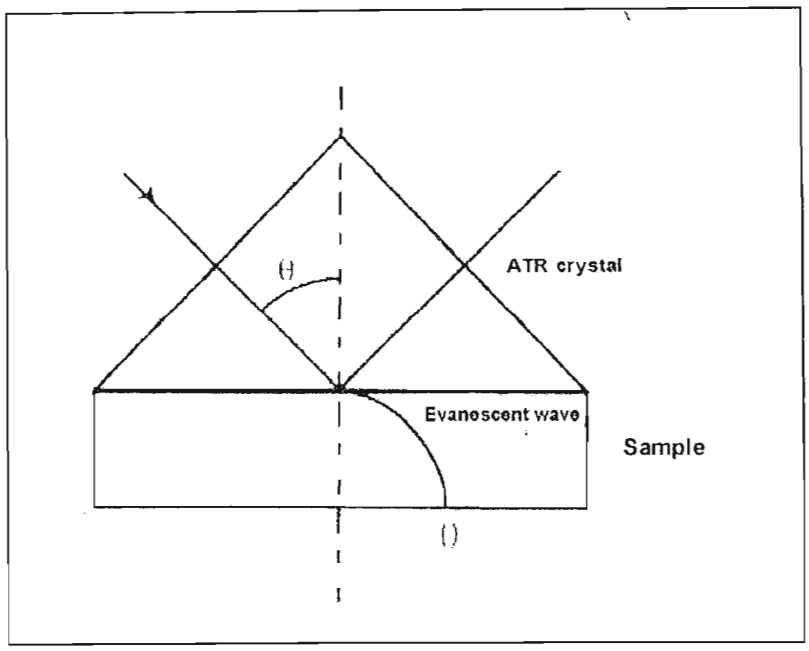

Fig. 4. Reflection of an IR beam off the interface between a sample and the ATR crystal and the resulting evanescent wave that is created.

Total internal reflection occurs when the angle of the incident radiation θ, exceeds the critical angle, θ_c. The critical angle is a function of the refractive indices of the sample and ATR crystal and is defined as:

$$\theta_c = \sin^{-1} \frac{n_2}{n_1}$$

where n_1 is the refractive index of the ATR crystal and n_2 is the refractive index of the sample (Chittur, K.; webpage). High refractive index materials are chosen for the ATR crystal to minimize the critical angle. The intensity of the evanescent wave decays exponentially with distance from the surface of the ATR crystal. A factor that affects the quality of an ATR spectrum is the efficient contact of sample with the crystal. Because the evanescent wave decays very rapidly with distance from the surface, it is important to have the sample in intimate

contact with the crystal. This is easily achieved by applying pressure on the powder sample against the crystal.

In the technique of attenuated total reflectance, the spectrum of the reflected radiation closely resembles the absorption curve (Miller, R.G.J. p137). When radiation passing through a medium of high refractive index strikes the interface between that medium and one of lower refractive index, it is reflected with little attenuation when the angle of incidence is greater than a certain critical angle. The attenuation is in fact dependant on the refractive index change. By placing a sample in optical contact with a material of high and constant refractive index, any change in its refractive index will give rise to a change in reflection at the interface. Since the refractive index of a material changes rapidly at those wavelengths where it absorbs, the plot of attenuated total reflectance will resemble the absorption spectrum.

Successful operation depends to a great extent upon intimate contact between the sample and the crystal, but this is usually readily achieved and direct measurements can be made. The reflectance curve is quite independent of thickness, but the angle of incidence is important and must be carefully chosen. This angle determines the apparent depth of beam penetration into the sample, a steep angle, i.e. small and of incidence, produces a deeper penetration than a shallow angle. Optimum results are generally obtained between two and five degrees above the critical angle. This angle depends on the relative values of refractive index of sample and crystal. The water bands in ATR do not blank out the rest of the spectrum to such an extent as in the KBr pellet method FT-IR.

A crystal material must have a high index of refraction to allow internal reflectance. Materials with a refractive index greater than 2.2 are normally chosen as ATR crystals. Zinc selenite has a refractive index of 2.4 and a transmission range from 20,000 to 650 cm^{-1}.

The spectrum shows much more detail than a reflection spectrum from air because the refractive index of the interface is below unity. The great advantage of an ATR spectrum is that it is recognizably similar to a transmission spectrum (FT-IR). However certain characteristic differences are usually observed compared with a transmission spectrum:

(i) The bands are shifted to longer wavelengths.

(ii) The bands at short wavelengths appear to be weaker.

(iii) The weaker bands appear more prominent and conversely very intense bands are less inclined to dominate the spectrum as much.

(iv) The character of the spectrum changes markedly with angle of incidence. It may be necessary to change the angle of incidence to achieve optimum results.

(v) The spectrum is that of the surface layer and, therefore, greases, dirt, grit, silicone, etc, will contaminate the spectrum more readily.

For these reasons the best identifications are performed by comparison of the unknown against an ATR spectrum produced under exactly identical conditions. The prime requirement for a good ATR spectrum is that the material under analysis should be brought into good physical contact with the face of the prism, therefore rubbery or soft materials produce the best ATR spectra (Miller, R.G.J; p 137).

[4]http://www.eb.uah.edu/~kchittur/bmreview/node3.html

4. X-ray spectrometry

Since the discovery of X-rays by Roentgen in 1896, the electromagnetic spectrum between 0.1 and 200 Å has been a source of significant contributions to our fundamental knowledge of atomic structure. Bombarding matter with high-energy particles such as electrons or protons generates X-rays. When an atom is bombarded in this manner, an electron is ejected from one of the inner shells of the atom. This vacancy is immediately filled by an electron from a higher-energy shell, creating a vacancy in that shell that is, in turn, filled by an electron from yet a higher shell. Thus, by a series of transitions, L $\rightarrow$K, M$\rightarrow$L, N$\rightarrow$M, each new vacancy is filled until the excited atom returns to its ground state. This electronic transition results in the emission of a characteristic X-ray spectral line whose energy, $h\nu$, is equal to the difference between the binding energies of the two electrons involved in the transition. Only certain electronic transitions are permitted by quantum-mechanical selection rules. The energies or wavelengths of the X-ray spectral lines are the basis for qualitative analysis.

4.1 Energy dispersive X-ray spectrometry (EDX)[5]

As the electron beam of the scanning electron microscope (SEM) is scanned across the sample surface, it generates X-ray fluorescence from the atoms in its path. The energy of each X-ray photon is characteristic of the element that produced it.

A solid-state detector composed of Si and Li, is responsive to the energies of the characteristic X-ray radiation. Instruments utilizing these detectors are called energy-dispersive X-ray spectrometers. The energy of a characteristic X-ray produces an electronic pulse-amplitude distribution in the detector. The EDX microanalysis system collects the X-rays, sorts and plots them by energy and automatically identifies and labels the elements responsible for the peaks in this energy distribution.

Hence, an entire X-ray spectrum from several elements in a specimen can be stored at one time.

The EDX data are typically compared to either known or computer-generated standards to produce a full quantitative analysis showing the sample composition. The EDX instrument is also capable of giving maps of distributions of elements over areas of interest.

The detector must operate at liquid-nitrogen temperatures, and a reservoir attached to the detector must be filled periodically with liquid nitrogen. The preamplifier, pulse processor and pileup-rejection circuitry constitute a sophisticated electronic package to maintain the quantitative properties of the signals produced in the detector. These are necessary to ensure high performance with respect to energy resolution, data-acquisition times and signal-to-noise ratio (i.e. detection limit).

[5]http://www2.arnes.si/~sgszmeral/eds/eds.html

4.2 Scanning electron microscopy (SEM)[6]

In the scanning electron microscope (SEM), a very fine "probe" of electrons with energies up to 40 keV is focused at the surface of the specimen in the microscope and scanned across it in a pattern of parallel lines. A number of phenomena occur at the surface under electron impact: most important for scanning microscopy is the emission of secondary electrons with energies of a few tens eV and re-emission or reflection of the high-energy backscattered electrons from the primary beam. The intensity of emission of both secondary and backscattered electrons is very sensitive to the angle at which the electron beam strikes the surface, i.e. to topological features on the specimen. The emitted electron current is collected and amplified; variations in the resulting signal strength as the electron probe scans across the specimen are used to vary the brightness of the trace of a cathode ray tube being scanned in synchronism with the probe. There is thus a direct positional correspondence between the electron beam scanning across the specimen and the fluorescent image on the cathode ray tube.

The magnification produced by the scanning microscope is the ratio between the dimensions of the final image display and the field scanned on the specimen. Usually, the magnification range of SEM is between 10 and 200 000 X and the resolution is between 4 and 10 nm (40 – 100 angstroms).

[6]http://www2.arnes.si/~sgszmera1/sem/sem/html

4.3 X-ray diffraction (XRD)

In wavelength-dispersive spectrometers, a schematic of which appears in Fig. 5, wavelengths are separated by Bragg diffraction from a single crystal. The X-ray tube is usually of high intensity (approx. 3 kW) with a stabilized high-voltage supply. This is necessary because large losses of characteristic radiation occur due to the relatively low reflectivity of the dispersive crystals. The detector is mounted on a goniometer, which allows the detector to accept one wavelength at a time at the 2θ diffraction angle, and covers a broad range from a few degrees to 150 degrees. Either a proportional or scintillation counter detector is used, or both in

tandem arrangement. The associated electronics include a DC power supply, linear amplifier and recorder.

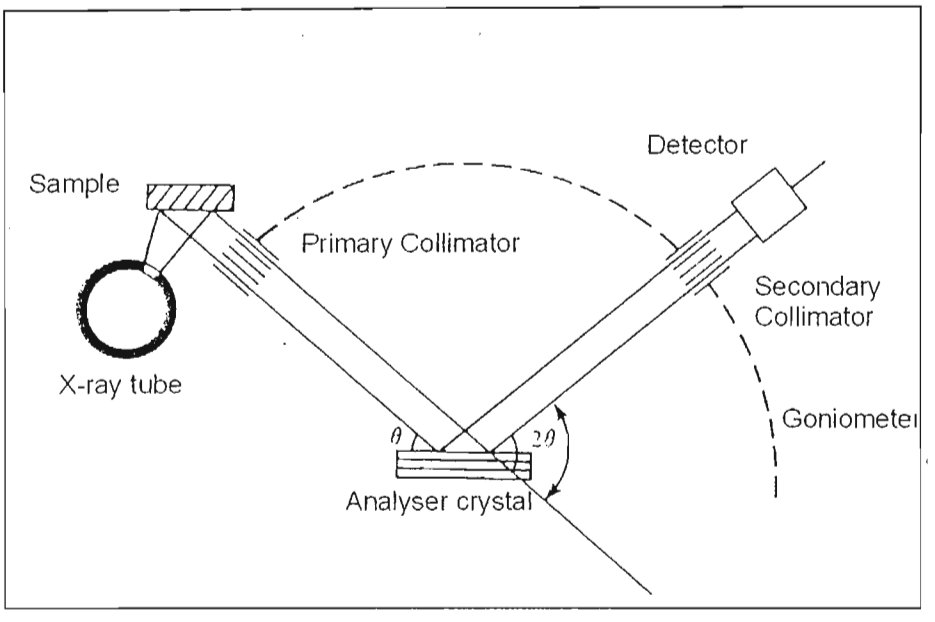

Fig. 5. A schematic representation of an XRD spectrometer

Bombarding a suitable target with electrons produces the X-rays. When the electrons hit the target, they "move" electrons around the orbitals, which results in a series of emission wavelengths as the atom returns to an unexcited state. The resulting electron excitation in the source produces a broad band of energies that are high energy X-rays. The sample is irradiated with the high energy X-rays to produce a secondary beam of fluorescent X-rays. These X-rays are passed through a collimator and thus directed to a single analyzer crystal that separates the wavelengths. The wavelengths of the X-rays produced by the powdered sample and diffracted by the analyzer crystal obey the Bragg equation:

$$\mathbf{n\lambda = 2dsin\theta}$$

where λ = wavelength of X-rays, d = spacings of atoms in powdered sample and n = integer.

The Bragg equation links the d-spacings on the powdered sample to the angle of turn of the analyzer crystal. The data obtained shows a series of lines of varying intensities at different 2θ values, obtained as the analyser crystal turns. A qualitative analysis of the sample is thus carried out (Brady, J.E. *et al.* (1993)).

References

Brady, J.E.; Holum, J.R.; *Chemistry: The Study of Matter and its Changes*; John Wiley and ons; p 386 Chapter 9 (1993)

Chittur, K.; *http://www.eb.uah.edu/~kchittur/bmreview/node3.html*

Miller, R.G.J.; *Laboratory Methods in Infrared Spectroscopy*; Heydon and Son Ltd,London, N.W.; p 137 (1988)

APPENDIX 4

MICROWAVE DIGESTION PROGRAM FOR CATALYST DIGESTION

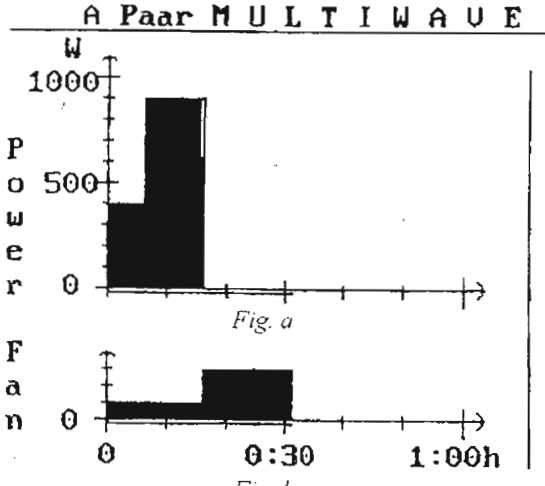

Fig. a

Fig. b

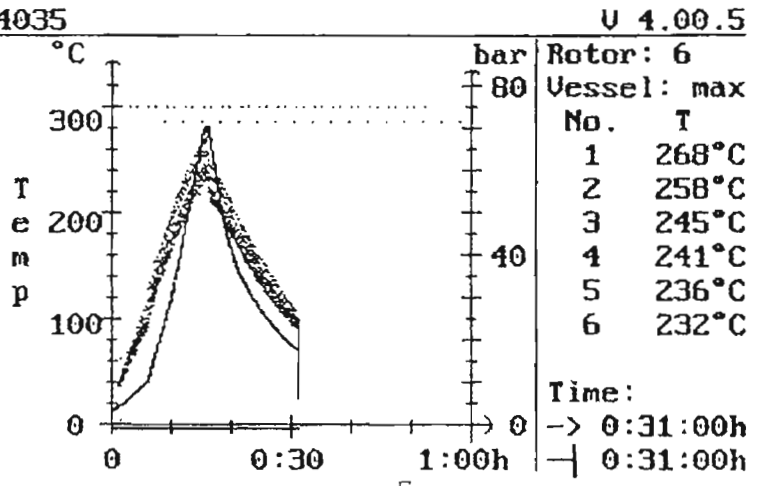

Fig. c

Fig. a is a graph of the power supplied to the microwave vs time. Fig. b is a graph of the power supplied to the fan in the microwave vs time. Six samples were digested at a time in separate vessels. The temperature in each vessel is shown in Fig. c which is a graph of temperature in each vessel vs time. The digestion time was 31 minutes.

Power W	Time mm:ss
400	6:00
900	10:00
0	15:00
0	0:00
0	0:00
0	0:00
0	0:00
0	0:00

Table 1

Ves	Weight max /g	Reag 1 /ml HCl	Reag 2 /ml HNO_3	Reag 3 /ml	Remark
1	0.100	3.50	1.50		
2	0.100	3.50	1.50		
3	0.100	3.50	1.50		
4	0.100	3.50	1.50		
5	0.100	3.50	1.50		
6	0.100	3.50	1.50		

Table 2

Table 1 shows the power supplied to the microwave over the digestion period. Table 2 shows the amounts of reagents the were added to the samples in the Anton Paar microwave digestion vessels containing the catalyst samples.

SEM image of residue obtained from digestion of VPO-1c

Elemental composition:

C	21.93 (wt%)
O	60.03
Cl	18.04

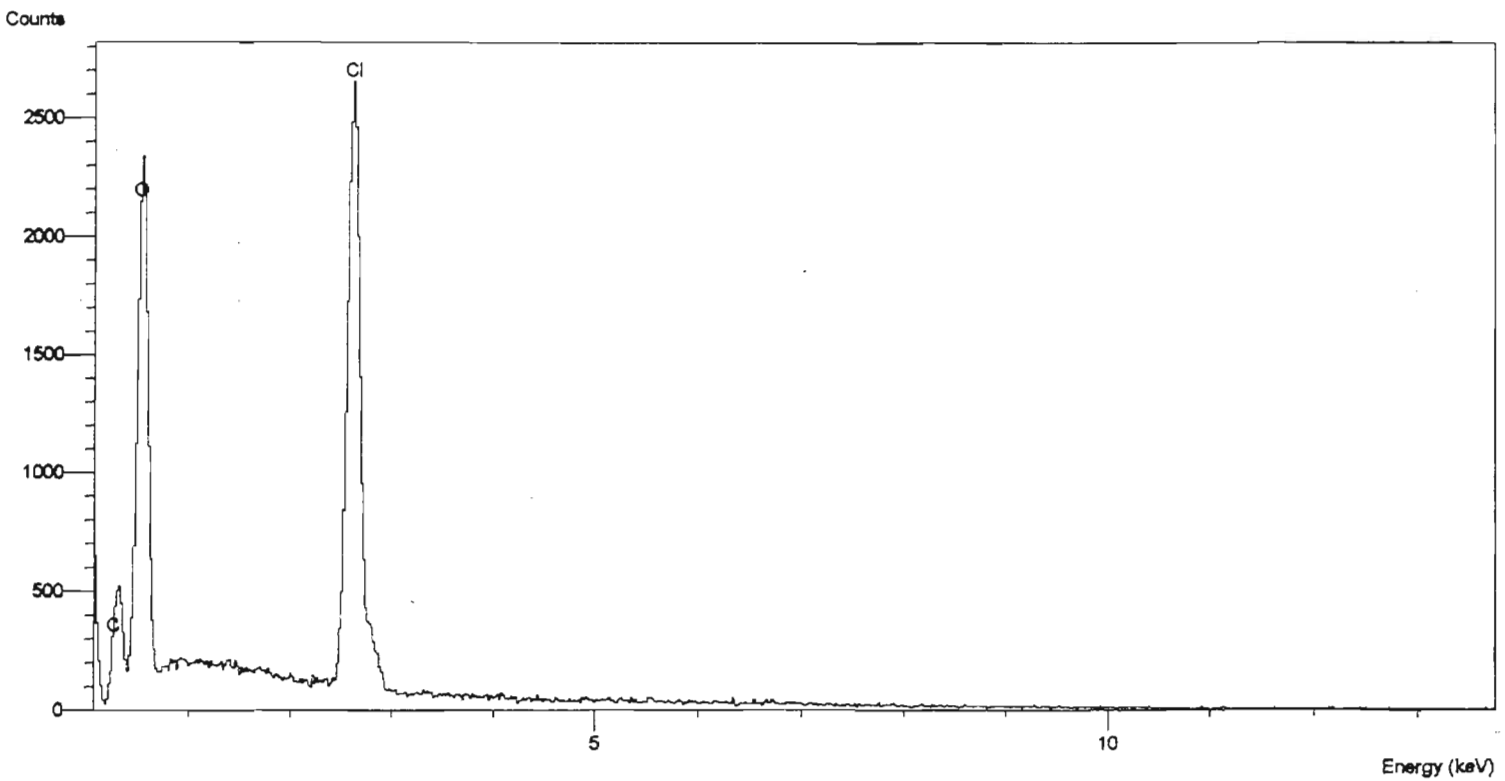

EDX spectrum of residue from VPO-1c digest

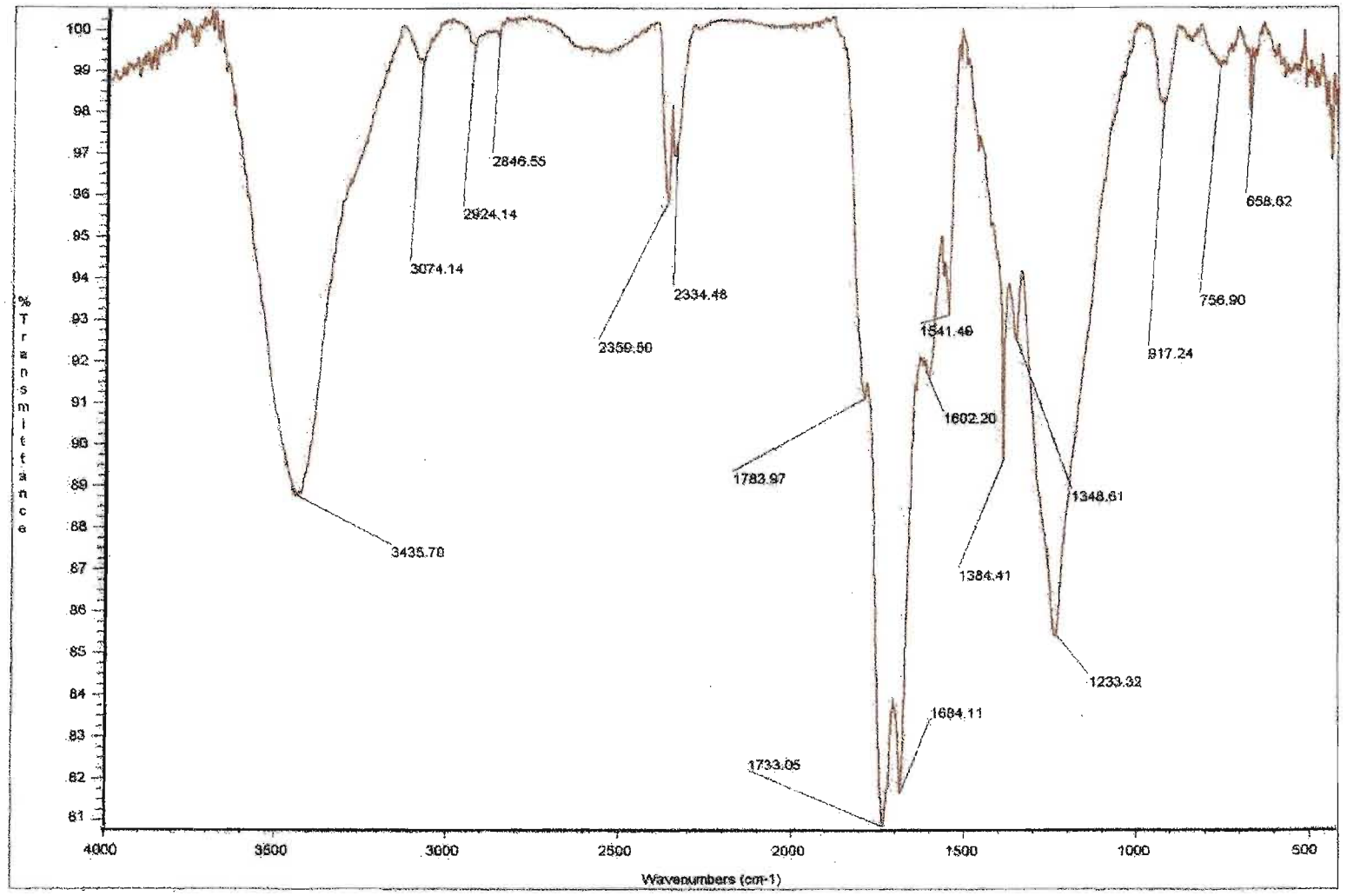

FT-IR spectrum of residue obtained from digestion of VPO-1c

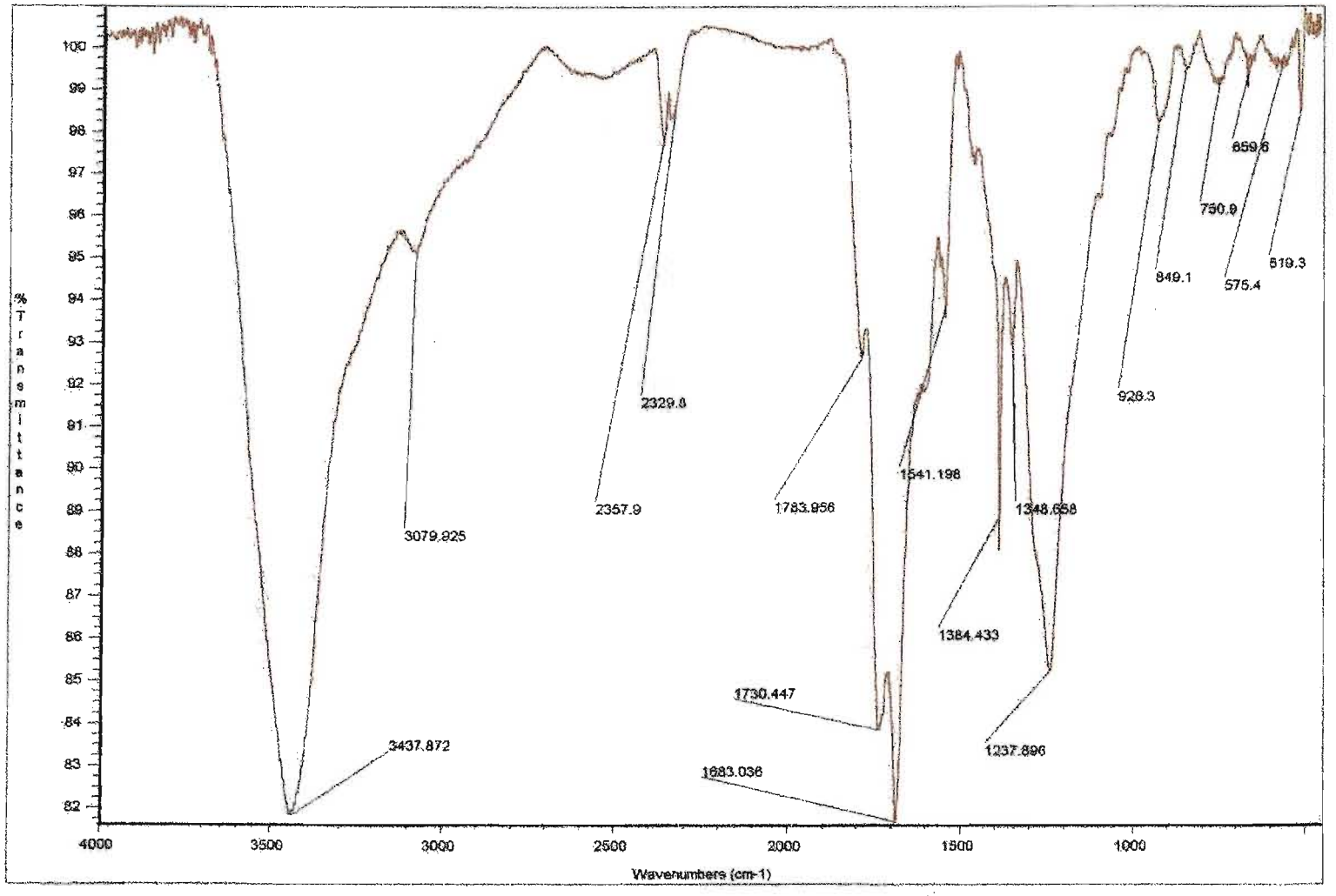

FT-IR spectrum of residue obtained from digestion of VPO-4c

APPENDIX 5

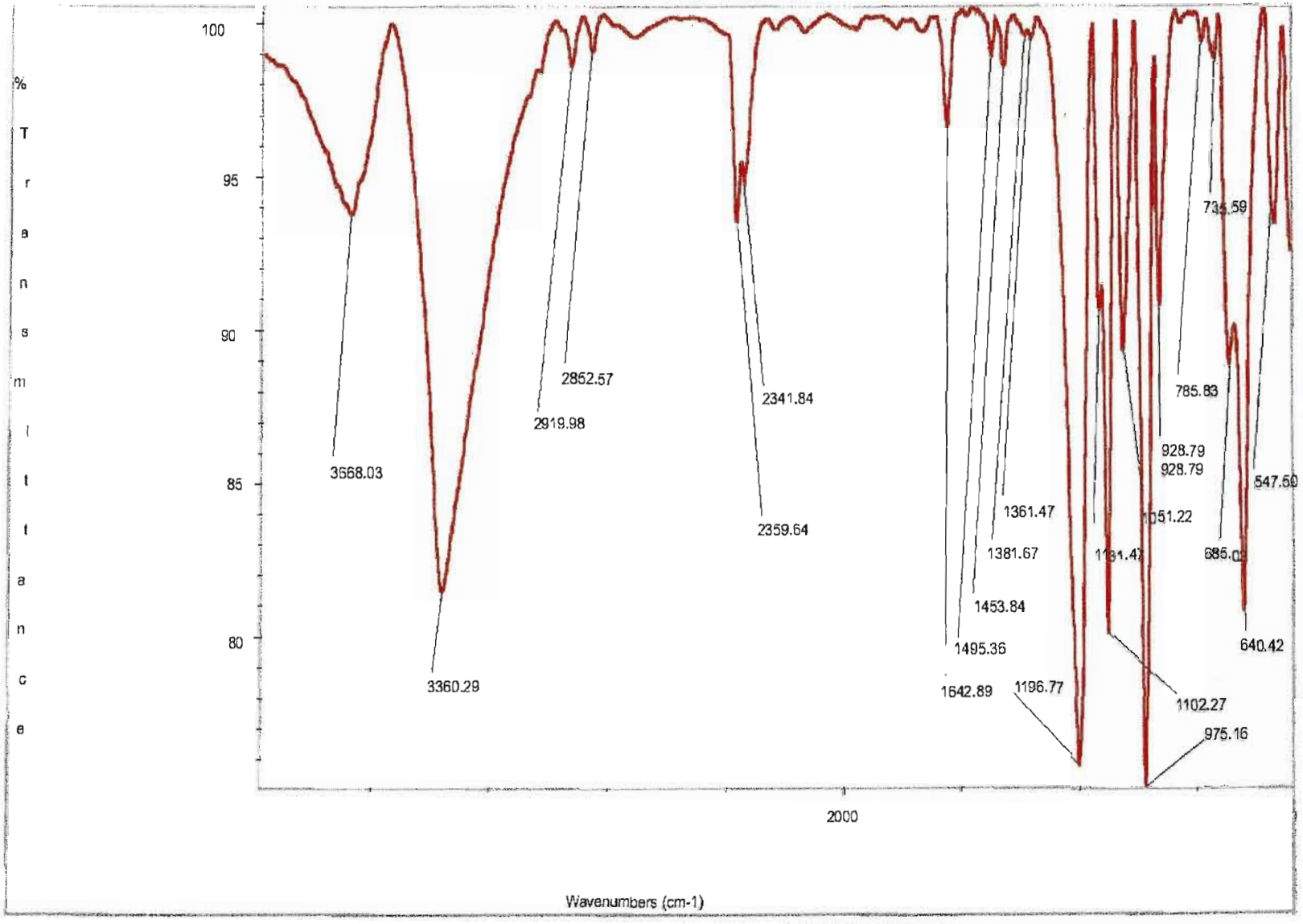

Fig. 1. FT-IR spectrum of VPO-1p

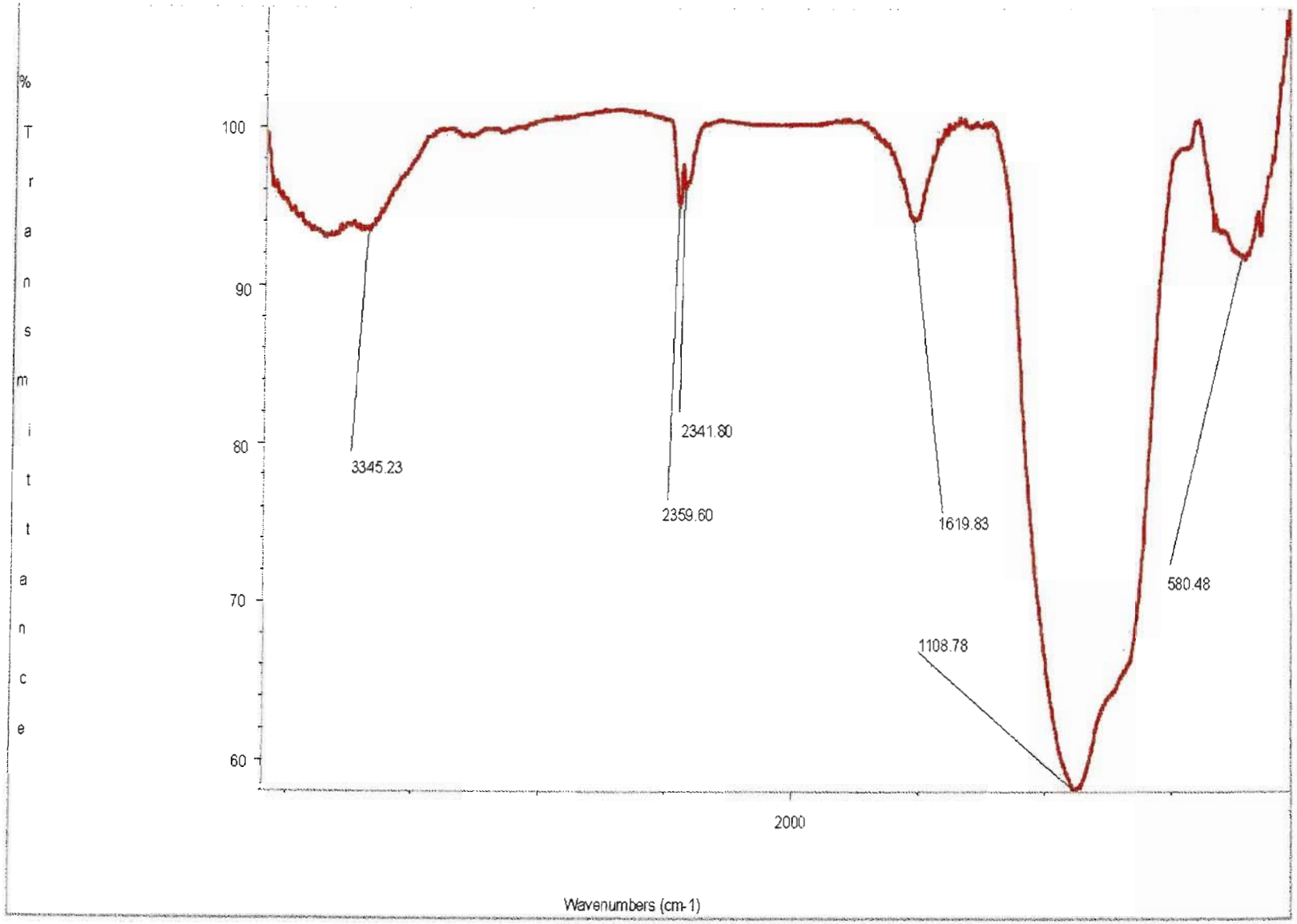

Fig. 2. FT-IR spectrum of VPO-1c

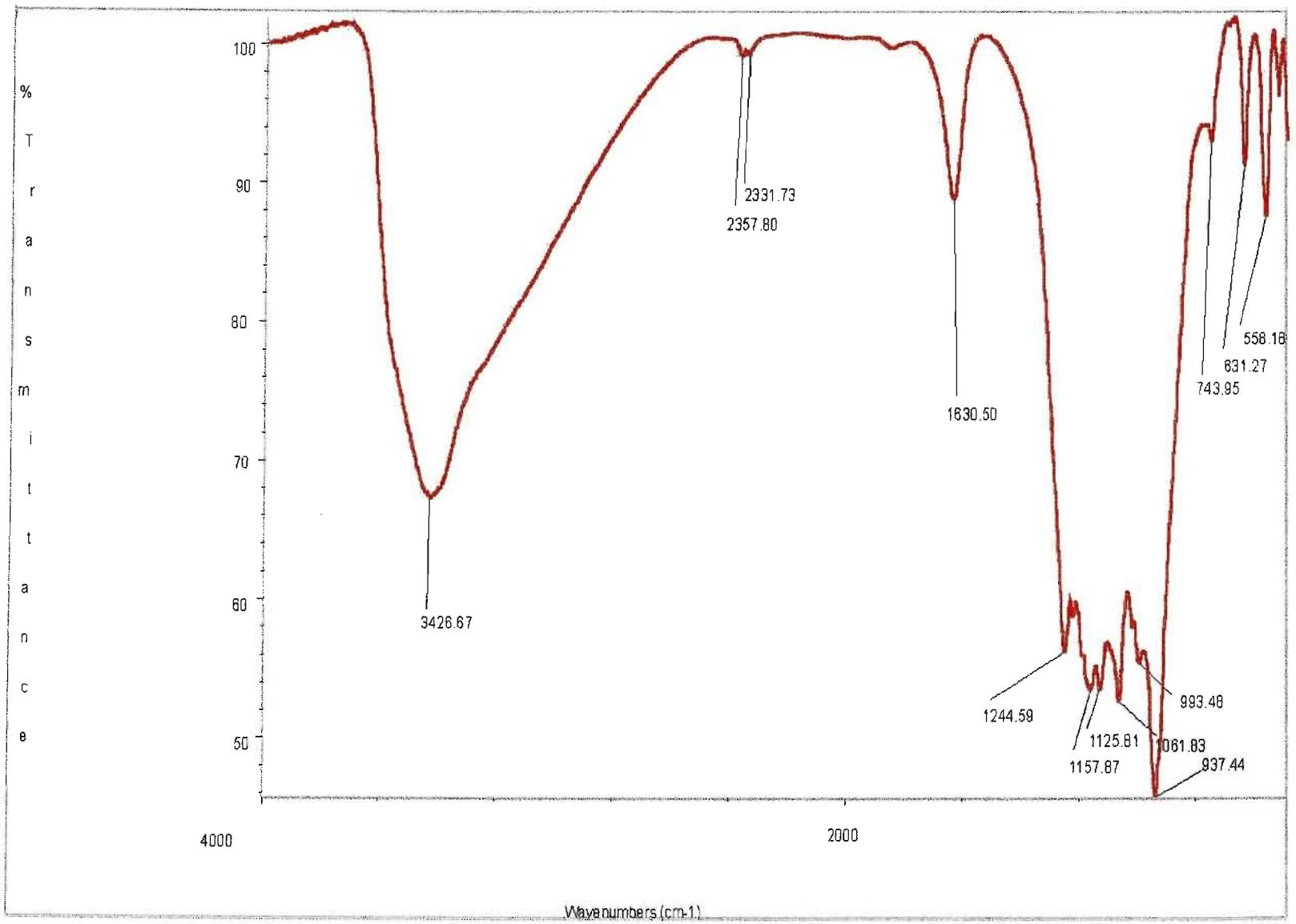

Fig. 3. FT-IR spectrum of VPO-1u

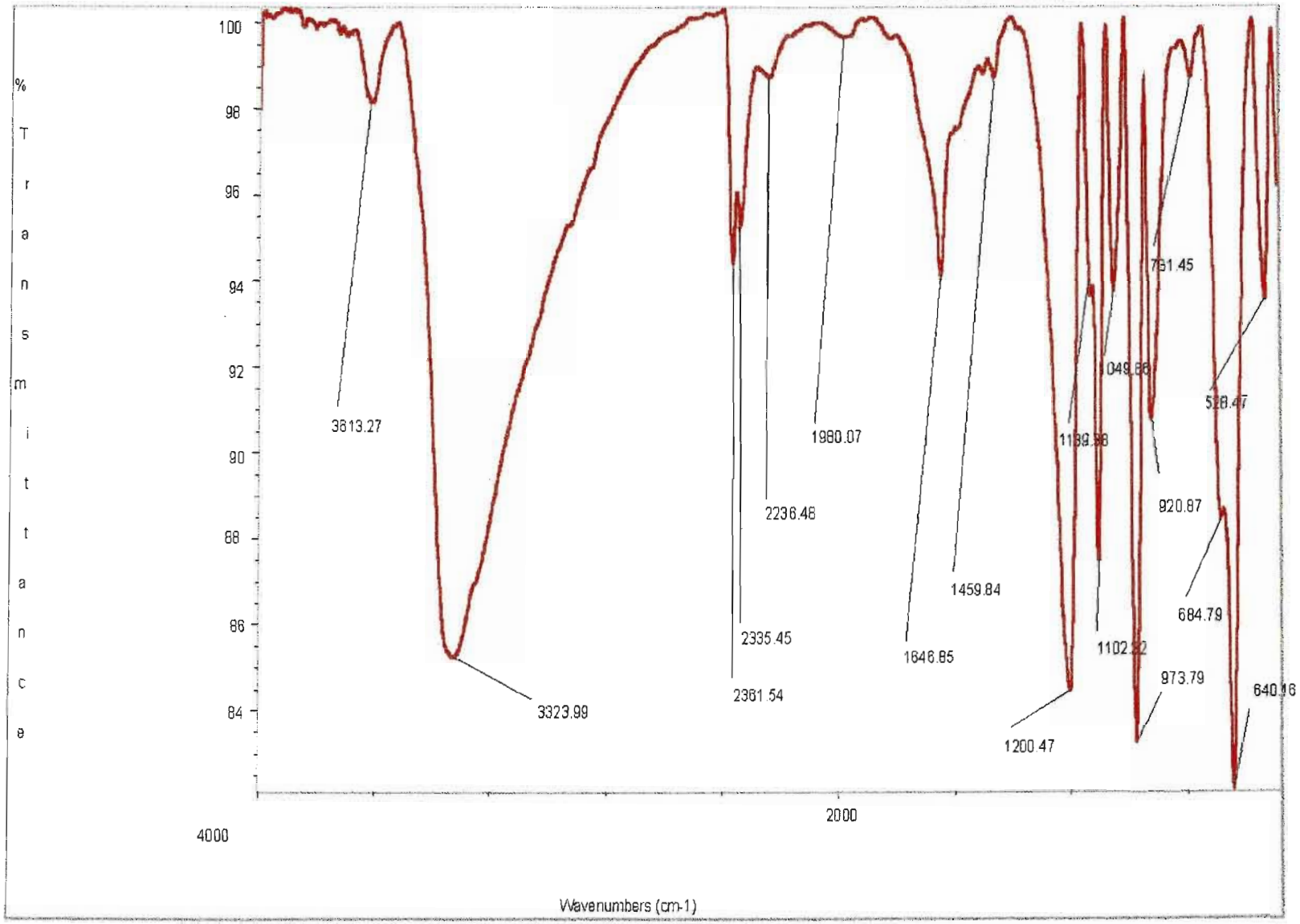

Fig. 4. FT-IR spectrum of VPO-2p

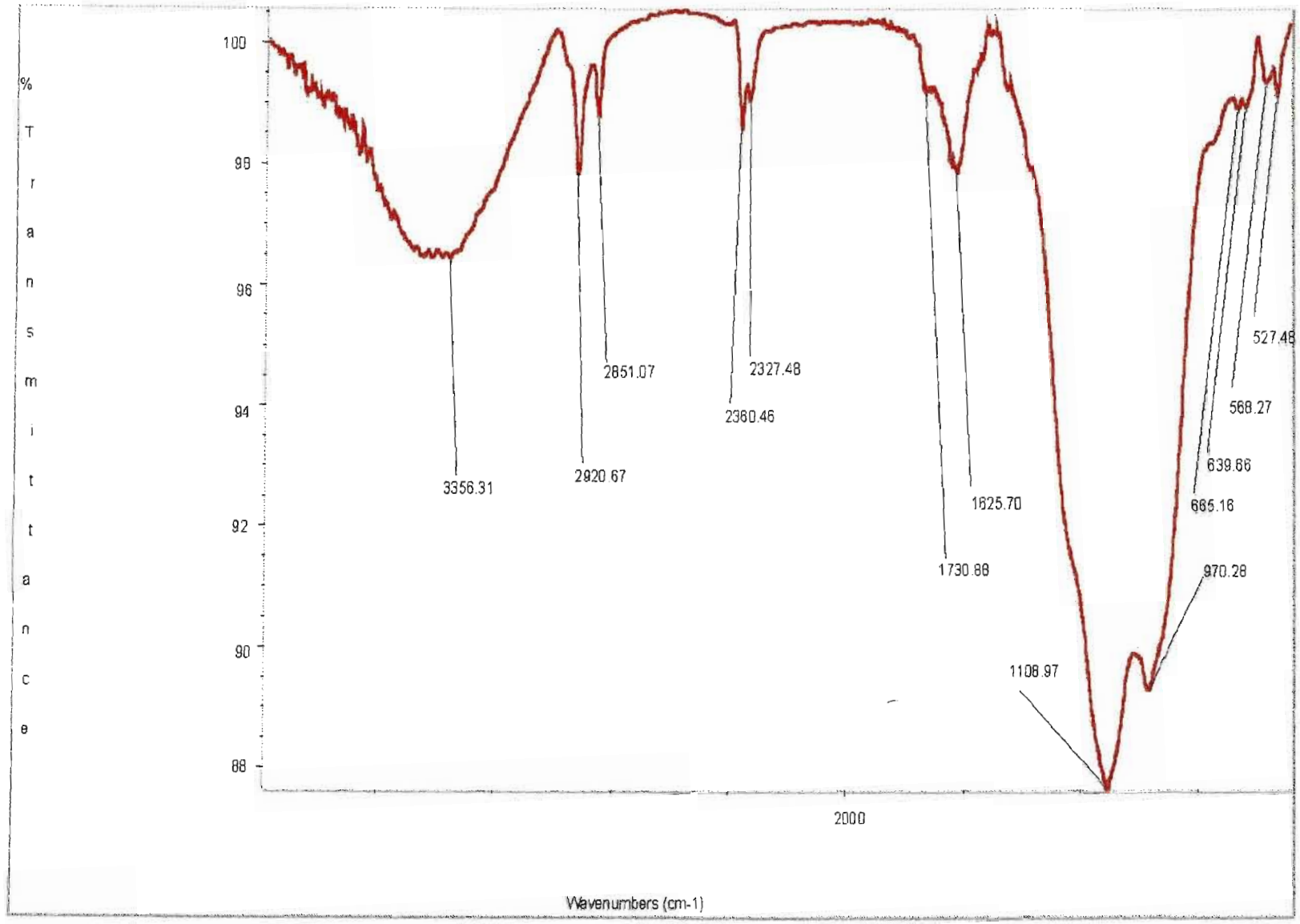

Fig. 5. FT-IR spectrum of VPO-2c

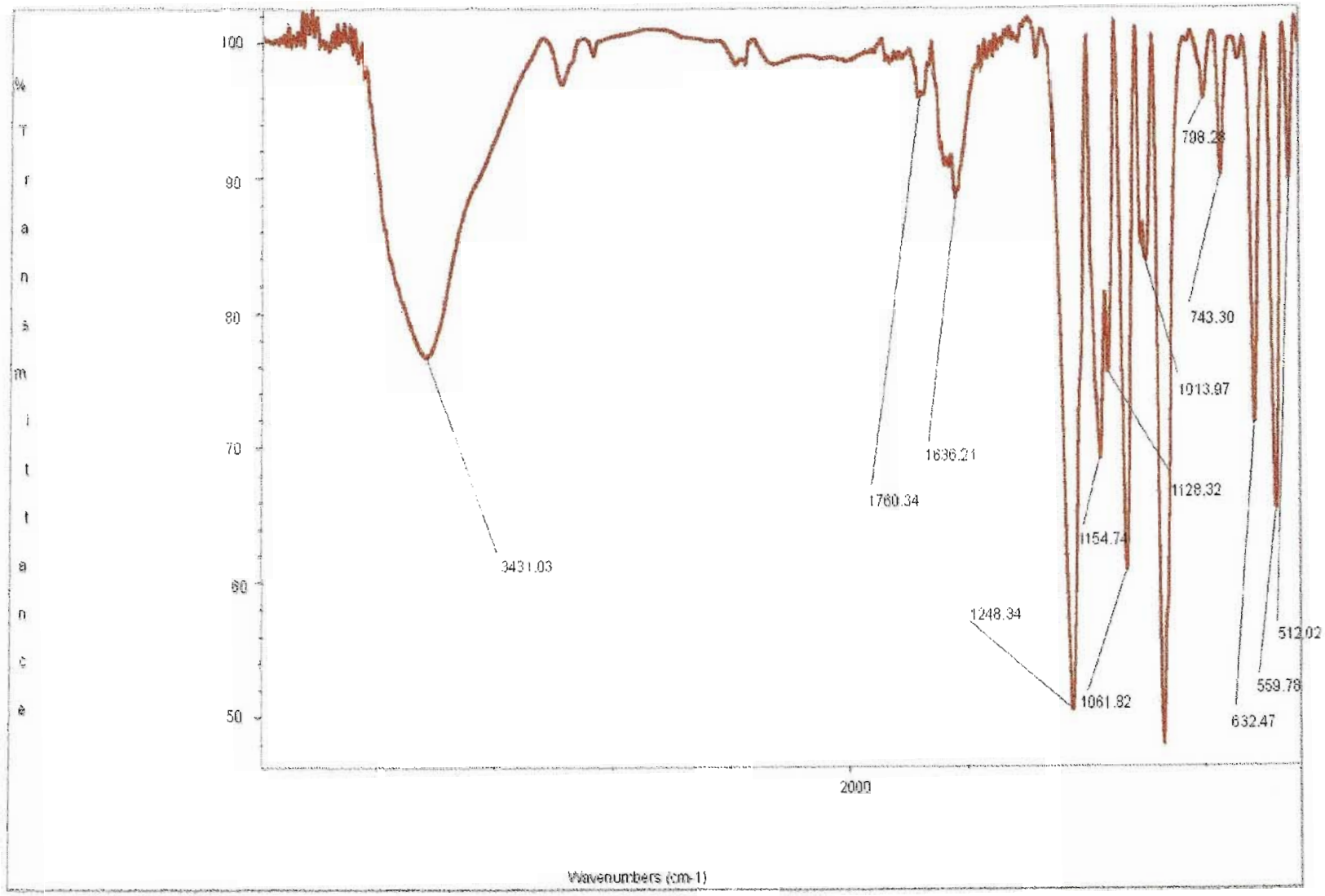

Fig. 6. FT-IR spectrum of VPO-2u

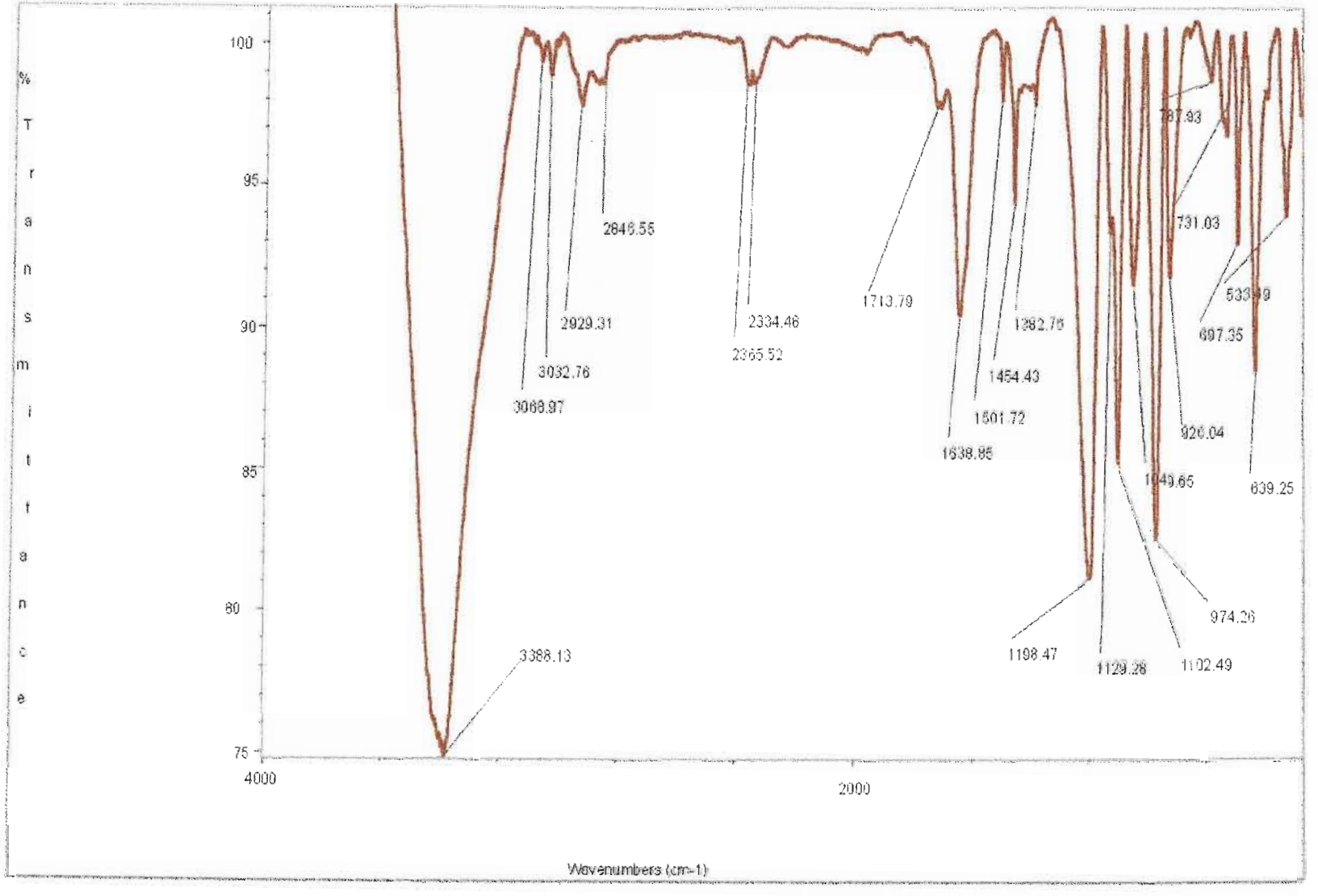

Fig. 7. FT-IR spectrum of VPO-3p

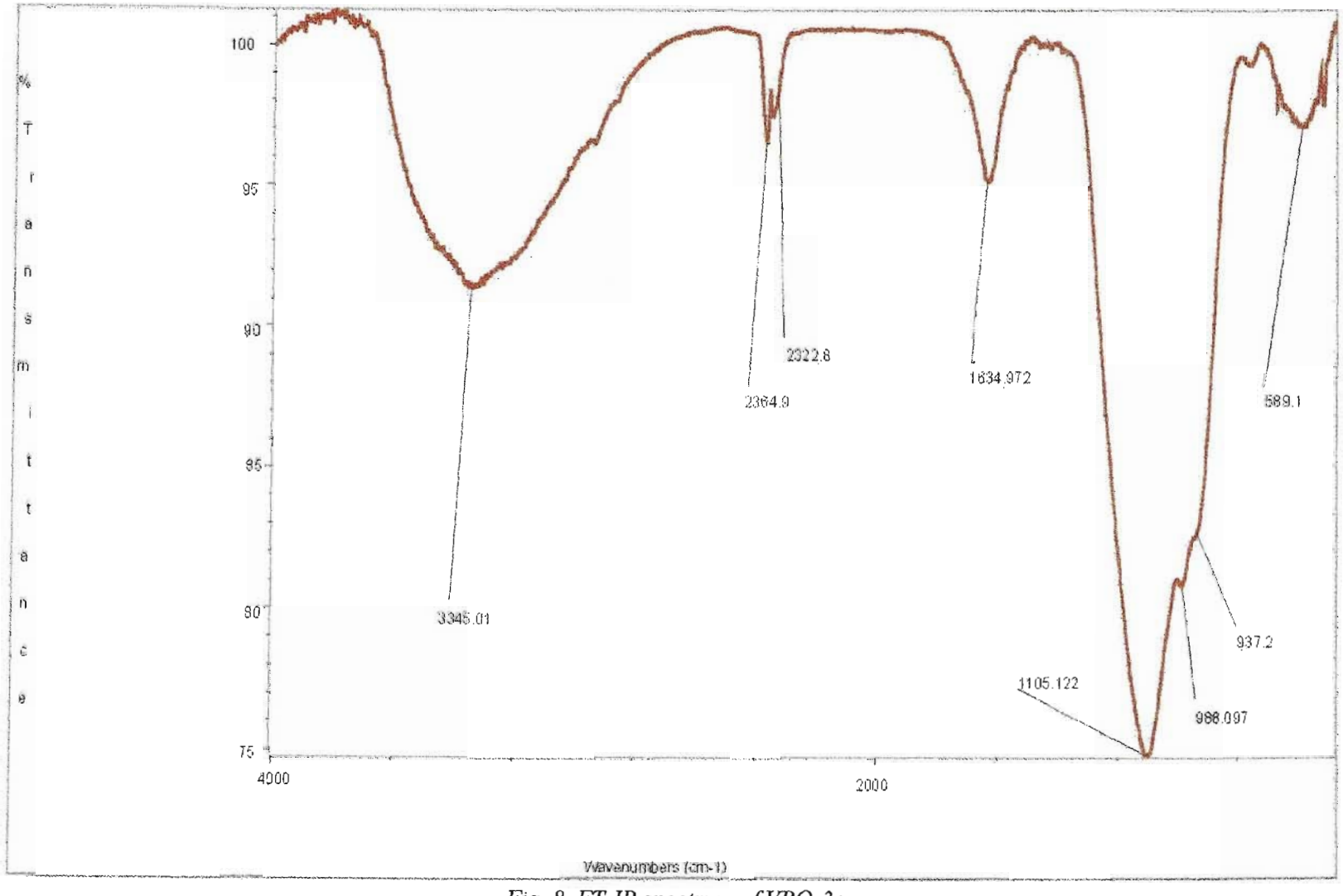

Fig. 8. FT-IR spectrum of VPO-3c

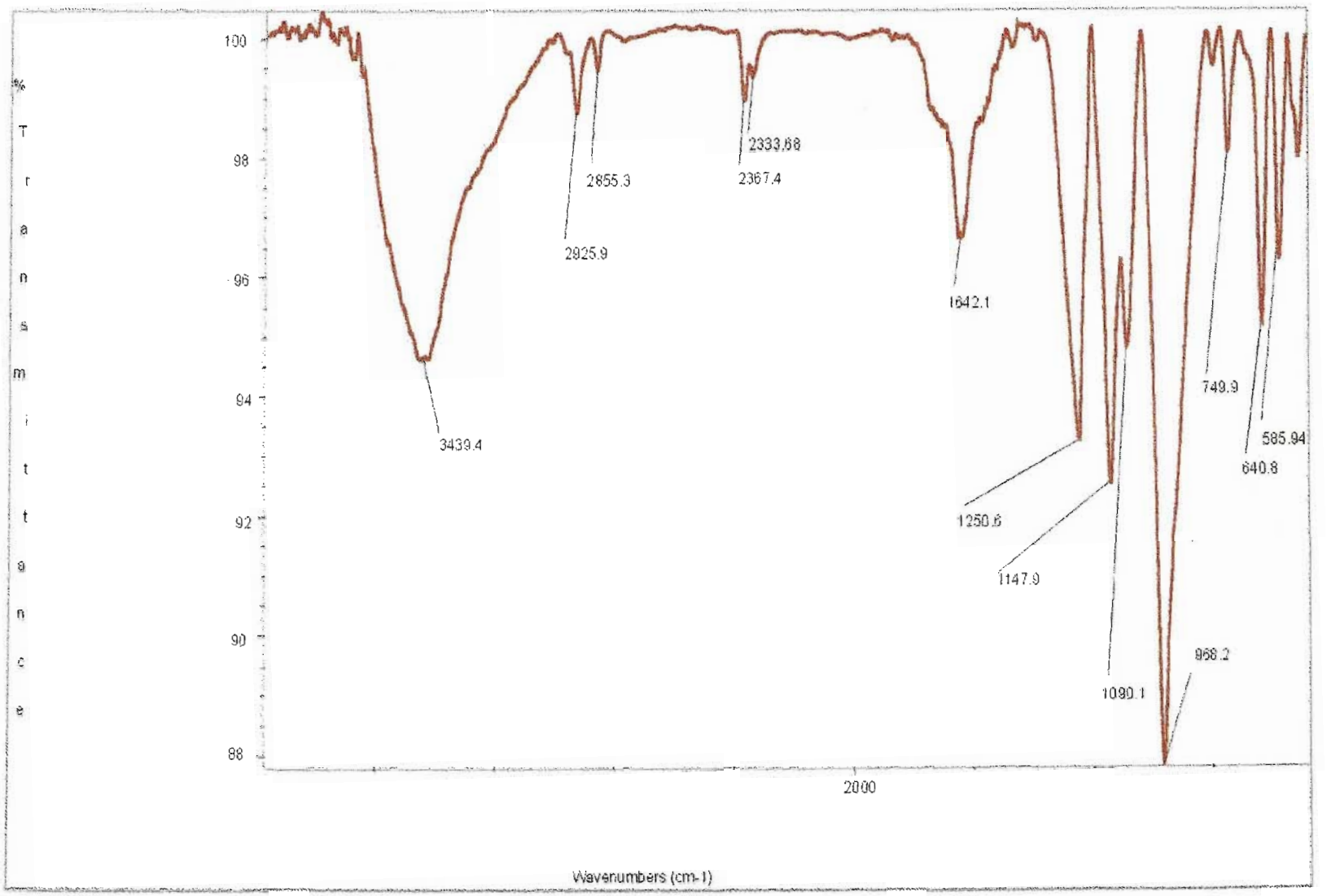

Fig. 9. FT-IR spectrum of VPO-3u

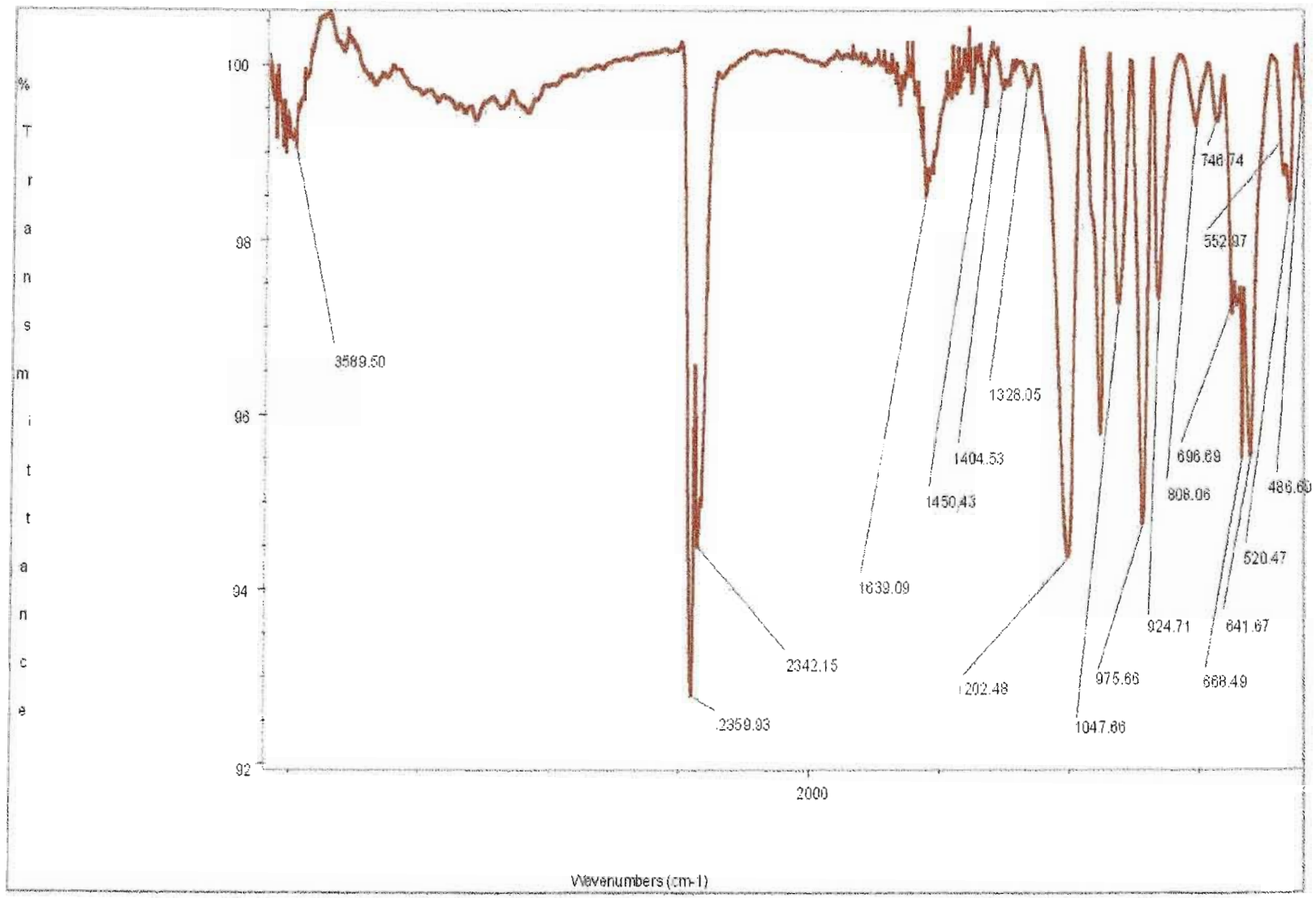

Fig. 10. FT-IR spectrum of VPO-4p

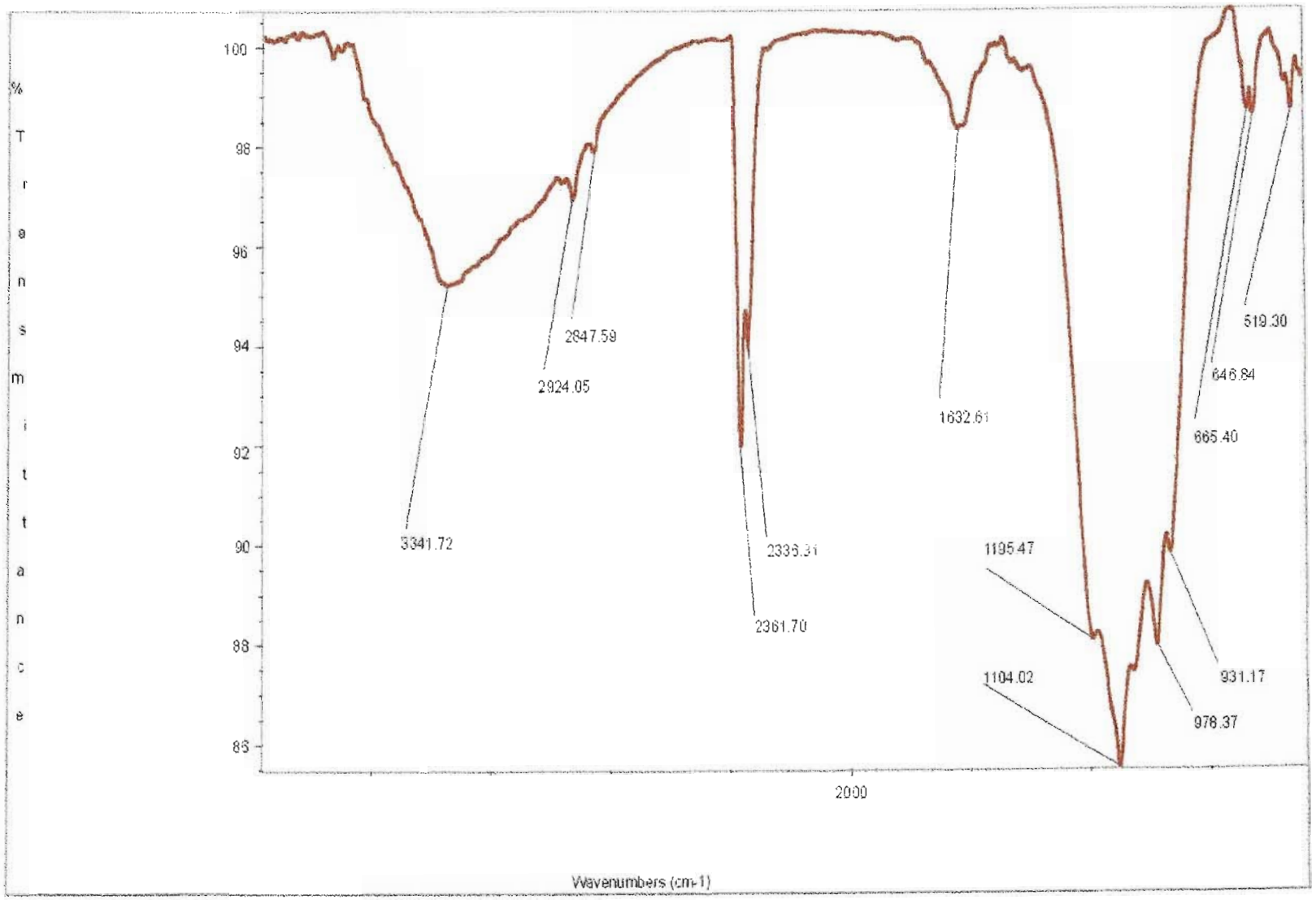

Fig. 11. FT-IR spectrum of VPO-4c

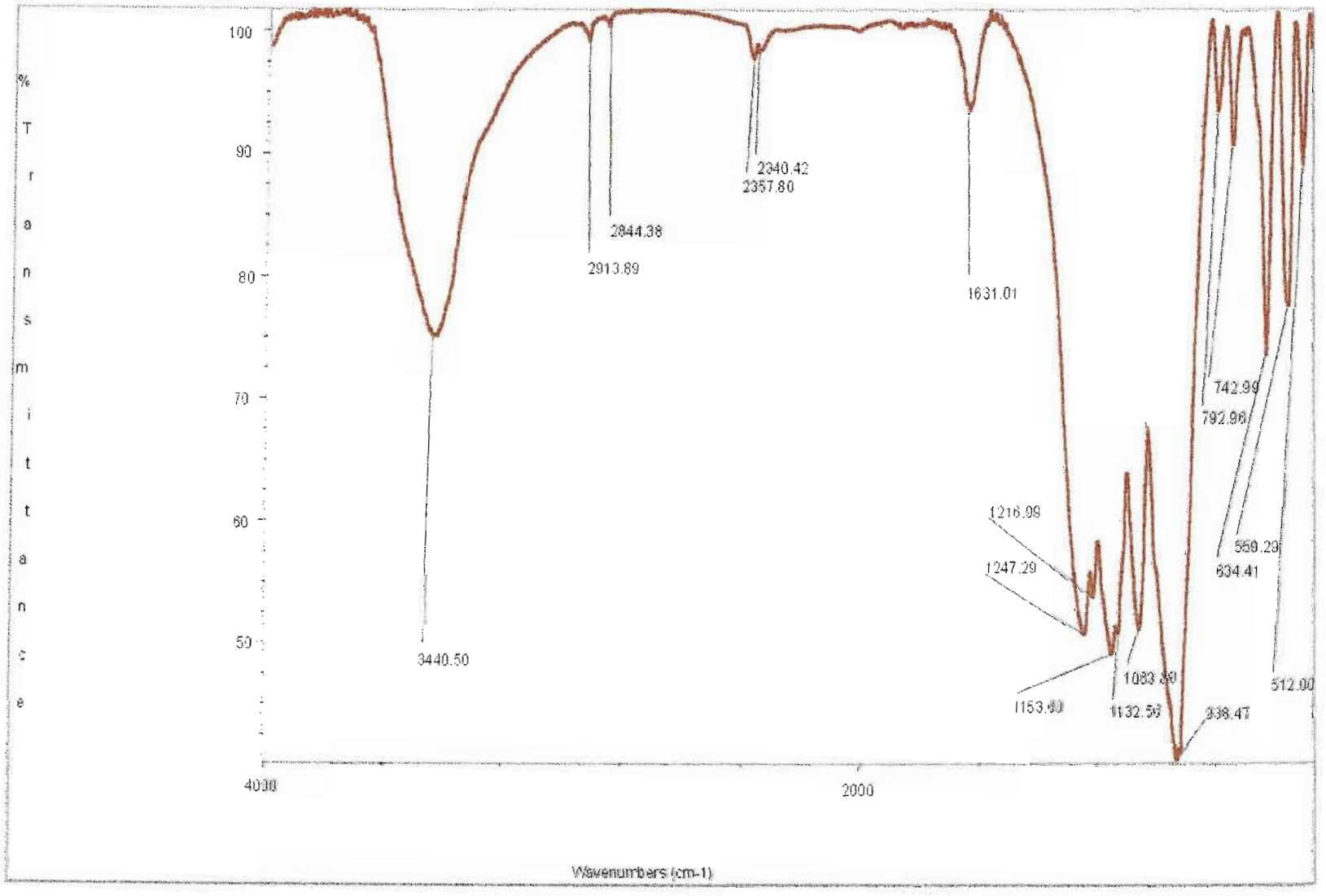

Fig. 12. FT-IR spectrum of VPO-4u

APPENDIX 6

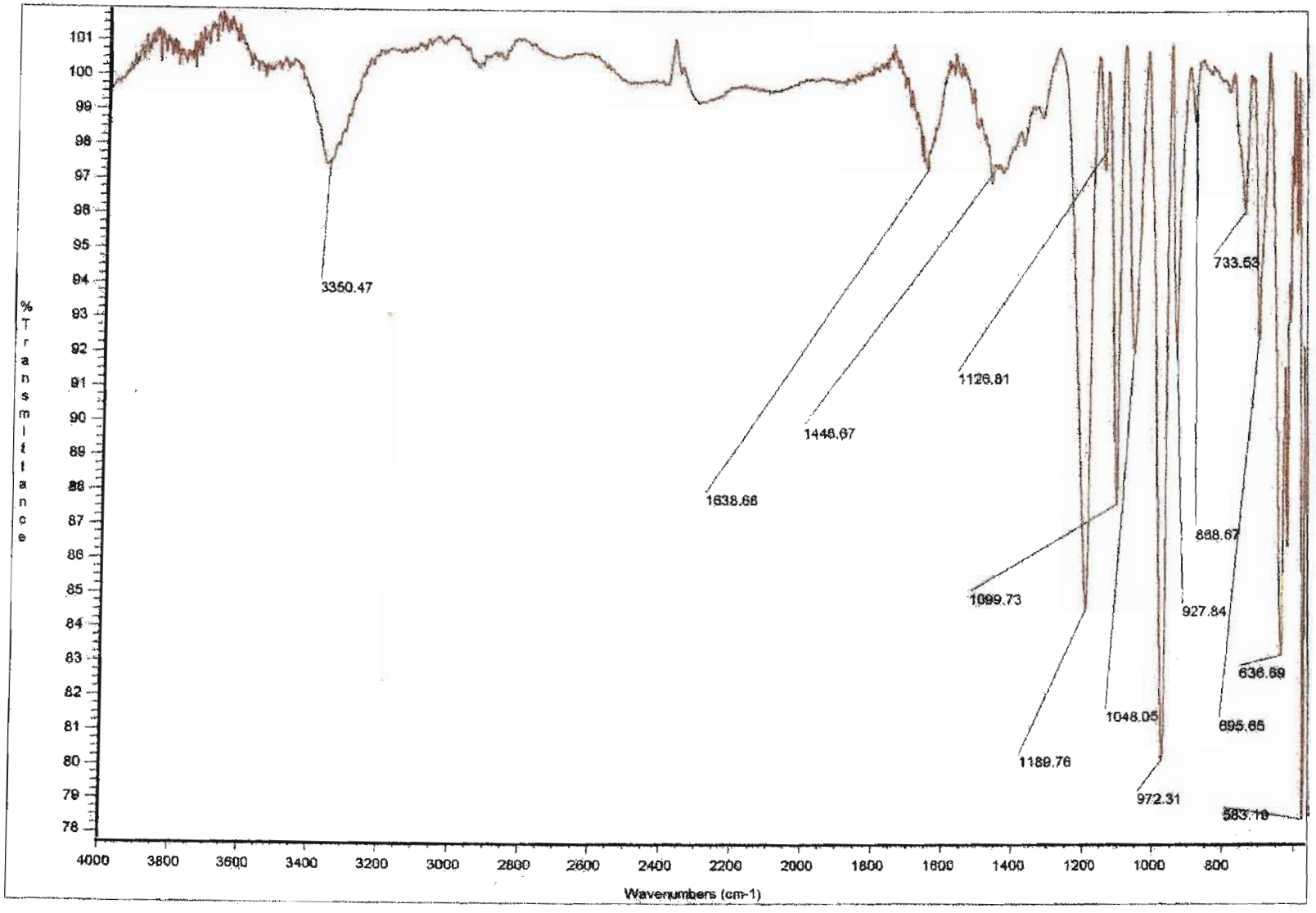

Fig. 1. ATR spectrum of VPO-1p

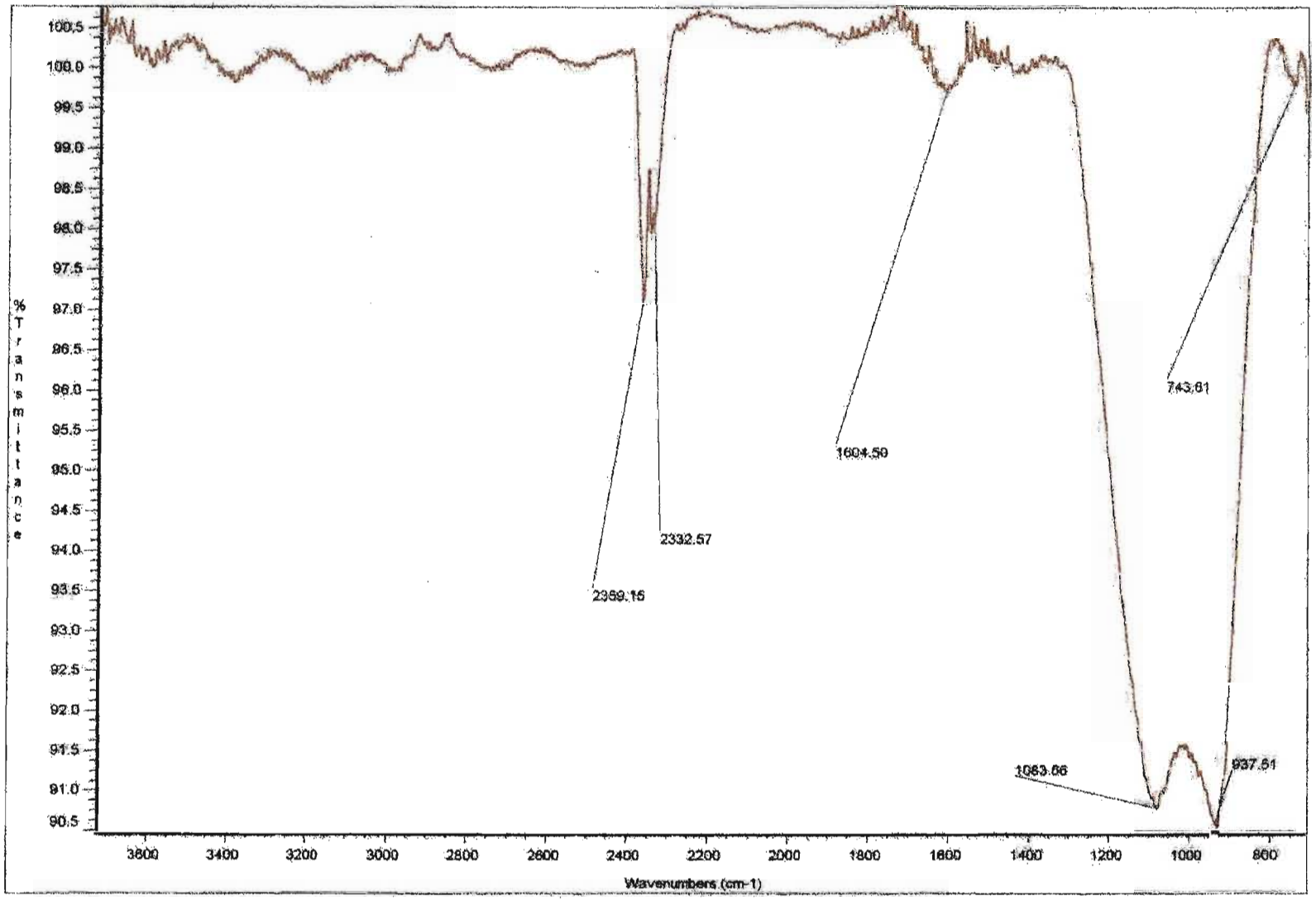

Fig. 2. ATR spectrum of VPO-1c

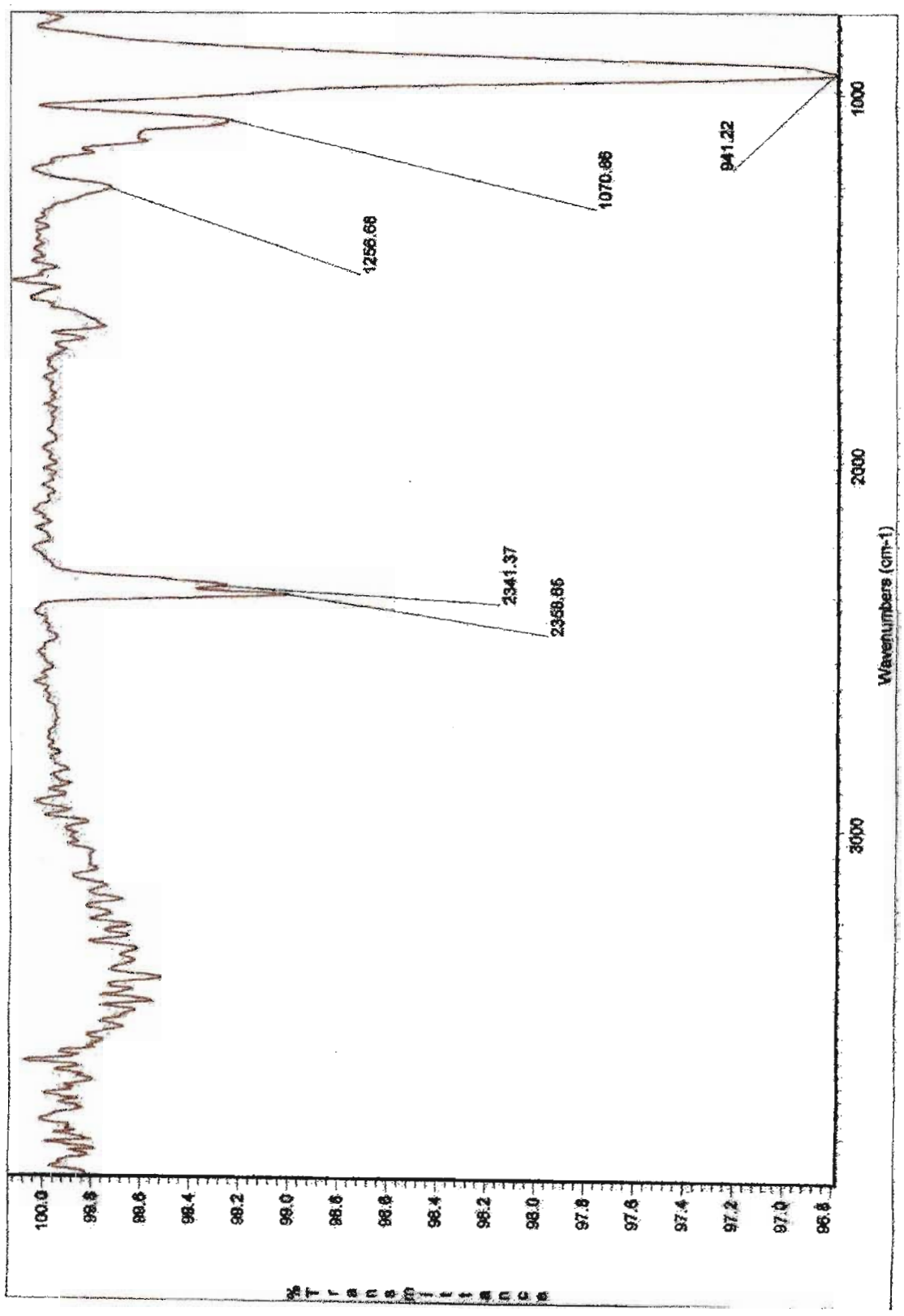

Fig. 3. ATR spectrum of VPO-1u

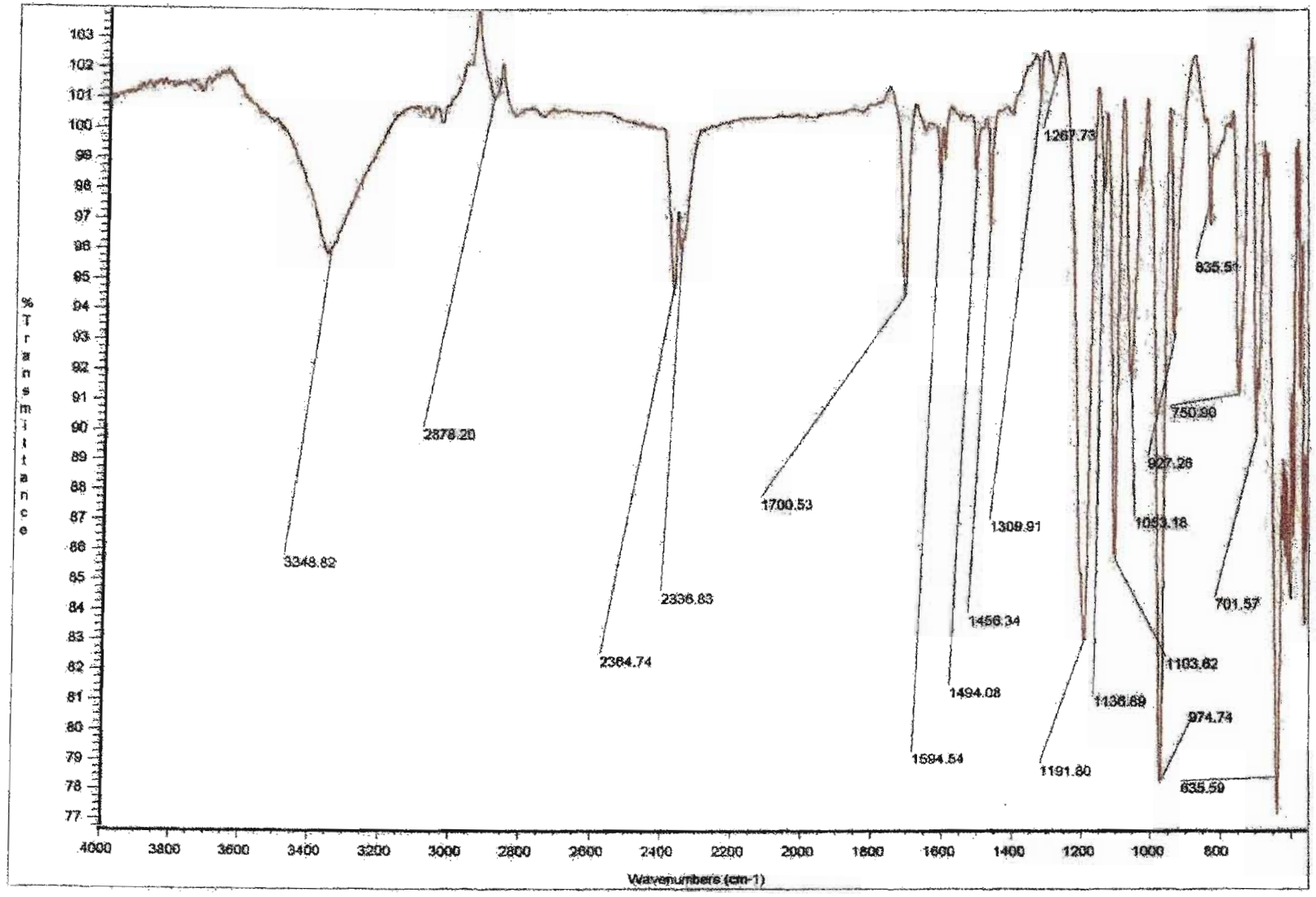

Fig. 4. ATR spectrum of VPO-2p

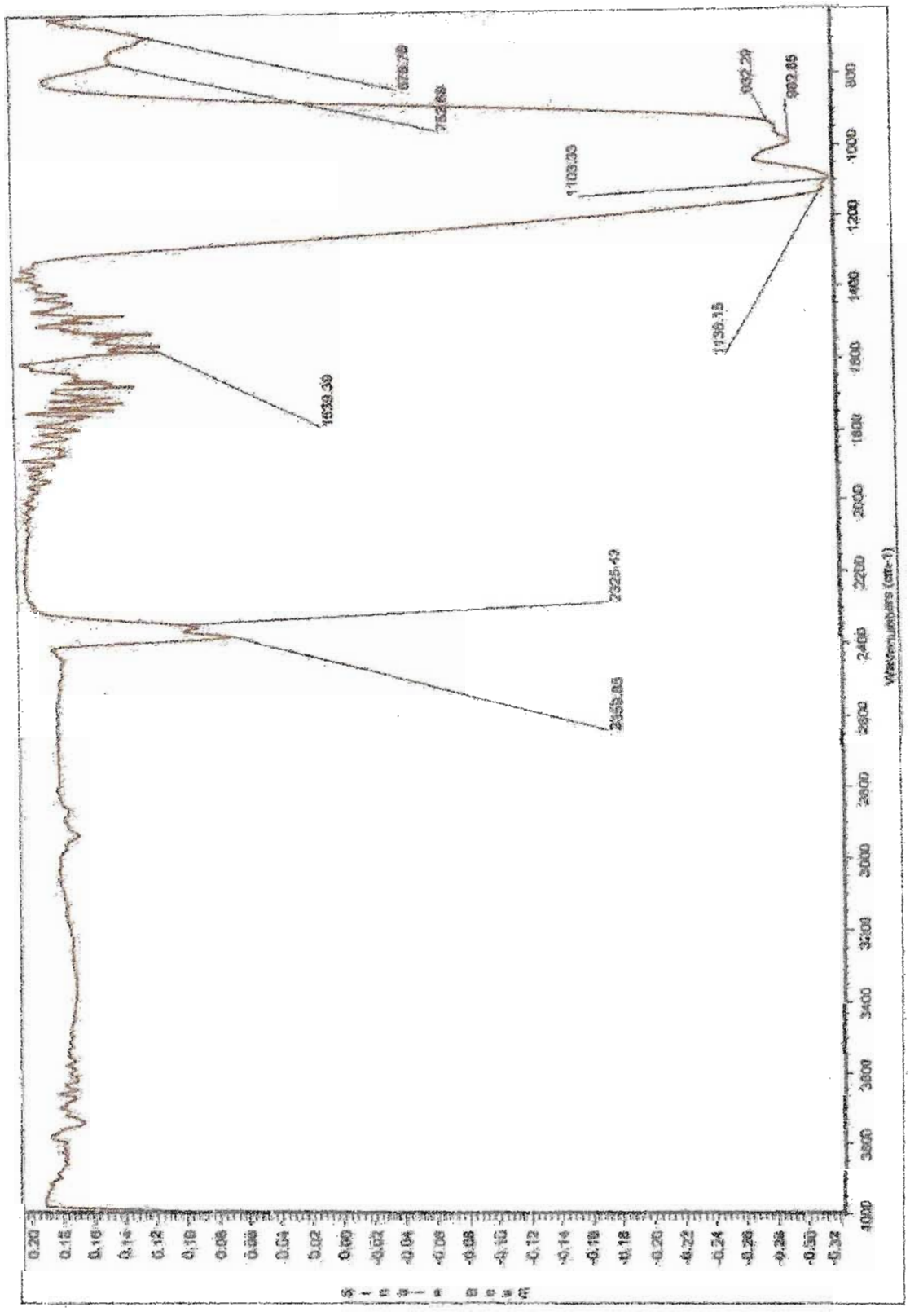

Fig. 5. ATR spectrum of VPO-2c

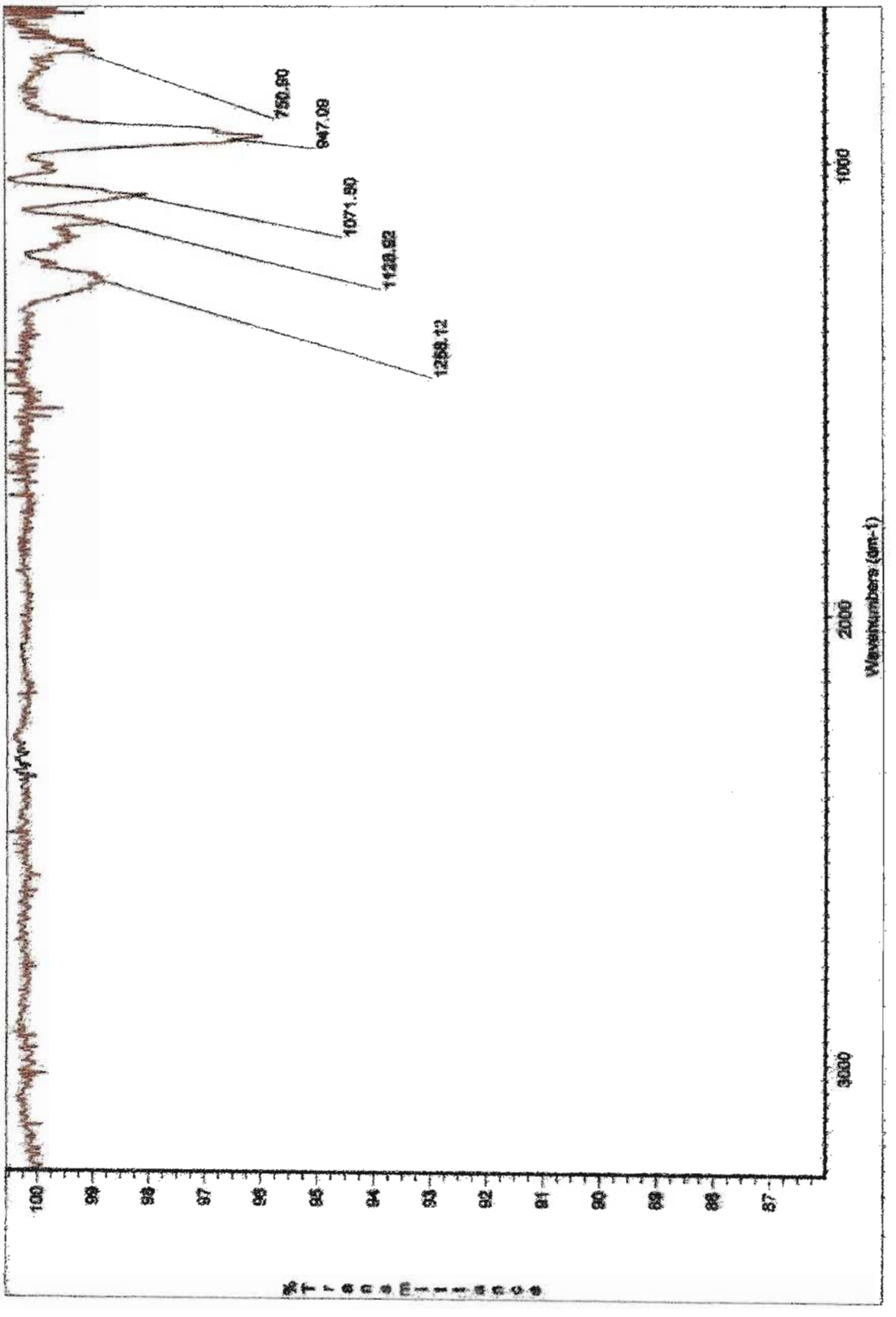

Fig. 6. ATR spectrum of VPO-2u

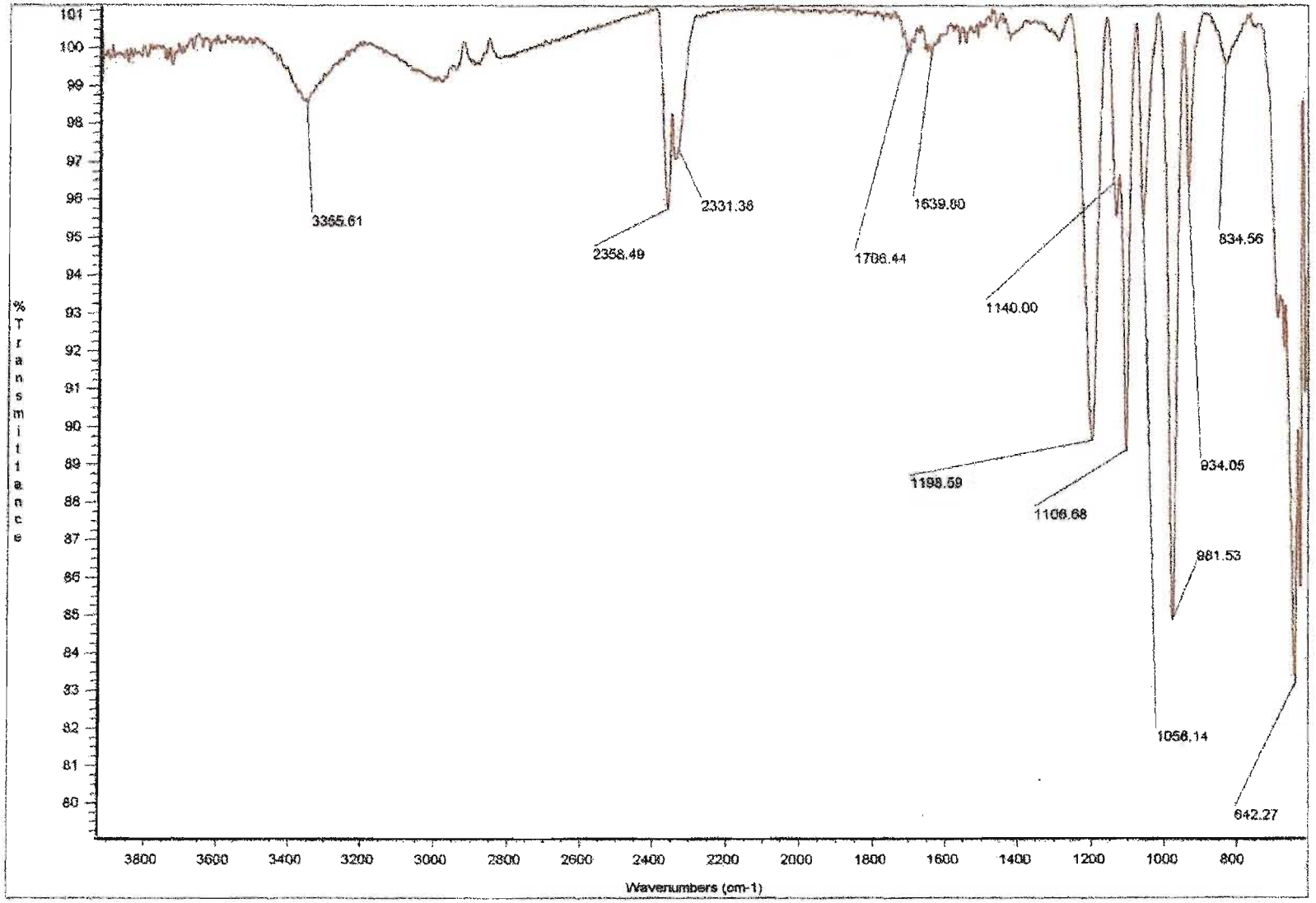

Fig. 7. ATR spectrum of VPO-5p

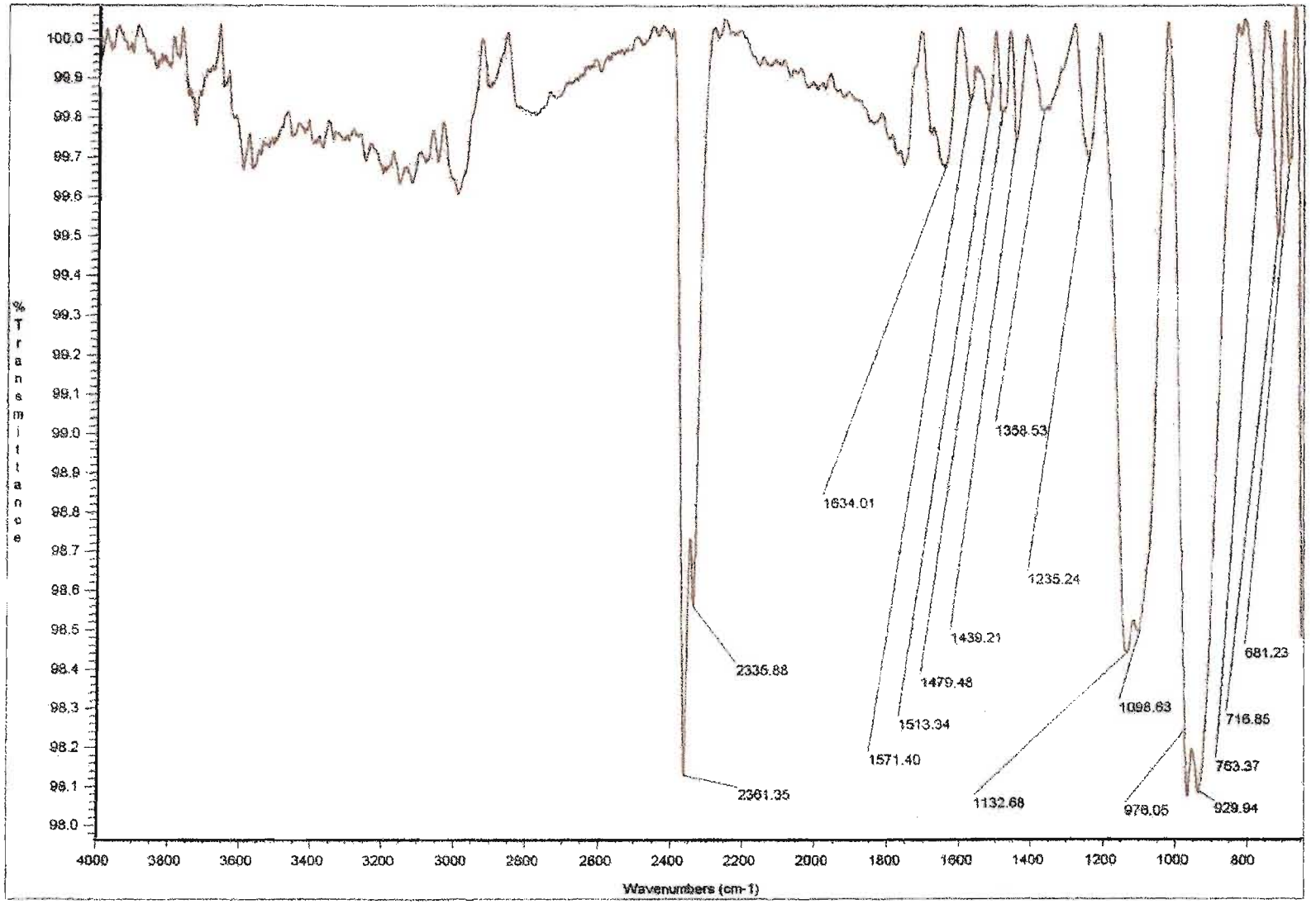

Fig. 8. ATR spectrum of VPO-3c

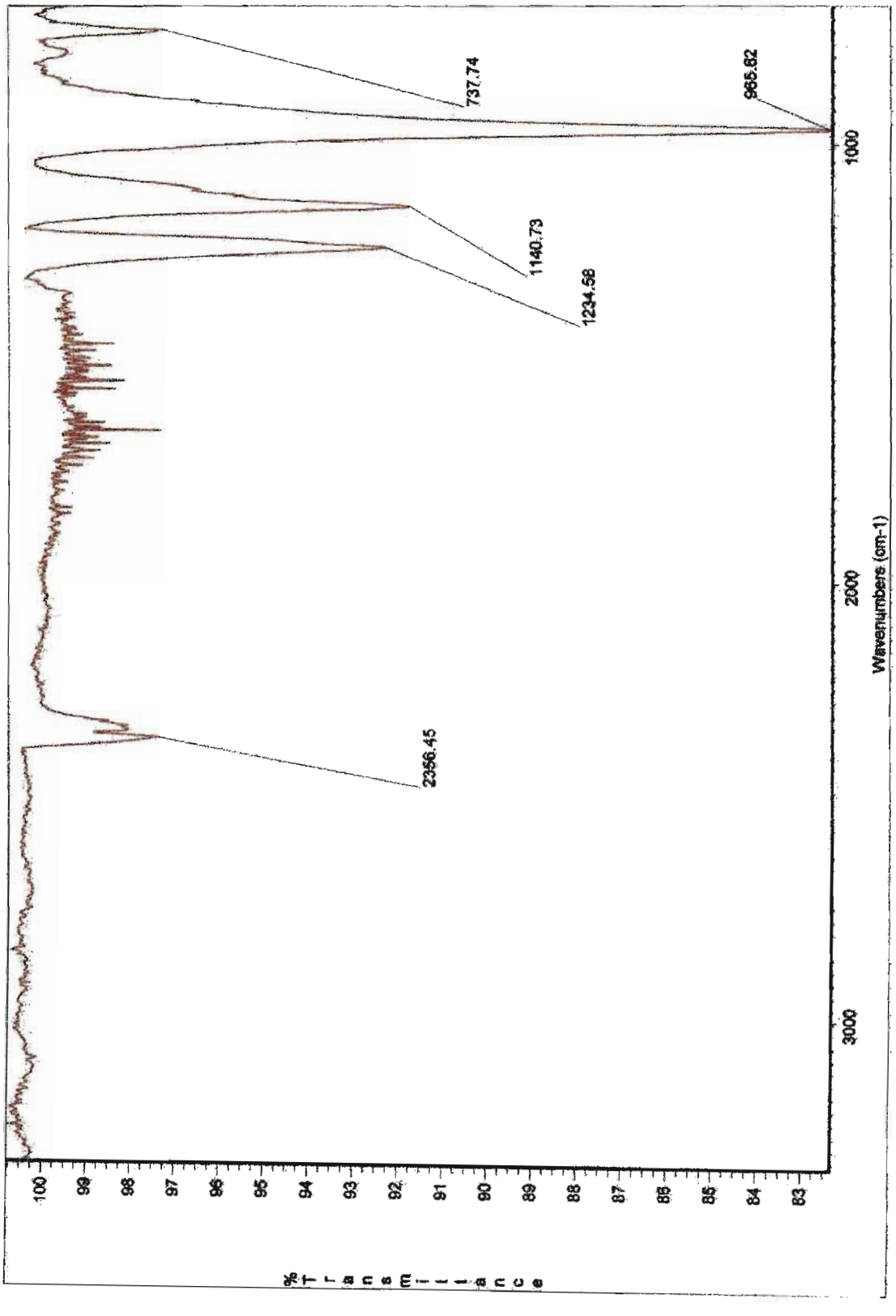

Fig. 9. ATR spectrum of VPO-3u

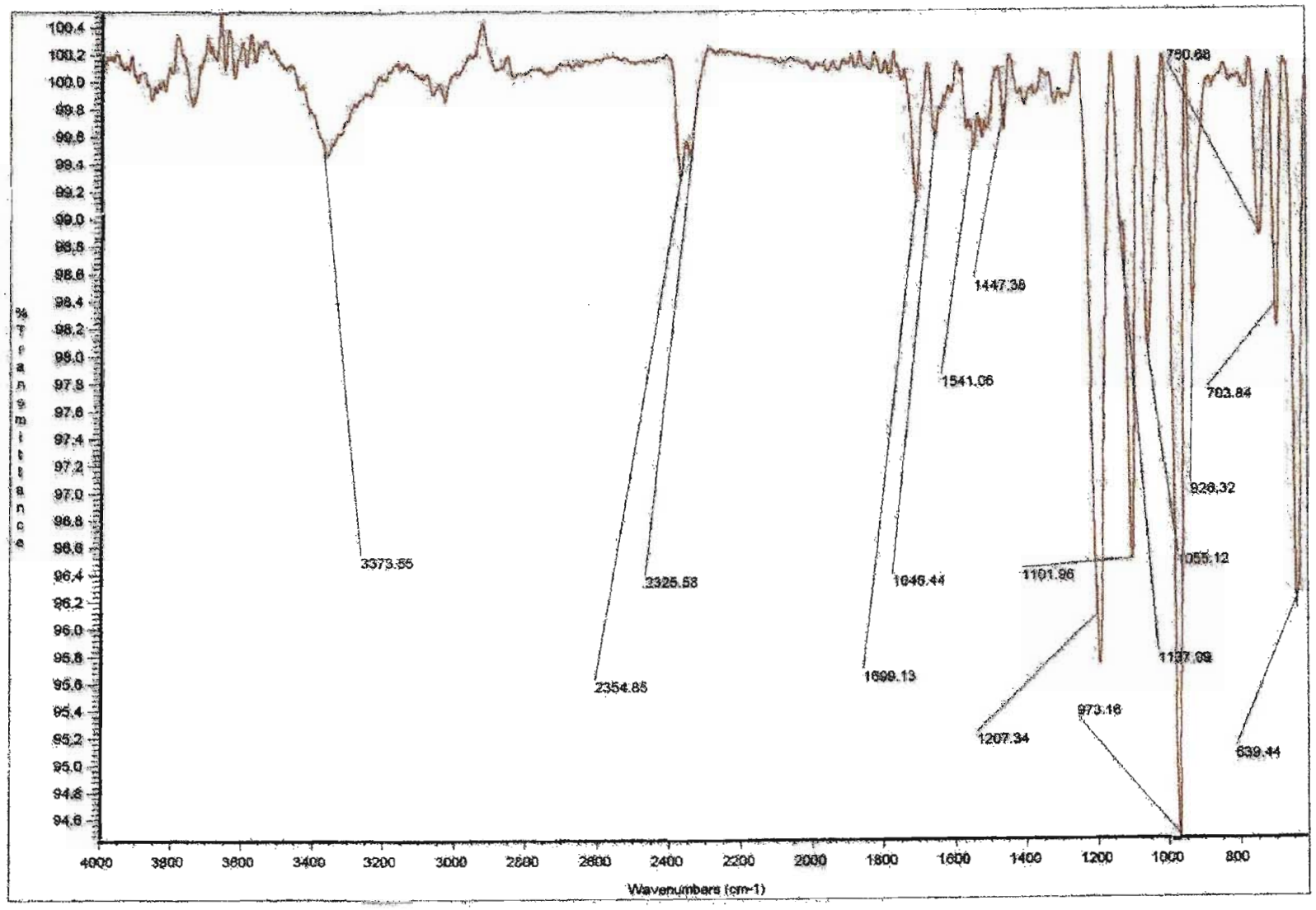

Fig. 10. ATR spectrum of VPO-4p

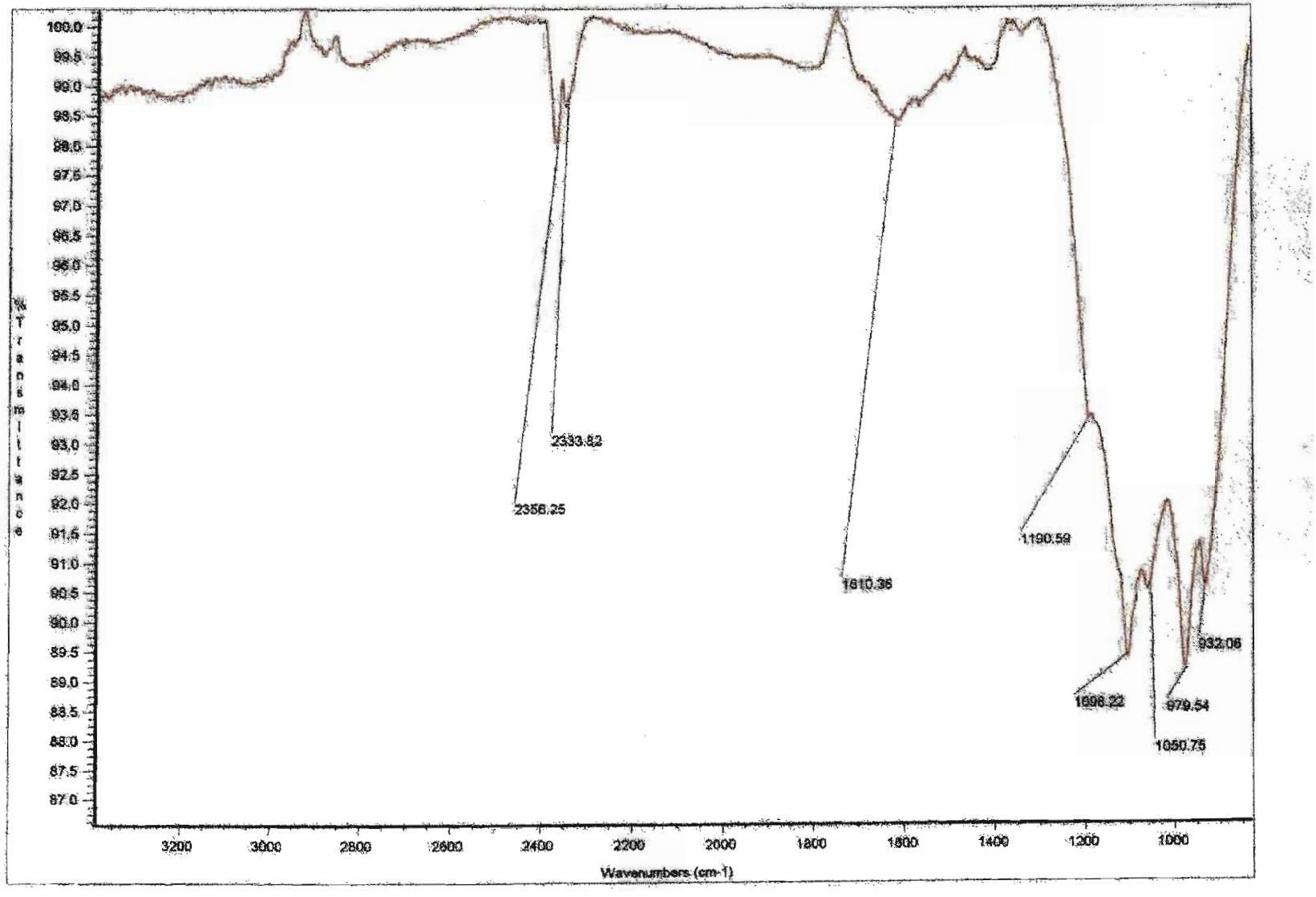

Fig. 11. ATR spectrum of VPO-4c

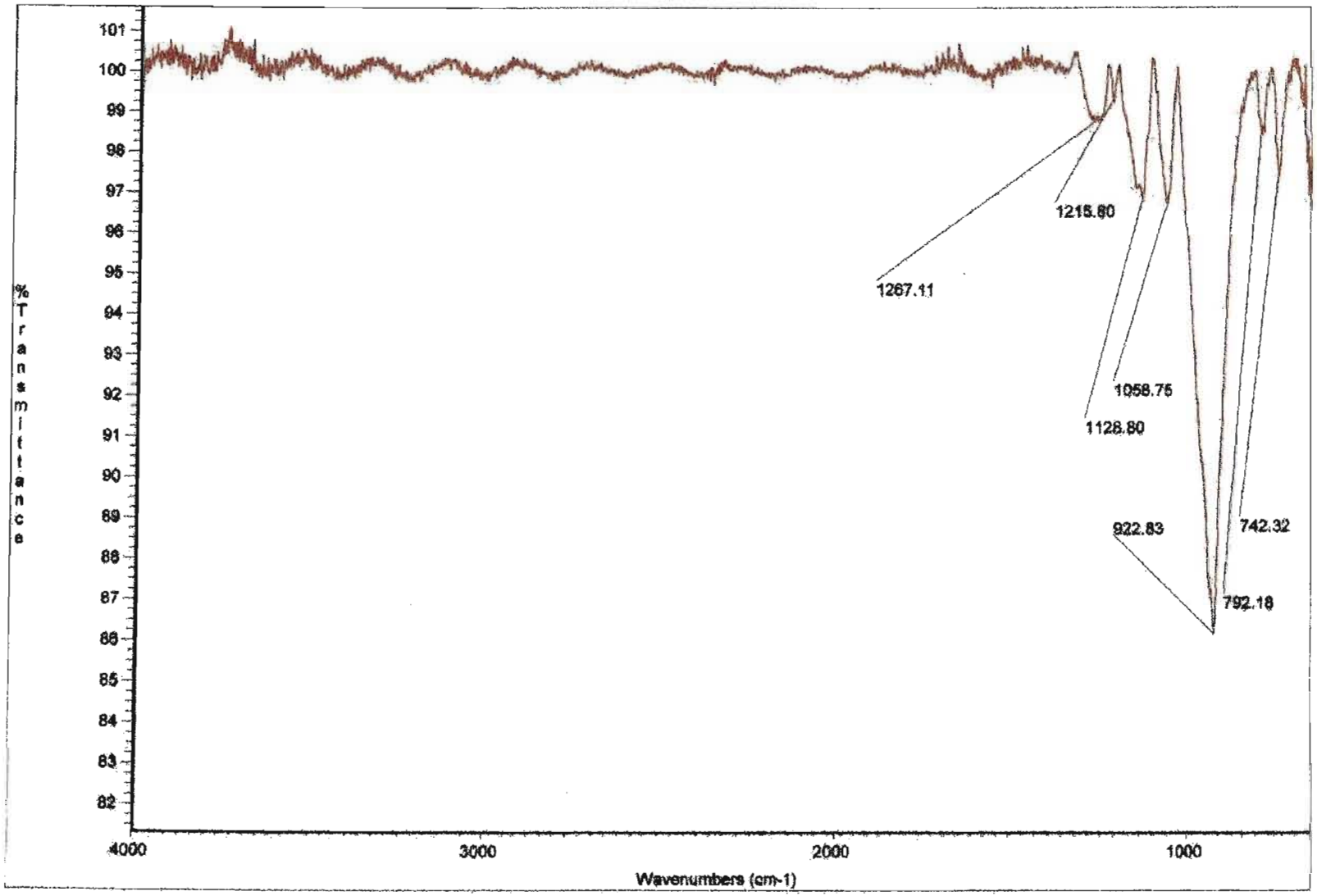

Fig. 12. ATR spectrum of VPO-4u

APPENDIX 7

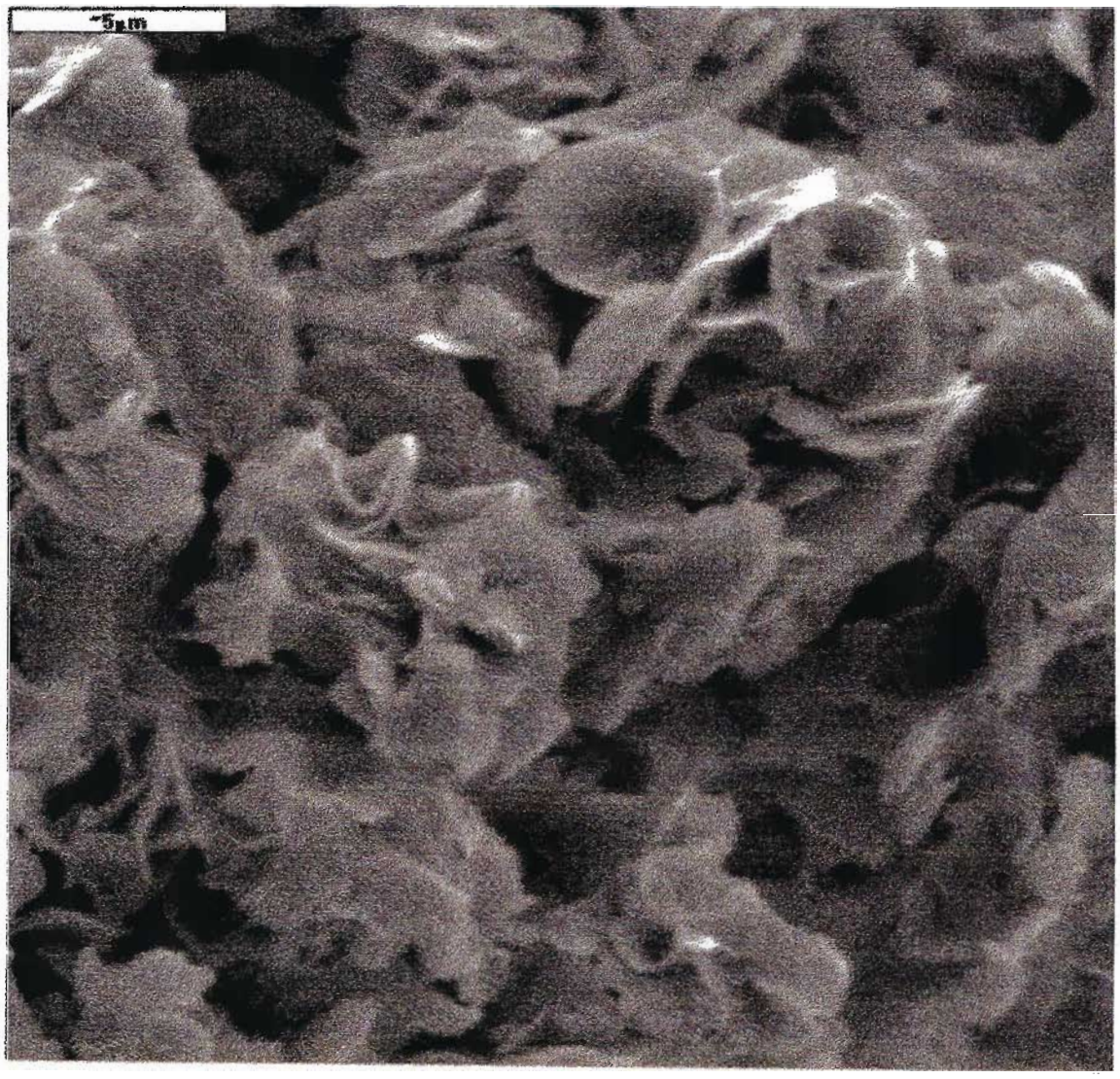

Fig. 1. SEM image of VPO-1p

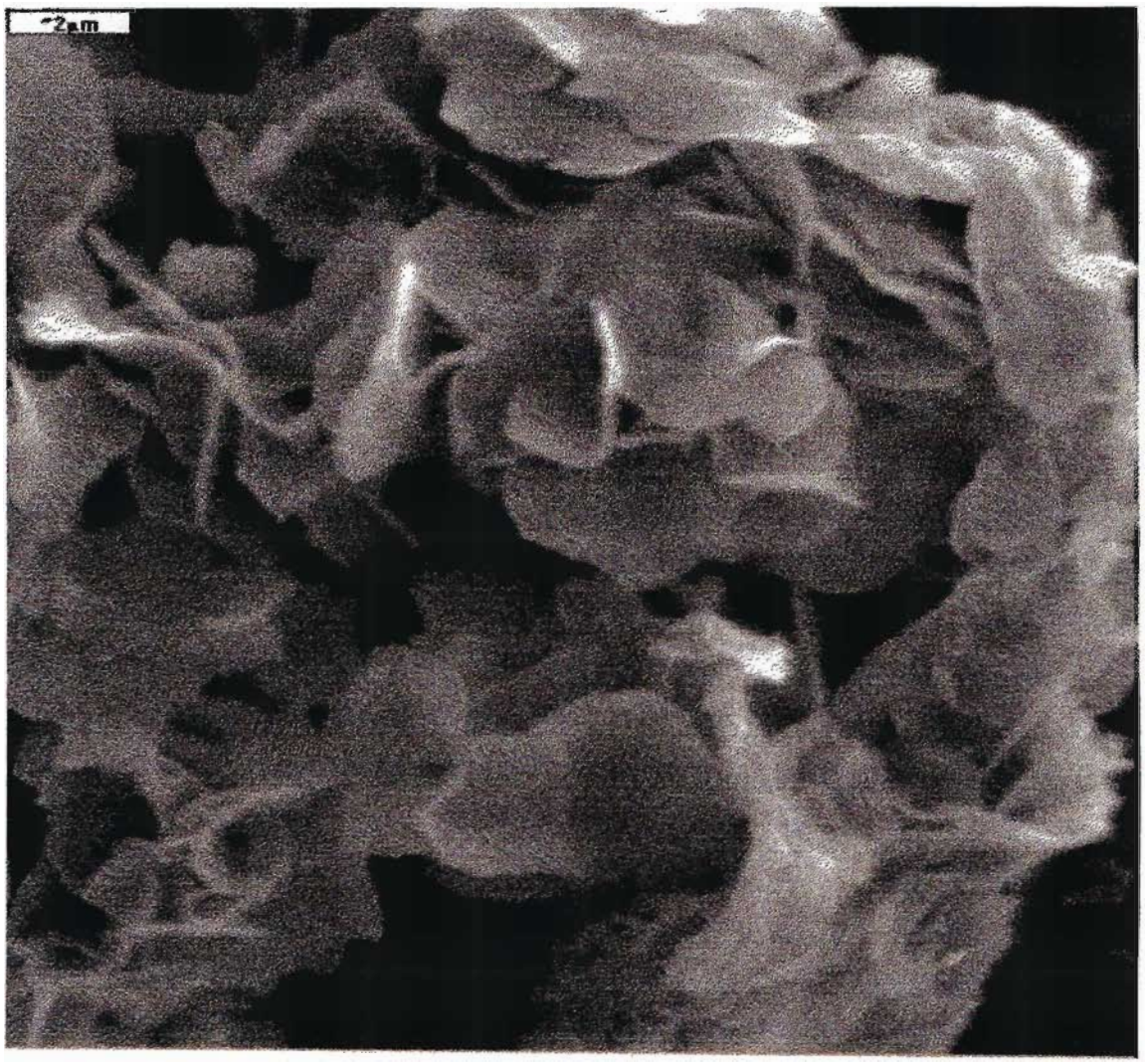

Fig. 2. SEM image of VPO-1c

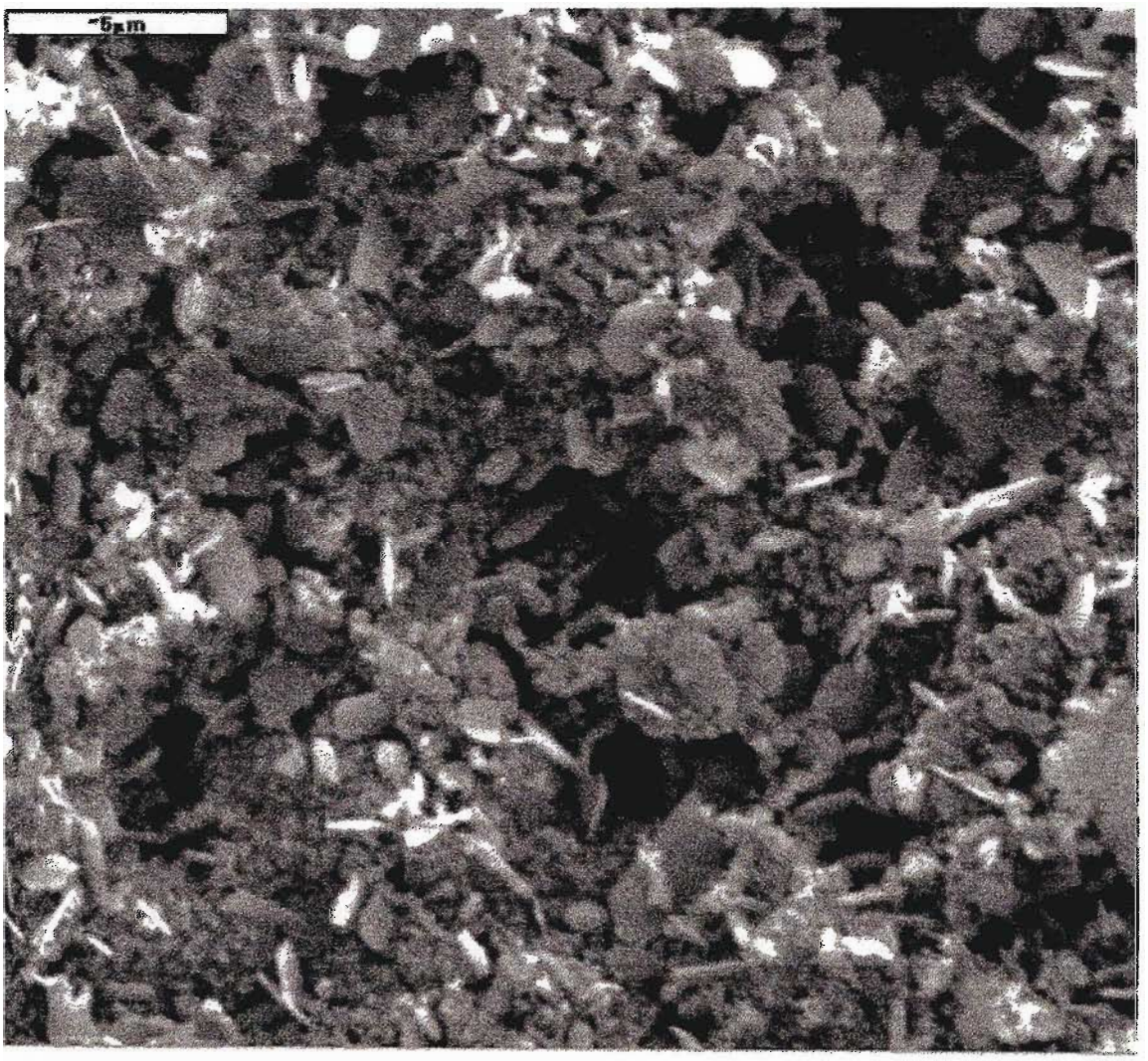

Fig. 3. SEM image of VPO-1u

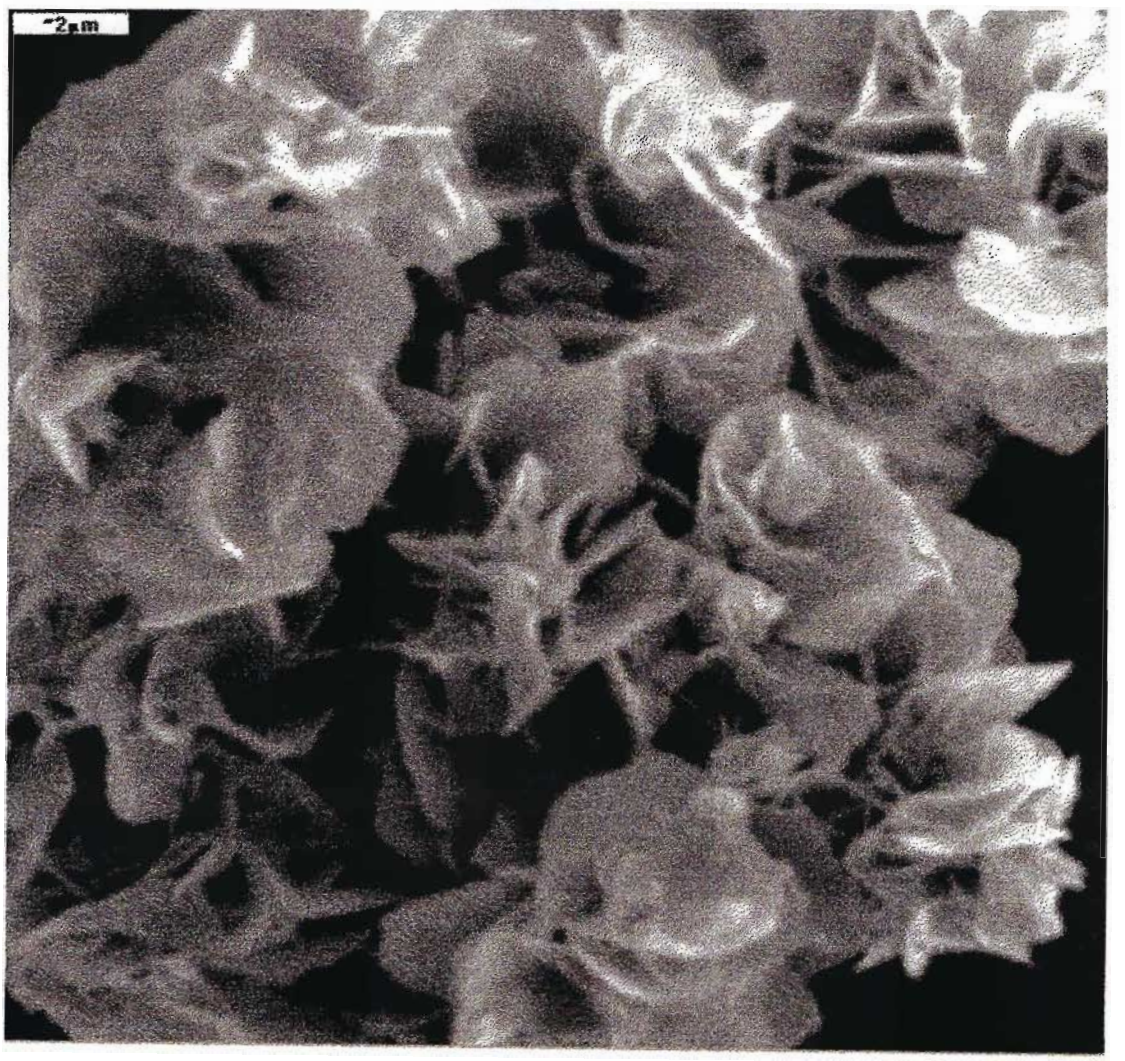

Fig. 4. SEM image of VPO-2p

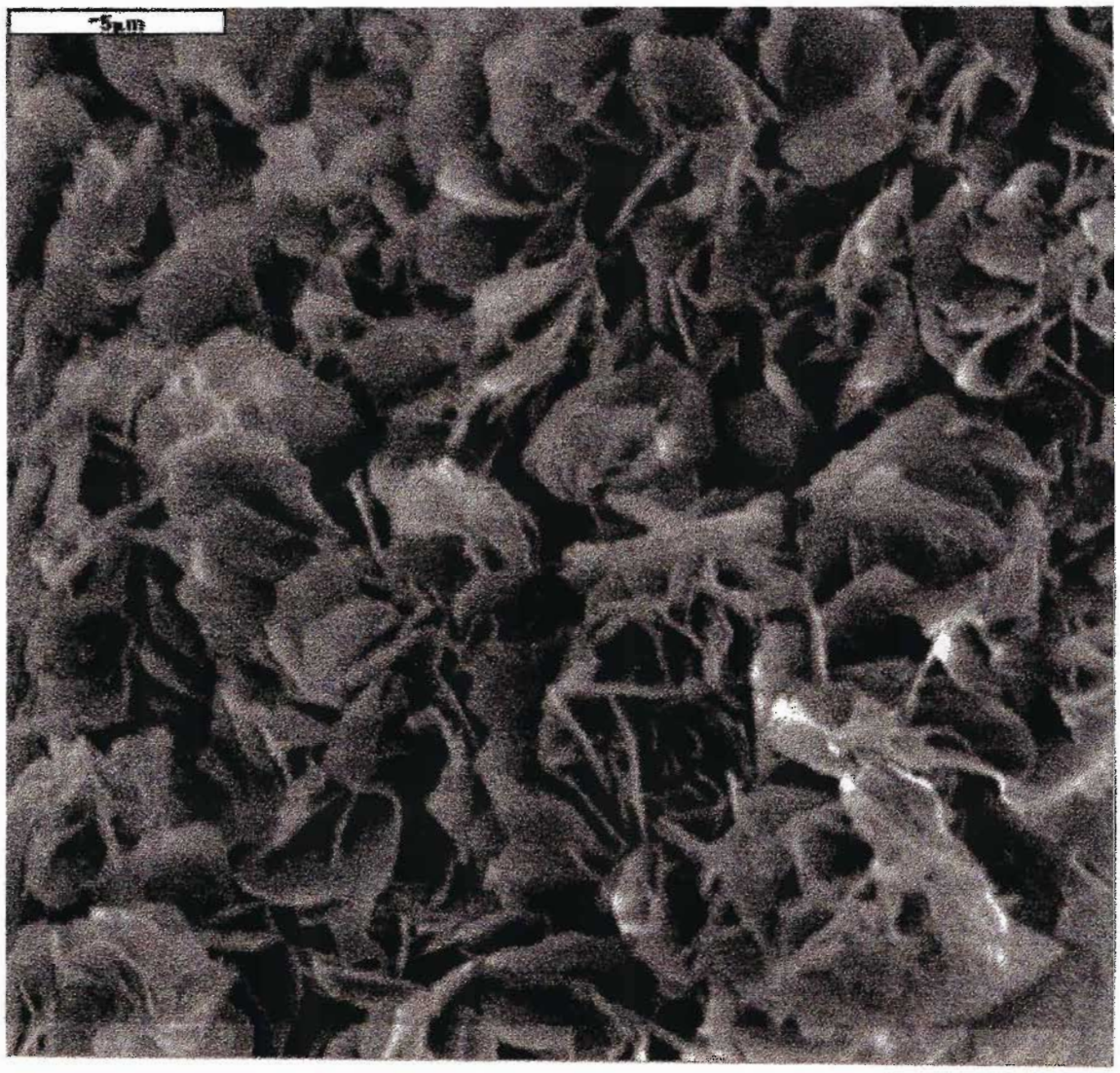

Fig. 5. SEM image of VPO-2c

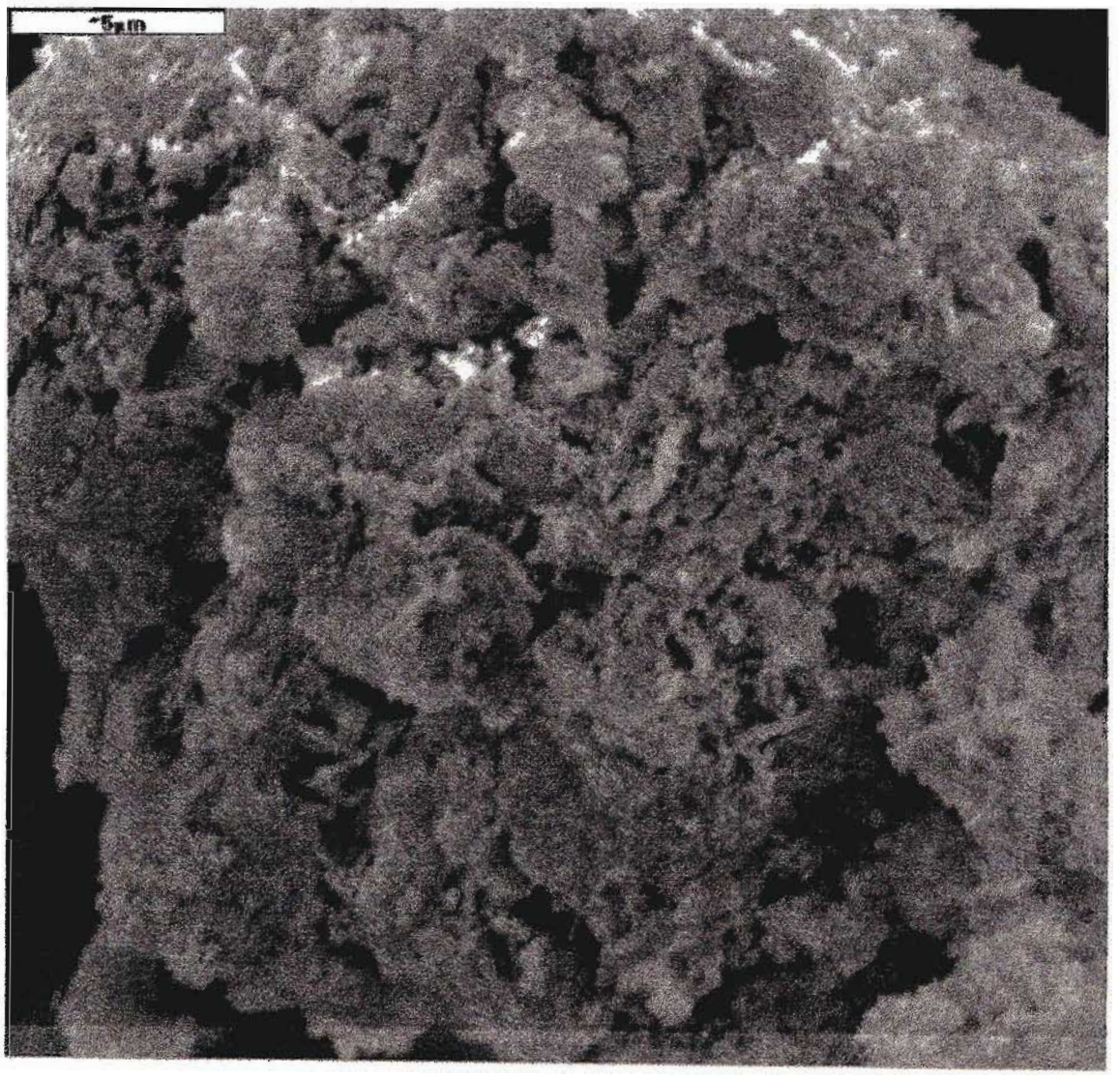

Fig. 6. SEM image of VPO-2u

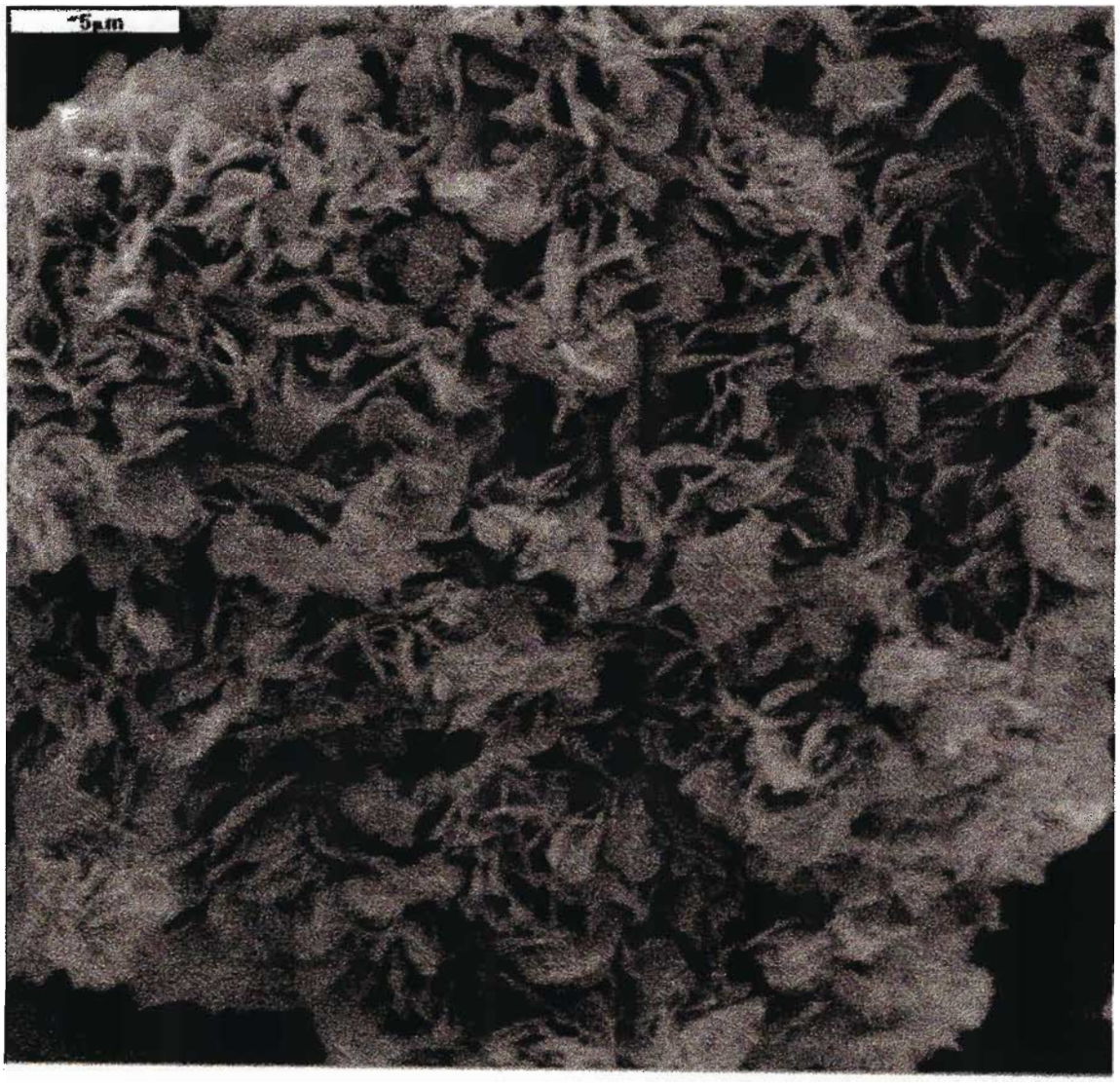

Fig. 7. SEM image of VPO-3p

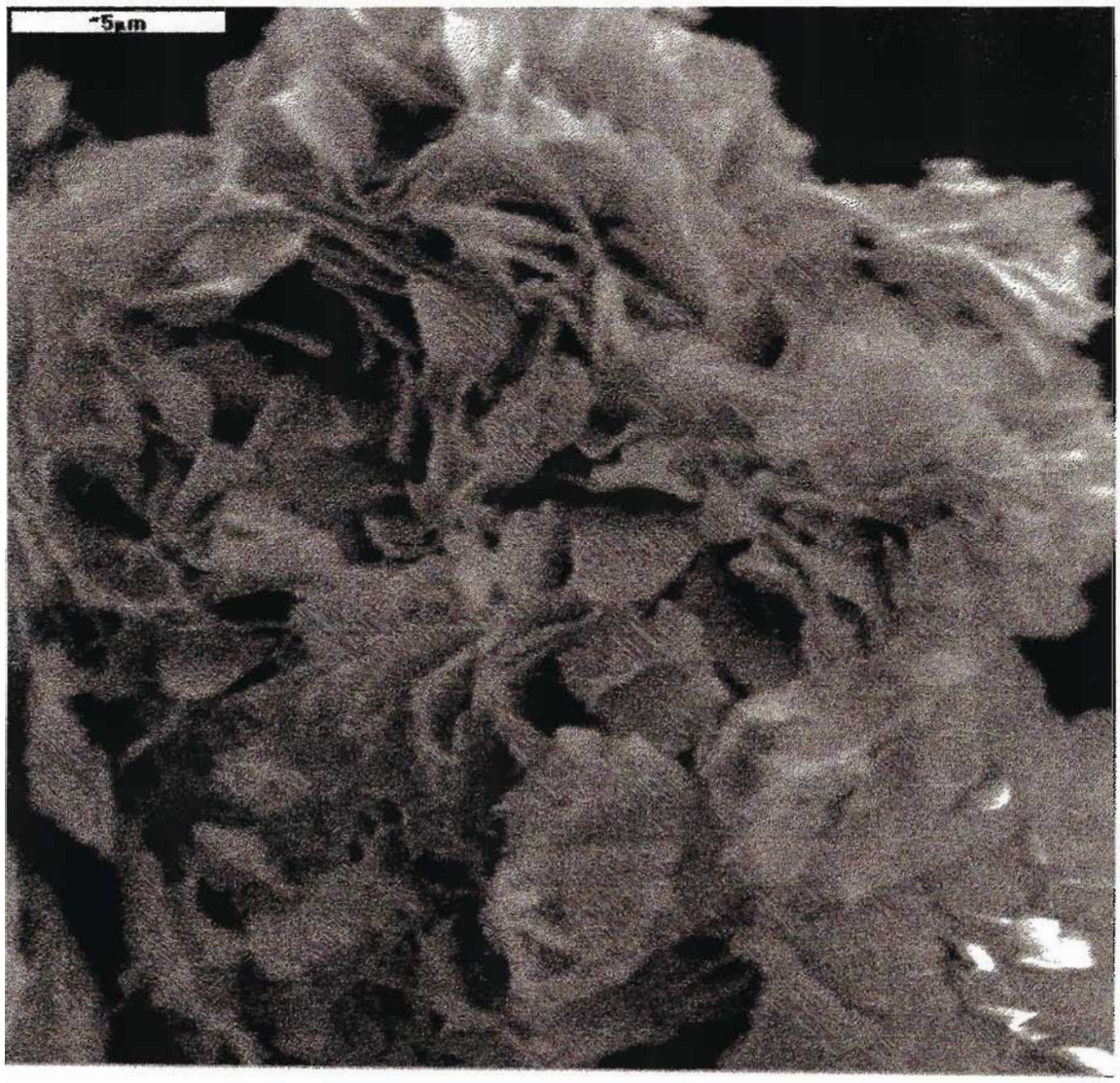

Fig. 8. SEM image of VPO-3c

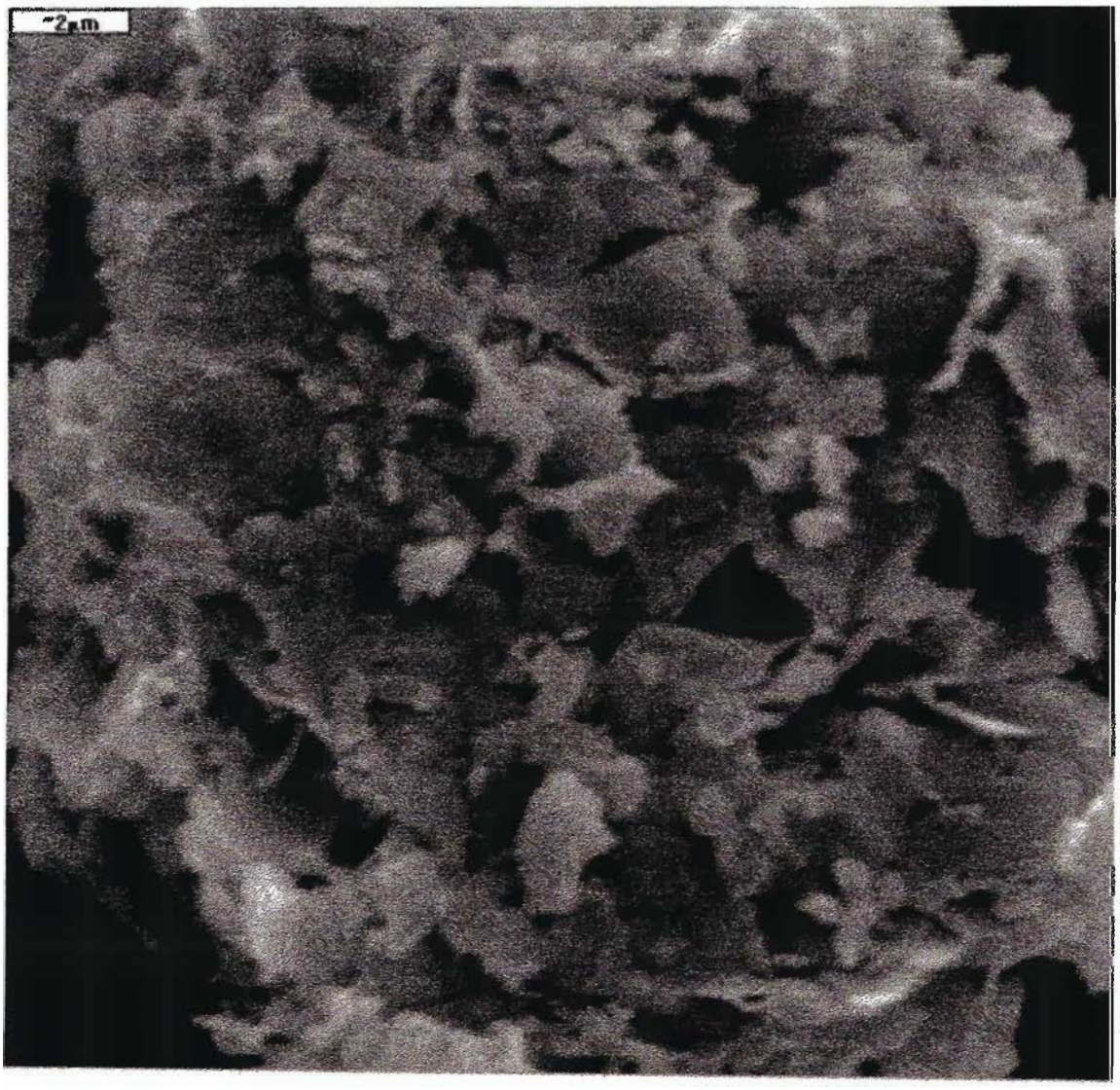

Fig. 9. SEM image of VPO-3u

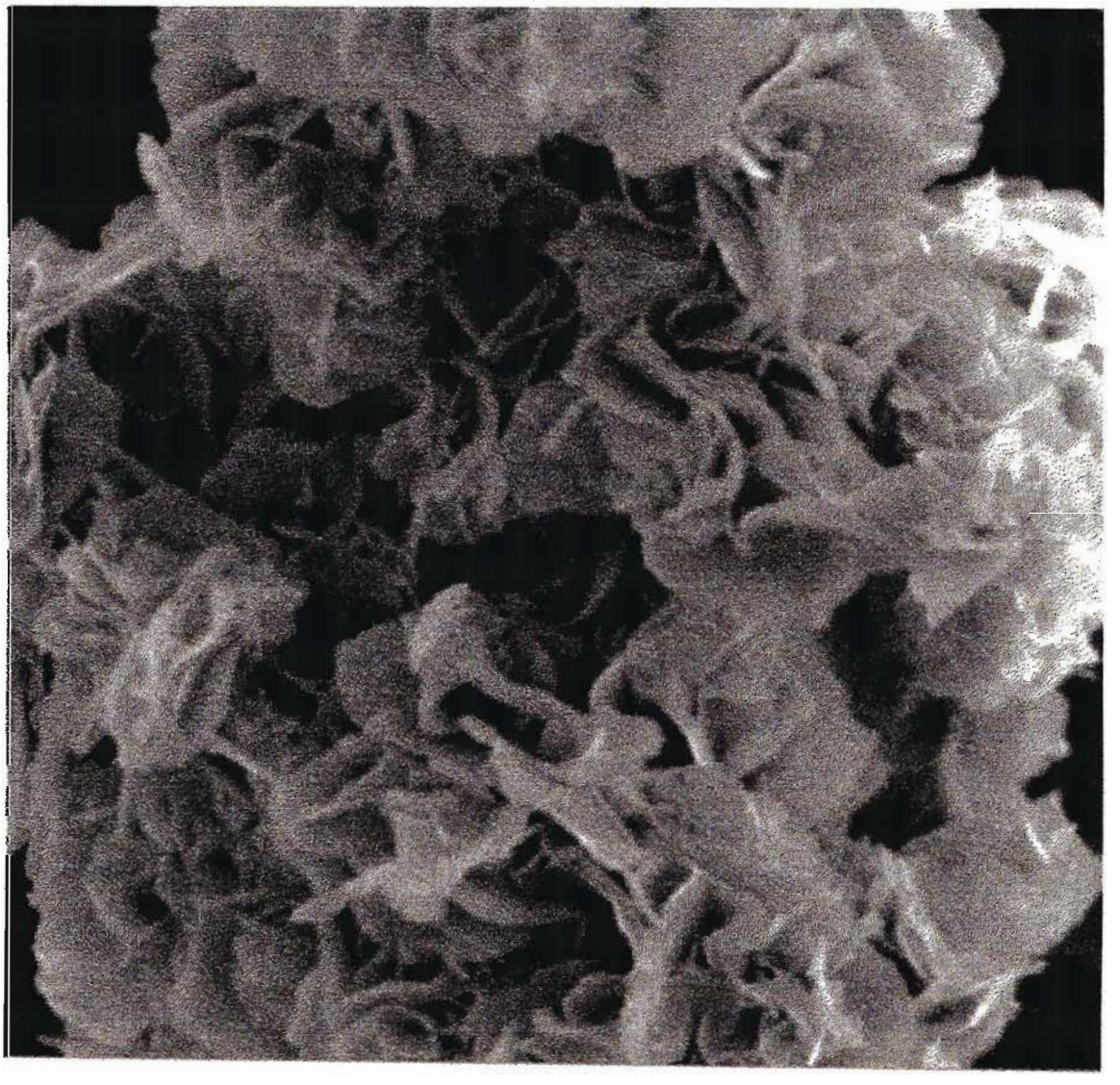

Fig. 10. SEM image of VPO-4p

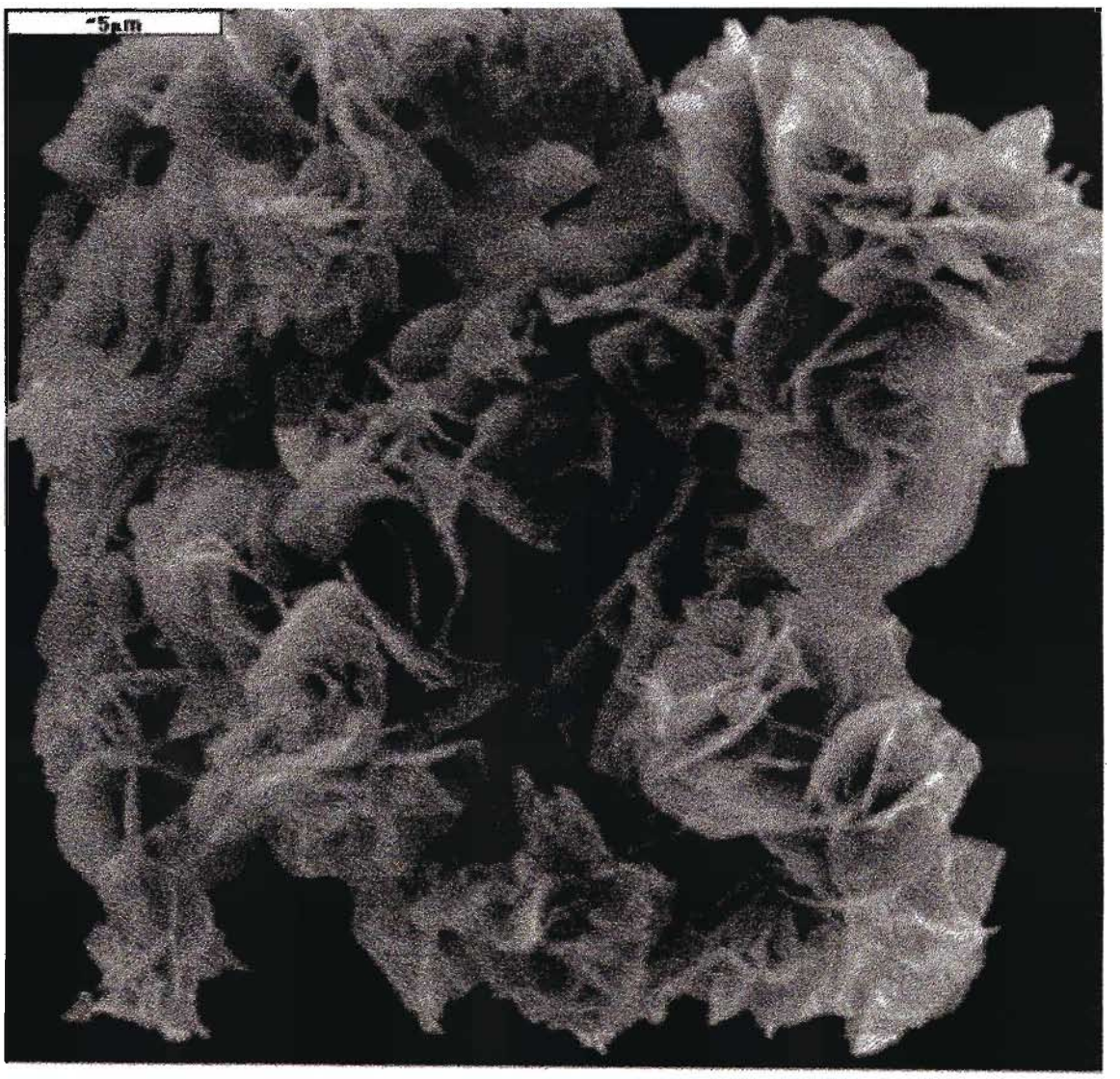

Fig. 11. SEM image of VPO-4c

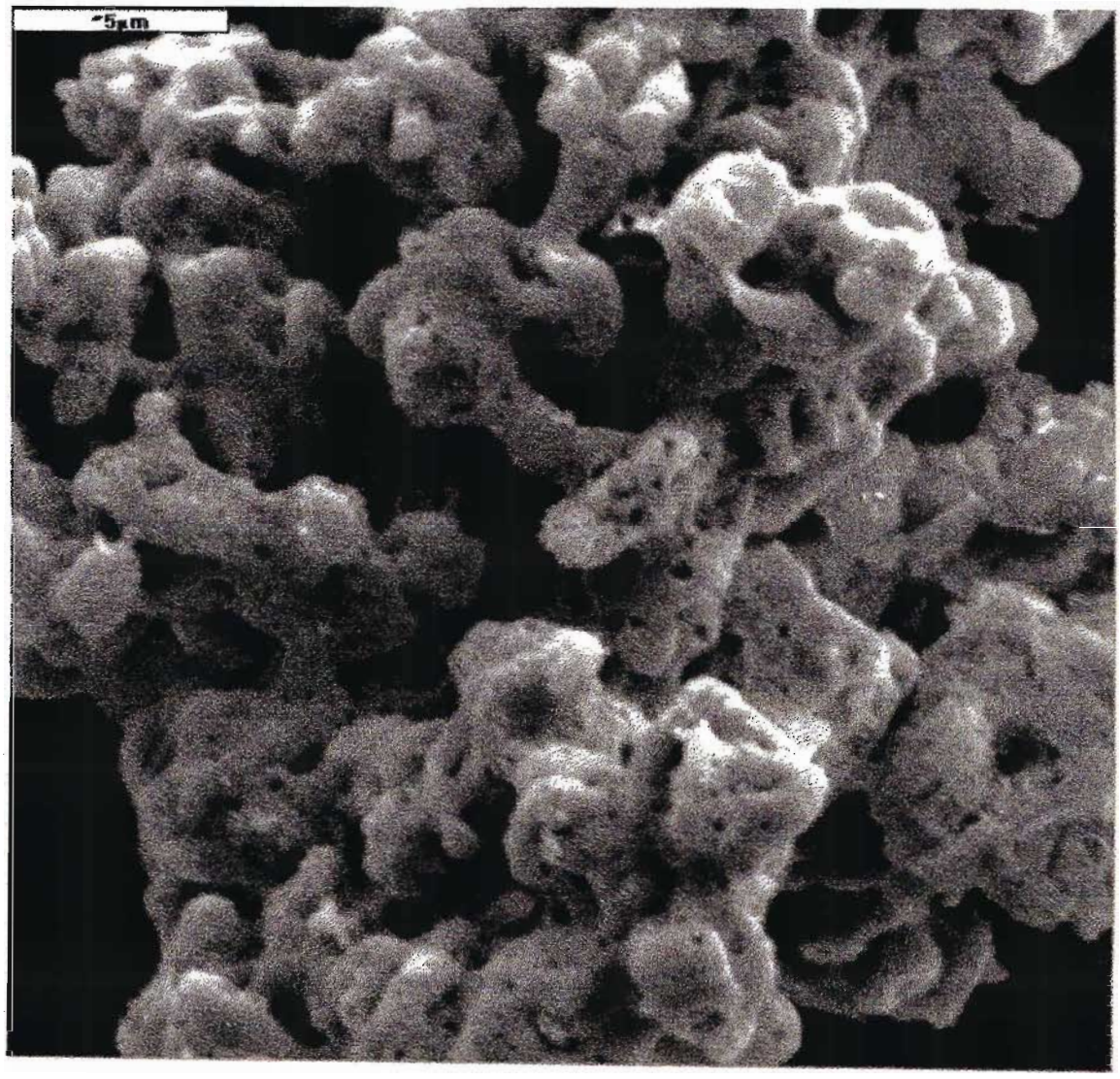

Fig. 12. SEM image of VPO-4u

APPENDIX 8

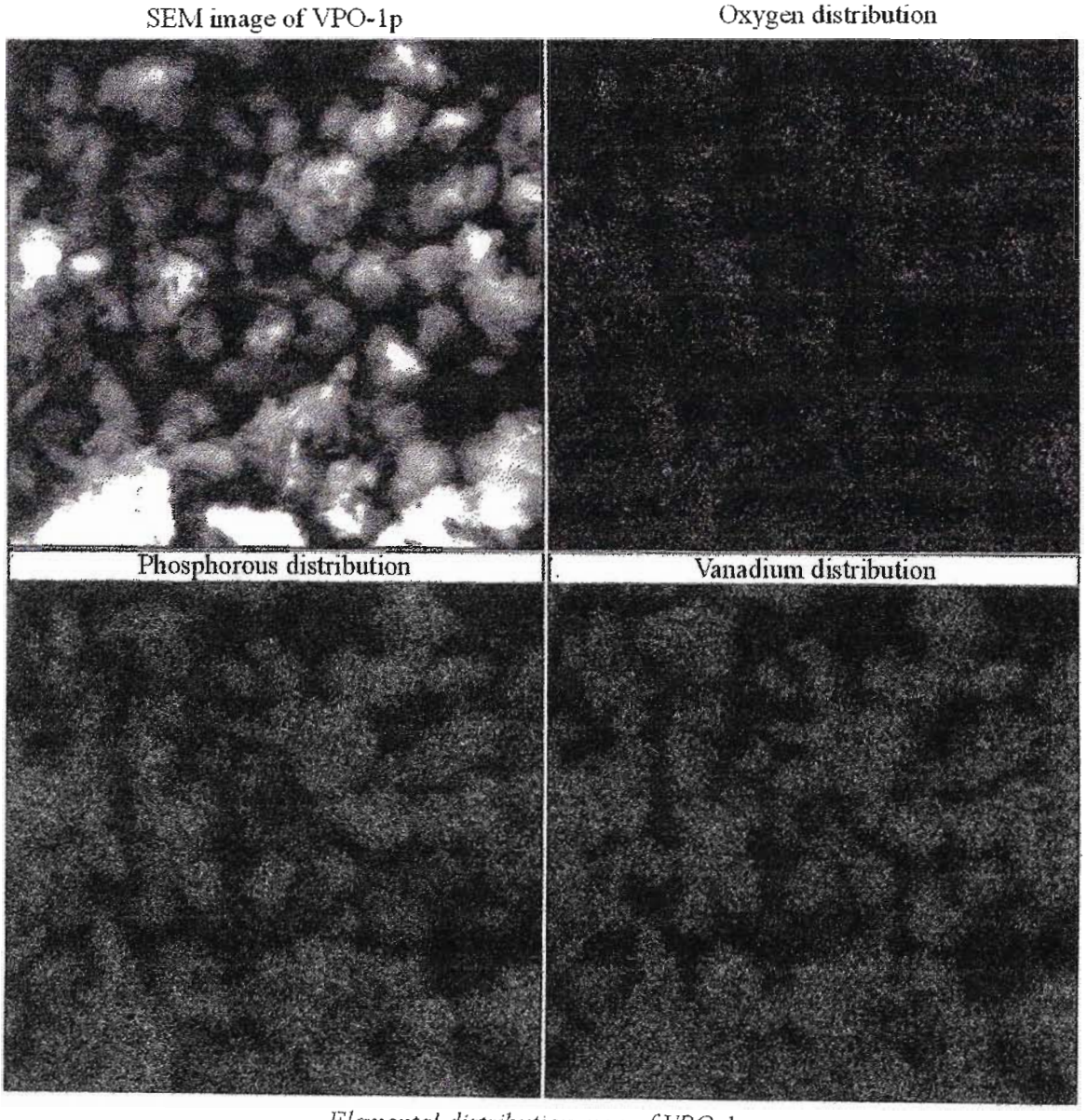

Elemental distribution map of VPO-1p

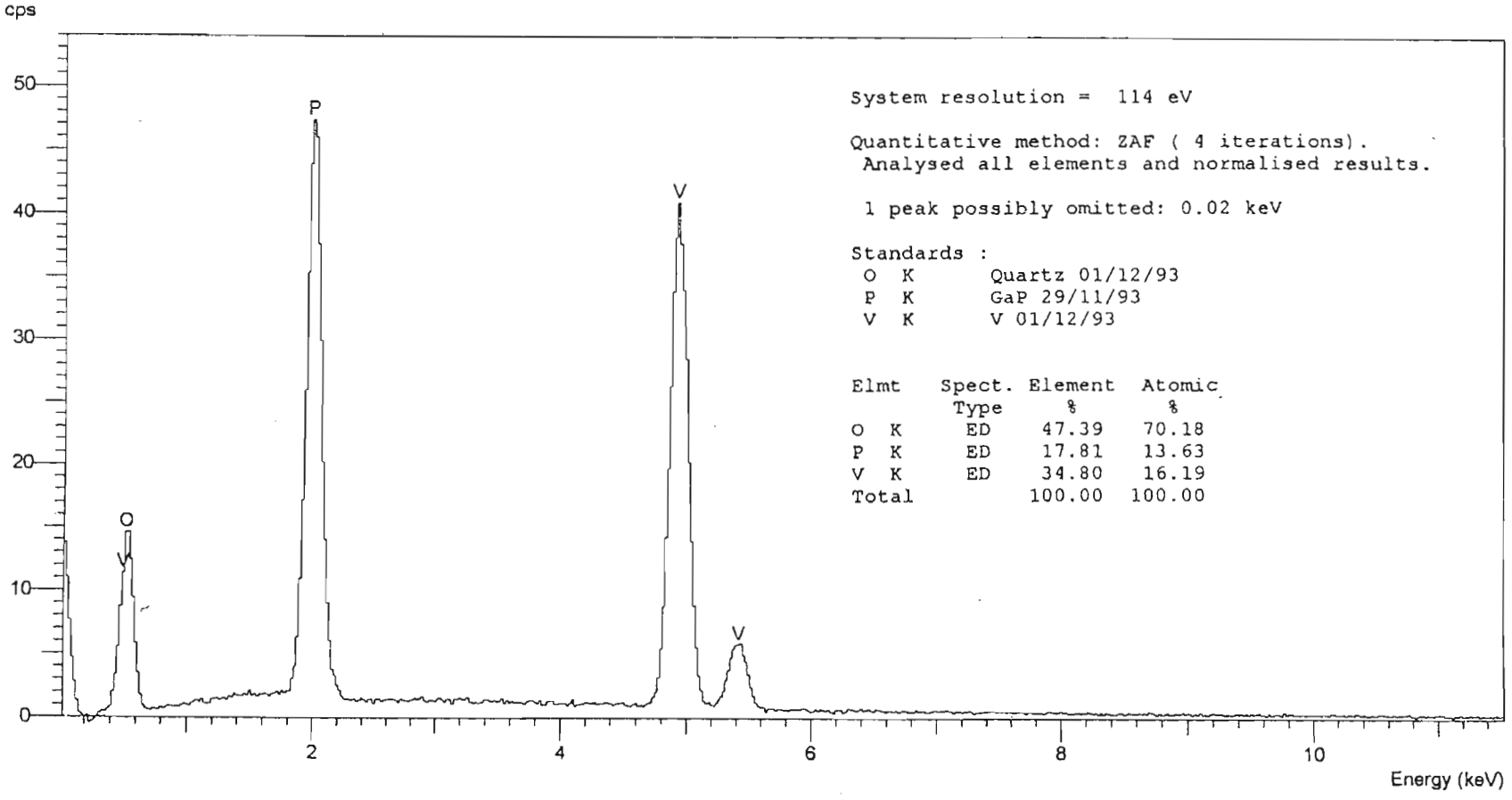

EDX spectrum of VPO-1p

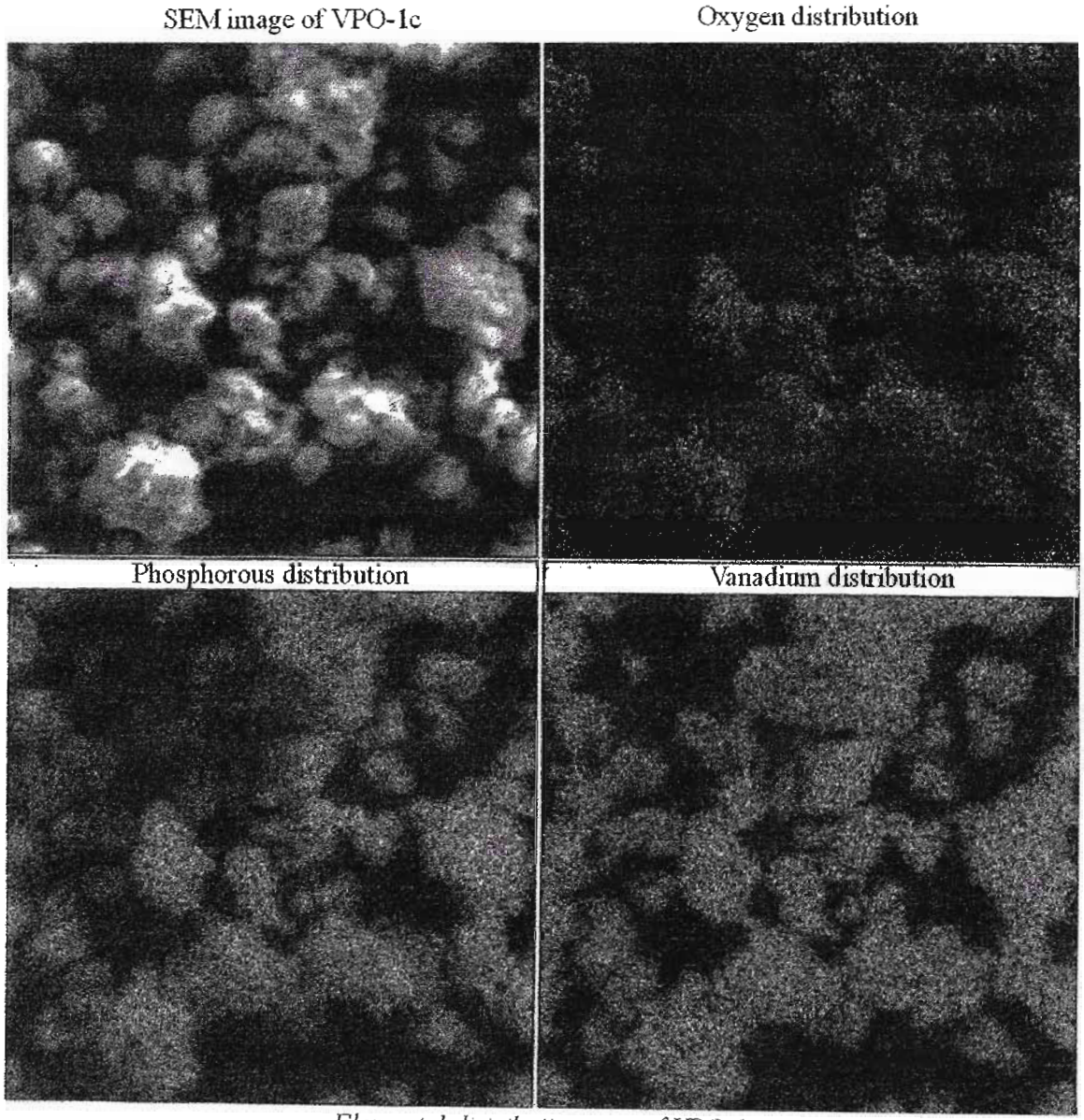

Elemental distribution map of VPO-1c

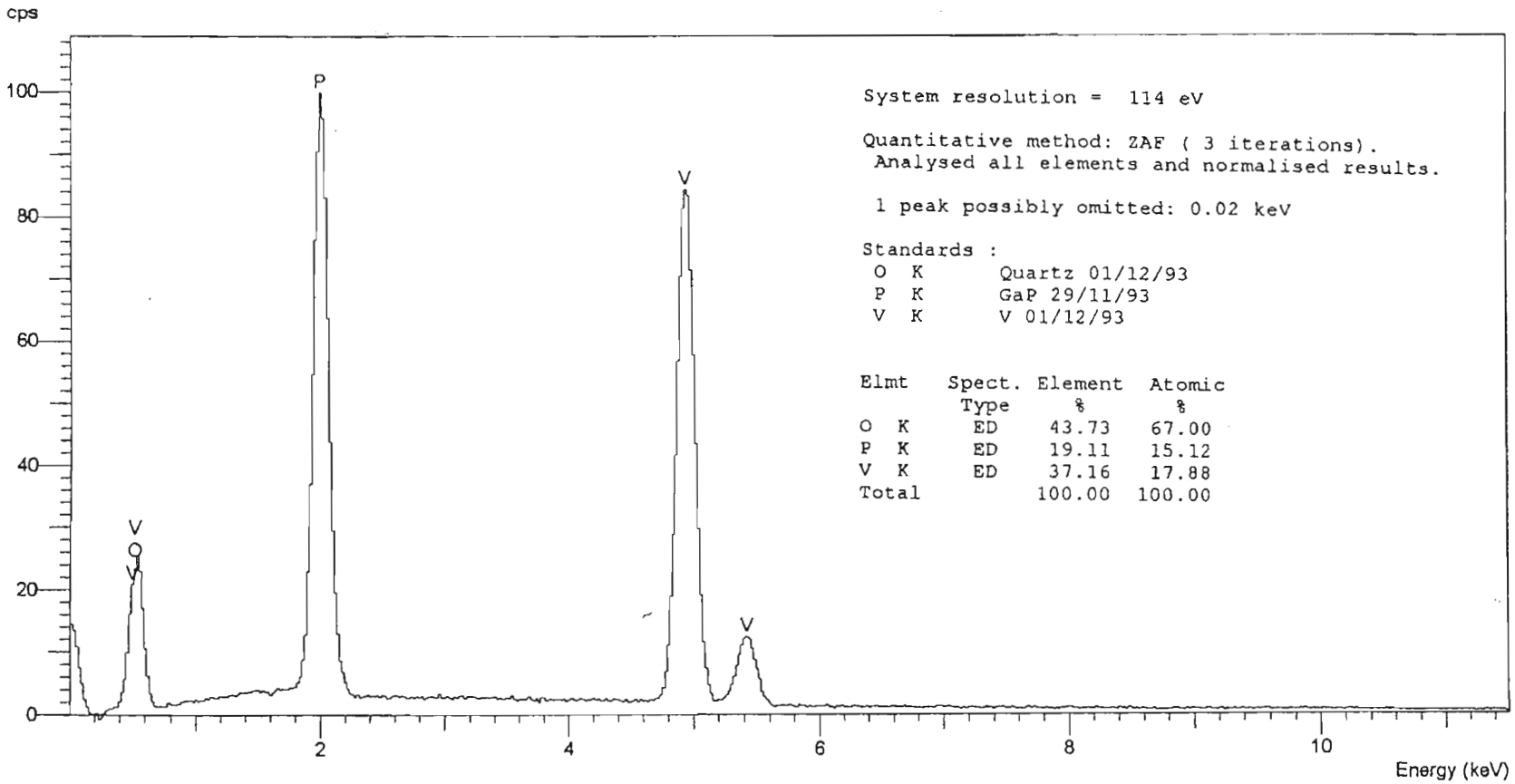

EDX spectrum of VPO-1c

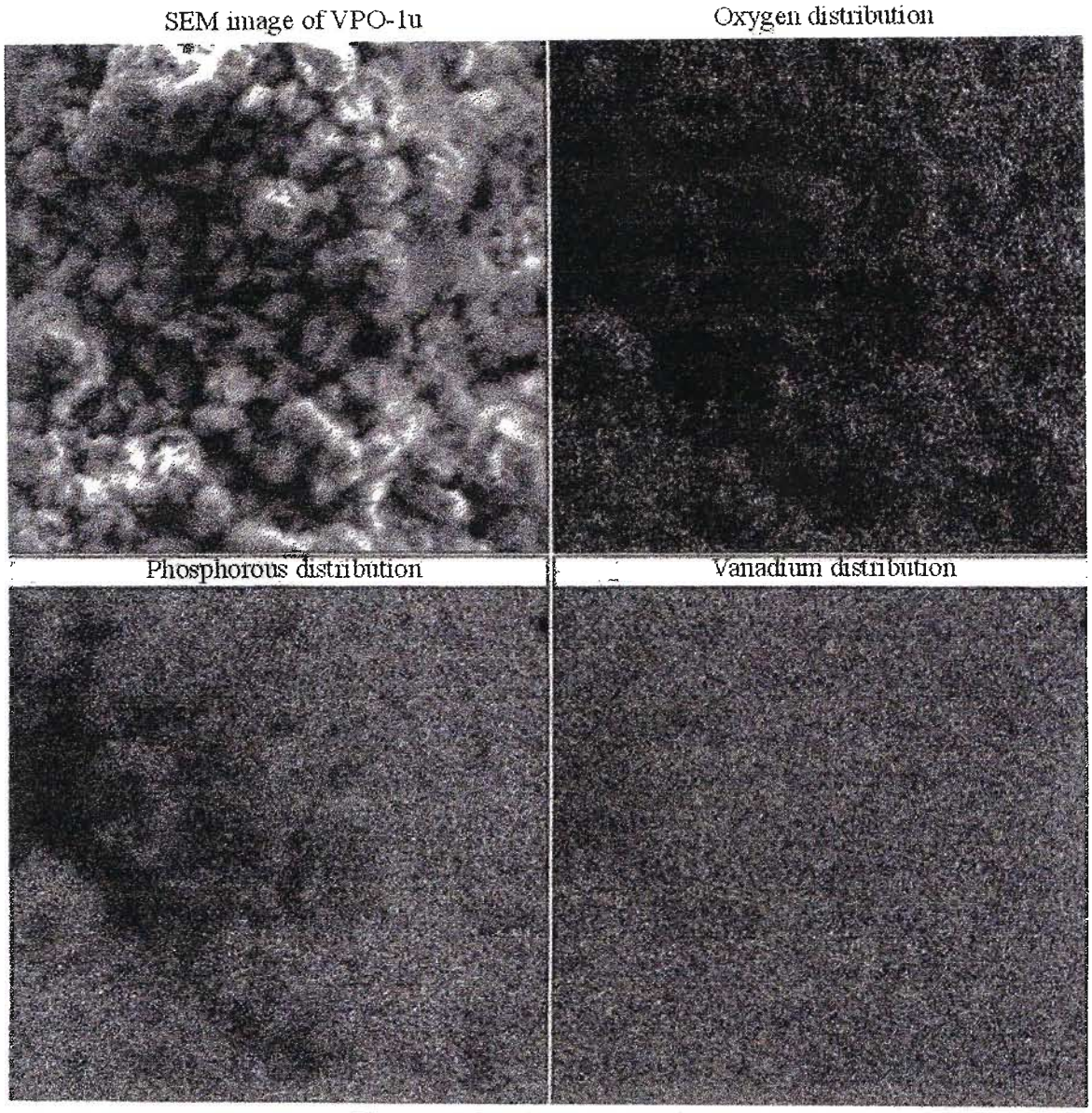

Elemental distribution map of VPO-1u

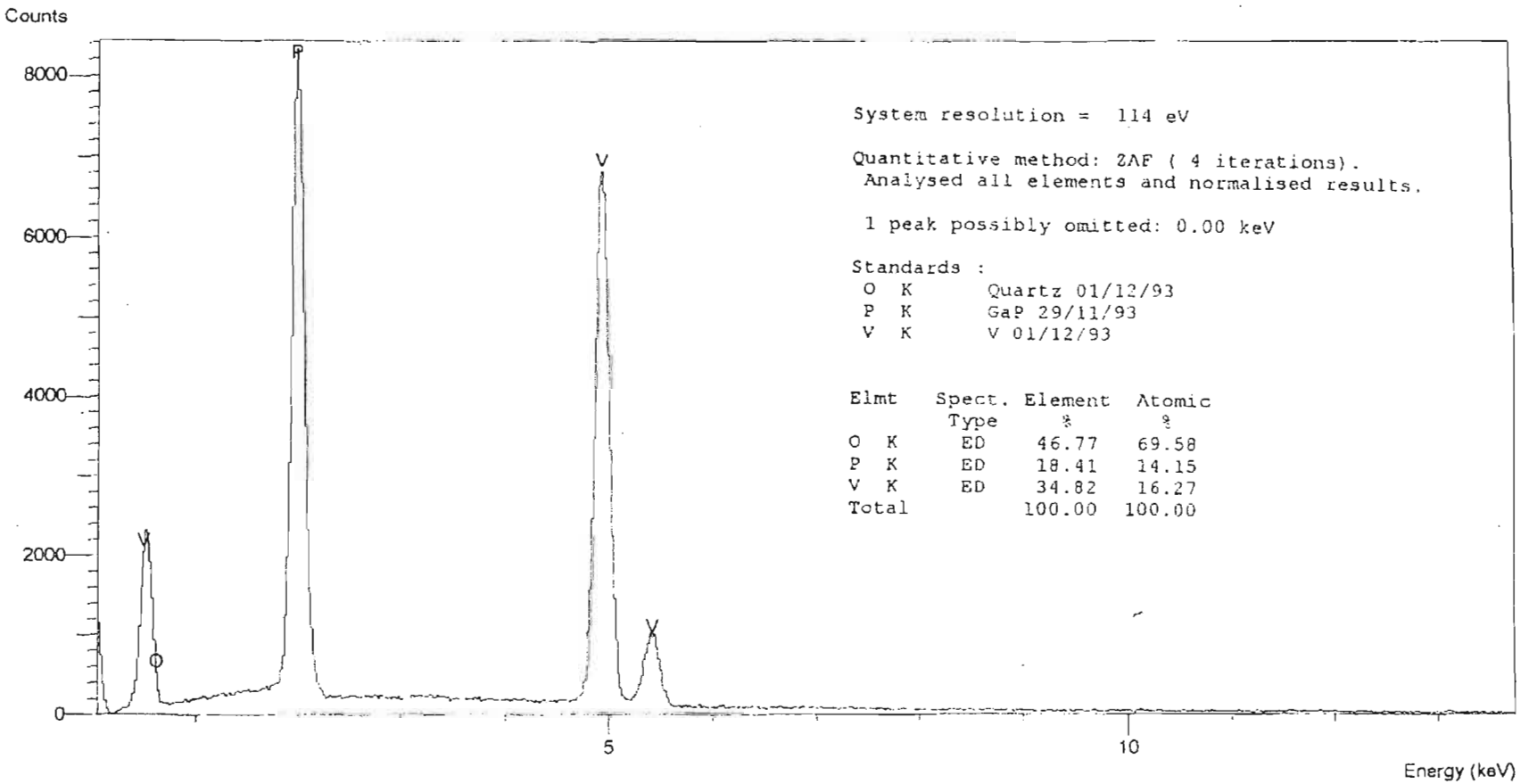

EDX spectrum of VPO-1u

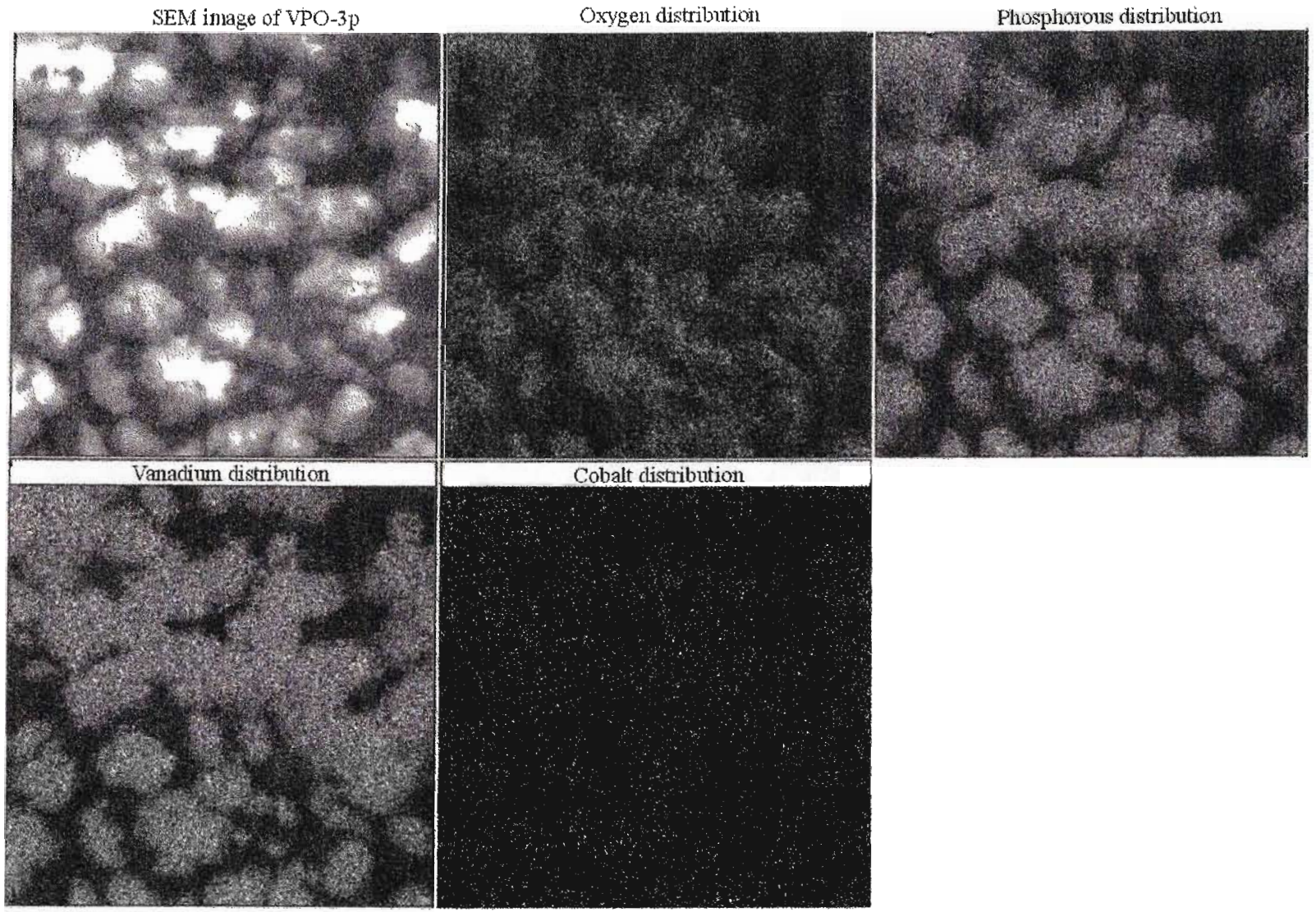

Elemental distribution map of VPO-3p

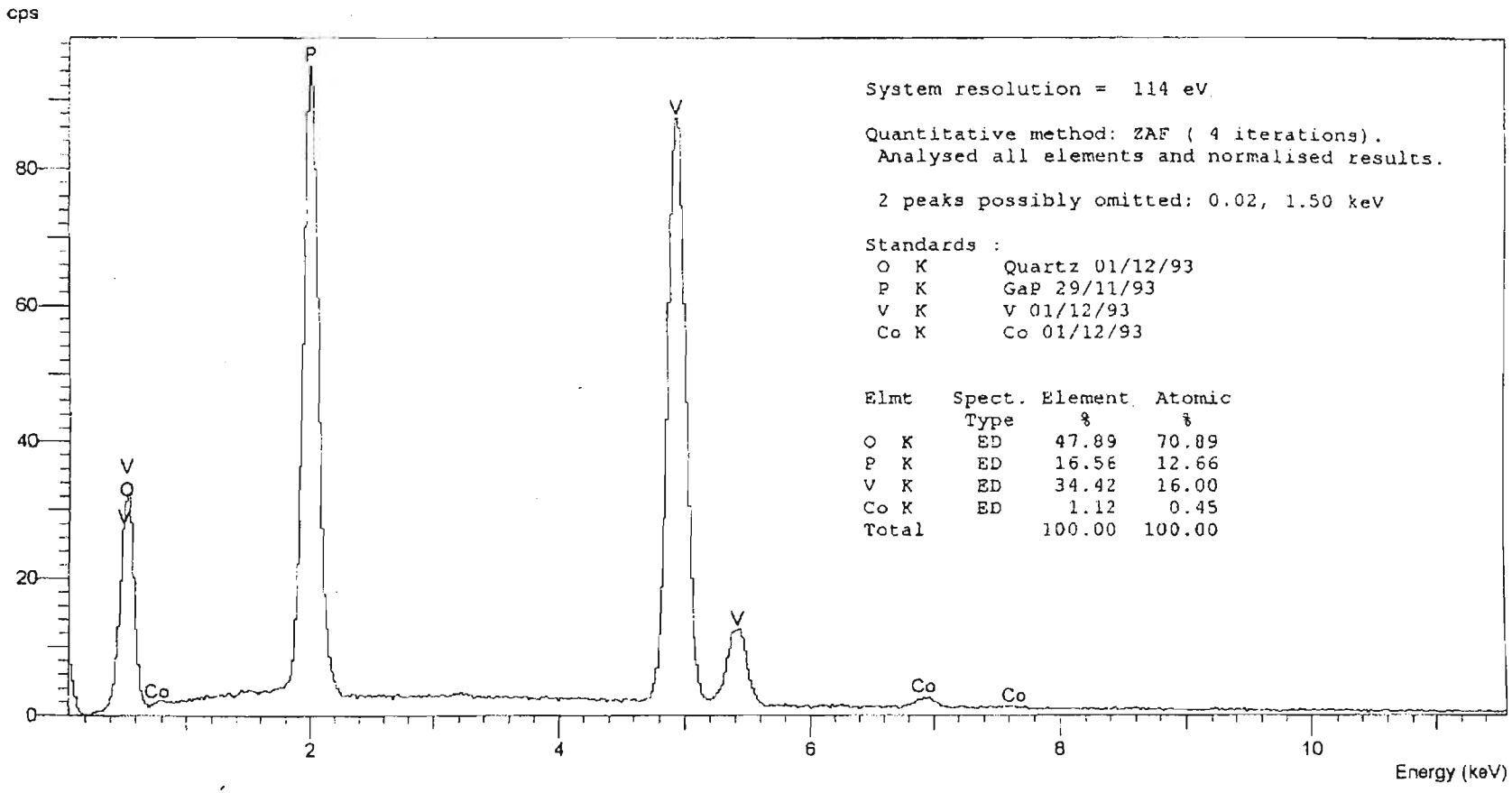

EDX spectrum of VPO-3p

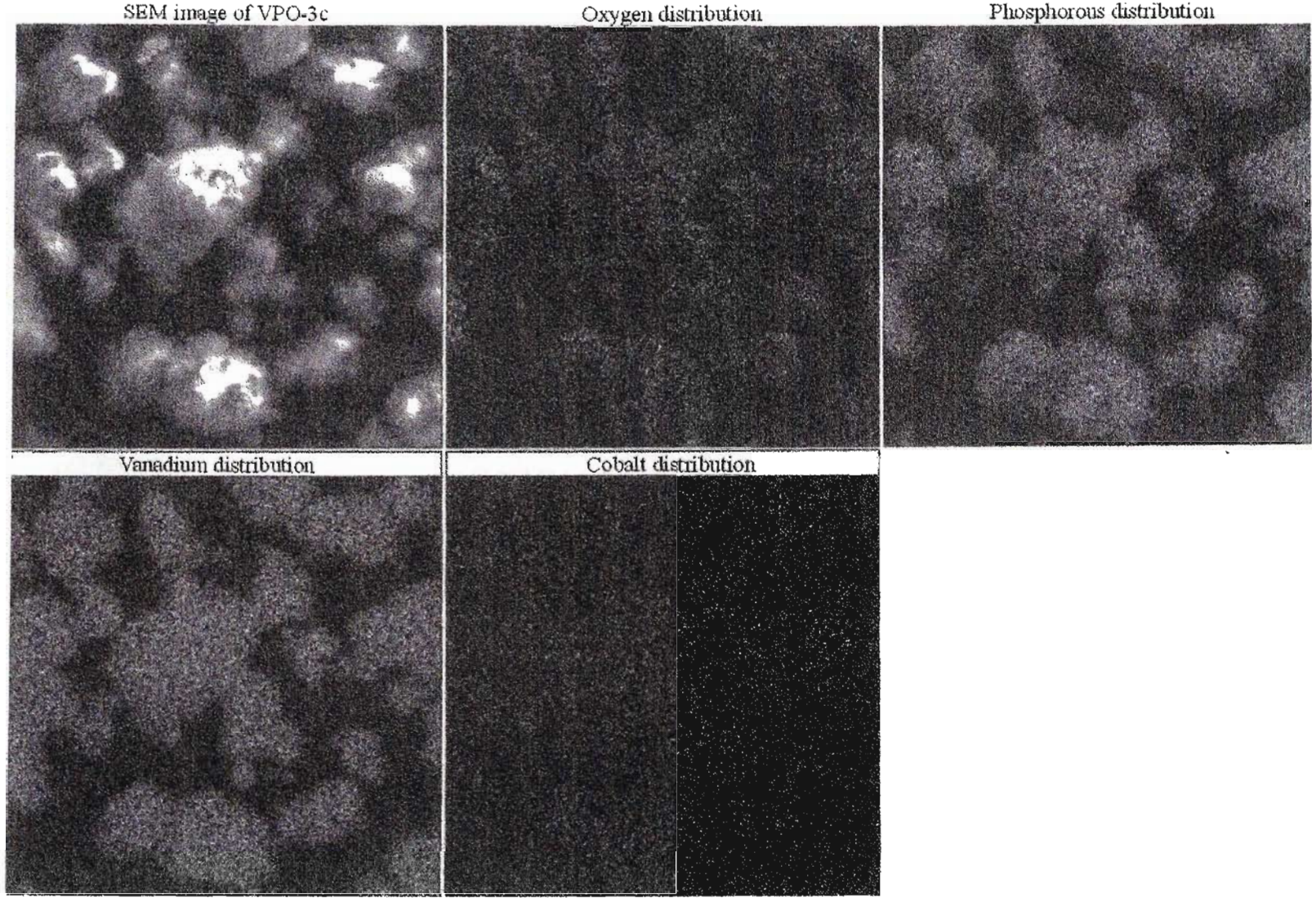

Elemental distribution map of VPO-3c

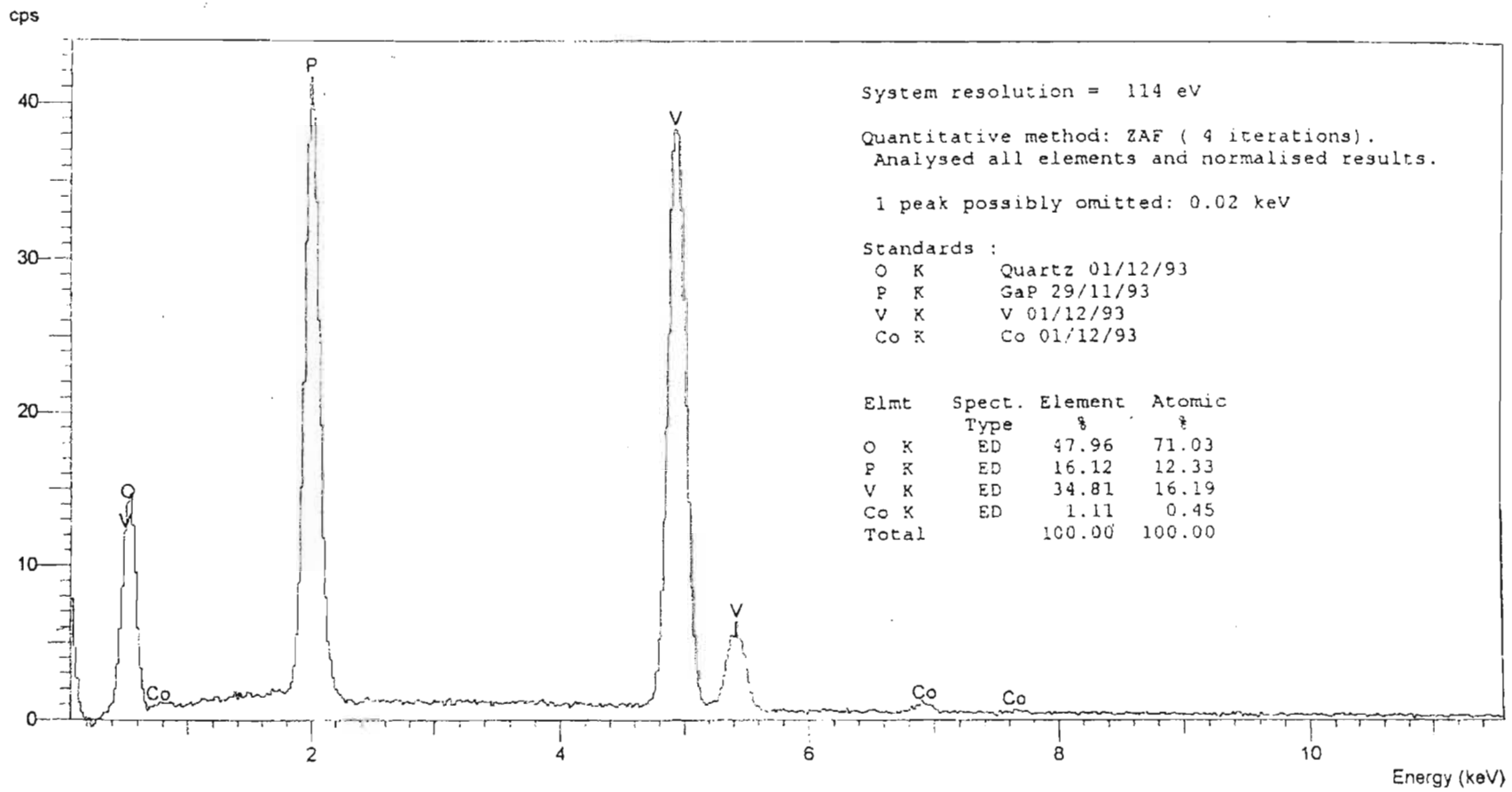

EDX spectrum of VPO-3c

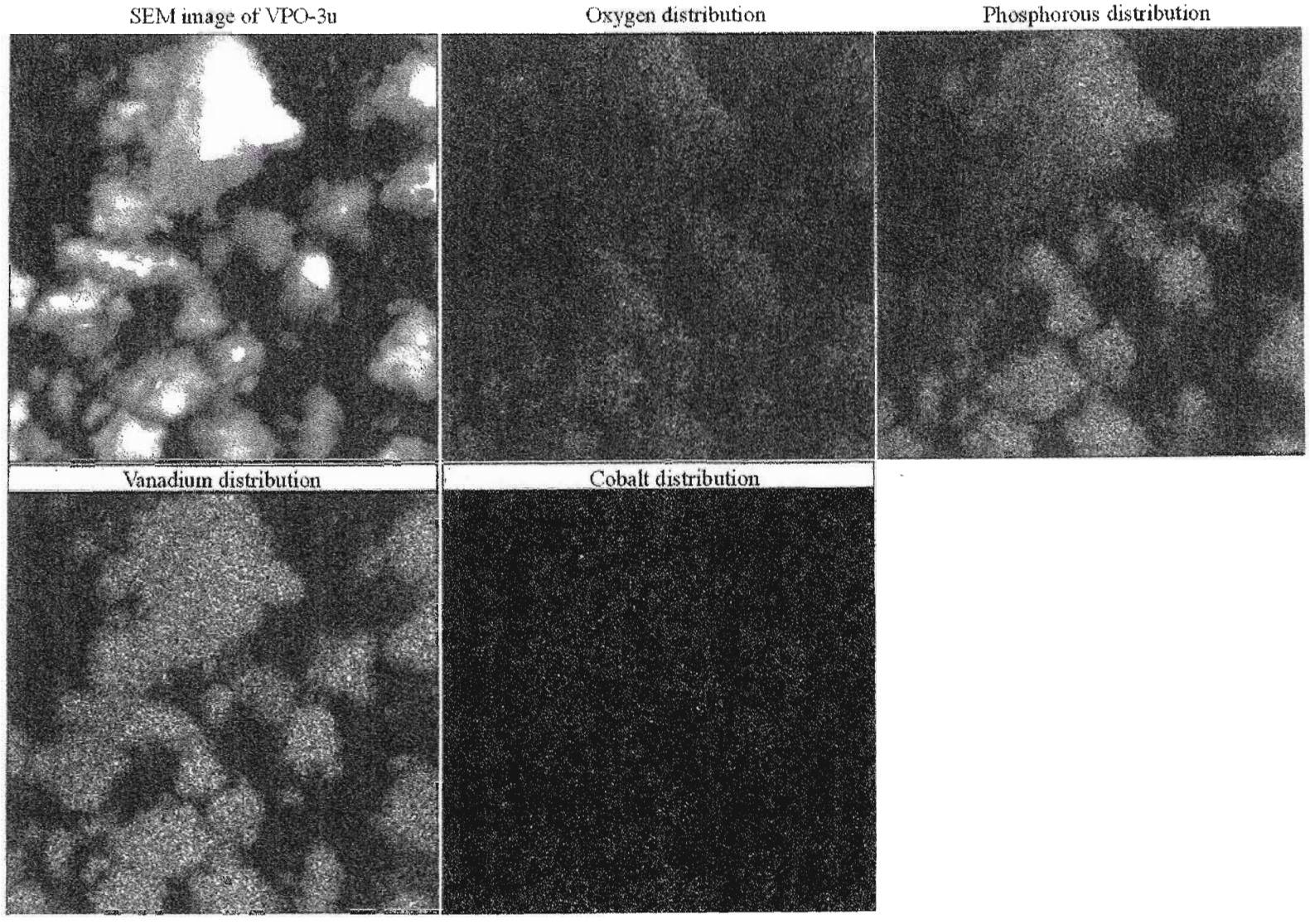

Elemental distribution map of VPO-3u

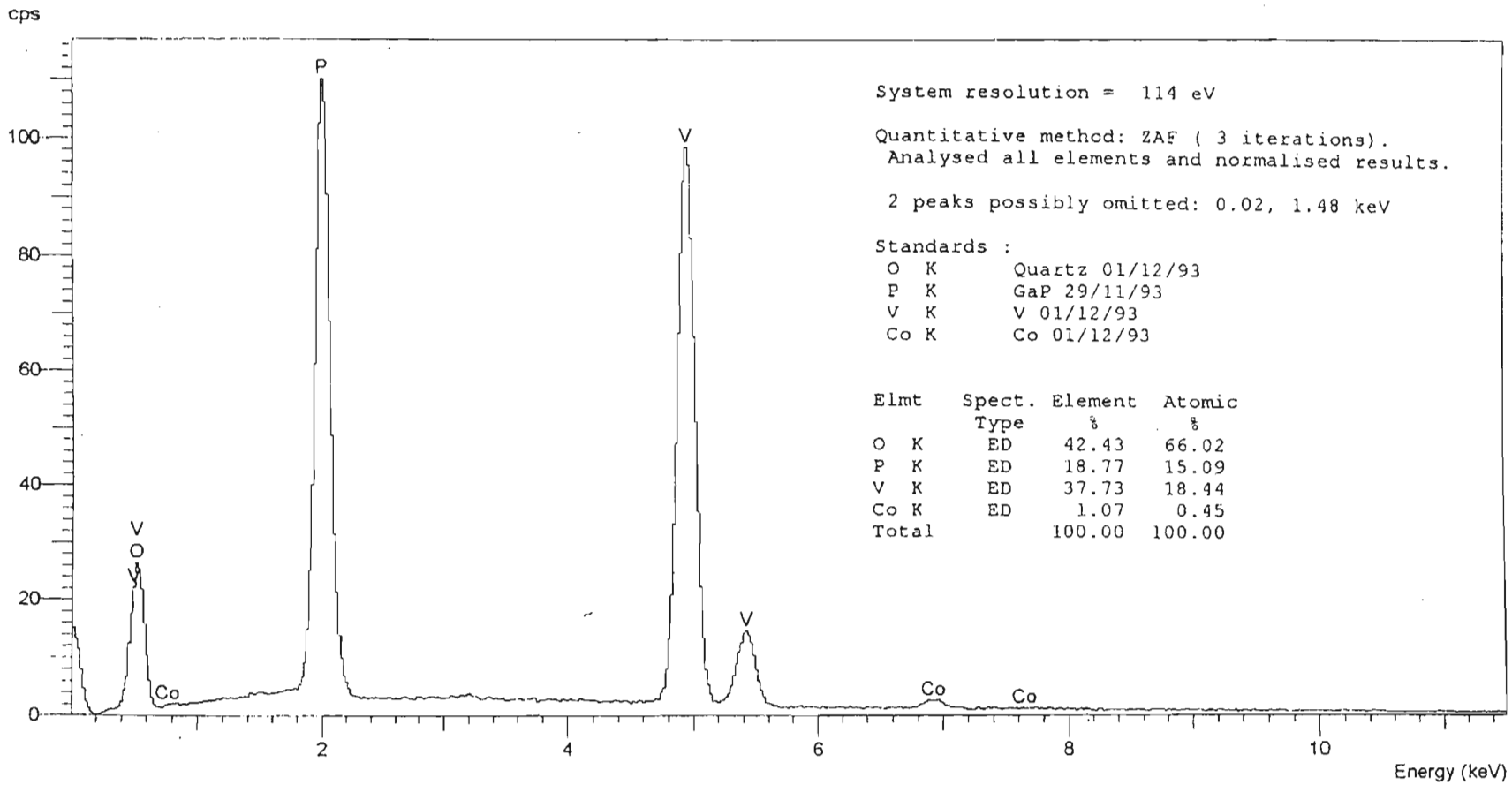

EDX spectrum of VPO-3u